

Nanostructures Across Oppositely Charged Surfactant–Polymer Interfaces



A thesis submitted for the degree of
Doctor of Philosophy

Submitted by
Kristian Joy Tangso
Bachelor of Pharmaceutical Sciences (Honours)
Monash University

January 2016



Drug Delivery, Disposition and Dynamics
Monash Institute of Pharmaceutical Sciences
Monash University (Parkville Campus)
381 Royal Parade, Parkville
Victoria, 3052, Australia

Copyright notice

© Kristian Joy Tangso (2016). Except as provided in the Copyright Act 1968, this thesis may not be reproduced in any form without the written permission of the author.

I certify that I have made all reasonable efforts to secure copyright permissions for third-party content included in this thesis and have not knowingly added copyright content to my work without the owner's permission.

Dedicated to my dearest parents, Marlene and Virgil Tangso

Acknowledgements

First and foremost, I would like to express my sincerest gratitude and appreciation to Doctor Father Ben Boyd for your guidance and encouragement to always strive to achieve my best and realise my full potential. Your time and shared expertise and experiences have been invaluable. I recall once having to reflect on ‘what is the meaning of life?’ during one of our end of year group meetings. Aside from acknowledging my dream of getting married and having children, I also shared one of my favourite quotes in which I live by: *“Sometimes opportunities float right past your nose. Work hard, apply yourself, and be ready. When an opportunity comes you can grab it.”* – Julie Andrews. Ben, thank you for all the opportunities I have had to learn, travel and grow both personally and professionally during my PhD candidature. I have had so many exciting, unexpected and unforgettable adventures and experiences through the past few years, where the wackiest of them all have unfortunately made it into ‘The Kristian Files’ (thanks Ben?!). It still astonishes me how your most brilliant of ideas are conceived over a glass of beer and that you never get tired of belting out that Elvis hit at karaoke. Moreover, your unfailing motivation, dedication and commitment to everything you do are commendable. There is no surprise as to why you are so successful and highly respected by your peers. It has been such a great privilege to have had you as a mentor and being part a friendly and intellectually stimulating work environment.

Thank you to Pat Spicer for your support and encouragement. Your expertise in rheology and your contributions from both academic and industrial perspectives have been invaluable. I’d also like to thank the Spicer family your hospitality during my short, but pleasant stay in Cincinnati.

To Pat Hartley and Seth Lindberg, thank you for your time and advice. I have had an interesting work experience during my visit at the CSIRO and P&G labs.

Thank you to Nigel Kirby, Stephen Mudie and Adrian Hawley for technical support on the SAXS/WAXS beamline at the Australian Synchrotron. Thanks to Brett Johnston, the Raman expert from The University of Melbourne, for training on the Raman microscope and your help in writing and working with scripts using 'R' - you'd be pleased to know that I managed to gain an appreciation of the program before I was on the brink of insanity. Thank you also to Robert Knott for your help with the SAXS experiments performed at the Bragg Institute.

The Australian Postgraduate Award, Australian Institute of Nuclear Science and Engineering Postgraduate Research Award, The Procter and Gamble Company and The Commonwealth Scientific and Industrial Research Organisation are acknowledged for their financial support.

To the Boyd group family who have been there through the best and worst of times - Stephanie Rietwyk, Khay Fong, Joanne Du, Linda Hong, Stefan Salentinig, Jamal Khan, Tang Li, Anna Pham, Nicolas Alcaraz, Nicole Bisset, Jessica Lyndon, Jason Liu, Charlie Dong, Graham Webster, Oliver Montagnat, Josephine Chong and Adam Tilley. Thank you for your friendship and support in and out of the lab. I will miss the office shenanigans!

To Martin and Katie, thank you for providing an excellent means of stress relief on campus. I have enjoyed all the boxing and yoga fitness classes over the years.

Thank you to my family and dearest friends for your moral support and always being there when I just needed a break from everything.

Most of all, I have to thank my number one supporters - mum and dad. Your unconditional love, sacrifices, selflessness and advice over the years have nurtured me in into

the person that I am today, and for that I am forever grateful. Thank you for always reminding me that anything is possible if you believe in it, and for your continued encouragement to pursue my dreams. Dad, thank you for the delicious meals you cook at home and for being my personal chauffeur at times- I will always be your little princess. Mum, or rather SUPER MUM, it amazes me how much you can accomplish in one day! I hope to be as kind-hearted, generous and successful as you, as well as a devoted and loving wife and mother. I am so blessed to have you both as my parents.

I thank You, Lord, for the strength, wisdom and patience You have given me during the preparation of my PhD thesis, as well as all the blessings I have received so far in life. I look forward to what You have planned for me next.

Contents

Abstract	i
Declaration of Authorship.....	ii
Publications	iii
Communications	iii
List of Abbreviations	v
Chapter 1: <i>Introduction</i>	1
1.1 Overview	2
1.2 Classification of Surfactants and Polymers.....	4
1.2.1 Surfactants.....	4
1.2.1.1 Liquid Crystalline Structures	5
1.2.2 Polymers.....	7
1.3 Oppositely Charged Surfactant and Polymer Systems	9
1.3.1 General Phase Behaviour	9
1.3.2 Commonly Studied Systems.....	13
1.3.3 Parameters that Influence the Formation of Nanostructured Complexes.....	16
1.3.3.1 Surfactant-to-Polymer Molar Charge Ratio.....	16
1.3.3.2 Polymer Structure.....	17
1.3.3.3 Surfactant Structure	17
1.3.3.4 Temperature	18
1.3.3.5 Salt Concentration.....	19
1.3.3.6 Solution pH.....	19
1.4 Practical Considerations for Studying the Equilibrium Behaviour of Oppositely Charged Surfactant and Polymer Systems.....	20
1.4.1 Method of Preparation	20
1.4.2 Rheology of Surfactant/Polymer Complexes	22
1.4.3 Exploitation of the Complex Salt.....	23
1.5 Techniques Commonly Employed to Characterise Mesophase Formation and Probe Molecular Interactions in Surfactant and Polymer Systems	25
1.5.1 Microscopic Techniques.....	27
1.5.1.1 Crossed-Polarised Light Microscopy	27
1.5.1.2 Scanning Electron Microscopy.....	29
1.5.1.3 Cryogenic-Transmission Electron Microscopy	29

1.5.1.4	Atomic Force Microscopy.....	30
1.5.1.5	Confocal Microscopy.....	31
1.5.2	Scattering Techniques.....	33
1.5.2.1	Dynamic Light Scattering.....	33
1.5.2.2	Electrophoretic Light Scattering.....	33
1.5.2.3	Small and Wide Angle X-ray Scattering.....	34
1.5.2.4	Small Angle Neutron Scattering.....	36
1.5.3	Other Techniques.....	36
1.6	A Statement of the Problem.....	37
1.7	Hypotheses.....	38
1.8	Aims.....	39
1.9	References.....	40

Chapter 2. *Developing a Novel Approach for Probing Structure and Composition Across Surfactant–Polymer Interfaces.....* 65

2.1	Introduction.....	66
2.2	Hypothesis and Aims.....	72
2.3	Materials.....	73
2.4	Methods.....	73
2.4.1	Selecting the Sample Cell.....	73
2.4.2	Sample Preparation.....	77
2.4.3	Characterisation of the Internal Structure of Liquid Crystalline Phases Across Surfactant–Polymer Interfaces.....	78
2.4.3.1	Crossed–Polarised Light Microscopy.....	78
2.4.3.2	Synchrotron Small Angle X-ray Scattering.....	78
2.4.4	Quantifying the Concentrations of Polymer, Surfactant, and Water Across SDS–PolyDADMAC Interfaces.....	81
2.4.4.1	Raman Microscopy.....	81
	<i>Developing and Validating Standard Curves.....</i>	81
	<i>Line Scans.....</i>	85
2.4.4.2	Synchrotron Small Angle X-ray Scattering.....	85
	<i>Developing Standard Curves for Quantifying SDS in Micellar Solutions or Hexagonal Phases.....</i>	85
	<i>Developing a Standard Curve for Measuring the Concentration of Water in Hexagonal Phases.....</i>	86
2.5	Results.....	88

2.5.1	Visualisation of Anisotropic Liquid Crystalline Structures Across Surfactant–Polymer Interfaces.....	88
2.5.2	Spatially Resolved Structural Information Across Surfactant–Polymer Interfaces	89
2.5.3	Generation of Calibration Curves to Quantify the Concentrations of Surfactant, Polymer, and Water Across SDS–PolyDADMAC Interfaces	91
2.5.3.1	Use of Raman Microscopy for Composition Analysis	91
	<i>PolyDADMAC/Water Binary Systems</i>	91
	<i>SDS/Water Binary Systems</i>	92
	<i>Water</i>	92
	<i>PolyDADMAC/SDS/Water Systems</i>	93
2.5.3.2	Use of Synchrotron Small Angle X-ray Scattering for Composition Analysis.....	94
	<i>SDS/Water Binary Systems</i>	94
	<i>Water</i>	96
2.6	Discussion	99
2.6.1	Probing Structures Across Surfactant–Polymer Interfaces.....	99
2.6.1.1	Imaging Birefringent Materials	99
2.6.1.2	Spatially Resolved SAXS Profiles with a Synchrotron Source	99
2.6.2	Determining Composition Across SDS–PolyDADMAC Interfaces.....	100
2.6.2.1	Advantages and Disadvantages of Raman Microscopy.....	100
2.6.2.2	Using SAXS to Interpret Composition.....	103
2.7	Conclusions	106
2.8	References	107

Chapter 3: *Investigation of Structure Formation Across the SDS–PolyDADMAC Interface*..... 113

3.1	Introduction.....	114
3.2	Hypotheses and Aims.....	120
3.3	Materials	121
3.4	Methods.....	121
3.4.1	Synthesis of the Complex Salt, PolyDADMADS.....	121
3.4.2	Preparation of Bulk Mixtures	122
3.4.2.1	Conventional Mixing Protocol	122
3.4.2.2	Employing the Complex Salt, PolyDADMADS	122
3.4.3	Characterisation of Mesophases in Bulk Mixtures	123

3.4.4	Studying the Phase Behaviour Across the SDS–PolyDADMAC Interface	123
3.4.4.1	Preparation of SDS–PolyDADMAC Interfaces	124
3.4.4.2	Characterisation of Nanostructures Formed Across the SDS–PolyDADMAC Interface	124
3.4.4.3	Quantifying the Concentrations of PolyDADMAC, SDS, and Water Across the SDS–PolyDADMAC Interface	125
3.5	Results	126
3.5.1	Phase Behaviour of SDS/PolyDADMAC Aqueous Mixtures	126
3.5.2	Structure Formation Across the SDS–PolyDADMAC Interface.....	129
3.5.3	Mapping Composition Across the SDS–PolyDADMAC Interface	134
3.5.4	Correlating Changes in Structure and Composition Across the SDS–PolyDADMAC Interface Over Time	138
3.6	Discussion	140
3.6.1	Formation of the Complex Salt in Bulk Mixtures.....	140
3.6.2	Self-Assembly of Nanostructures Across the SDS–PolyDADMAC Interface .	141
3.6.2.1	Development of Micellar and Hexagonal Phases Towards the Bulk SDS Region.....	142
3.6.2.2	Diffusion–Controlled Rate of Structure Formation Across the SDS–PolyDADMAC Interface	143
3.6.3.3	The Slow Kinetics Involved in the Formation of Equilibrium Structures Across the SDS–PolyDADMAC Interface	144
3.7	Conclusions	146
3.8	References	147
3.9	Appendix	154
A3.1	Phase Behaviour of an Industrially Relevant Surfactant/Polymer System	154
A3.2	Equilibrium Structure of the 20 wt% SDS: 20 wt% PolyDADMAC System as a Bulk Mixture	155
A3.3	Structural Characterisation of a Concentrated Aqueous Mixture of SDS and Water by SAXS.....	156

Chapter 4. *Controlling the Mobility of System Components Across Surfactant–Polymer Interfaces*

4.1	Introduction.....	158
4.2	Hypotheses and Aims.....	162
4.3	Materials.....	164
4.4	Methods.....	164

4.4.1	Synthesis of the Cross-linked Polyacrylate Macrogel.....	164
4.4.2	Preparation of the Surfactant–Polymer Interfaces.....	165
4.4.2.1	CTAB/Polyacrylate Macrogel System.....	165
4.4.2.2	SDS _{H1} /PolyDADMAC System.....	165
4.4.3	Characterisation of Nanostructures Across Surfactant–Polymer Interfaces.....	166
4.4.4	Determining the Distribution of System Components Across Surfactant–Polymer Interfaces.....	166
4.4.4.1	CTAB/Polyacrylate Macrogel System.....	166
4.4.4.2	SDS _{H1} /PolyDADMAC System.....	167
4.5	Results.....	168
4.5.1	Kinetics of Structure Formation Across the CTAB–Polyacrylate Macrogel Interface.....	168
4.5.1.1	Growth of Mesophases Within the Polyacrylate Macrogel.....	168
4.5.1.2	Frontal Diffusion of CTAB Molecules into the PA Macrogel.....	171
4.5.2	Dynamics of Structure Formation Upon Contact of SDS Hexagonal Phase with Dilute PolyDADMAC Solution.....	172
4.5.2.1	Mesophases Formed Across the SDS _{H1} –PolyDADMAC Interface.....	172
4.5.2.2	Correlating Changes in Composition with the Formation of Mesophases Across the SDS _{H1} –PolyDADMAC Interface.....	176
4.6	Discussion.....	178
4.6.1	Dynamic Phase Behaviour Across the Cross-linked Polyacrylate Gel Upon Contact with CTAB Solution.....	178
4.6.2	Implications of Cross-linked Polymers and Oppositely Charged Molecules in Drug Delivery.....	181
4.6.3	The Importance of SDS Concentration in the Formation of Micellar-like Ordered Structures Upon Contact with Solutions of Mobile PolyDADMAC Molecules.....	182
4.7	Conclusions.....	185
4.8	References.....	186
4.9	Appendix.....	192
A4.1	Structural Characterisation of Mesophases Formed Across the CTAB–Polyacrylate Macrogel Interface by SAXS.....	192
A4.2	Structural Characterisation of Bulk Aqueous Mixtures of SDS and PolyDADMAC by SAXS.....	193
Chapter 5: <i>Toward the Formation of Equilibrium Structures in SDS and PolyDADMAC Dispersions</i>.....		194

5.1	Introduction.....	195
5.2	Hypotheses and Aims.....	198
5.3	Materials.....	199
5.4	Methods.....	199
5.4.1	Sample Preparation.....	199
5.4.2	Characterisation of Mesophases in SDS and PolyDADMAC Dispersions.....	200
5.4.2.1	Dynamic Light Scattering.....	200
5.4.2.2	Small Angle X-ray Scattering.....	201
5.4.2.3	Cryogenic-Transmission Electron Microscopy.....	201
5.5	Results.....	202
5.5.1	Evolution of Nanostructures in Dispersed SDS and PolyDADMAC Systems.....	202
5.5.2	Effect of Additives on Nanostructure Phase Behaviour.....	205
5.6	Discussion.....	207
5.6.1	Effect of the PolyDADMAC-to-SDS Molar Charge Ratio on the Lattice Parameter of Hexagonal Phases Formed in SDS/PolyDADMAC Mixtures.....	207
5.6.2	The Importance of the Absolute Concentrations in Determining the Global Morphology of Mesophases Formed in Surfactant/Polymer Mixtures.....	208
5.6.3	Understanding the Relationship Between the Local Composition and the Existence of Equilibrium Structures in Surfactant/Polymer Mixtures.....	211
5.6.4	Formation of Normal Hexagonal (H ₁) Phase in SDS and PolyDADMAC Systems.....	213
5.6.5	Implications for Use as Bioactive Delivery Systems.....	214
5.7	Conclusions.....	215
5.8	References.....	216
5.9	Appendix.....	223

Chapter 6: *Novel Stimuli-Responsive Drug Delivery Systems Created Using Nanostructures Formed Across Surfactant-Polymer Interfaces.....* 225

6.1	Introduction.....	226
6.1.1	SDS/PolyDADMAC System.....	228
6.1.2	CTAB/PAAm-AA System.....	229
6.1.3	Bile Salt/Chitosan System.....	231
6.1.4	Studying the Release Behaviour from Structured Capsules.....	232
6.2	Hypotheses and Aims.....	233
6.3	Materials.....	234
6.3.1	Surfactant/Polymer System Composition.....	234

6.3.1.1	SDS/PolyDADMAC System.....	234
6.3.1.2	CTAB/PAAm-AA System.....	235
6.3.1.3	Bile Salt/Chitosan System.....	235
6.4	Methods.....	236
6.4.1	Characterisation of the Internal Structure of Liquid Crystalline Phases.....	236
6.4.1.1	Mesophases Across Surfactant-Polymer Interfaces.....	236
	<i>Sample Preparation</i>	236
	<i>Crossed-Polarised Light Microscopy</i>	237
	<i>Hot Stage Crossed-Polarised Light Microscopy</i>	237
	<i>Synchrotron Small Angle X-ray Scattering</i>	238
6.4.1.2	Temperature Scan of Bulk Mixtures.....	238
6.4.2	<i>In Vitro</i> Release Studies.....	239
6.4.2.1	Release of Model Drug from Nanostructured Capsules.....	239
6.4.2.2	Rhodamine B Assay by Fluorescence Spectroscopy.....	241
6.4.2.3	Data Analysis.....	241
6.5	Results.....	242
6.5.1	Nanostructures Across the SDS-PolyDADMAC Interface.....	242
6.5.1.1	Effect of Temperature on Hexagonal Phases.....	242
6.5.1.2	Effect of Salt Concentration on Hexagonal Phases.....	243
6.5.2	Nanostructures Across the CTAB-PAAM-AA Interface.....	244
6.5.2.1	Growth and Development of Coexisting <i>Pm3n</i> Cubic and Hexagonal Phases.....	244
6.5.2.2	Effect of Temperature on CTAB-PAAM-AA Mesophases.....	246
6.5.2.3	Effect of pH on CTAB-PAAM-AA Mesophases.....	247
6.5.3	Nanostructures Across the Bile Salt-Chitosan Interface.....	248
6.5.3.1	Growth and Development of Bile Salt-Chitosan Mesophases.....	248
6.5.3.2	Effect of Temperature on Bile Salt-Chitosan Lamellar Phase.....	249
6.5.3.3	Effect of Salt Concentration on Bile Salt-Chitosan Lamellar Phase....	250
6.5.4	Diffusivity of Rhodamine B from Nanostructured Capsules.....	251
6.5.4.1	Triggered Release from Nanostructured Capsules.....	252
	<i>Thermally Stable Hexagonal SDS/PolyDADMAC Capsules</i>	252
	<i>pH-Responsive Cubic/Hexagonal Phase CTAB/PAAm-AA Capsules</i>	252
	<i>Temperature-Responsive Lamellar Phase Bile Salt/Chitosan Capsules</i>	252
6.6	Discussion.....	255
6.6.1	Nanostructure-Controlled Diffusion of Molecules from Surfactant/Polymer Complexes.....	255

6.6.2	Potential Applications of Thermally Stable and Salt-Sensitive SDS/PolyDADMAC Micellar/Hexagonal Phases.....	257
6.6.3	Novel Cubic/Hexagonal Phase Cetyltrimethylammonium Bromide/Poly(acrylamide-acrylic acid) Capsules for pH Stimulated Release	259
6.6.4	Novel Temperature-Sensitive Lamellar Phase Bile Salt/Chitosan Oral Dosage Forms	260
6.6.4.1	<i>In Situ</i> Self-Assembly of Lamellar Phase in Simulated Gastrointestinal Fluids.....	261
6.6.5	Novel Colistin/Heparin Lamellar Phase Complexes for Antimicrobial Coating of Biomedical Devices.....	262
6.7	Conclusions	264
6.8	References	265
6.9	Appendix	273
A6.1	Effect of pH on the Bile Salt/Chitosan System	273
A6.2	Visualising the Growth of Nanostructures Across the Bile Salt-Chitosan Interface by CPLM.....	274
A6.3	Phase Behaviour of Chitosan in Biorelevant Bile Solutions.....	274
A6.4	Characterisation of Mesophases Formed Across the CTAB-PAAm-AA Interface by Synchrotron SAXS	276
A6.5	Identification of Coexisting <i>Pm3n</i> Cubic and Hexagonal Phases Across the CTAB-PAAm-AA Interface	276
A6.6	Temperature-Dependent Equilibrium Phase Behaviour of the CTAB and PAAm-AA System	277
A6.7	Calibration Curve for Rhodamine B by Fluorescence Spectroscopy.....	278
Chapter 7: <i>Summary and Outlook</i>.....		279
7.1	Summary of Findings.....	280
7.1.1	Novel Approaches to Study the Dynamics of Structure Formation Across Solution Interfaces	280
7.1.2	New Insights into the Formation of Equilibrium and Nonequilibrium Structures in Oppositely Charged Surfactant and Polymer Systems	283
7.1.3	Tailored Release Nanomaterials.....	285
7.2	Future Directions.....	286
7.3	References	287

Abstract

Oppositely charged surfactant and polymer systems have received increasing interest as they offer great versatility and control of highly ordered structures formed in solution for exploitation in various industrial and pharmaceutical applications. Early studies have focused on the phase behaviour of these systems as bulk mixtures or dispersions, however investigation across surfactant–polymer solution interfaces has been scarce.

A novel approach was developed to study the kinetics of structure formation across such interfaces. Line scans were performed with synchrotron small angle X-ray scattering and Raman microscopy to obtain structural and compositional data spatially across SDS–polyDADMAC interfaces at various time points. Structures identified across these interfaces were compared with those formed in dispersions or bulk mixtures prepared at the same molar charge ratio to comment on their state of equilibrium. The release behaviour of model hydrophilic drug from a range of industrially and biologically relevant oppositely charged surfactant and polymer structured capsules to certain stimuli was also assessed.

Results demonstrated the existence of both equilibrium and nonequilibrium nanostructures locally across SDS–polyDADMAC interfaces. The rate of structure formation across these interfaces and the extent to which equilibrium was reached was determined by the structure and concentration gradients existing at a given time and the mobility of the components within or from bulk regions, and across hexagonal and/or micellar phases.

New insights gained into the slow mixing, equilibrium phase behaviour and structural attributes of oppositely charged surfactant and polymer systems can be applied in the development cost-effective formulations with the desired physicochemical properties and functionality, as well as the design of novel stimuli-responsive drug delivery systems.

Declaration of Authorship

In accordance with Monash University Doctorate Regulation, 17/Doctor of Philosophy and Master of Philosophy (MPhil) regulations, the following declarations are made:

I hereby declare that this thesis contains no material which has been accepted for the award of any other degree or diploma at any university or equivalent institution and that, to the best of my knowledge and belief, this thesis contains no material previously published or written by another person, except where due reference is made in the text of the thesis.

This thesis includes studies and figures from two original papers published in peer reviewed journals. The core theme of the thesis is nanostructures across oppositely charged surfactant–polymer interfaces. The ideas, development and authorship of all the papers in the thesis were the principal responsibility of myself, the candidate, working within the theme of Drug Delivery, Disposition and Dynamics at the Monash Institute of Pharmaceutical Sciences, under the supervision of Professor Ben J. Boyd.

The inclusion of co-authors in the published papers reflects the fact that this work came from active collaborations.

Signed:



Date: 15/01/2016

Publications

First Author

1. Tangso, K. J., Lindberg, S., Hartley, P. G., Knott, R., Spicer, P.T., Boyd, B. J., *Formation of Liquid Crystalline Structures in the Bile Salt–Chitosan System and Triggered Release from Lamellar Phase Bile Salt–Chitosan Capsules*. ACS Appl. Mater. Interfaces. 2015, 6, (15), 12565–12571.
2. Tangso, K. J., Patel, H., Lindberg, S., Hartley, P. G., Knott, R., Spicer, P.T., Boyd, B. J., *Controlling the Mesosstructure Formation within the Shell of Novel Cubic/Hexagonal Phase Cetyltrimethylammonium bromide–Poly(acrylamide–acrylic acid) Capsules for pH Stimulated Release*. ACS Appl. Mater. Interfaces. 2015, 7, (44), 24501–24509.
3. Tangso, K. J., C.D da Cunha, P.H., Spicer, P.T., Li, J., Boyd, B. J., *Antimicrobial Activity from Colistin/Heparin Lamellar Phase Complexes for Coating of Biomedical Devices*. Biomaterials Science. Submitted.

Communications

1. Tangso, K. J. *et al.*, *Probing the Interface Between Oppositely Charged Surfactant–Polymer Solutions for Complex Nanostructures Using Small Angle X-ray Scattering*, abstract in the 15th International Small-Angle Scattering Conference; Sydney; November 2012. Poster presentation.

2. Tangso, K. J. *et al.*, *Examining the Interface Between Oppositely Charged Chitosan and Bile Salt Solutions for Liquid Crystalline Nanostructures*, abstract in the Drug Delivery Australia meeting; Victoria; November 2012. Poster presentation.
3. Tangso, K. J. *et al.*, *Linking Nanostructure, Composition and Microrheology of Mesophases Formed Across Oppositely Charged Surfactant–Polymer Interfaces*, abstract in the 6th Biennial Australian Colloid and Interface Symposium; Queensland; February 2013. Poster presentation.
4. Tangso, K. J. *et al.*, *Nanostructures Across Oppositely Charged Surfactant–Polymer Interfaces as Tailored Release Nanomaterials*, abstract in the 50th Annual Meeting and Exposition of the Controlled Release Society; Honolulu; abstract in the 8th Pacific Rim International Congress on Advanced Materials and Processing; Waikoloa; July 2013. Poster presentations.
5. Tangso, K. J. *et al.*, *Nanostructures Across Oppositely Charged Surfactant–Polymer Interfaces as Tailored Release Nanomaterials*, abstract in the Drug Delivery Australia meeting; Sydney; November 2013. Oral presentation.
6. Tangso, K. J. *et al.*, *Triggered Release from Oppositely Charged Surfactant and Polymer Nanostructured Capsules*, abstract in the 5th FIP Pharmaceutical Sciences World Congress Melbourne; Victoria; April 2014; abstract in the Nanotechnology and Medicines for Tomorrow symposium; Victoria; November 2014. Poster presentations.
7. Tangso, K. J. *et al.*, *Nanostructures Across Oppositely Charged Surfactant–Polymer Interfaces*, abstract in the 7th Biennial Australian Colloid and Interface Symposium; Hobart; February 2015. Oral presentation.

List of Abbreviations

AES	alkyl ethoxysulphates
AFM	atomic force microscopy
AP	ammonium persulphate
A.U.	arbitrary units
A.U.C.	area under the curve
C ₁₂ E _x	ethylene glycol monododecyl ether
cac	critical aggregation concentration
cat-HEC	cationic hydroxyethylcellulose (commercial name: JR-400)
cmc	critical micellar concentration
CPLM	crossed-polarised light microscopy
CPP	critical packing parameter
cryo-SEM	cryogenic-scanning electron microscopy
cryo-TEM	cryogenic-transmission electron microscopy
CSIRO	Commonwealth Scientific and Industrial Research Organisation
CTAB	cetyltrimethylammonium bromide
CTAPA	cetyltrimethylammonium-polyacrylate complex salt
DAC	dodecylammonium chloride
DDAB	didecyldimethylammonium bromide
DLS	dynamic light scattering
DNA	deoxyribonucleic acid
DOPC	dioleoylphosphatidylcholine
DOPE	dioleoylphosphatidylethanolamine
DTA ₂ CO ₃	dodecyltrimethylammonium carbonate
DTAB	dodecyltrimethylammonium bromide
ELS	electrophoretic light scattering
EtOH	ethanol
FC ₇	sodium perfluorooctanoate
H ₁	normal hexagonal phase
H ₂	inverse hexagonal phase
HCl	hydrochloric acid
HCPS	hexagonal close-packed spheres
HD	n-hexadecane
HPLC	high performance liquid chromatography
I ₁	normal discrete cubic phases

I ₂	inverse discrete cubic phases
KOH	potassium hydroxide
L ₁	normal micelles
L ₂	inverse micelles
LC	liquid crystalline
L.P.	lattice parameter
L _α	lamellar phase
MEHQ	mono methyl ether of hydroquinone
MW	molecular weight
NaCl	sodium chloride
NaOH	sodium hydroxide
NaPA	sodium polyacrylate
Nd:YAG	neodymium-doped yttrium aluminium garnet
NMBA	N,N'-methylenebis(acrylamide)
P&G	Procter and Gamble
PA	polyacrylate
PAAm-AA	poly(acrylamide-acrylic acid)
PNIPAM	poly(N-isopropylacrylamide)
polyDADMAC	poly(diallyldimethylammonium chloride)
polyDADMADS	poly(diallyldimethylammonium-dodecyl sulphate)
RhB	Rhodamine B
SANS	small angle neutron scattering
SAXS	small angle X-ray scattering
S.D.	standard deviation
SDS	sodium dodecyl sulphate
SEM	scanning electron microscopy
STDC	sodium taurodeoxycholate hydrate
TEMED	N,N,N',N'-tetramethylethylenediamine
TFA	tetrafluoroacetic acid
UV	ultra violet
V ₁	normal bicontinuous cubic phase
V ₂	inverse bicontinuous cubic phase
WAXS	wide angle X-ray scattering
1D	one-dimensional
2D	two-dimensional
3D	three-dimensional

Chapter 1: *Introduction*

1. Introduction

1.1 Overview

Over the past few decades, oppositely charged surfactant and polymer systems have received great interest for their versatility in various pharmaceutical¹⁻⁶ and industrial⁷⁻¹² applications. The rate of mixing of surfactant and polymer solutions can be significantly influenced by the concentration, viscosity, the order of addition of each component, and the amount of energy introduced to the system.¹⁵⁻¹⁷ The slow equilibration kinetics experienced in such systems often leads to formation of kinetically trapped nonequilibrium structures.¹⁸⁻²² However, there is little understanding of how changes in structure and composition locally within the mixtures can give rise to equilibrium or nonequilibrium mesophases in oppositely charged surfactant and polymer systems.

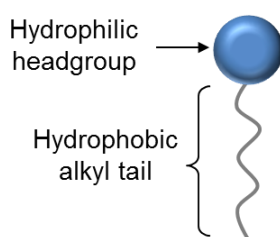
Research into the dynamics of structure formation at the interface between solutions of oppositely charged surfactant and polymer molecules has been scarce. Studying surfactant–polymer interfaces can provide an interesting means of probing changes in the distribution of surfactant, polymer, and water molecules with the formation of liquid crystalline structures over time as the system approaches equilibrium. Therefore, there is a great need for suitable techniques, or a methodology, that enables characterisation of the internal structure of mesophases, as well as quantification of the concentrations of surfactant, polymer, and water spatially across surfactant–polymer interfaces. The findings obtained can provide new insights into experimental parameters that lead to the existence of equilibrium and nonequilibrium nanostructures across oppositely charged surfactant–polymer interfaces, as well as in concentrated bulk aqueous mixtures and dilute dispersions.

This chapter gives a general background to the classification and function of surfactant and polymers individually, followed by an introduction to the significance of oppositely charged surfactant and polymer systems. Factors influencing the phase behaviour and structure formation in commonly studied industrially and biologically relevant systems are discussed, and their potential applications as drug delivery systems are addressed. In addition, parameters that may have important implications in studying the state of equilibrium in aqueous mixtures of surfactant and polymer are considered. Lastly, methods commonly employed that indirectly measure composition and structurally characterise mesophases formed in bulk surfactant and polymer mixtures are outlined and assessed for their applicability for examining the dynamics across surfactant–polymer interfaces.

1.2 Classification of Surfactants and Polymers

1.2.1 Surfactants

Surfactants are amphiphilic molecules that possess both hydrophobic and hydrophilic moieties (Schematic 1.1) and are often classified into four main types, namely: anionic (negatively charged), cationic (positively charged), zwitterionic (possess both positive and negative charges), and nonionic (uncharged) surfactants.



Schematic 1.1 Structure of a surfactant molecule.

Anionic surfactants, such as alkyl-, alkyl aryl- and ether- sulphates, carboxylates and sulphonates, are commonly used as detergents and dispersants in soaps, laundry powder, and personal care products (e.g. skin cleansers, shampoos, hand soaps, oral care products, and surgical scrubs).^{34, 35}

Cationic surfactants, such as quaternary ammonium salts, are often used as pharmaceutical preservatives³⁶, sewage flocculants,³⁷ softeners,^{38, 39} conditioners,⁴⁰ and disinfectants⁴¹ in formulations including mouth washes, sanitisers, antistatics, fabric softeners, and hair conditioners.

Nonionic surfactants, such as polysorbates and carboxylic- esters and amides, are generally used as emulgents,⁴² solubilisers,⁴³ and wetting agents.⁴⁴

Biosurfactants are often of microbial origin possessing antibacterial,⁴⁵ antifungal, and antiviral activity, and are frequently used in the removal of pollutants.⁴⁶ They are

biodegradable,⁴⁷ less toxic,⁴⁸ and effective at extreme temperatures⁴⁹ and pH values,⁵⁰ which make them advantageous in the treatment of certain diseases.⁵¹ Perhaps the most common classes of biological surfactants are phospholipids, which carry a zwitterionic charge and are the most abundant component of cellular membranes,⁵² and bile salts, which usually carry a negative charge and are the primary detergents in the gastrointestinal tract for solubilisation of fats.⁵³

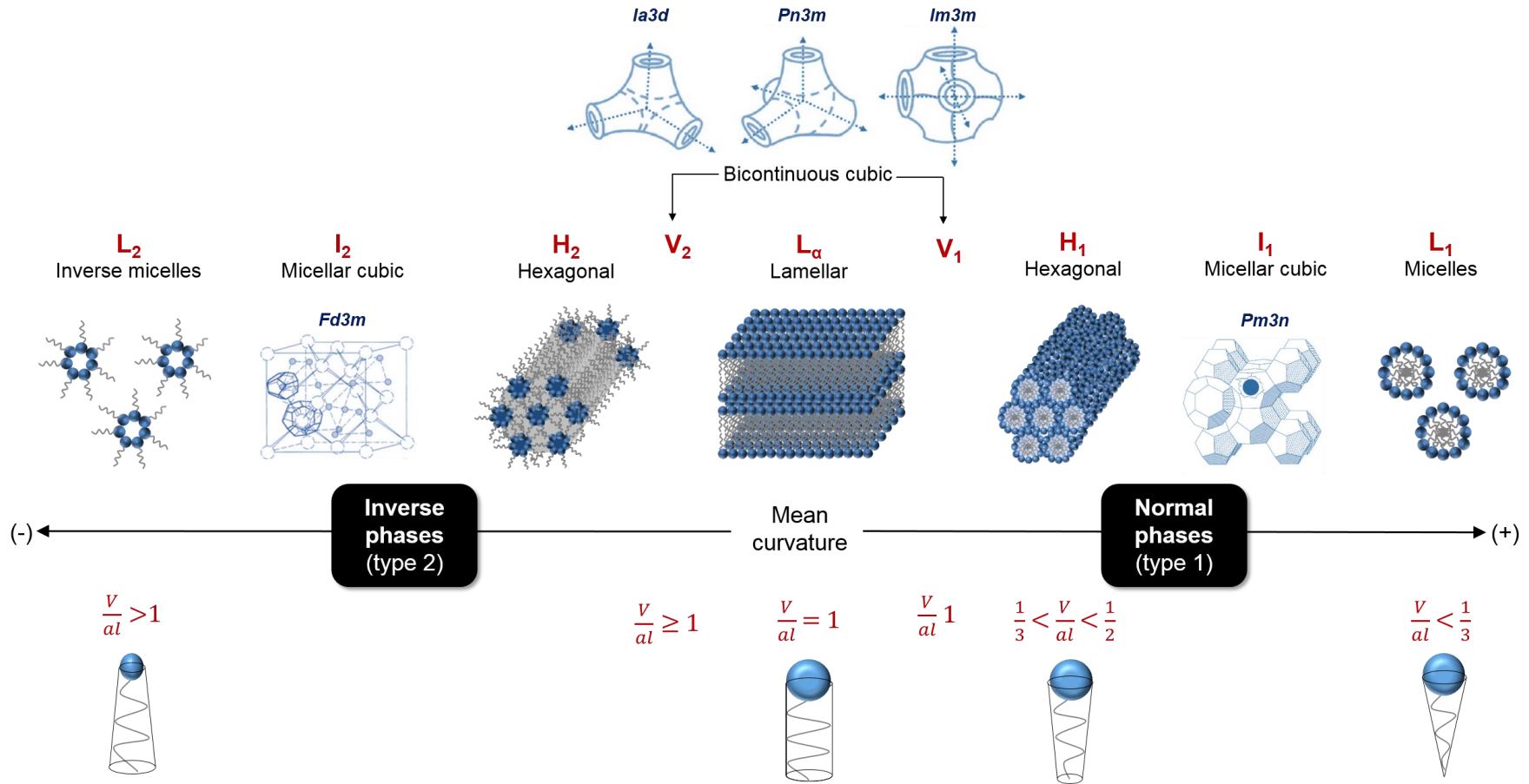
Above the critical micelle concentration (*cmc*), surfactants are able to self-assemble into aggregates, one type of which is known as micelles. At higher concentrations they can form more highly ordered thermodynamically stable liquid crystalline structures (often termed ‘mesophases’).^{23, 54-57} The geometric packing of the surfactant molecules in solution dictates the type of structure that is formed, which can be described by the critical packing parameter (CPP):⁵⁸

$$CPP = \frac{V}{al} \quad [1.1]$$

where , V , is the effective chain volume, a , is the area per surfactant molecule at the headgroup/chain interface, and l is the chain length of the molecule in its molten state.³¹

1.2.1.1 *Liquid Crystalline Structures*

Mesophases can be further categorised into two types of phases which are dependent upon their mean curvature (Schematic 1.2). For type 1 phases, also known as the normal mesophases, the hydrophilic–hydrophobic interface curves away from the water phase leading to ‘oil-in-water’ type structures. On the other hand, for type 2 phases, also called inverse mesophases, the polar–apolar interface curves towards the water phase resulting in ‘water-in-oil’ type structures.



Schematic 1.2 Common self-assembled structures illustrating the importance of the molecular packing geometry on the mesophase formed in excess water. Adapted from Holmberg *et al.*²³ Cubic structures reproduced from Hyde *et al.*,³¹ Kulkarni *et al.*,³² and Tresset *et al.*³³

Lamellar (L_{α}/L_{β}) phases are the most commonly encountered mesophases and are comprised of planar, parallel stacks of amphiphile bilayers forming a one-dimensional lattice. They are generally less viscous than hexagonal and bicontinuous cubic phases.³¹

The hexagonal (H_1/H_2) phase is highly viscous and consists of cylindrical micelles that are packed on a two-dimensional hexagonal lattice.³¹

Cubic phases can be further divided into two different types: discrete (I_1, I_2) and bicontinuous (V_1, V_2), both of which are very viscous. The first class can be defined as spherical micelle aggregates that are commonly faceted with cubic crystallographic space groups, namely $Pm3n$, $Fm3m$, $Fd3m$, and the less encountered hexagonally close-packed ($P6/mmc$) phase.³¹ Bicontinuous cubic phases are the most complex spatially organised liquid crystalline structures. They are portrayed as being ‘warped lamellar phases’ composed of a continuous lipid bilayer that is intertwined with a continuous network of aqueous channels, or vice versa, forming a three-dimensional symmetric cubic structure.³¹ Three types of bicontinuous cubic phases that have been observed experimentally include the gyroid ($Ia3d$), diamond ($Pn3m$), and primitive ($Im3m$) surface (Schematic 1.2).⁵⁹

Liquid crystalline phases have the ability to solubilise a range of therapeutics. It is also well known that the nanostructure controls the rate of drug release from these matrices, which make them applicable as drug delivery systems.^{60, 61}

1.2.2 Polymers

Polymers are macromolecules that have repeating structural units and are often classified as either homopolymers ($A-A-A-A = -A_n-$), copolymers ($A-B-A-B = -(AB)_n-$), random ($A-B-B-A$), or block copolymers ($A-A-A-A-B-B-B-B$). As with surfactants, polymers can also be categorised based on their charge.

Naturally occurring polymers such as proteins, nucleic acids, and polysaccharides comprise the building blocks that regulate biological processes and functioning within the human body.⁶² Their biocompatibility⁶³⁻⁶⁵ allows them to be implemented in a variety of biosensors, such as tactile sensors^{66, 67} for use in medical robotics and thermal sensors^{68, 69} as diagnostic tools. They are also employed in thermographic imaging and as probing devices to detect temperature changes in particular regions in the body during surgery.^{70, 71}

Polymers have also been applied to modify surface properties, such as wettability and adsorption,⁷²⁻⁷⁴ functionalisation of nanoparticle surfaces for targeted drug delivery, and promoting protein interaction by selecting the appropriate surface charge.⁷⁵⁻⁷⁸ They also play a role in regulating cell behaviour (adhesion, migration, and differentiation),⁷⁹⁻⁸¹ improving the biocompatibility of implants,⁸²⁻⁸⁴ and in the encapsulation of cargo into liposomes and subsequent release at the site of interest in response to a stimulus.⁸⁵⁻⁹⁰

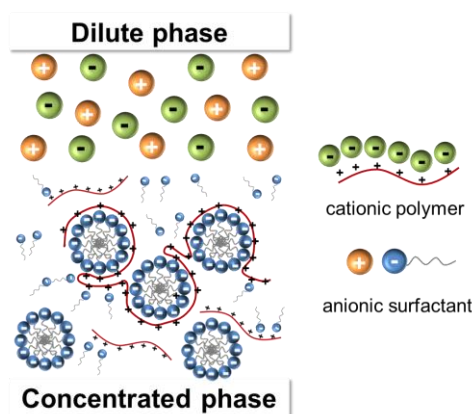
Ionic polymers are of particular interest as they are able to form electrostatic interactions with oppositely charged ionic species, which are inherently stronger than the van der Waals forces and hydrophobic interactions often present between nonionic structures. The layer-by-layer assembly of nanoparticles is a prominent example of a technique that takes advantage of the physicochemical properties of oppositely charged polyelectrolytes to engineer smart drug delivery systems.⁹¹⁻⁹⁹ Surfactants in their own right can self-assemble into ordered mesophases in aqueous media, but their inclusion into polymeric systems provides a larger library of chemical structures to select from, offering superior control over structure manipulation, which is advantageous in attaining the desired phase behaviour at different conditions. Furthermore, a diversity of hierarchical structures can arise in systems of oppositely charged surfactant and polymer that often do not form by layer-by-layer polyelectrolyte assembly.

1.3 Oppositely Charged Surfactant and Polymer Systems

It has been known for at least four decades that mesophases can arise in mixtures of oppositely charged surfactant and polymer systems.¹⁰⁰ As mentioned earlier, the mesophase formed depends on the packing geometry of the molecules,⁵⁸ therefore significant interest has been invested in the study of how various parameters can influence the primary interactions that govern the self-assembly of highly ordered structures. Contributions to literature have increasingly lead to a better understanding of how the structural attributes of these systems can be controlled and exploited in various industrial and biomedical applications, particularly as stimuli-responsive drug delivery systems.^{2, 5, 101-105}

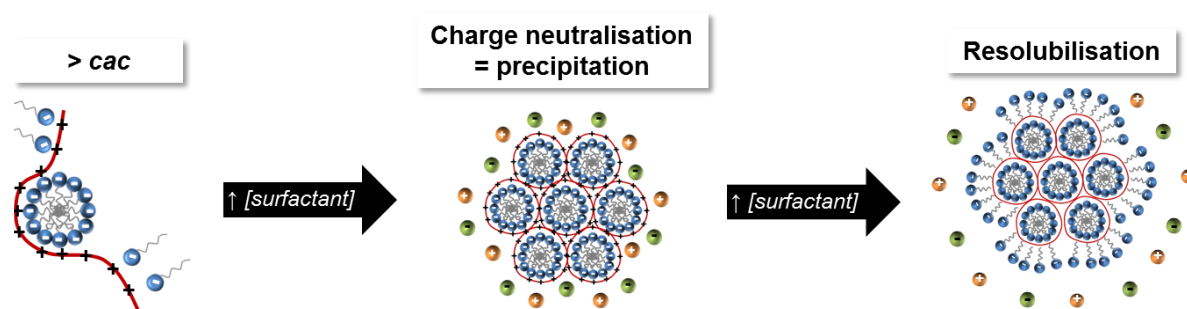
1.3.1 General Phase Behaviour

Interactions between molecules in solutions of oppositely charged surfactants and polymers often involve a cooperative binding process that frequently leads to an associative phase separation. This is where one phase is concentrated with the surfactant ion and polyion wherein a precipitate or liquid crystalline phase is often formed, while the dilute phase is comprised of the simple salts (Schematic 1.3). This phenomenon is sometimes referred to as coacervation, where the resulting complexes formed are known as coacervates.



Schematic 1.3 Associative phase separation.

The concentration at which the surfactant begins to bind polymer chains is known as the critical aggregation concentration (*cac*), which typically occurs more than 2–4 times lower than the critical micellar concentration due to the strong attractive forces between the opposing charges on the two species. It has been proposed that polymer chains wrap around surfactant aggregates forming a ‘pearl necklace’ structure.^{106, 107} Once the complex has reached stoichiometric charge neutralisation, precipitation often occurs as the complex loses its ‘charge’ and becomes hydrophobic. As the surfactant concentration is increased above the point at which the observed maximum precipitation occurs, at a certain polymer concentration the precipitate ‘dissolves’ and the system becomes dispersed once again. This can be explained by the adsorption of a second layer of surfactant, which transforms the aggregate into a soluble charged structure following charge inversion.^{108, 109} It should be noted that the redissolution of the coacervate is not universal and most likely time dependent. The three distinct zones that describe the general phase behaviour demonstrated by aqueous mixtures of an anionic surfactant and a cationic polymer upon increasing surfactant concentration are illustrated in Schematic 1.4.



Schematic 1.4 Typical phase behaviour of oppositely charged surfactant and polymer complexes upon increasing concentration of surfactant in solution.

Furthermore, the degree of binding of surfactant aggregates to the polymer and the resulting morphology of the colloidal particles has a direct correlation with the viscosity exhibited by the system at a given composition. Mukherjee *et al.* demonstrated changes in the viscosity of bulk aqueous mixtures of sodium dodecyl sulphate (SDS) and poly(diallyldimethylammonium chloride) (polyDADMAC) as a function of surfactant concentration relative to the measured viscosity of the SDS/water binary solution (Figure 1.1).³⁰ Upon addition of surfactant to a solution of polymer, the viscosity of the mixture decreased as the *cac* (C^*) is approached due to compaction of the polymer chain by neutralisation of its charges with the oppositely charged headgroup of the surfactant (Figure 1.1).³⁰ A significant increase in the viscosity is generally observed after the *cac* is exceeded, reaching a maximum at the concentration at which complete complexation of surfactant and polymer molecules has occurred, C_s (Figure 1.1).³⁰ The magnitude in which the viscosity increased depends on the expansion of the polymer chain by electrostatic repulsion among attached surfactant/polymer complexes or formation of aggregates in solution.³⁰ A further increase in the surfactant concentration (C_f) led to a decrease in the viscosity of the solution due to the solubilisation of the complexes by the excess surfactant molecules (Figure 1.1).³⁰

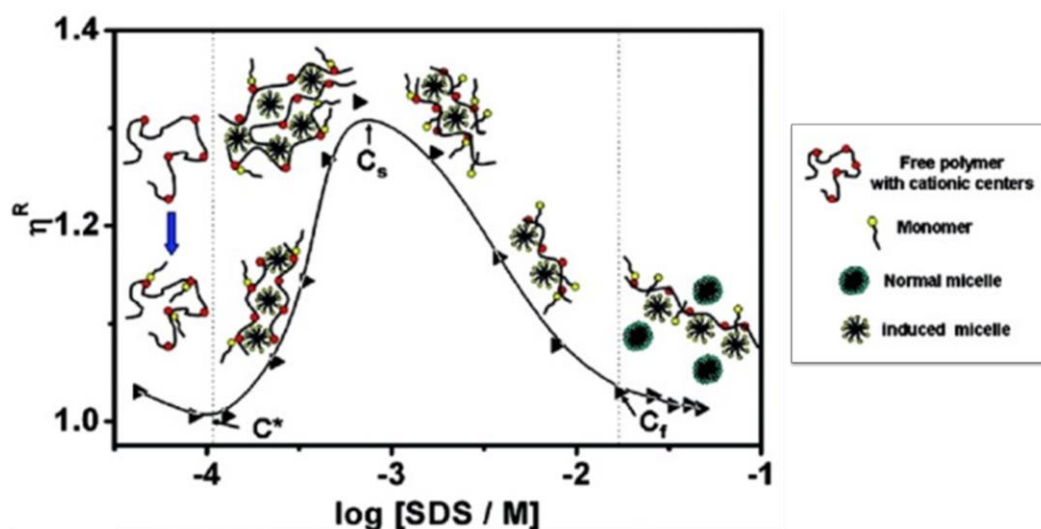


Figure 1.1 Effect of surfactant concentration on the interaction of 0.005 % (w/v) polyDADMAC with SDS in water, and subsequently on the relative viscosity (η^R) of the aqueous mixtures. Annotations- C^* : critical aggregation concentration, C_s : maximum concentration of SDS that led to coacervation, and C_f : SDS in excess which led to resolubilisation of the complexes. Reproduced from Mukherjee *et al.*³⁰

Data acquired through measurements of the viscosity,^{30, 110, 111} the strength of interactions between surfactant and polymer molecules, and the system composition by rheometry,^{30, 110, 111} isothermal calorimetry,¹¹²⁻¹¹⁶ or self-diffusion¹¹⁷⁻¹²¹ experiments may therefore be used to infer information on the other parameters stated. The relationship between structure, composition, rheology, and the interactions between surfactant and polymer molecules is therefore important in rationalising the equilibrium phase behaviour displayed by oppositely charged surfactant and polymer systems, a subject that will later be discussed in further detail. The phase behaviour described here is often exhibited in aqueous mixtures of various oppositely charged surfactant and polymer solutions (Schematic 1.4).^{108.}

1.3.2 Commonly Studied Systems

The most commonly studied oppositely charged surfactant and polymer systems are materials that are relevant to industrial or pharmaceutical applications (Table 1.1).

The physicochemical properties and phase behaviour displayed by systems comprised of the anionic surfactant, SDS, with either polyDADMAC^{30, 114, 126-137} or cationic hydroxyethylcellulose (cat-HEC, commercially known as JR-400),^{122, 124, 138-143} are of particular interest in the formulation of personal care and cleaning products. Knowledge of how the complexes will respond to exposure to different conditions, such as dilution, high or low temperatures, certain additives, or stress prior to or during application is valuable when considering the impact they have on, for example, the stability, aesthetics, feel, surface deposition,⁹ and flow behaviour of the product.

Similarly, diverse hierarchical structures are encountered when the antimicrobial cationic surfactant, cetyltrimethylammonium bromide (CTAB) is combined with counter charged polymers, including poly(acrylamide-acrylic acid),¹⁴⁴ carboxymethyl cellulose,¹⁴⁵ poly(sodium methacrylate-co-N-isopropylacrylamide),^{146, 147} sodium polyacrylate,¹⁴⁸⁻¹⁵⁰ and sodium poly(α ,L-glutamate),^{151, 152} rendering these systems amenable to a wide range of purposes (Table 1.1).

Lastly, the use of biomaterials is advantageous for application within the body, especially with the incorporation of therapeutics. Generally, these are biocompatible, biodegradable, and non-toxic, and are produced synthetically or often exist naturally in the body (Table 1.1). For example, DNA has been delivered with the cationic lipids,² surfactants,^{4, 153-156} or polymers,^{1, 157} as an approach to enhance transfection in gene therapy.

What makes these oppositely charged surfactant and polymer systems very interesting is the ability to control the structural attributes of the complexes formed.

Table 1.1 Factors that influence the mesophases formed in commonly studied oppositely charged surfactant and polymer systems.

Variable	Impact on the surfactant/polymer complexes	References
Surfactant-to-polymer molar charge ratio	Minimum viscosity and particle size displayed by complexes at low [surfactant] due to initial extension of polymer chains.	1, 4, 127, 131, 140, 145
	Formation of kinetically stable colloidal dispersions increases with increasing [surfactant].	156, 158, 159
	SAXS intensity and d-spacing of compact structures increases with increasing [surfactant].	1, 4, 128, 131, 145, 160
	Particle size of complexes increases with increasing [surfactant] as charge neutralisation is approached, leading to precipitation/phase separation.	1, 127, 140, 149, 161
	Maximum viscosity is achieved for complexes formed at charge equivalence.	162
	Particle size decreases when [surfactant] is in excess due to resolubilisation of complexes.	127, 138, 140, 162
Polymer structure	Use of polyelectrolytes with low charge density often forms less ordered structures.	163–165
	SAXS intensity and degree of order (lattice parameter) of complexes formed increases with increasing polymer charge density.	128, 166–168
	Viscosity of complexes formed is enhanced by increasing the polymer charge density, MW, or introducing cross-links within the polymer network.	163, 169–172
	High loading capacity is observed by complexes comprised of a high charge density polymer.	105
	Flexible polymers tend to produce more compact complexes.	167, 168
Surfactant structure	Structure of surfactant significantly influences the type of LC structure formed.	164, 173
	Degree of order of LC structures formed increases with increasing alkyl chain length.	13, 126, 145, 151, 152, 174
	L.P. and melting temperature of LC structures formed, as well as the size of the two-phase region in ternary phase diagrams increases with increasing surfactant chain length.	126, 129, 130, 175

Abbreviations: SAXS (small angle X-ray scattering), L.P. (lattice parameter), MW (molecular weight), LC (liquid crystalline).

Variable	Impact on the surfactant/polymer complexes	References
Temperature	Lattice parameter of lamellar phase often decreases with increasing temperature due to changes in the thickness of the bilayer structure.	176, 177
	Lamellar to hexagonal phase transition results from the release of counterions upon an increase in temperature in systems comprised of DNA, DTAB, and DOPE.	4, 153
	Reversible <i>Ia3d</i> to <i>Im3m</i> cubic phase transition in mixtures of the complex salt of CTAB and PAA (CTAPA) with C ₁₂ E ₅ as the temperature decreases from 25 °C to 15 °C.	178
Salt concentration	Addition of high [salt] often decreases the kinetic stability of nanoparticles due to the ‘screening effect’ of the electrostatic attraction between oppositely charged molecules.	5, 15, 19, 21, 22, 109, 156, 158, 159, 179-182
	Addition of low to moderate [salt] often increases the electrostatic interactions between the oppositely charged species and facilitates the self-assembly of ordered structures.	15, 127, 181-183
Solution pH	pH influences the degree of ionisation of acidic or basic functional groups on the polymer chains, and the subsequent formation of structured complexes.	158, 184-186
	Alginate-reinforced oligochitosan complexes provide sustained release in acidic environments and simulated gastrointestinal fluids.	187

Abbreviations: DNA (deoxyribonucleic acid), DTAB (dodecyltrimethylammonium bromide), DOPE (dioleoylphosphatidyl ethanolamine), CTAB (hexadecyltrimethylammonium bromide), PAA (poly(acrylic acid)), CTAPA (cetyltrimethylammonium-polyacrylate complex salt), C₁₂E₅ (penta(ethylene glycol) monododecyl ether).

1.3.3 Parameters that Influence the Formation of Nanostructured Complexes

It is well established that the electrostatic and hydrophobic interactions that arise between oppositely charged surfactant and polymer molecules and the entropic gain experienced by the system from the subsequent release of counterions into the bulk solution both play an important role in driving the self-assembly of mesophases in such systems.^{144, 153, 164, 188, 189} The interplay between the charged species will in turn impact the geometric packing of the molecules that dictates the resulting liquid crystalline structure. Therefore, rational design of such outcomes would be of great value when engineering tunable structured nanomaterials.

1.3.3.1 Surfactant-to-Polymer Molar Charge Ratio

The surfactant-to-polymer molar charge ratio is a significant parameter that must be considered during the development of formulations (Table 1.1). The phase behaviour exhibited by these systems is a reflection of the physical changes that transpire upon varying the concentration of molecules present in the mixture. The system composition is indicative of the initial number of molecules available to form interactions with each other, however it does not necessarily mean that all molecules will participate in the self-assembly of mesophases. This often results in phase separation and may also lead to the existence of kinetically trapped nonequilibrium structures.^{109, 190} This problem may be exacerbated when the inherent viscosity of the surfactant and/or polymer solution limits the ability of charged species to form new associations with unbound or pre-existing structures in the mixture by slowing diffusive transport by the same factor as the increase in viscosity.^{17, 25} Therefore, the strength of the interactions formed at a given surfactant-to-polymer molar charge ratio will

dictate the structure and rheology of the coacervates, and the subsequent phase behaviour demonstrated upon changes in the composition of the system.¹¹²⁻¹¹⁶

1.3.3.2 Polymer Structure

The charge density of the polyelectrolyte is another parameter that influences the electrostatic interactions between oppositely charged surfactants and polymers (Table 1.1). It refers to how closely or widely the charged monomer units are distributed along the polymer backbone. Use of polymers with low charge density often results in complexes that are loosely associated, thus producing low viscosity solutions.¹⁹¹ On the other hand, a high charge density polymer enhances the electrostatic attraction between charged surfactant molecules or micellar aggregates, and the formation of highly ordered complexes.^{146, 147, 192, 193} This in turn produces complexes that are more compact, stable, and resistant to changes in environmental conditions.^{158, 159}

In addition, the molecular weight, flexibility, and degree of cross-linking of the polymer also affects the size of complexes formed and the viscosity of the oppositely charged surfactant and polymer system.^{163, 167-172}

1.3.3.3 Surfactant Structure

The chemical structure of the surfactant is also important in achieving the desired nanostructure within surfactant and polymer systems, where the hydrophilic-lipophilic balance associated with the surfactant dictates the strength of interactions formed (Table 1.1).¹⁴ The effect of the surfactant electrostatic charge, hydrophobicity, and the size of its headgroup on the strength of interactions between surfactant and polymer molecules was emphasised with the use of a nonionic polymer, poly(N-isopropyl acrylamide) (PNIPAM). Loh *et al.* demonstrated through measuring changes in enthalpy, the onset on binding of the

surfactants, which is often an exothermic process, with PNIPAM was greatest between an anionic surfactant, sodium dodecyl sulphate (SDS), followed by the cationic surfactants cetyltrimethylammonium bromide (CTAB), dodecylammonium chloride (DAC), then dodecyltrimethylammonium bromide (DTAB).¹⁹⁴ The differences Loh *et al.* found between the enthalpic behaviour demonstrated by the various systems with increasing surfactant concentration could be explained by the following reasons. Firstly, it is known that anionic surfactants interact more strongly with nonionic polymers than do cationic surfactants.¹⁹⁵ Secondly, a surfactant with a longer chain length (CTAB vs. DTAB) has a much greater hydrophobic effect, resulting in an increase in entropy due to expulsion of water molecules into the bulk solution, which favours micellisation and subsequent adsorption onto the surface of the polymer structure. Lastly, the size of the headgroup dictates the degree of repulsion between like charges. Therefore, a smaller headgroup would again favour association of surfactant molecules into micelles more readily than surfactants with a larger headgroup (DAC vs. DTAB), which the polymer can wrap around to form the typical ‘pearl-necklace’ structure.^{106, 107} In summary, the degree of dehydration experienced by the polymer and the strength of interactions and arrangement between surfactant and polymer molecules can dictate the type, size, and stability of colloidal structures formed (Table 1.1).

1.3.3.4 Temperature

The influence of temperature on the equilibrium phase behaviour of liquid crystalline systems has widely been studied as a means to indirectly attain information on the nature of interactions that dominate in the formation of mesophases. Typically, these are hydrophobic or hydrogen bonding forces. Depending on the strength of these interactions, the heat applied

to the material may enhance the mobility of the molecules within the structured matrix, which most often stimulates a phase transition (Table 1.1).^{61, 196}

1.3.3.5 Salt Concentration

The formation of highly ordered structures in aqueous mixtures of surfactant and polymer is primarily a consequence of the gain in entropy from the release of counterions into the bulk solution as simple salts.^{149, 153, 188} Further addition of salt is known to significantly influence the electrostatic interactions between charged ions which depend on the concentration and chemical structure¹⁵ of the salt added (Table 1.1). Addition of low salt concentrations introduces a screening effect, which often leads to a considerable drop in the density of packing within the nanostructures. This has been shown to enhance the molecular mobility of surfactant/polymer complexes and the self-ordering process.^{15, 182} Conversely, addition of intermediate to high concentrations of salt have resulted in the partial or complete dissociation of the complexes due to the more complete screening effect of salt that intrinsically lowers the electrostatic association between charged species.^{179, 180}

1.3.3.6 Solution pH

Many drug delivery systems have been rendered responsive to pH by employing materials that carry an ionisable functional group.¹⁹⁷⁻²⁰⁰ Changes in the ionisation state of an acidic or basic moiety, particularly for oppositely charged surfactant and polymer systems, is the key determinant dictating the charge density of the polyelectrolyte (Table 1.1), which has considerable influence over the electrostatic interactions involved in the self-assembly of nanostructured complexes.^{185, 189}

Various parameters have been demonstrated to significantly influence the nanostructure, size, stability, flow properties, and phase behaviour of colloidal complexes formed in oppositely charged surfactant and polymer systems. However, limited research has addressed the important factors that should be considered when assessing whether equilibrium structures are truly formed in such systems and what causes the formation of kinetically trapped nonequilibrium structures.

1.4 Practical Considerations for Studying the Equilibrium Behaviour of Oppositely Charged Surfactant and Polymer Systems

Oppositely charged surfactant and polymer systems have been extensively studied as either dispersions or bulk mixtures, but much less at solution interfaces. Here, different strategies and experimental parameters that are influential to the equilibrium phase behaviour displayed by these systems are explored. Insight into physicochemical changes that are likely to affect the rate of mixing and the existence of equilibrium or nonequilibrium structures in dispersions and bulk aqueous mixtures, such as mesophase formation, solution viscosity, and the diffusivity of surfactant and polymer molecules within the system, will guide the development of hypotheses regarding the dynamics across surfactant–polymer interfaces.

1.4.1 Method of Preparation

Recent studies have brought to light the impact of how selecting different routes of sample preparation can lead to aqueous mixtures of surfactant and polymer with the same

composition and internal structure, however possessing entirely different morphology, rheology, or other surface properties.^{131, 162, 201}

It has been demonstrated that the mixing protocol or blending method has a significant effect on the resulting particle size and the occurrence of precipitation. The two main methods of mixing reported in literature are either slow/gentle mixing or stop-flow mixing.^{20-22, 109} Slow/gentle mixing involves adding a solution of one component dropwise to an equal volume of the other solution after which the sample is slowly inverted. Whereas stop-flow mixing often employs an apparatus that mixes equal volumes of both solutions within 10 milliseconds and is designed to monitor the kinetics of chemical reactions and/or coagulation of colloidal particles. This approach is said to provide gentler mixing rather than vigorous mixing exhibited by a stirrer bar. Generally, transparent mixtures are observed in samples prepared by stop-flow mixing that are on average smaller in particle size.¹⁰⁹ Conversely, larger complexes are formed by gentle mixing and have a greater tendency to precipitate and appear extremely turbid at high surfactant concentrations. From a formulation perspective, a clear objective would be to discover a means of avoiding phase separation. This may be achieved by producing a colloidal dispersion where the particles are trapped in a charged-stabilised nonequilibrium state. Pojják *et al.* described through the application of rapid mixing of both components, charged surfactant molecules can adsorb onto the surface of complexes sufficiently rapidly before any precipitate can form.¹⁹ Contrary to their findings, it has been thought that the nonequilibrium nature of structures formed in oppositely charged surfactant and polymer systems would depend highly on whether or not the system displays redissolution or which side of charge neutrality it exists, rather than the speed of mixing.

The order of addition of oppositely charged solutions, whether it is surfactant to polymer or polymer to surfactant, may also influence the state of equilibrium of structures

formed in such mixtures. The outcomes would depend on the concentration of each solution and their apparent viscosities, and how much time is allowed for the polymer and surfactant molecules to evenly distribute within the mixture.²¹

1.4.2 Rheology of Surfactant/Polymer Complexes

The rheology of surfactant/polymer complexes greatly depends on the concentration of each component, the strength of interactions between surfactant and polymer molecules, as well as their morphology. Self-diffusion measurements by nuclear magnetic resonance or time-resolved fluorescence have demonstrated that the diffusion of polymer or surfactant-bound polymer is much slower than solutions comprised of free micelles,^{13, 119, 181} and that the rate of diffusion of surfactant is significantly slower within the core of cross-linked polymer gel networks.¹¹⁸ More notable than the effect of concentration on the diffusivity of molecules within solutions or gels is the type of mesophase formed. Mezzenga *et al.* showed that monoglyceride lipids formed temperature-dependent viscoelastic *Pn3m* and *Ia3d* bicontinuous cubic phases that exhibited longer relaxation times than hexagonal phases (Figure 1.2).²⁴ Therefore, the formation of mesophases in oppositely charged surfactant and polymer systems could introduce a highly viscous barrier through which existing molecules must diffuse in order to reach equilibrium.

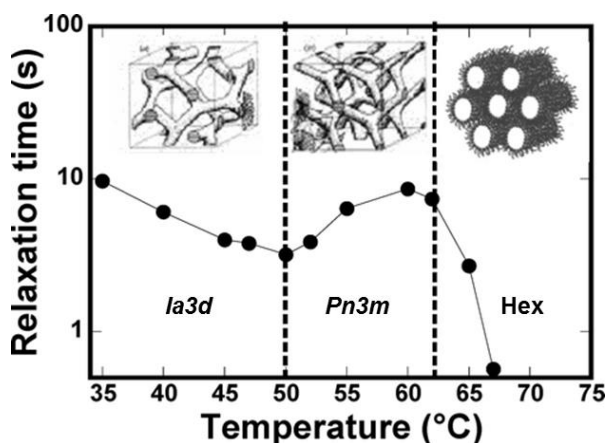
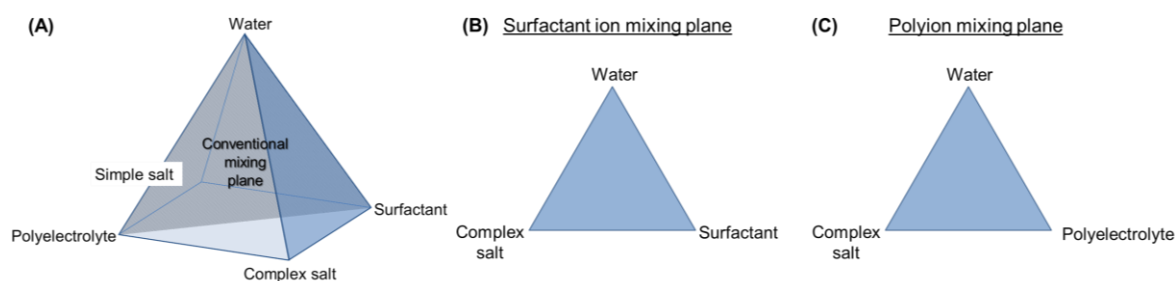


Figure 1.2 A comparison of viscoelastic properties of temperature-dependent mesophases formed in monoglyceride/water systems. Reproduced from Mezzenga *et al.*²⁴

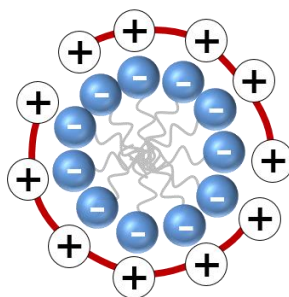
1.4.3 Exploitation of the Complex Salt

Oppositely charged surfactant and polymer systems are comprised of four components. The surfactant is comprised of the surfactant ion and its counterion, while the polyelectrolyte is comprised of the polyion and its counterion. Hence, these systems can only be fully described by a three-dimensional phase diagram, such as the pyramid phase diagram proposed by Svensson *et al.* (Schematic 1.5-A).^{26, 27, 141, 149, 150}



Schematic 1.5 Illustration of the three-dimensional phase diagram (A) developed to study a truly ternary system within the surfactant ion (B) or the polyion (C) mixing plane which encompasses the complex salt. Adapted from Svensson *et al.*²⁷

A relatively new approach to better understand the phase behaviour of such systems involves inclusion of the ‘complex salt’ (Schematic 1.6).^{26, 27, 148, 202-206}



Schematic 1.6 Illustration of an oppositely charged surfactant/polymer complex salt which is comprised of a single surfactant ion per polyion charge and the absence of other ions. Adapted from Svensson *et al.*²⁶

The complex salt is the precipitate that is formed from the reaction between the polyion and surfactant ion which is most often stoichiometric,¹⁴⁴ but sometimes can be nonstoichiometric.^{163, 183} This can be achieved in one of two ways. The most common method involves titration of the hydroxide form of the surfactant with the acid form of the polymer or vice versa. Alternatively, a solution of surfactant (in excess) is reacted with a limiting concentration of polymer and washed with copious amounts of water to remove excess surfactant. In both procedures, the precipitate formed is further diluted with water to ensure complete removal of any uncomplexed molecules, collected and freeze-dried. An elemental analysis of the specimen is then conducted to confirm its molar charge ratio.

Employing the complex salt, where the same counterions are present, eliminates the production of simple salts and provides a true three-component system for investigation (Schematic 1.5). There is the assumption that the liquid crystalline structure that exists when the complex salt is present is at 'equilibrium', and therefore acts as a point of reference. This offers a more strategic route to studying how the equilibrium nanostructures deviate from the complex salt formed upon dilution and/or addition of respective surfactant or polymer. An extensive review of various oppositely charged surfactant and polymer systems explored by this methodology has been detailed by Piculell *et al.*^{207, 208} Briefly, as with surfactant/polymer complexes investigated in the conventional manner, formation of highly ordered structures is often suppressed when polyions with low charge density are used.²⁰⁹ Interestingly, incorporation of a nonionic surfactant, ethylene glycol monododecyl ether ($C_{12}E_x$) into a system comprised of the cetyltrimethylammonium–polyacrylate (CTAPA) complex salt described the first occurrence of a bicontinuous cubic phase at certain surfactant concentrations.¹⁷⁸ Addition of the nonionic surfactant improved the stability of the complexes formed and a reversible phase transition between *Ia3d* and *Im3m* cubic phases was induced

by switching the temperature between 25 °C and 15 °C, respectively.²¹⁰ A similar effect was also demonstrated by complex salts prepared with hexadecyltrimethylammonium hydroxide and the random copolymers poly(methacrylic acid-*co*-methacrylate ethoxylated).²¹¹

It has been established that the exploitation of the complex salt can yield attractive properties in these oppositely charged surfactant and polymer systems. However, it would be inconvenient in real life applications to add the complex salt as a discrete component. It is unknown whether or not the complex salt is formed *in situ*. Perhaps formation of the complex salt upon contact between oppositely charged solutions of surfactant and polymer can eliminate phase separation from occurring and produce kinetically stable liquid crystalline structures.

Examination of liquid–liquid interfaces can offer a means of enhancing understanding the equilibrium behaviour of oppositely charged surfactant and polymer systems. Therefore, methods that enable acquisition of spatially resolved information on structure and composition across surfactant–polymer interfaces are required.

1.5 Techniques Commonly Employed to Characterise Mesophase Formation and Probe Molecular Interactions in Surfactant and Polymer Systems

Various techniques have been utilised to characterise the liquid crystalline structures formed and to study the interactions between oppositely charged surfactant and polymer molecules in bulk aqueous mixtures. The feasibility of these approaches to probe changes in structure and composition across surfactant–polymer interfaces are assessed (Table 1.2).

Table 1.2 An assessment of the techniques commonly used to characterise structures formed in bulk aqueous mixtures of surfactant and polymer for their applicability in studying surfactant–polymer interfaces. Abbreviations in the table are defined in the coming text.

Technique	Advantages	Disadvantages
CPLM	Can visualise the formation of mesophases through changes in optical properties of the material. Suitable for the study of interfaces.	Transmission of light through opaque or thick samples may be affected.
Cryo-SEM/ Cryo-TEM	Can image the morphology and internal structure of complexes formed.	Preparation of samples is a lengthy process.
AFM	Analysis of surface properties and particle size.	Slow scan time which can cause thermal drift of sample.
Confocal microscopy	Can view cross-sections of the sample in the z-direction. Can image the internal and external morphology of gel particles. Suitable for the study of interfaces, however on a three-dimensional scale.	Charged fluorescent dye may interfere with the interactions normally arising between oppositely charged surfactant and polymer molecules in the absence of the probe.
DLS ELS	Measures the particle size distribution and surface charge of particles, respectively.	Assumes that all particles are spherical in shape. Only suitable for dispersions.
SAXS/WAXS	Synchrotron X-ray source enables acquisition of spatially and temporally resolved information on the internal structure of mesophases and provides an adaptable sample working environment suitable for the study of interfaces.	Low signal-to-noise ratio detection from bench-top instruments result in weakly resolved scattering.
SANS	Contrast variation allows conclusions to be drawn on the composition and arrangement of molecules in liquid crystalline structures.	Very limited access. Large amount of sample required. Low fluxes prohibit kinetic studies.

1.5.1 Microscopic Techniques

1.5.1.1 Crossed-Polarised Light Microscopy

Crossed-polarised light microscopy (CPLM) is a technique commonly used to identify liquid crystalline phases formed in bulk samples. Polarisers are optical filters that pass light of particular polarisation and blocks out others. When two polarisers overlap in a parallel orientation, light is able to pass through. However, when the overlying polarisers are crossed perpendicularly, light is blocked. Structures that rotate the polarised light will allow the vertically polarised light to be viewed through the horizontal filter, whereas non-rotated light is completely blocked. Cubic and micellar phases appear dark under crossed-polarised light as they are isotropic and do not rotate light. In contrast, the anisotropic structure of hexagonal and lamellar phases rotates the polarisation of light, which is then able to pass through the second polariser and be observed with characteristic textures that are birefringent.²¹² Hexagonal phases usually appear smoke-like or fan-like.²¹³ While lamellar phases most often display streaky mosaic-like patterns, 'Maltese crosses', or are occasionally exhibited as spirals.

In addition, CPLM has also been used to visualise the penetration of aqueous solvent into lipids or surfactants.^{28, 214} The viscosity of isotropic mesophases formed and/or the appearance of textured birefringence are often indicative of the structures present at the phase boundaries formed upon initial contact between water and solid material, and the subsequent diffusion of the solvent into the other component (Figure 1.3).

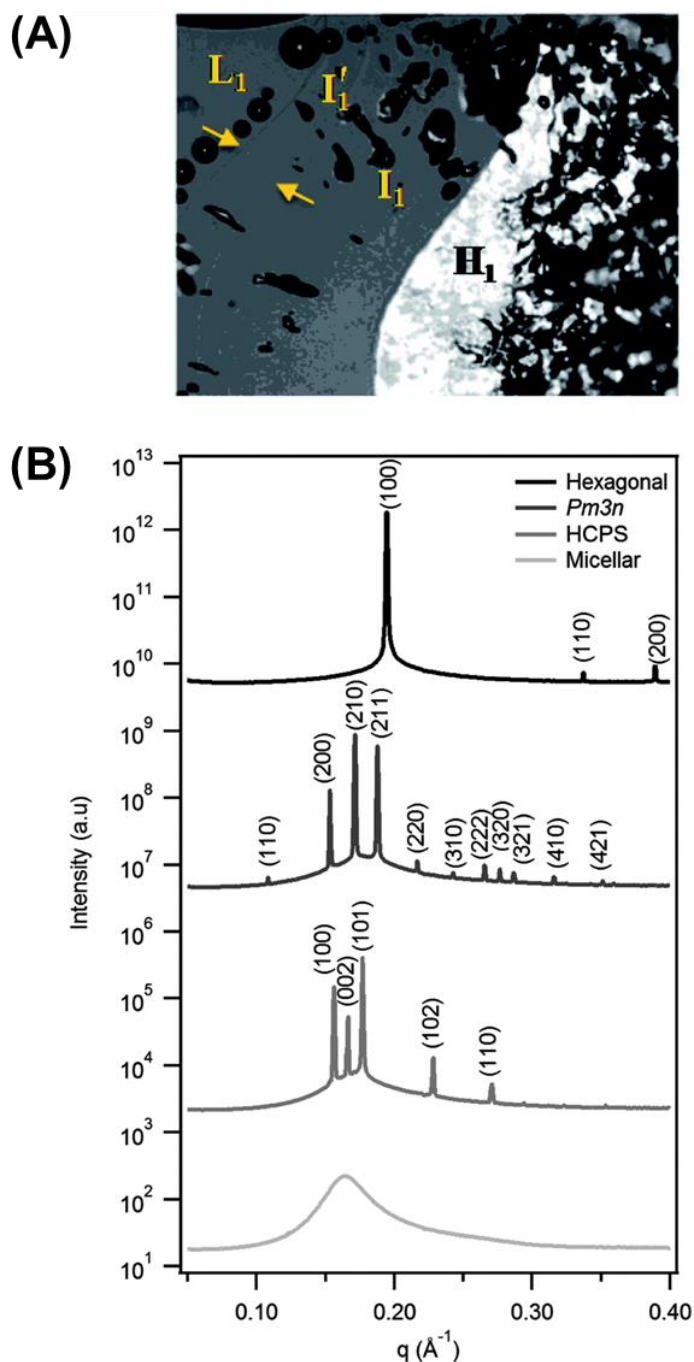


Figure 1.3 CPLM images (A) and corresponding synchrotron SAXS diffraction patterns (B) showing the phase sequence for DTA_2CO_3 in a concentration gradient scan. SAXS patterns show increasing concentrations from bottom to top. The phases and symmetry/space group are identified as micelles (L_1), I_1 HCPS ($F6_3/mmc$), I_1 cubic ($Pm\bar{3}n$), and H_1 hexagonal ($p6m$) phases. Curves are offset for clarity. Reproduced from Liu *et al.*²⁸

1.5.1.2 Scanning Electron Microscopy

Scanning electron microscopy (SEM) involves focussing a beam of electrons onto the sample of interest to gain information on the external morphology (texture) and orientation of materials in the form of highly resolved three-dimensional images. In addition, semi-quantitative information, such as the chemical composition, can sometimes be attained (Table 1.2). This technique is only viable for examination of solid state materials that are stable under vacuum and its use is limited to the size of the solids. To prevent charging of the specimen from exposure to electron irradiation during imaging and increase the signal-to-noise ratio, a thin layer of electrically conducting material is usually deposited onto the sample. This approach is known as ‘sputter coating’ which typically uses gold or palladium. On the other hand, dispersions may be plunged into liquid nitrogen to produce frozen samples suitable for analysis with cryo-SEM (Table 1.2).¹²¹

1.5.1.3 Cryogenic-Transmission Electron Microscopy

While SEM provides information primarily on surface morphology of materials, cryogenic-transmission electron microscopy (cryo-TEM) generates images that provide information on the morphology of particles and internal structure of soft matter (Table 1.2). Samples are rapidly vitrified under liquid nitrogen to preserve the specimen in a snapshot of its solution state with minimal artefacts and hence it is commonly employed to confirm mesophases that remain unidentified after investigation by X-ray or neutron scattering techniques. Nizri *et al.* revealed an evolution of mesophases formed as the surfactant-to-polymer molar charge ratio in dispersions comprised of cetyltrimethylammonium bromide (CTAB) and sodium polyacrylate (NaPA) with cryo-TEM (Figure 1.4).¹³

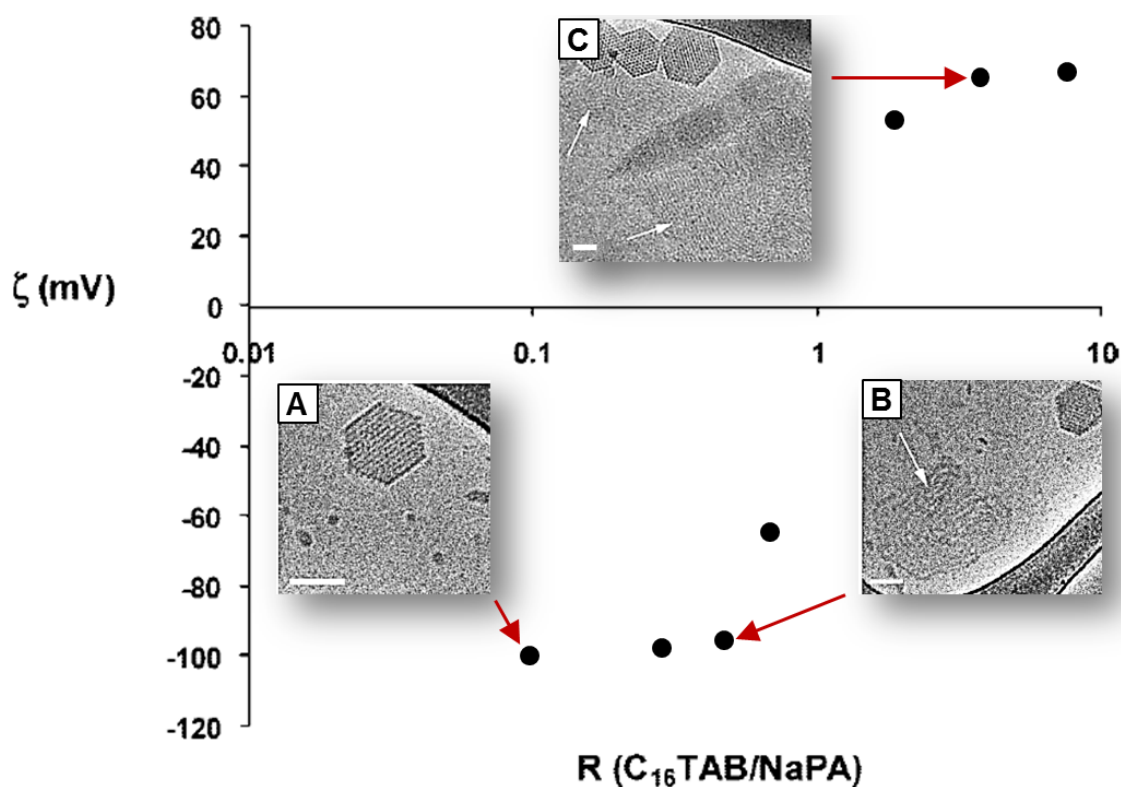


Figure 1.4 Effect of the surfactant-to-polymer molar charge ratio (R) on the zeta potential (ζ) and internal structure of C_{16} TAB/NaPA complexes measured by electrophoretic light scattering and cryo-TEM, respectively. Appearance of highly ordered hexagonal structures (A), thread-like micelles (B), and ‘fingerprint’ patterns as highlighted by the white arrows (C). Scale bars = 50 nm. Adapted from Nizri *et al.*^{13, 14}

1.5.1.4 Atomic Force Microscopy

Atomic force microscopy (AFM) operates by measuring the force between the scanning probe and the sample. The solution of interest is deposited onto the surface of a mica disk and the vertical and lateral deflection of the cantilever is measured by the optical lever, which reflects the laser beam off the cantilever to be detected. Information on the size, morphology, or hardness of surfaces can be obtained.^{12, 215} However, AFM is not suitable for examining solution interfaces as analysis of samples in solid form is more ideal (Table 1.2).

Although these microscopic techniques provide great detail on structure, a major limitation is their inability to deliver a global representation of the sample as usually only a small portion of the sample size is captured (Table 1.2).

1.5.1.5 Confocal Microscopy

Confocal microscopy is another optical technique that has been used to visualise the internal and external structure of surfactant/polymer complexes. This is one of only a few methods that has been employed to probe the structural attributes at surfactant–polymer interfaces (Table 1.2). Specifically, these interfaces were created between droplets of polymer solution that were surrounded by a solution of oppositely charged surfactant.^{17, 216, 217}

Lapitsky *et al.* demonstrated the formation of bead-like gel particles, where the kinetics of gelation and release of solvent was viewed under a confocal microscope whilst loaded in a flow chamber designed for these experiments.²¹⁸ The morphology of the gel particles depended on the concentration of the surfactant and polymer in solution (Figure 1.5), as well as the droplet size delivered and its rate of addition.²⁹

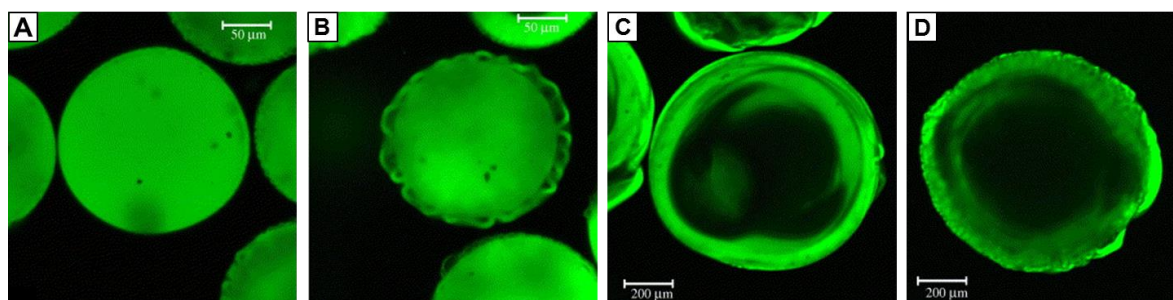


Figure 1.5 Confocal microscopy images of JR-400/CTAB/FC₇ gel particles prepared at varying compositions with a 0.11 mm needle. Smooth solid gel particle (A), gel particle with a flower-like corona layer (B), smooth hollow particle with dense thin gel shell (C), and gel particle with a gel corona (D). Reproduced from Lapitsky *et al.*²⁹

Closer examination of the fluorescently labelled gel particles revealed that the structure formed at the surfactant–polymer interface was comprised of three layers: a dense shell, a sparse and porous interstitial layer, and a homogeneous core (Figure 1.6).²⁵

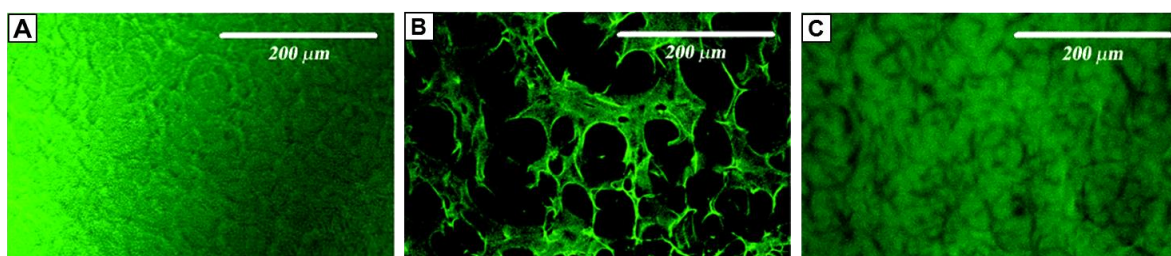


Figure 1.6 Fluorescent confocal micrographs showing cross-sections of the outer layer (A), the interstitial layer (B), and the core (C) of a sparsely cross-linked JR-400 gel particle (4–5 mm in diameter) following a 2 min reaction. Reproduced from Lapitsky *et al.*²⁵

Furthermore, utilisation of optical tweezers by incorporation of tracer particles was able to probe the transport of polymer, surfactant, and water molecules between the continuous phase (surfactant solution) and the gel particles. This also provided information on the microrheology of the structures,²⁵ which gives an indication of the existing mesophase.²¹⁹

While both these techniques show promise for gaining a better appreciation of the equilibrium phase behaviour across oppositely charged surfactant and polymer interfaces, they also have limitations (Table 1.2). Interestingly, the globular three-dimensional shape of the gel particles offer a different perspective on the growth of structures across the interfaces formed. However for simplicity, it would be ideal to study the formation of nanostructures and distribution of molecules across planar surfactant–polymer interfaces.

1.5.2 Scattering Techniques

Unlike microscopic approaches utilised to observe the structural features of oppositely charged surfactant and polymer systems, scattering techniques offer a more statistically representative characterisation of the sample.

1.5.2.1 *Dynamic Light Scattering*

Dynamic light scattering (DLS) indirectly measures the size of particles based on the Brownian diffusion experienced by the solutes in solution, as given by the Stokes–Einstein equation:

$$H_R = \frac{k_B T}{6\pi\eta D} \quad [1.2]$$

where H_R is the hydrodynamic radius, k_B is the Boltzmann constant, T is the absolute temperature, η is the solvent viscosity, and D is the diffusion coefficient. The Stokes–Einstein law for diffusion in solutions is only valid for measurement of spherical particles. Therefore, a different treatment is required to analyse the particle size of non-spherical molecules which considers both the rotational and translational diffusion coefficients.^{220, 221} Data is normally plotted as a size distribution and the correlation function for a given sample is often provided for each measurement to statistically support that the behaviour of the nanoparticles is not a random event. DLS has been commonly used to study how changes in the surfactant-to-polymer molar charge ratio influences the size of the complexes formed in dispersions and bulk aqueous mixtures of surfactant and polymer.^{1, 127, 185}

1.5.2.2 *Electrophoretic Light Scattering*

Electrophoretic light scattering (ELS) is based on dynamic light scattering, however it applies an oscillating electric field that causes movement of charged particles. This method

allows measurement of the electrophoretic mobility and calculation of the zeta potential of dispersed particles. The velocity at which the particles move is translated into the zeta potential, which also describes the magnitude of the electrostatic forces the charged particles experience, whether it is repulsive or attractive. Study of this parameter as well as size measurements provide useful information pertaining to the colloidal stability of dispersions; knowledge that would be valuable in the optimisation of formulations, particularly in prolonging their shelf-life.

Over the years, ELS has become a fundamental means of examining the surface charge of surfactant and polymer complexes. Nizri *et al.* demonstrated that at low surfactant-to-polymer molar charge ratios, the nanoparticles carried a negative charge owing to the presence of the anionic polymer, NaPA, in excess. The repulsive forces between the negatively charged complexes decreased as the system approached charge neutrality. Above this composition, the concentration of the cationic surfactant, CTAB, was greater than that of the NaPA in solution, and thus displayed an overall positive charge (Figure 1.4).¹³

1.5.2.3 *Small and Wide Angle X-ray Scattering*

X-ray scattering techniques have become universal for the identification of liquid crystalline phases. When a beam of X-ray with a known wavelength, λ , is passed through a given sample, it interacts with the electrons and scatters the radiation at dissimilar angles, 2θ , based on the differences in electron density of the material. These two-dimensional scattering patterns are detected where the scattering intensities are usually presented as a function of the length of the scattering vector, q . Information on the shape, also known as the ‘form factor’, can be obtained for dilute samples, such as micelles. Whereas for more concentrated samples, the ‘structure factor’ can be acquired with the appearance of pronounced peaks,

which reveal the presence of a highly ordered structure (Figure 1.3). The position of the maximum Bragg peak, q_{peak} , indicates the distance, d (in units of length), between the aligned particles by using Bragg's law:

$$q = \frac{4\pi}{\lambda} \cdot \sin(\theta) \quad [1.3]$$

The relative peak positions from a scattering profile allow characterisation of specific mesophases within the material. The lattice parameter, which defines the internal dimensions of the liquid crystalline phase, can be calculated from the absolute position of the peaks i.e. the interplanar distance within the matrix, d , when the corresponding scattering law is used for the mesophase present.

$$d = \frac{2\pi}{q_{peak}} \quad [1.4]$$

The main difference between small angle X-ray scattering (SAXS) and wide angle X-ray scattering (WAXS) is that the distance from the sample to the detector is longer in SAXS, thus smaller angles are probed which correlates to larger structures (e.g. colloidal dimensions), compared to probing molecular dimensions with WAXS.

The capabilities of these instruments are greatly broadened when coupled to a synchrotron source where the experimental setup and sample environment can be modified to achieve the desired requirements (Table 1.2).²²² In addition, spatially resolved data can be acquired in short time frames (Figure 1.3), which also allows kinetic processes to be studied. These features would be advantageous when probing the phase behaviour across surfactant-polymer interfaces.

1.5.2.4 *Small Angle Neutron Scattering*

Neutron scattering occurs from the interaction between a neutron and the nuclei of samples. Neutrons have high penetration for most elements making the technique useful for probing bulk mixtures. Small angle neutron scattering (SANS) often exploits the phenomenon of ‘contrast variation’, whereby one component is rendered ‘invisible’ by matching the scattering length density selectively with other components of the system, such as a continuous aqueous phase. This allows for determination of the shape and disposition of labelled and unlabelled components within a complex (Table 1.2).

1.5.3 Other Techniques

Structural characterisation of the mesophases formed across oppositely charged surfactant–polymer interfaces is valuable for understanding the equilibrium phase behaviour of these systems. However, quantitative information pertaining to changes in the distribution of molecules across the interface with the formation of mesophases over time is also of great importance. Study of the interactions between surfactant and polymer molecules have included the direct measurement of properties such as the viscosity,^{30, 162, 223–226} surface tension,^{30, 125, 227–230} conductance,^{112, 125, 131, 231, 232} self-diffusion,^{121, 210, 233, 234} and thermochemical parameters,^{111, 112, 115, 116, 125, 189, 194, 235–242} however, only in bulk aqueous mixtures. A suitable approach to determine the concentrations of surfactant, polymer, and water spatially across surfactant–polymer interfaces is needed. Only then can comments be made regarding the kinetics of structure formation and the existence of equilibrium and/or nonequilibrium structures across surfactant–polymer interfaces.

1.6 A Statement of the Problem

Existing literature on oppositely charged surfactant and polymer systems focusses on the study of dispersions and bulk mixtures, however little is known about the equilibrium phase behaviour at smaller length scales or across surfactant–polymer interfaces.

In seeking to better understand the factors that influence the formation of equilibrium or nonequilibrium structures across surfactant–polymer interfaces, new approaches to spatially characterise the mesophases formed and quantify the concentrations of surfactant, polymer, and water across these interfaces are needed.

Studying the dynamics across the interfacial region created between solutions of oppositely charged surfactants and polymers will provide a new means of determining how certain systems will behave upon mixing. Furthermore, insights may be gained to circumvent phase separation and the existence of kinetically trapped nonequilibrium nanostructures in dispersions or bulk mixtures, which are the main issues relating to instability and limit the ability to design materials from a formulation perspective. Therefore, strategies to develop systems with the desired properties and improve the method of preparation would be advantageous for industrial applications.

Stimuli-responsive liquid crystalline phases have received great attention for applications in the field of drug delivery.^{61, 200, 243, 244} Oppositely charged surfactant and polymer systems have shown promise in this area for the versatility they provide in controlling the interactions that govern the self-assembly of a diversity of mesophases. Knowledge of how the structural attributes of various industrially and biologically relevant oppositely charged surfactant and polymer respond to changes in environmental conditions can produce novel nanomaterials for use in a wide range of pharmaceutical applications.

These are the core issues that formed the basis of the hypotheses and aims developed in this thesis, which are outlined in their corresponding chapters.

1.7 Hypotheses

The broad hypotheses developed in this thesis were:

- i. That the phase behaviour demonstrated by aqueous mixtures of surfactant and polymer will be similar to those prepared with the complex salt, indicating the complex salt can be formed *in situ*.
- ii. That structure and concentration gradients will arise across the interface formed on contact between oppositely charged surfactant and polymer solutions.
- iii. That nanostructures at equilibrium are formed locally across surfactant–polymer interfaces, despite the existence of a global nonequilibrium state.
- iv. That systems comprised of the same surfactant-to-polymer molar charge ratio, but prepared at different concentration regimes will produce mesophases with similar internal structures, but different global morphologies.
- v. That the diffusivity of a model hydrophilic drug from nanostructured capsules formed by contact between oppositely charged surfactant and polymer solutions can be modulated by changes in solution temperature, salt concentration, or pH depending on the system studied.

1.8 Aims

In order to address the broad hypotheses stated earlier, the following aims were achieved.

- i. To generate and compare ternary phase diagrams of bulk aqueous mixtures of surfactant and polymer prepared either by the conventional mixing protocol or with incorporation of the complex salt.
- ii. To develop an approach to spatially resolve the formation of liquid crystalline structures across surfactant–polymer interfaces.
- iii. To develop an approach to spatially resolve composition (surfactant, polymer, and water concentrations) across surfactant–polymer interfaces.
- iv. To correlate changes in structure with changes in composition across surfactant–polymer interfaces over time.
- v. To study factors that can influence the rate and direction of structure formation across surfactant–polymer interfaces.
- vi. To structurally characterise a series of surfactant and polymer dispersions with varying surfactant-to-polymer molar charge ratios, and compare the structures formed with those arising in bulk aqueous mixtures, and across surfactant–polymer interfaces at similar compositions.
- vii. To study the structural attributes of a range of both industrially and biologically relevant oppositely charged surfactant and polymer systems and assess their potential as novel tailored release nanomaterials.

1.9 References

1. Liu, W.; Sun, S.; Cao, Z.; Zhang, X.; Yao, K.; Lu, W. W.; Luk, K. D. K., *An Investigation on the Physicochemical Properties of Chitosan/DNA Polyelectrolyte Complexes*. *Biomaterials*. 2005, 26, 2705–2711.
2. Amar-Yuli, I.; Adamcik, J.; Blau, S.; Aserin, A.; Garti, N.; Mezzenga, R., *Controlled Embedment and Release of DNA from Lipidic Reverse Columnar Hexagonal Mesophases*. *Soft Matter*. 2011, 7, 8162–8168.
3. Lin, H.; Zhu, G.; Xing, J.; Gao, B.; Qiu, S., *Polymer–Mesoporous Silica Materials Templated with an Oppositely Charged Surfactant/Polymer System for Drug Delivery*. *Langmuir*. 2009, 25, 10159–10164.
4. Hsu, W.-L.; Chen, H.-L.; Liou, W.; Lin, H.-K.; Liu, W.-L., *Mesomorphic Complexes of DNA with the Mixtures of a Cationic Surfactant and a Neutral lipid*. *Langmuir*. 2005, 21, 9426–9431.
5. Morán, M. C.; Miguel, M. G.; Lindman, B., *Surfactant–DNA Gel Particles: Formation and Release Characteristics*. *Biomacromolecules*. 2007, 8, 3886–3892.
6. Boukhnikachvili, T.; Aguerre–Chariol, O.; Airiau, M.; Lesieur, S.; Ollivon, M.; Vacus, J., *Structure of In-Serum Transfecting DNA–Cationic Lipid Complexes*. *FEBS Letters*. 1997, 409, 188–194.
7. Somasundaran, P.; Chakraborty, S.; Qiang, Q.; Deo, P.; Wang, J.; Zhang, R., *Surfactants, Polymers and their Nanoparticles for Personal Care Applications*. *J Cosmet Sci*. 2004, 55.
8. Miyake, M.; Kakizawa, Y., *Morphological Study of Cationic Polymer–Anionic Surfactant Complex Precipitated in Solution during the Dilution Process*. *J. Cosmet. Sci*. 2010, 61, 289–301.
9. Svensson, A. V.; Johnson, E. S.; Nylander, T.; Piculell, L., *Surface Deposition and Phase Behavior of Oppositely Charged Polyion–Surfactant Ion Complexes. 2. A Means to Deliver Silicone Oil to Hydrophilic Surfaces*. *ACS Appl. Mater. Interfaces*. 2010, 2, 143–156.

10. Lochhead, R. Y., *Shampoo and Conditioner Science*. In *Practical Modern Hair Science*, 2012; pp 75–116.
11. Clauzel, M.; Johnson, E. S.; Nylander, T.; Panandiker, R. K.; Sivik, M. R.; Piculell, L., *Surface Deposition and Phase Behavior of Oppositely Charged Polyion–Surfactant Ion Complexes. Delivery of Silicone Oil Emulsions to Hydrophobic and Hydrophilic Surfaces*. *ACS Appl. Mater. Interfaces*. 2011, 3, 2451–2462.
12. Lochhaas, K. H.; Thünemann, A. F.; Antonietti, M., *Polyelectrolyte–Surfactant Complexes with Fluorinated Surfactants. A New Type of Material for Coatings*. *Surface Coatings International*. 1999, 82, 451–455.
13. Nizri, G.; Makarsky, A.; Magdassi, S.; Talmon, Y., *Nanostructures Formed by Self-Assembly of Negatively Charged Polymer and Cationic Surfactants*. *Langmuir*. 2009, 25, 1980–1985.
14. Mezei, A.; Pons, R.; Morán, M. C., *The Nanostructure of Surfactant–DNA Complexes with Different Arrangements*. *Colloids Surf., B*. 2013, 111, 663–671.
15. Mironov, A. V.; Starodoubtsev, S. G.; Khokhlov, A. R.; Dembo, A. T.; Dembo, K. A., *Effect of Chemical Nature of 1,1–Salt on Structure of Polyelectrolyte Gel–Surfactant Complexes*. *J. Phys. Chem. B*. 2001, 105, 5612–5617.
16. Lapitsky, Y.; Kaler, E. W., *Formation of Surfactant and Polyelectrolyte Gel Particles in Aqueous Solutions*. *Colloids Surf, A*. 2004, 250, 179–187.
17. Babak, V. G.; Merkovich, E. A.; Galbraikh, L. S.; Shtykova, E. V.; Rinaudo, M., *Kinetics of Diffusionally Induced Gelation and Ordered Nanostructure Formation in Surfactant–Polyelectrolyte Complexes Formed at Water/Water Emulsion Type Interfaces*. *Mendeleev Commun*. 2000, 10, 94–95.
18. Fegyver, E.; Mészáros, R., *Fine-Tuning the Nonequilibrium Behavior of Oppositely Charged Macromolecule/Surfactant Mixtures via the Addition of Nonionic Amphiphiles*. *Langmuir*. 2014, 30, 15114–15126.
19. Pojják, K.; Mészáros, R., *Novel Self-Assemblies of Oppositely Charged Polyelectrolytes and Surfactants in the Presence of Neutral Polymer*. *Langmuir*. 2009, 25, 13336–13339.

20. Mezei, A.; Mészáros, R.; Varga, I.; Gilányi, T., *Effect of Mixing on the Formation of Complexes of Hyperbranched Cationic Polyelectrolytes and Anionic Surfactants*. *Langmuir*. 2007, 23, 4237–4247.
21. Naderi, A.; Claesson, P. M.; Bergström, M.; Dédinaite, A., *Trapped Non-Equilibrium States in Aqueous Solutions of Oppositely Charged Polyelectrolytes and Surfactants: Effects of Mixing Protocol and Salt Concentration*. *Colloids and Surfaces A: Physicochem. Eng. Aspects*. 2005, 253, 83–93.
22. Naderi, A.; Claesson, P. M., *Association between Poly(vinylamine) and Sodium Dodecyl Sulfate: Effects of Mixing Protocol, Blending Procedure, and Salt Concentration*. *J. Dispersion Sci. Technol.* 2005, 26, 329–340.
23. Holmberg, K.; Jönsson, B.; Kronberg, B.; Lindman, B., *Surfactants and Polymers in Aqueous Solution*. John Wiley & Sons, Ltd.: 2002.
24. Mezzenga, R.; Meyer, C.; Servais, C.; Romoscanu, A. I.; Sagalowicz, L.; Hayward, R. C., *Shear Rheology of Lyotropic Liquid Crystals: A Case Study*. *Langmuir*. 2005, 21, 3322–3333.
25. Lapitsky, Y.; Eskuchen, W. J.; Kaler, E. W., *Surfactant and Polyelectrolyte Gel Particles that Swell Reversibly*. *Langmuir*. 2006, 22, 6375–6379.
26. Svensson, A.; Norrman, J.; Piculell, L., *Phase Behaviour of Polyion–Surfactant Ion Complex Salts: Effects of Surfactant Chain Length and Polyion Length*. *J. Phys. Chem. B*. 2006, 110, 10332–10340.
27. Svensson, A.; Piculell, L.; Cabane, B.; Ilékti, P., *A New Approach to the Phase Behaviour of Oppositely Charged Polymers and Surfactants*. *J. Phys. Chem. B*. 2002, 106, 1013–1018.
28. Liu, C. K.; Warr, G. G., *Hexagonal Closest-Packed Spheres Liquid Crystalline Phases Stabilised by Strongly Hydrated Counterions*. *Soft Matter*. 2014, 10, 83–87.
29. Lapitsky, Y.; Kaler, E. W., *Formation of Surfactant and Polyelectrolyte Gel Particles in Aqueous Solutions*. *Colloids Surf., A*. 2004, 250, 179–187.

30. Mukherjee, S.; Dan, A.; Bhattacharya, S. C.; Panda, A. K.; Moulik, S. P., *Physicochemistry of Interaction between the Cationic Polymer Poly(diallyldimethylammonium chloride) and the Anionic Surfactants Sodium Dodecyl Sulfate, Sodium Dodecylbenzenesulfonate, and Sodium N-Dodecanoylsarcosinate in Water and Isopropyl Alcohol– Water Media*. Langmuir. 2011, 27, 5222–5233.
31. Hyde, S., *Chapter 16– Identification of Lyotropic Liquid Crystalline Mesophases*. In Handbook of Applied Surface and Colloid Chemistry, Holmberg, K., Ed. John Wiley & Sons, Ltd. 2001 pp 299–332.
32. Kulkarni, C. V.; Wachter, W.; Iglesias–Salto, G.; Engelskirchen, S.; Ahualli, S., *Monolein: A Magic Lipid?* Phys. Chem. Chem. Phys. 2011, 13, 3004–3021.
33. Tresset, G., *The Multiple Faces of Self–Assembled Lipidic Systems*. PMC Biophys. 2009, 2, 3–3.
34. Stache W., H., *Anionic Surfactants: Organic Chemistry*. 1996; Vol. 56.
35. Painter, H. A., *Anionic Surfactants*. In Detergents, de Oude, N. T., Ed. Springer Berlin Heidelberg, 1992; Vol. 3 / 3F, pp 1–88.
36. Öztekin, N.; Erim, F. B., *Determination of Cationic Surfactants as the Preservatives in an Oral Solution and a Cosmetic Product by Capillary Electrophoresis*. J. Pharm. Biomed. Anal. 2005, 37, 1121–1124.
37. Besra, L.; Sengupta, D. K.; Roy, S. K.; Ay, P., *Studies on Flocculation and Dewatering of Kaolin Suspensions by Anionic Polyacrylamide Flocculant in the Presence of Some Surfactants*. Int. J. Miner. Process. 2002, 66, 1–28.
38. Giolando, S. T.; Rapaport, R. A.; Larson, R. J.; Federle, T. W.; Stalmans, M.; Masscheleyn, P., *Environmental Fate and Effects of DEEDMAC: A New Rapidly Biodegradable Cationic Surfactant for Use in Fabric Softeners*. Chemosphere. 1995, 30, 1067–1083.
39. Mishra, S.; Tyagi, V. K., *Ester Quats: The Novel Class of Cationic Fabric Softeners*. J Oleo Sci. 2007, 56, 269–276.
40. Tsai, P.-C.; Ding, W.-H., *Determination of Alkyltrimethylammonium Surfactants in Hair Conditioners and Fabric Softeners by Gas Chromatography–Mass Spectrometry*

- with *Electron–Impact and Chemical Ionisation*. J. Chromatogr. A. 2004, 1027, 103–108.
41. Morrow, A. P.; Kassim, O. O.; Ayorinde, F. O., *Detection of Cationic Surfactants in Oral Rinses and a Disinfectant Formulation using Matrix–Assisted Laser Desorption/Ionisation Time–of–Flight Mass Spectrometry*. Rapid Commun Mass Spectrom. 2001, 15, 767–770.
42. Lim, H.; Kassim, A.; Huang, N.; Ambar Yarmo, M., *Palm–Based Nonionic Surfactants as Emulsifiers for High Internal Phase Emulsions*. J Surfact Deterg. 2009, 12, 355–362.
43. de la Maza, A.; Parra, J. L., *Solubilising Effects Caused by the Nonionic Surfactant Dodecylmaltoside in Phosphatidylcholine Liposomes*. Biophys. J. 72, 1668–1675.
44. Tiberg, F.; Cazabat, A. M., *Self–Assembly and Spreading of Non–Ionic Trisiloxane Surfactants*. EPL (Europhysics Letters). 1994, 25, 205.
45. Gomaa, E. Z., *Antimicrobial Activity of a Biosurfactant Produced by Bacillus Licheniformis Strain M104 Grown on Whey*. Braz. Arch. Biol. Technol. 2013, 56, 259–268.
46. Mulligan, C. N., *Environmental Applications for Biosurfactants*. Environ. Pollut. 2005, 133, 183–198.
47. Hirata, Y.; Ryu, M.; Oda, Y.; Igarashi, K.; Nagatsuka, A.; Furuta, T.; Sugiura, M., *Novel Characteristics of Sophorolipids, Yeast Glycolipid Biosurfactants, as Biodegradable Low–Foaming Surfactants*. J. Biosci. Bioeng. 2009, 108, 142–146.
48. Flasz, A.; Rocha, C. A.; Mosquera, B.; Sajo, C., *A Comparative Study of the Toxicity of a Synthetic Surfactant and One Produced by Pseudomonas Aeruginosa ATCC 55925*. Med Sci Res. 1998, 26, 181–185.
49. McInerney, M.; Javaheri, M.; Nagle, D., Jr., *Properties of the Biosurfactant Produced by Bacillus Licheniformis Strain JF–2*. J. Ind. Microbiol. 1990, 5, 95–101.
50. Nitschke, M.; Pastore, G. M., *Production and Properties of a Surfactant Obtained from Bacillus Subtilis Grown on Cassava Wastewater*. Bioresour. Technol. 2006, 97, 336–341.

51. Banat, I. M.; Makkar, R. S.; Cameotra, S. S., *Potential Commercial Applications of Microbial Surfactants*. Appl Microbiol Biotechnol. 2000, 53, 495–508.
52. Cooper, G. M., *The Cell: A Molecular Approach (2nd edition)*. 2000.
53. Borgström, B., *Fat Digestion and Solubilisation*. In Bile Acids in Health and Disease, Northfield, T.; Jazrawi, R.; Zentler–Munro, P., Eds. Springer Netherlands: 1988; pp 217–228.
54. Kékicheff, P., *Phase Diagram of Sodium Dodecyl Sulfate–Water System. 2. Complementary Isoplethal and Isothermal Phase Studies*. J. Colloid Interface Sci. 1989, 131, 133–152.
55. Yalcilla, M. T.; Herrington, K. L.; Brasher, L. L.; Kaler, E. W.; Chiruvolu, S.; Zasadzinski, J. A., *Phase Behavior of Aqueous Mixtures of Cetyltrimethylammonium Bromide (CTAB) and Sodium Octyl Sulfate (SOS)*. J Phys Chem. 1996, 100, 5874–5879.
56. Balmbra, R. R.; Clunie, J. S.; Goodman, J. F., *Cubic Mesomorphic Phases*. Nature. 1969, 222, 1159–1160.
57. Kratzat, K.; Schmidt, C.; Finkelmann, H., *A Doubly Branched Nonionic Oligooxyethylene ν -Amphiphile. Effect of Molecular Geometry on Liquid–Crystalline Phase Behaviour*. J. Colloid Interface Sci. 1994, 163, 190–198.
58. Israelachvili, J. N.; Mitchell, D. J.; Ninham, B. W., *Theory of Self-Assembly of Hydrocarbon Amphiphiles into Micelles and Bilayers*. J. Chem. Soc., Faraday Trans. 2. 1976, 72, 1525–1568.
59. Kaasgaard, T.; Drummond, C. J., *Ordered 2-D and 3-D Nanostructured Amphiphile Self-Assembly Materials Stable in Excess Solvent*. Phys. Chem. Chem. Phys. 2006, 8, 4957–4975.
60. Phan, S.; Fong, W.-K.; Kirby, N.; Hanley, T.; Boyd, B. J., *Evaluating the Link Between Self-Assembled Mesophase Structure and Drug Release*. Int. J. Pharm. 2011, 421, 176–182.

61. Fong, W.-K.; Hanley, T.; Boyd, B. J., *Stimuli Responsive Liquid Crystals Provide 'On-Demand' Drug Delivery In Vitro and In Vivo*. *J. Controlled Release*. 2009, 135, 218–226.
62. Ravve, A., *Naturally Occurring Polymers*. In *Principles of Polymer Chemistry*, Springer US: 2000; pp 449–475.
63. Zhao, K.; Deng, Y.; Chun Chen, J.; Chen, G.-Q., *Polyhydroxyalkanoate (PHA) Scaffolds with Good Mechanical Properties and Biocompatibility*. *Biomaterials*. 2003, 24, 1041–1045.
64. Clarotti, G.; Schue, F.; Sledz, J.; Aoumar, A. A. B.; Geckeler, K. E.; Orsetti, A.; Paleirac, G., *Modification of the Biocompatible and Haemocompatible Properties of Polymer Substrates by Plasma-Deposited Fluorocarbon Coatings*. *Biomaterials*. 1992, 13, 832–840.
65. Shuai, X.; Merdan, T.; Unger, F.; Kissel, T., *Supramolecular Gene Delivery Vectors Showing Enhanced Transgene Expression and Good Biocompatibility*. *Bioconjugate Chem*. 2005, 16, 322–329.
66. Castellanos-Ramos, J.; Navas-González, R.; Macicior, H.; Sikora, T.; Ochoteco, E.; Vidal-Verdú, F., *Tactile Sensors Based on Conductive Polymers*. *Microsyst Technol*. 2010, 16, 765–776.
67. Engel, J.; Chen, J.; Fan, Z.; Liu, C., *Polymer Micromachined Multimodal Tactile Sensors*. *Sens Actuators, A*. 2005, 117, 50–61.
68. Pelletier, N.; Beche, B.; Gaviot, E.; Camberlein, L.; Grossard, N.; Polet, F.; Zyss, J., *Single-Mode Rib Optical Waveguides on SOG/SU-8 Polymer and Integrated Mach-Zehnder for Designing Thermal Sensors*. *IEEE Sens. J*. 2006, 6, 565–570.
69. Uchiyama, S.; Tsuji, T.; Ikado, K.; Yoshida, A.; Kawamoto, K.; Hayashi, T.; Inada, N., *A Cationic Fluorescent Polymeric Thermometer for the Ratiometric Sensing of Intracellular Temperature*. *Analyst*. 2015, 140, 4498–4506.
70. Hammiche, A.; Hourston, D. J.; Pollock, H. M.; Reading, M.; Song, M., *Scanning Thermal Microscopy: Subsurface Imaging, Thermal Mapping of Polymer Blends, and Localised Calorimetry*. *J. Vac. Sci. Technol., B*. 1996, 14, 1486–1491.

71. Okabe, K.; Inada, N.; Gota, C.; Harada, Y.; Funatsu, T.; Uchiyama, S., *Intracellular Temperature Mapping with a Fluorescent Polymeric Thermometer and Fluorescence Lifetime Imaging Microscopy*. Nat. Commun. 2012, 3.
72. Yoo, D.; Shiratori, S. S.; Rubner, M. F., *Controlling Bilayer Composition and Surface Wettability of Sequentially Adsorbed Multilayers of Weak Polyelectrolytes*. Macromolecules. 1998, 31, 4309–4318.
73. Arima, Y.; Iwata, H., *Effect of Wettability and Surface Functional Groups on Protein Adsorption and Cell Adhesion Using Well-Defined Mixed Self-Assembled Monolayers*. Biomaterials. 2007, 28, 3074–3082.
74. Jianhua, W.; Toshio, I.; Naoto, O.; Takayasu, I.; Takashi, M.; Baolin, L.; Masao, Y., *Influence of Surface Wettability on Competitive Protein Adsorption and Initial Attachment of Osteoblasts*. Biomed. Mater. 2009, 4, 045002.
75. Ma, Z.; Mao, Z.; Gao, C., *Surface Modification and Property Analysis of Biomedical Polymers Used for Tissue Engineering*. Colloids Surf., B. 2007, 60, 137–157.
76. Yoo, H. S.; Kim, T. G.; Park, T. G., *Surface-Functionalised Electrospun Nanofibers for Tissue Engineering and Drug Delivery*. Adv. Drug Delivery Rev. 2009, 61, 1033–1042.
77. Patil, Y. B.; Toti, U. S.; Khdair, A.; Ma, L.; Panyam, J., *Single-Step Surface Functionalisation of Polymeric Nanoparticles for Targeted Drug Delivery*. Biomaterials. 2009, 30, 859–866.
78. Cheng, J.; Teply, B. A.; Sherifi, I.; Sung, J.; Luther, G.; Gu, F. X.; Levy-Nissenbaum, E.; Radovic-Moreno, A. F.; Langer, R.; Farokhzad, O. C., *Formulation of Functionalised PLGA-PEG Nanoparticles for In Vivo Targeted Drug Delivery*. Biomaterials. 2007, 28, 869–876.
79. Racine, J.; Luong-Van, E.; Sadikin, Y.; Kang, R. K. C.; Chu, Y. S.; Racine, V.; Thiery, J. P.; Birch, W. R., *A Versatile Gradient of Biomolecules for Regulating Cell Behaviour*. J. Adhes. Sci. Technol. 2010, 24, 975–992.
80. Kimura, D., *Cell Growth Processes: New Research*. Nova Science Publishers: 2008.

81. Boccaccini, A. R.; Gough, J. E., *Tissue Engineering Using Ceramics and Polymers*. Woodhead Publishing Limited and CRC Press LLC: Abington, 2007.
82. Mändl, S.; Rauschenbach, B., *Improving the Biocompatibility of Medical Implants with Plasma Immersion Ion Implantation*. Surf. Coat Technol. 2002, 156, 276–283.
83. Gulati, K.; Ramakrishnan, S.; Aw, M. S.; Atkins, G. J.; Findlay, D. M.; Losic, D., *Biocompatible Polymer Coating of Titania Nanotube Arrays for Improved Drug Elution and Osteoblast Adhesion*. Acta Biomater. 2012, 8, 449–456.
84. Whelan, D. M.; van der Giessen, W. J.; Krabbendam, S. C.; van Vliet, E. A.; Verdouw, P. D.; Serruys, P. W.; van Beusekom, H. M. M., *Biocompatibility of Phosphorylcholine Coated Stents in Normal Porcine Coronary Arteries*. Heart. 2000, 83, 338–345.
85. Kokuryo, D.; Nakashima, S.; Ozaki, F.; Yuba, E.; Chuang, K.-H.; Aoshima, S.; Ishizaka, Y.; Saga, T.; Kono, K.; Aoki, I., *Evaluation of Thermo-Triggered Drug Release in Intramuscular-Transplanted Tumors Using Thermosensitive Polymer-Modified Liposomes and MRI*. Nanomedicine. 2015, 11, 229–238.
86. Lee, J.; Ivkov, R.; Blumenthal, R., *Magnetically Triggered Drug Release from Liposome Embedded Gel*. J. Nanomedicine Biotherapeutic Discov. . 2014, 4, 130.
87. Huang, S.-L.; MacDonald, R. C., *Acoustically Active Liposomes for Drug Encapsulation and Ultrasound-Triggered Release*. Biochimica et Biophysica Acta 2004, 1665, 134–141.
88. Ta, T.; Porter, T. M., *Thermosensitive Liposomes for Localised Delivery and Triggered Release of Chemotherapy*. J. Controlled Release. 169, 112–125.
89. Basel, M. T.; Shrestha, T. B.; Troyer, D. L.; Bossmann, S. H., *Protease-Sensitive, Polymer-Caged Liposomes: A Method for Making Highly Targeted Liposomes Using Triggered Release*. ACS Nano. 2011, 5, 2162–2175.
90. van Elk, M.; Deckers, R.; Oerlemans, C.; Shi, Y.; Storm, G.; Vermonden, T.; Hennink, W. E., *Triggered Release of Doxorubicin from Temperature-Sensitive Poly(N-(2-hydroxypropyl)-methacrylamide mono/dilactate) Grafted Liposomes*. Biomacromolecules. 2014, 15, 1002–1009.

91. Johnston, A. P. R.; Cortez, C.; Angelatos, A. S.; Caruso, F., *Layer-by-Layer Engineered Capsules and Their Applications*. *Curr. Opin. Colloid Interface Sci.* 2006, 11, 203–209.
92. Zhao, X.; Liu, P., *pH-Sensitive Fluorescent Hepatocyte-Targeting Multilayer Polyelectrolyte Hollow Microspheres as a Smart Drug Delivery System*. *Mol. Pharmaceutics*. 2014, 11, 1599–1610.
93. Deng, Z. J.; Morton, S. W.; Ben-Akiva, E.; Dreaden, E. C.; Shopsowitz, K. E.; Hammond, P. T., *Layer-by-Layer Nanoparticles for Systemic Codelivery of an Anticancer Drug and siRNA for Potential Triple-Negative Breast Cancer Treatment*. *ACS Nano*. 2013, 7, 9571–9584.
94. Poon, Z.; Chang, D.; Zhao, X.; Hammond, P. T., *Layer-by-Layer Nanoparticles with a pH-Sheddable Layer for in Vivo Targeting of Tumor Hypoxia*. *ACS Nano*. 2011, 5, 4284–4292.
95. Romero, G.; Murray, R.; Qiu, Y.; Sanz, D.; Moya, S., *Layer by Layer Surface Engineering of Poly (lactide-co-glycolide) Nanoparticles: A Versatile Tool for Nanoparticle Engineering for Targeted Drug Delivery*. *Sci. China Chem.* 2013, 56, 1029–1039.
96. Huang, J.; Shu, Q.; Wang, L.; Wu, H.; Wang, A. Y.; Mao, H., *Layer-by-layer Assembled Milk Protein Coated Magnetic Nanoparticle Enabled Oral Drug Delivery with High Stability in Stomach and Enzyme-Responsive Release in Small Intestine*. *Biomaterials*. 2015, 39, 105–113.
97. Kim, B.-S.; Park, S. W.; Hammond, P. T., *Hydrogen-Bonding Layer-by-Layer-Assembled Biodegradable Polymeric Micelles as Drug Delivery Vehicles from Surfaces*. *ACS Nano*. 2008, 2, 386–392.
98. Elbakry, A.; Zaky, A.; Liebl, R.; Rachel, R.; Goepferich, A.; Breunig, M., *Layer-by-Layer Assembled Gold Nanoparticles for siRNA Delivery*. *Nano Letters*. 2009, 9, 2059–2064.
99. Zhou, J.; Pishko, M. V.; Lutkenhaus, J. L., *Thermoresponsive Layer-by-Layer Assemblies for Nanoparticle-Based Drug Delivery*. *Langmuir*. 2014, 30, 5903–5910.
100. Leung, P. S.; Goddard, E. D.; Han, C.; Glinka, C. J., *A Study of Polycation—Anionic-Surfactant Systems*. *Colloid Surface*. 1985, 13, 47–62.

101. Lapitsky, Y.; Kaler, E. W., *Surfactant and Polyelectrolyte Gel Particles for Encapsulation and Release of Aromatic Oils*. *Soft Matter*. 2006, 2, 779–784.
102. Takka, S.; Çali, A. G., *Bile Salt-Reinforced Alginate–Chitosan Beads*. *Pharm. Dev. Technol.* 2012, 17, 23–29.
103. Qiu, L.; Li, Z.; Qiao, M.; Long, M.; Wang, M.; Zhang, X.; Tian, C.; Chen, D., *Self-Assembled pH-Responsive Hyaluronic Acid–g–Poly(l-histidine) Copolymer Micelles for Targeted Intracellular Delivery of Doxorubicin*. *Acta Biomater.* 2014, 10, 2024–2035.
104. Wang, Y.; Hosta-Rigau, L.; Lomas, H.; Caruso, F., *Nanostructured Polymer Assemblies Formed at Interfaces: Applications from Immobilisation and Encapsulation to Stimuli-Responsive Release*. *Phys. Chem. Chem. Phys.* 2011, 13, 4782–4801.
105. Wang, W.; Sande, S. A., *Kinetics of Re-Equilibrium of Oppositely Charged Hydrogel–Surfactant System and Its Application in Controlled Release*. *Langmuir*. 2013, 29, 6697–6705.
106. Kogej, K.; Evmenenko, G.; Theunissen, E.; Berghmans, H.; Reynaers, H., *Investigation of Structures in Polyelectrolyte/Surfactant Complexes by X-ray Scattering*. *Langmuir*. 2001, 17, 3175–3184.
107. Kwak, J. C. T., *Polymer–Surfactant Systems*. Marcel Dekker: New York, 1998.
108. Goddard, E.; Hannan, R., *Polymer/Surfactant Interactions*. *J. Am. Oil Chem. Soc.* 1977, 54, 561–566.
109. Pojják, K.; Bertalanits, E.; Mészáros, R., *Effect of Salt on the Equilibrium and Nonequilibrium Features of Polyelectrolyte/Surfactant Association*. *Langmuir*. 2011, 27, 9139–9147.
110. Dan, A.; Ghosh, S.; Moulik, S. P., *Physicochemistry of the Interaction between Inulin and Alkyltrimethylammonium Bromides in Aqueous Medium and the Formed Coacervates*. *J. Phys. Chem. B*. 2009, 113, 8505–8513.

111. Samuel, G.; Daragh, M.; Nirmesh, J.; Michel, D.; Dominique, L., *Polyelectrolyte–Surfactant Complexes at Interfaces and in Bulk*. J. Phys.: Condens. Matter. 2003, 15, S219.
112. Winnik, M. A.; Bystryak, S. M.; Chassenieux, C.; Strashko, V.; Macdonald, P. M.; Siddiqui, J., *Study of Interaction of Poly(ethylene imine) with Sodium Dodecyl Sulfate in Aqueous Solution by Light Scattering, Conductometry, NMR, and Microcalorimetry*. Langmuir. 2000, 16, 4495–4510.
113. Thongngam, M.; McClements, D. J., *Isothermal Titration Calorimetry Study of the Interactions between Chitosan and a Bile Salt (Sodium Taurocholate)*. Food Hydrocolloids. 2005, 19, 813–819.
114. Nizri, G.; Lagerge, S.; Kamyshny, A.; Major, D. T.; Magdassi, S., *Polymer–Surfactant Interactions: Binding Mechanism of Sodium Dodecyl Sulfate to Poly(diallyldimethylammonium chloride)*. J. Colloid Interface Sci. 2008, 320, 74–81.
115. Courtois, J.; Berret, J. F., *Probing Oppositely Charged Surfactant and Copolymer Interactions by Isothermal Titration Microcalorimetry*. Langmuir. 2010, 26, 11750–11758.
116. Brinatti, C.; Mello, L. B.; Loh, W., *Thermodynamic Study of the Micellization of Zwitterionic Surfactants and Their Interaction with Polymers in Water by Isothermal Titration Calorimetry*. Langmuir. 2014, 30, 6002–6010.
117. Thalberg, K.; Van Stam, J.; Lindblad, C.; Almgren, M.; Lindman, B., *Time-Resolved Fluorescence and Self-Diffusion Studies in Systems of a Cationic Surfactant and an Anionic Polyelectrolyte*. J. Phys. Chem. 1991, 95, 8975–8982.
118. Philippova, O. E.; Starodoubtzev, S. G., *Interaction of Slightly Cross-linked Gels of Poly(diallyldimethylammonium bromide) with Sodium Dodecyl Sulfate. Diffusion of Surfactant Ions in Gel*. J. Polym. Sci., Part B: Polym. Phys. 1993, 31, 1471–1476.
119. Svensson, A.; Topgaard, D.; Piculell, L.; Söderman, O., *Molecular Self-Diffusion in Micellar and Discrete Cubic Phases of an Ionic Surfactant with Mixed Monovalent/Polymeric Counterions*. J. Phys. Chem. B. 2003, 107, 13241–13250.

120. Gao, H.; Zhu, R.; Yang, X.; Mao, S.; Zhao, S.; Yu, J.; Du, Y., *Properties of Polyethylene Glycol (23) Lauryl Ether with Cetyltrimethylammonium Bromide in Mixed Aqueous Solutions Studied by Self-Diffusion Coefficient NMR*. J. Colloid Interface Sci. 2004, 273, 626–631.
121. Totland, C.; Martinez–Santiago, J.; Ananthapadmanabhan, K. P.; Somasundaran, P., *Composition and Structural Transitions of Polyelectrolyte–Surfactant Complexes in the Presence of Fatty Acid Studied by NMR and Cryo–SEM*. Langmuir. 2015, 31, 1623–1631.
122. Goddard, E. D.; Hannan, R. B., *Cationic Polymer/Anionic Surfactant Interactions*. J. Colloid Interface Sci. 1976, 55, 73–79.
123. Anthony, O.; Marques, C. M.; Richetti, P., *Bulk and Surface Behavior of Cationic Guar in Solutions of Oppositely Charged Surfactants*. Langmuir. 1998, 14, 6086–6095.
124. Zhou, S.; Xu, C.; Wang, J.; Golas, P.; Batteas, J.; Kreeger, L., *Phase Behavior of Cationic Hydroxyethyl Cellulose–Sodium Dodecyl Sulfate Mixtures. Effects of Molecular Weight and Ethylene Oxide Side Chain Length of Polymers*. Langmuir. 2004, 20, 8482–8489.
125. Chakraborty, T.; Chakraborty, I.; Ghosh, S., *Sodium Carboxymethylcellulose–CTAB Interaction. A Detailed Thermodynamic Study of Polymer–Surfactant Interaction with Opposite Charges*. Langmuir. 2006, 22, 9905–9913.
126. Sokolov, E.; Yeh, F.; Khokhlov, A.; Grinberg, V. Y.; Chu, B., *Nanostructure Formation in Polyelectrolyte–Surfactant Complexes*. J. Phys. Chem. B. 1998, 102, 7091–7098.
127. Nizri, G.; Magdassi, S.; Schmidt, J.; Cohen, Y.; Talmon, Y., *Microstructural Characterisation of Micro- and Nanoparticles Formed by Polymer–Surfactant Interactions*. Langmuir. 2004, 20, 4380–4385.
128. Yeh, F.; Sokolov, E. L.; Khokhlov, A. R.; Chu, B., *Nanoscale Supramolecular Structures in the Gels of Poly(diallyldimethylammonium chloride) Interacting with Sodium Dodecyl Sulfate*. J. Am. Chem. Soc. 1996, 118, 6615–6618.

129. Sokolov, E. L.; Yeh, F.; Khokhlov, A.; Chu, B., *Nanoscale Supramolecular Ordering in Gel–Surfactant Complexes: Sodium Alkyl Sulfates in Poly(diallyldimethylammonium chloride)*. *Langmuir*. 1996, 12, 6229–6234.
130. Chu, B.; Yeh, F.; Sokolov, E. L.; Starodoubtsev, S. G.; Khokhlov, A. R., *Interaction of Slightly Cross-Linked Gels of Poly(diallyldimethylammonium chloride) with Surfactants*. *Macromolecules*. 1995, 28, 8447–8449.
131. Kong, L.; Cao, M.; Hai, M., *Investigation on the Interaction between Sodium Dodecyl Sulfate and Cationic Polymer by Dynamic Light Scattering, Rheological, and Conductivity Measurements*. *J. Chem. Eng. Data*. 2007, 52, 721–726.
132. Fegyver, E.; Meszaros, R., *Fine-Tuning the Nonequilibrium Behavior of Oppositely Charged Macromolecule/Surfactant Mixtures via the Addition of Nonionic Amphiphiles*. *Langmuir*. 2014.
133. Carnali, J. O.; Shah, P., *Correlation of Surfactant/Polymer Phase Behavior with Adsorption on Target Surfaces*. *J. Phys. Chem. B*. 2008, 112, 7171–7182.
134. Staples, E.; Tucker, I.; Penfold, J.; Warren, N.; Thomas, R. K.; Taylor, D. J. F., *Organisation of Polymer–Surfactant Mixtures at the Air–Water Interface: Sodium Dodecyl Sulfate and Poly(dimethyldiallylammonium chloride)*. *Langmuir*. 2002, 18, 5147–5153.
135. Lee, J.; Moroi, Y., *Investigation of the Interaction between Sodium Dodecyl Sulfate and Cationic Polymers*. *Langmuir*. 2004, 20, 4376–4379.
136. Lee, J.; Moroi, Y., *Binding of Sodium Dodecyl Sulfate to a Cationic Polymer of High Charge Density*. *Bull. Chem. Soc. Jpn.* 2003, 76, 2099–2102.
137. Lee, J.; Moroi, Y., *Solubilisation Study for Aggregates of Sodium Dodecyl Sulfate and Cationic Polymer of High Charge Density*. *J. Colloid Interface Sci.* 2004, 273, 645–650.
138. Li, D.; Kelkar, M. S.; Wagner, N. J., *Phase Behaviour and Molecular Thermodynamics of Coacervation in Oppositely Charged Polyelectrolyte/Surfactant Systems: A Cationic Polymer JR 400 and Anionic Surfactant SDS Mixture*. *Langmuir*. 2012, 28, 10348–10362.

139. Wang, W.; Sande, S. A., *Kinetics of Re-Equilibrium of Oppositely Charged Hydrogel-Surfactant System and its Application in Controlled Release*. Langmuir. 2013.
140. Goldraich, M.; Schwartz, J. R.; Burns, J. L.; Talmon, Y., *Microstructures Formed in a Mixed System of a Cationic Polymer and an Anionic Surfactant*. Colloid Surface Physicochem. Eng. Aspect. 1997, 125, 231-244.
141. Svensson, A.; Sjöström, J.; Scheel, T.; Piculell, L., *Phases and Structures of a Polyion-Surfactant Ion Complex Salt in Aqueous Mixtures: Cationic Hydroxyethyl Cellulose with Dodecylsulfate Counterions*. Colloid Surface Physicochem. Eng. Aspect. 2003, 228, 91-106.
142. Terada, E.; Samoshina, Y.; Nylander, T.; Lindman, B., *Adsorption of Cationic Cellulose Derivatives/Anionic Surfactant Complexes onto Solid Surfaces. I. Silica Surfaces*. Langmuir. 2004, 20, 1753-1762.
143. Zimin, D.; Craig, V. S. J.; Kunz, W., *Adsorption Pattern of Mixtures of Trimethylammonium-Modified Hydroxyethylcellulose and Sodium Dodecyl Sulfate at Solid-Liquid Interfaces*. Langmuir. 2004, 20, 2282-2291.
144. Leonard, M. J.; Strey, H. H., *Phase Diagrams of Stoichiometric Polyelectrolyte-Surfactant Complexes*. Macromolecules. 2003, 36, 9549-9558.
145. Trabelsi, S.; Guillot, S.; Ritacco, H.; Boué, F.; Langevin, D., *Nanostructures of Colloidal Complexes Formed in Oppositely Charged Polyelectrolyte/Surfactant Dilute Aqueous Solutions*. Eur. Phys. J. E. 2007, 23, 305-311.
146. Zhou, S.; Burger, C.; Yeh, F.; Chu, B., *Charge Density Effect of Polyelectrolyte Chains on the Nanostructures of Polyelectrolyte-Surfactant Complexes*. Macromolecules. 1998, 31, 8157-8163.
147. Zhou, S.; Yeh, F.; Burger, C.; Chu, B., *Nanostructures of Polyelectrolyte Gel-Surfactant Complexes*. J. Polymer Sci. B Polymer Phys. 1999, 37, 2165-2172.
148. Ilekli, P.; Piculell, L.; Tournilhac, F.; Cabane, B., *How to Concentrate an Aqueous Polyelectrolyte/Surfactant Mixture by Adding Water*. J. Phys. Chem. B. 1998, 102, 344-351.

149. Ilkkti, P.; Martin, T.; Cabane, B.; Piculell, L., *Effects of Polyelectrolytes on the Structures and Interactions of Surfactant Aggregates*. J. Phys. Chem. B. 1999, 103, 9831–9840.
150. Svensson, A.; Piculell, L.; Karlsson, L.; Cabane, B.; Jönsson, B., *Phase Behaviour of an Ionic Surfactant with Mixed Monovalent/Polymeric Counterions*. J. Phys. Chem. B. 2003, 107, 8119–8130.
151. Ponomarenko, E. A.; Waddon, A. J.; Bakeev, K. N.; Tirrell, D. A.; MacKnight, W. J., *Self-Assembled Complexes of Synthetic Polypeptides and Oppositely Charged Low Molecular Weight Surfactants. Solid-State Properties*. Macromolecules. 1996, 29, 4340–4345.
152. Ponomarenko, E. A.; Waddon, A. J.; Tirrell, D. A.; MacKnight, W. J., *Structure and Properties of Stoichiometric Complexes Formed by Sodium Poly(α , β -glutamate) and Oppositely Charged Surfactants*. Langmuir. 1996, 12, 2169–2172.
153. Hsu, W.-L.; Li, Y.-C.; Chen, H.-L.; Liou, W.; Jeng, U. S.; Lin, H.-K.; Liu, W.-L.; Hsu, C.-S., *Thermally-Induced Order–Order Transition of DNA–Cationic Surfactant Complexes*. Langmuir. 2006, 22, 7521–7527.
154. McLoughlin, D.; Delsanti, M.; Tribet, C.; Langevin, D., *DNA Bundle Formation Induced by Cationic Surfactants*. EPL (Europhysics Letters). 2005, 69, 461.
155. McLoughlin, D.; Impéror-Clerc, M.; Langevin, D., *A New Cubic Phase Containing DNA and a Surfactant*. ChemPhysChem. 2004, 5, 1619–1623.
156. Bilalov, A.; Olsson, U.; Lindman, B., *DNA–Lipid Self-Assembly. Phase Behaviour and Phase Structures of a DNA–Surfactant Complex Mixed with Lecithin and Water*. Soft Matter. 2011, 7, 730–742.
157. Alatorre-Meda, M.; Taboada, P.; Sabin, J.; Krajewska, B.; Varela, L. M.; Rodriguez, J. R., *DNA–Chitosan Complexation. A Dynamic Light Scattering Study*. Colloids Surf., A. 2009, 339, 145–152.
158. Mezei, A. I.; Ábrahám, A. g.; Pojják, K.; Mészáros, R. b., *The Impact of Electrolyte on the Aggregation of the Complexes of Hyperbranched Poly(ethyleneimine) and Sodium Dodecyl Sulfate*. Langmuir. 2009, 25, 7304–7312.

159. Abraham, A.; Mezei, A.; Meszaros, R., *The Effect of Salt on the Association Between Linear Cationic Polyelectrolytes and Sodium Dodecyl Sulfate*. *Soft Matter*. 2009, 5, 3718–3726.
160. Agzenai, Y.; Lindman, B.; Alfredsson, V.; Topgaard, D.; Renamayor, C. S.; Pacios, I. E., *In Situ X-ray Polymerization: From Swollen Lamellae to Polymer–Surfactant Complexes*. *J. Phys. Chem. B*. 2014, 118, 1159–1167.
161. Li, Y.; Dubin, P. L.; Havel, H. A.; Edwards, S. L.; Dautzenberg, H., *Complex Cormation Between Polyelectrolyte and Oppositely Charged Mixed Micelles: Soluble Complexes vs Coacervation*. *Langmuir*. 1995, 11, 2486–2492.
162. Hoffmann, I.; Heunemann, P.; Prévost, S.; Schweins, R.; Wagner, N. J.; Gradzielski, M., *Self-Aggregation of Mixtures of Oppositely Charged Polyelectrolytes and Surfactants Studied by Rheology, Dynamic Light Scattering and Small-Angle Neutron Scattering*. *Langmuir*. 2011, 27, 4386–4396.
163. Agzenai, Y.; Renamayor, C.; Pacios, I., *Nonstoichiometric Polymer–Surfactant Complexes Obtained in a Lamellar Lyotropic Medium*. *Colloid Polym. Sci.* 2012, 290, 1123–1132.
164. Merta, J.; Torkkeli, M.; Ikonen, T.; Serimaa, R.; Stenius, P., *Structure of Cationic Starch (CS)/Anionic Surfactant Complexes Studied by Small-Angle X-ray Scattering (SAXS)*. *Macromolecules*. 2001, 34, 2937–2946.
165. Kogej, K., *Study of the Effect of Polyion Charge Density on Structural Properties of Complexes Between Poly(acrylic acid) and Alkylpyridinium Surfactants*. *J. Phys. Chem. B*. 2003, 107, 8003–8010.
166. Kogej, K.; Theunissen, E.; Reynaers, H., *Effect of Polyion Charge Density on the Morphology of Nanostructures in Polyelectrolyte–Surfactant Complexes*. *Langmuir*. 2002, 18, 8799–8805.
167. Macdonald, P. M.; Tang, A., *¹H and ²H NMR Studies of Poly(acrylate) and Poly(sodium styrenesulfonate) Interactions with Cationic Surfactant Micelles*. *Langmuir*. 1997, 13, 2259–2265.

168. Vleugels, L. F. W.; Pollet, J.; Tuinier, R., *Polycation–Sodium Lauryl Ether Sulfate–Type Surfactant Complexes: Influence of Ethylene Oxide Length*. J. Phys. Chem. B. 2015, 119, 6338–6347.
169. Zhou, S.; Liang, D.; Burger, C.; Yeh, F.; Chu, B., *Nanostructures of Complexes Formed by Calf Thymus DNA Interacting with Cationic Surfactants*. Biomacromolecules. 2004, 5, 1256–1261.
170. Chronakis, I. S.; Alexandridis, P., *Rheological Properties of Oppositely Charged Polyelectrolyte–Surfactant Mixtures: Effect of Polymer Molecular Weight and Surfactant Architecture*. Macromolecules. 2001, 34, 5005–5018.
171. Antunes, F. E.; Marques, E. F.; Gomes, R.; Thuresson, K.; Lindman, B.; Miguel, M. G., *Network Formation of Catanionic Vesicles and Oppositely Charged Polyelectrolytes: Effect of Polymer Charge Density and Hydrophobic Modification*. Langmuir. 2004, 20, 4647–4656.
172. Agzenai, Y.; Pacios, I. E.; Renamayor, C. S., *Copolymer–Surfactant Complexes Obtained in a Lamellar Lyotropic Medium*. J. Phys. Chem. B. 2013, 117, 3019–3027.
173. Chiappisi, L.; Prévost, S.; Grillo, I.; Gradzielski, M., *From Crab Shells to Smart Systems: Chitosan–Alkylethoxy Carboxylate Complexes*. Langmuir. 2014.
174. Rosa, M.; del Carmen Morán, M.; da Graça Miguel, M.; Lindman, B., *The Association of DNA and Stable Catanionic Amino Acid–Based Vesicles*. Colloids Surf., A. 2007, 301, 361–375.
175. Thalberg, K.; Lindman, B.; Karlstroem, G., *Phase Behaviour of Systems of Cationic Surfactant and Anionic Polyelectrolyte: Influence of Surfactant Chain Length and Polyelectrolyte Molecular Weight*. J. Phys. Chem. 1991, 95, 3370–3376.
176. Uhríková, D.; Rapp, G.; Balgavý, P., *Condensed Lamellar Phase in Ternary DNA–DLPC–Cationic Gemini Surfactant System: A Small-Angle Synchrotron X-ray Diffraction Study*. Bioelectrochemistry. 2002, 58, 87–95.
177. Zantl, R.; Artzner, F.; Rapp, G.; Rädler, J. O., *Thermotropic Structural Changes of Saturated–Cationic–Lipid–DNA Complexes*. EPL (Europhysics Letters). 1999, 45, 90.

178. Janiak, J.; Bayati, S.; Galantini, L.; Pavel, N. V.; Schillén, K., *Nanoparticles with a Bicontinuous Cubic Internal Structure Formed by Cationic and Non-Ionic Surfactants and an Anionic Polyelectrolyte*. Langmuir. 2012, 28, 16536–16546.
179. Hellebust, S.; Blokhuis, A. M.; Nilsson, S., *Associative and Segregative Phase Behaviour of a Mixed Aqueous Cationic Surfactant and Anionic Hydrophilic Polymer System*. Colloid Surface Physicochem. Eng. Aspect. 2004, 243, 133–138.
180. Annaka, M., *Salt Effect on Microscopic Structure and Stability of Colloidal Complex Obtained from Neutral/Polyelectrolyte Block Copolymer and Oppositely Charged Surfactant*. Colloids Surf., B. 2012, 99, 127–135.
181. Thalberg, K.; Lindman, B.; Karlstroem, G., *Phase Behaviour of a System of Cationic Surfactant and Anionic Polyelectrolyte. The Effect of Salt*. J. Phys. Chem. 1991, 95, 6004–6011.
182. Zhao, X.; Shang, Y.; Liu, H.; Hu, Y., *Complexation of DNA with Cationic Gemini Surfactant in Aqueous Solution*. J. Colloid Interface Sci. 2007, 314, 478–483.
183. Mironov, A. V.; Starodoubtsev, S. G.; Khokhlov, A. R.; Dembo, A. T.; Yakunin, A. N., *Ordered Nonstoichiometric Polymer Gel–Surfactant Complexes in Aqueous Medium with High Ionic Strength*. Macromolecules. 1998, 31, 7698–7705.
184. Putnam, F. W.; Neurath, H., *The Precipitation of Proteins by Synthetic Detergents*. J. Am. Chem. Soc. 1944, 66, 692–697.
185. Chiappisi, L.; Prévost, S.; Grillo, I.; Gradzielski, M., *Chitosan/Alkylethoxy Carboxylates: A Surprising Variety of Structures*. Langmuir. 2014, 30, 1778–1787.
186. Zhou, S.; Hu, H.; Burger, C.; Chu, B., *Phase Structural Transitions of Polyelectrolyte–Surfactant Complexes between Poly(vinylamine hydrochloride) and Oppositely Charged Sodium Alkyl Sulfate*. Macromolecules. 2001, 34, 1772–1778.
187. Čalijski, B.; Cekić, N.; Savić, S.; Daniels, R.; Marković, B.; Milić, J., *pH-sensitive Microparticles for Oral Drug Delivery Based on Alginate/Oligochitosan/Eudragit® L100–55 “Sandwich” Polyelectrolyte Complex*. Colloids Surf., B. 2013, 110, 395–402.

188. Wagner, K.; Harries, D.; May, S.; Kahl, V.; Rädler, J. O.; Ben-Shaul, A., *Direct Evidence for Counterion Release Upon Cationic Lipid–DNA Condensation*. *Langmuir*. 1999, 16, 303–306.
189. Wang, H.; Wang, Y.; Yan, H.; Zhang, J.; Thomas, R. K., *Binding of Sodium Dodecyl Sulfate with Linear and Branched Polyethyleneimines in Aqueous Solution at Different pH Values*. *Langmuir*. 2006, 22, 1526–1533.
190. Mezei, A. I.; Pojják, K.; Mészáros, R. B., *Nonequilibrium Features of the Association between Poly(vinylamine) and Sodium Dodecyl Sulfate. The Validity of the Colloid Dispersion Concept*. *J. Phys. Chem. B*. 2008, 112, 9693–9699.
191. Ruppelt, D.; Kötz, J.; Jaeger, W.; Friberg, S. E.; Mackay, R. A., *Influence of Cationic Polyelectrolytes on Structure Formation in Lamellar Liquid Crystalline Systems*. *Langmuir*. 1997, 13, 3316–3319.
192. Starodubtsev, S. G.; Dembo, A. T.; Dembo, K. A., *Effect of Polymer Charge Density and Ionic Strength on the Formation of Complexes Between Sodium Arylamido–2-methyl-1-propane-sulfonate-co-acrylamide Gels and Cetylpyridinium Chloride*. *Langmuir*. 2004, 20, 6599–6604.
193. Zhou, S.; Yeh, F.; Burger, C.; Chu, B., *Highly Ordered Supramolecular Structures From Self-Assembly of Ionic Surfactants in Oppositely Charged Polyelectrolyte Gels*. In *Scattering from polymers*, American Chemical Society: 1999; Vol. 739, pp 244–260.
194. Loh, W.; Teixeira, L. A. C.; Lee, L.-T., *Isothermal Calorimetric Investigation of the Interaction of Poly(N-isopropylacrylamide) and Ionic Surfactants*. *J. Phys. Chem. B*. 2004, 108, 3196–3201.
195. Myers, D., *Physical Properties of Surfactant Used in Cosmetics*. In *Surfactants in Cosmetics*, Second Edition, Reiger, M. M.; Rhein, L. D., Eds. CRC Press: USA, 1997; Vol. 68, pp 29–82.
196. Tangso, K. J.; Fong, W.-K.; Darwish, T.; Kirby, N.; Boyd, B. J.; Hanley, T. L., *Novel Spiropyran Amphiphiles and Their Application as Light-Responsive Liquid Crystalline Components*. *J. Phys. Chem. B*. 2013, 117, 10203–10210.

197. Negrini, R.; Fong, W.-K.; Boyd, B. J.; Mezzenga, R., *pH-responsive Lyotropic Liquid Crystals and Their Potential Therapeutic Role in Cancer Treatment*. Chem. Commun. 2015, 51, 6671–6674.
198. Salentinig, S.; Tangso, K. J.; Hawley, A.; Boyd, B. J., *pH-driven Colloidal Transformations Based on the Vasoactive Drug Nicergoline*. Langmuir. 2014, 30, 14776–14781.
199. Salentinig, S.; Phan, S.; Darwish, T. A.; Kirby, N.; Boyd, B. J.; Gilbert, E. P., *pH-responsive Micelles Based on Caprylic Acid*. Langmuir. 2014, 30, 7296–7303.
200. Du, J. D.; Liu, Q.; Salentinig, S.; Nguyen, T.-H.; Boyd, B. J., *A Novel Approach to Enhance the Mucoadhesion of Lipid Drug Nanocarriers for Improved Drug Delivery to the Buccal Mucosa*. Int. J. Pharm. 2014, 471, 358–365.
201. Campbell, R. A.; Yanez Arteta, M.; Angus-Smyth, A.; Nylander, T.; Varga, I., *Effects of Bulk Colloidal Stability on Adsorption Layers of Poly(diallyldimethylammonium chloride)/Sodium Dodecyl Sulfate at the Air–Water Interface Studied by Neutron Reflectometry*. J. Phys. Chem. B. 2011, 115, 15202–15213.
202. Vitorazi, L.; Berret, J.-F.; Loh, W., *Self-Assembly of Complex Salts of Cationic Surfactants and Anionic–Neutral Block Copolymers. Dispersions with Liquid-Crystalline Internal Structure*. Langmuir. 2013, 29, 14024–14033.
203. Percebom, A. M.; Piculell, L.; Loh, W., *Polyion–Surfactant Ion Complex Salts Formed by a Random Anionic Copolyacid at Different Molar Ratios of Cationic Surfactant. Phase Behavior with Water and n-Alcohols*. J. Phys. Chem. B. 2012, 116, 2376–2384.
204. Bernardes, J. S.; Piculell, L.; Loh, W., *Self-Assembly of Polyion–Surfactant Ion Complex Salts in Mixtures with Water and n-Alcohols*. J. Phys. Chem. B. 2011, 115, 9050–9058.
205. Percebom, A. M.; Bernardes, J. S.; Loh, W., *Complex Salts Formed by Anionic Copolymers with Hexadecyltrimethylammonium. Phase Equilibrium and Structural Characterisation using SAXS*. AIP Conf. Proc. 2009, 1092, 173–175.
206. Bernardes, J. S.; Loh, W., *Structure and Phase Equilibria of Mixtures of the Complex Salt Hexadecyltrimethylammonium Polymethacrylate, Water and Different Oils*. J. Colloid Interface Sci. 2008, 318, 411–420.

207. Piculell, L., *Understanding and Exploiting the Phase Behaviour of Mixtures of Oppositely Charged Polymers and Surfactants in Water*. Langmuir. 2013, 29, 10313–10329.
208. Piculell, L.; Svensson, A.; Norrman, J.; Bernardes, J. S.; Karlsson, L.; Loh, W., Controlling Structure in Associating Polymer–Surfactant Mixtures. In *Pure Appl Chem*, 2007; Vol. 79, p 1419.
209. Norrman, J.; Lynch, I.; Piculell, L., *Phase Behaviour of Aqueous Polyion–Surfactant Ion Complex Salts: Effects of Polyion Charge Density*. J. Phys. Chem. B. 2007, 111, 8402–8410.
210. Janiak, J.; Tomšič, M.; Lundberg, D.; Olofsson, G.; Piculell, L.; Schillén, K., *Soluble Aggregates in Aqueous Solutions of Polyion–Surfactant Ion Complex Salts and a Nonionic Surfactant*. J. Phys. Chem. B. 2014.
211. Percebom, A. M.; Barbosa, L. R. S.; Itri, R.; Loh, W., *How Does the Ethoxylated Grafting of Polyelectrolytes Affect the Self-Assembly of Polyanion–Cationic Surfactant Complex Salts?* Langmuir. 2014.
212. Rosevear, F. B., *The Microscopy of the Liquid Crystalline Neat and Middle Phases of Soaps and Synthetic Detergents*. J. Am. Oil Chem. Soc. 1954, 31, 628–639.
213. Fontell, K., *X-ray Diffraction by Liquid Crystals – Amphiphilic Systems*. In *Liquid crystals and plastic crystals*, 1974; Vol. 2, pp 80–109.
214. Boyd, B. J.; Dong, Y.-D.; Rades, T., *Nonlamellar Liquid Crystalline Nanostructured Particles: Advances in Materials and Structure Determination*. J. Liposome Res. 2009, 19, 12–28.
215. Cheng, Y.; Wu, Q.; Li, Y.; Hu, J.; Xu, T., *New Insights Into the Interactions Between Dendrimers and Surfactants: 2. Design of New Drug Formulations Based on Dendrimer–Surfactant Aggregates*. J. Phys. Chem. B. 2009, 113, 8339–8346.
216. Babak, V. G.; Merkovich, E. A.; Desbrières, J.; Rinaudo, M., *Formation of An Ordered Nanostructure in Surfactant–Polyelectrolyte Complexes Formed by Interfacial Diffusion*. Polym. Bull. 2000, 45, 77–81.

217. Vikhoreva, G. A.; Babak, V. G.; Galich, E. F.; Gal'braikh, L. S., *Complex Formation in the Sodium Dodecyl Sulfate–Chitosan System*. Polym. Sci., Ser. A. 1997, 39, 617–622.
218. Lapitsky, Y.; Kaler, E. W., *Formation and Structural Control of Surfactant and Polyelectrolyte Gels*. Colloids Surf., A. 2006, 282–283, 118–128.
219. Alam, M. M.; Mezzenga, R., *Particle Tracking Microrheology of Lyotropic Liquid Crystals*. Langmuir. 2011, 27, 6171–6178.
220. Rodríguez–Fernández, J.; Pérez–Juste, J.; Liz–Marzán, L. M.; Lang, P. R., *Dynamic Light Scattering of Short Au Rods with Low Aspect Ratios*. J Phys Chem C. 2007, 111, 5020–5025.
221. Aragón, S. R.; Pecora, R., *Theory of Dynamic Light Scattering from Polydisperse Systems*. J. Chem. Phys. 1976, 64, 2395–2404.
222. Kirby, N. M.; Mudie, S. T.; Hawley, A. M.; Cookson, D. J.; Mertens, H. D. T.; Cowieson, N.; Samardzic–Boban, V., *A Low–Background–Intensity Focusing Small–Angle X–ray Scattering Undulator Beamline*. J Appl. Crystallogr. 2013, 46, 1670–1680.
223. Plucktaveesak, N.; Konop, A. J.; Colby, R. H., *Viscosity of Polyelectrolyte Solutions with Oppositely Charged Surfactant*. J. Phys. Chem. B. 2003, 107, 8166–8171.
224. Buajarern, J.; Mitchem, L.; Reid, J. P., *Manipulation and Characterisation of Aqueous Sodium Dodecyl Sulfate/Sodium Chloride Aerosol Particles*. J. Phys. Chem. A. 2007, 111, 13038–13045.
225. Bhattacharyya, A.; Monroy, F.; Langevin, D.; Argillier, J.–F., *Surface Rheology and Foam Stability of Mixed Surfactant– Polyelectrolyte Solutions*. Langmuir. 2000, 16, 8727–8732.
226. Shrestha, R. G.; Shrestha, L. K.; Aramaki, K., *Formation of Wormlike Micelle in a Mixed Amino–Acid Based Anionic Surfactant and Cationic Surfactant Systems*. J. Colloid Interface Sci. 2007, 311, 276–284.
227. Zhao, X.; Shang, Y.; Hu, J.; Liu, H.; Hu, Y., *Biophysical Characterisation of Complexation of DNA with Oppositely Charged Gemini Surfactant 12–3–12*. Biophys. Chem. 2008, 138, 144–149.

228. Goddard, E. D.; Leung, P. S., *Studies of Gel Formation, Phase Behaviour and Surface Tension in Mixtures of a Hydrophobically Modified Cationic Cellulose Polymer and Surfactant*. Colloid Surface. 1992, 65, 211–219.
229. Campbell, R. A.; Angus-Smyth, A.; Yanez Arteta, M.; Tonigold, K.; Nylander, T.; Varga, I., *New Perspective on the Cliff Edge Peak in the Surface Tension of Oppositely Charged Polyelectrolyte/Surfactant Mixtures*. J. Phys. Chem. Letters. 2010, 1, 3021–3026.
230. Asnacios, A.; Langevin, D.; Argillier, J. F., *Mixed Monolayers of Cationic Surfactants and Anionic Polymers at the Air–Water Interface. Surface Tension and Ellipsometry Studies*. Eur. Phys. J. B. 1998, 5, 905–911.
231. Onésippe, C.; Lagerge, S., *Studies of the Association of Chitosan and Alkylated Chitosan with Oppositely Charged Sodium Dodecyl Sulfate*. Colloid Surface Physicochem. Eng. Aspect. 2008, 330, 201–206.
232. Abraham, T.; Giasson, S., *Interactions of Partially Screened Polyelectrolyte Layers with Oppositely Charged Surfactant in Confined Environment*. Colloid Surface Physicochem. Eng. Aspect. 2001, 180, 103–110.
233. Bastardo, L. A.; Iruthayaraj, J.; Lundin, M.; Dedinaite, A.; Vareikis, A.; Makuška, R.; van der Wal, A.; Furó, I.; Garamus, V. M.; Claesson, P. M., *Soluble Complexes in Aqueous Mixtures of Low Charge Density Comb Polyelectrolyte and Oppositely Charged Surfactant Probed by Scattering and NMR*. J. Colloid Interface Sci. 2007, 312, 21–33.
234. Percebom, A. M.; Janiak, J.; Schillen, K.; Piculell, L.; Loh, W., *Micellization of Water-Soluble Complex Salts of an Ionic Surfactant with Hairy Polymeric Counterions*. Soft Matter. 2013, 9, 515–526.
235. Covis, R.; Vives, T.; Gaillard, C.; Benoit, M.; Benvegna, T., *Interactions and Hybrid Complex Formation of Anionic Algal Polysaccharides with a Cationic Glycine Detaine-Derived Surfactant*. Carbohydrate Polymers. 2015, 121, 436–448.
236. Li, Y.; Xu, R.; Couderc, S.; Bloor, D. M.; Warr, J.; Penfold, J.; Holzwarth, J. F.; Wyn-Jones, E., *Structure of the Complexes Formed between Sodium Dodecyl Sulfate and a Charged and Uncharged Ethoxylated Polyethyleneimine. Small-Angle Neutron Scattering*.

- Electromotive Force, and Isothermal Titration Calorimetry Measurements.* Langmuir. 2001, 17, 5657–5665.
237. Wang, C.; Tam, K. C., *New Insights on the Interaction Mechanism within Oppositely Charged Polymer/Surfactant Systems.* Langmuir. 2002, 18, 6484–6490.
238. Bai, G.; Nichifor, M.; Lopes, A.; Bastos, M., *Thermodynamic Characterization of the Interaction Behavior of a Hydrophobically Modified Polyelectrolyte and Oppositely Charged Surfactants in Aqueous Solution: Effect of Surfactant Alkyl Chain Length.* J. Phys. Chem. B 2005, 109, 518–525.
239. Wang, C.; Tam, K. C.; Jenkins, R. D.; Tan, C. B., *Interactions between Methacrylic Acid/Ethyl Acrylate Copolymers and Dodecyltrimethylammonium Bromide.* J. Phys. Chem. B 2003, 107, 4667–4675.
240. Wang, C.; Tam, K. C., *Interaction between Polyelectrolyte and Oppositely Charged Surfactant: Effect of Charge Density.* J. Phys. Chem. B. 2004, 108, 8976–8982.
241. Berret, J.-F., *Evidence of Overcharging in the Complexation between Oppositely Charged Polymers and Surfactants.* J. Chem. Phys. 2005, 123, 164703.
242. Ksenija, K., *Association and Structure Formation in Oppositely Charged Polyelectrolyte–Surfactant Mixtures.* Adv. Colloid Interface Sci. 2010, 158, 68–83.
243. Salentinig, S.; Tangso, K. J.; Hawley, A.; Boyd, B. J., *pH-Driven Colloidal Transformations Based on the Vasoactive Drug Nicergoline.* Langmuir. 2014, 30, 14776–14781.
244. Negrini, R.; Fong, W.-K.; Boyd, B. J.; Mezzenga, R., *pH-Responsive Lyotropic Liquid Crystals and Their Potential Therapeutic Role in Cancer Treatment.* Chem. Commun. 2015.

Chapter 2: *Developing a Novel Approach for Probing
Structure and Composition Across
Surfactant–Polymer Interfaces*

2. Developing a Novel Approach for Probing Structure and Composition Across Surfactant–Polymer Interfaces

2.1 Introduction

The general phase behaviour exhibited by oppositely charged surfactant and polymer systems at varying compositions has extensively been reported for bulk aqueous mixtures,¹⁻⁹ however little is known about the kinetics of structure formation and distribution of molecules across surfactant–polymer solution interfaces.¹⁰⁻¹⁴ The mixing of oppositely charged surfactant and polymer solutions is often not an instantaneous event.^{12, 14, 15} The existence of kinetically trapped nonequilibrium structures depend on the order and speed in which the components are mixed,¹⁶⁻¹⁹ the viscosity of the bulk solutions, and the type of mesophase formed.²⁰ These variables may play a significant role in the extent to which equilibrium structures are formed across such interfaces. Studying the dynamics of structure formation across surfactant–polymer solution interfaces presents a means of gaining a better appreciation of the changes in the local concentrations of surfactant, polymer, and water constituting the mesophases formed at a given time as the system approaches equilibrium without any input of energy. By this approach, it is anticipated that the mixing process would be driven by the diffusivity of molecules in solution and through mesophases formed across the interface. The slow kinetics can be monitored over a longer time scale and the resulting structures can be compared to those arising in bulk aqueous mixtures. It is hypothesised that a concentration gradient will form across the liquid–liquid interface after contact between oppositely charged solutions of surfactants and polymers, inducing a gradient in self-assembled structures which may or may not exist at local equilibrium.

Liu *et al.* developed a ‘concentration gradient’ method based on the methodology pioneered by Caffrey²¹ as a means of reducing the time involved in preparing and structurally characterising numerous samples required for generating surfactant/water binary phase diagrams.²² The fundamentals of this method involved adding water to a solid form of surfactant that was placed in between a microscope slide and a cover slip. The evolution of different mesophases was observed under crossed-polarisers due to the existence of a concentration gradient across the surfactant–water interface (Figure 1.3-A).²² This technique is analogous to the ‘flooding’ or ‘penetration’ experiments commonly employed to visualise phase boundaries formed upon introducing water to lipid based formulations.²³ Furthermore, Laughlin *et al.* has demonstrated the diffusive transport of molecules across interfacial regions through isothermal swelling studies and that near-infrared microscopy can be employed to quantify the concentration of water across such interfaces.^{24, 25}

Synchrotron small angle X-ray scattering (SAXS) was used to identify the mesophases formed across the surfactant–water interface. In this approach, the solid mass of surfactant was loaded into the bottom half of a standard SAXS capillary (~1.5 mm in diameter) then topped with water. Scattering curves were acquired at ~800 µm increments vertically across the sample showing a progression of structures from micelles, to hexagonally close-packed spheres, to *Pm3n* cubic phase, and finally hexagonal phase with increasing surfactant concentration (Figure 1.3-B).²² This technique allows the identification of liquid crystalline phases and localisation of phase boundaries. It also presents a non-destructive means of determining artifacts due to non-random sample orientation and enables rapid data collection that is applicable to characterising a wide range of liquid crystalline systems.^{21, 26} However, a major limitation is the need for access to a synchrotron source and the inability to measure the concentration of surfactant and water comprising the lyotropic mesophases.

As an extension to the methodology developed by Caffrey, Ricoul *et al.* demonstrated a means of determining the composition along the structure gradient upon contact between a solid mixture of a glycolipid and the cationic surfactant, didodecyldimethylammonium bromide, and excess water.²⁶ The concentration of the glycolipid was measured by autoradiography of the molecule radioactively labelled with ¹⁴C, while the concentrations of the surfactant and water were deduced from the sample X-ray transmission measurements which depended on the weight fractions of the three components averaged on the illuminated fraction of the sample, their weight adsorption coefficients, and their densities.²⁶ It was found that a large error in quantifying the concentration of these molecules by SAXS came from the experimental error in the thickness of the capillaries.²⁶ Although determining the composition of mesophases formed after the diffusion of water into the solid material was achieved through measurements by SAXS and autoradiography, the use of non-radioactive materials would be more favourable, particularly to avoid contamination of the interior surfaces of the capillary in experiments involving addition or removal of solutions from the interface.

There are several other methods that are capable of determining the composition of bulk mixtures which may also be feasible for quantifying the concentration of molecules distributed across surfactant–polymer interfaces (Table 2.1). Many of these techniques can produce high resolution images or spectra of the sample that are necessary to gain quantitative information. However, their use may be limited to various experimental factors, such as restrictions on the size or thickness of the sample (Table 2.1). For example, thicker samples would increase the detection of protons and improve the signal-to-noise ratio with magnetic resonance imaging (Table 2.1). As a consequence, this particular sample configuration would not be suitable for structural characterisation with synchrotron SAXS where thinner samples are preferred for efficient transmission of X-rays through the sample.

Samples prepared at larger volumes would increase the likelihood of creating surfactant–polymer interfaces that are not well defined, as well as further slowing down the mixing kinetics of the two solutions to form mesophases. In addition, exposure to a high vacuum environment, as in the case for infrared spectroscopy, time-of-flight secondary ion mass spectroscopy and scanning electron microscopy, requires the sample to be dry which is impractical as surfactant–polymer interfaces must obviously be hydrated to be able to measure the concentration of water (Table 2.1). Coherent anti-Stokes Raman spectroscopy and laser ablation inductively coupled plasma mass spectrometry can damage the samples, which make them unfeasible for studying the kinetics of structure formation across surfactant–polymer interfaces at multiple time points (Table 2.1). More so, the formation of anisotropic mesophases across surfactant–polymer interfaces may significantly affect the transmission of light through the sample and accurate detection of the sample composition, particularly with spectroscopic techniques, such as near infrared thermal imaging (Table 2.1).

Raman microscopy is frequently employed to analyse the chemistry and structure of materials. Briefly, when a sample is irradiated by an intense monochromatic laser beam, usually in the UV–visible region, the light interacts with the molecules and a change in its frequency is characteristic of the nature of each vibrational bond present.²⁷ The Raman spectrum obtained is therefore a unique vibrational fingerprint of a given material. Water is a weak Raman scatterer, which gives Raman spectroscopy a major advantage over infrared spectroscopy. This signifies that Raman microscopy may be suitable for the study of aqueous solutions since Raman spectra may be obtained without major interference from water vibrations,²⁷ and therefore seems the most feasible at measuring the concentrations of surfactant, polymer, and water across oppositely charged surfactant–polymer interfaces.

Table 2.1 Summary of the advantages and disadvantages of the various techniques explored to potentially quantify the composition across surfactant–polymer interfaces.

Technique	Advantages	Disadvantages
Synchrotron Infrared Microspectroscopy	High signal-to-noise ratio. 3–8 μm spatial resolution. Motorised stage allows for automated spectral mapping.	Sample must be dry. Sample thickness (3–10 μm). Strong absorption of water.
Coherent Anti-Stokes Raman Spectroscopy	High spectral resolution. Issues associated with fluorescence is eliminated.	Samples must be optically transparent and not be easily damaged by high power lasers. Narrow spectral range.
Time-of-Flight Secondary Ion Mass Spectrometry	High mass resolution. Mapping of 3D images after analysis of full mass spectrum.	Surface sensitive. Operates under high vacuum. Qualitative analysis.
Laser Ablation Inductively Coupled Plasma Mass Spectrometry	Highly sensitive chemical analysis. Speed. Sub-microscale sample size.	Destructive. Sample thickness and integrity is important.
Scanning Electron Microscopy	3D and topographical imaging. Obtain morphological and compositional information.	Operates under high vacuum. Can only detect C and O; possibly N, Na, S, and Cl. Qualitative analysis only.
Near-infrared Thermal Imaging	Whole sample imaging. Measures water content. Non-destructive.	Transmission at interface may be hindered by the presence of liquid crystalline structure.
Magnetic Resonance Imaging	Map differences in proton density across samples.	Sample geometry. Speed.
Raman Microscopy	Low absorption of water. Semi-quantitative.	Fluorescence of some samples. Refractive index influences accuracy of measured intensity.
Nuclear Magnetic Resonance	High spectral resolution. Self-diffusion measurements.	Limited sample geometry.

In this chapter, the development of novel approaches to examine the kinetics of structure formation across oppositely charged surfactant-polymer interfaces is described. Through examination of what is occurring specifically across the interface between solutions of surfactant and polymer, new insights into the structural and compositional changes that occur as the system approaches equilibrium will be gained. Thus, careful considerations must be made in order to select the appropriate sample cell and the toolbox of techniques that would enable spatially- and time-resolved characterisation of structures formed and quantification of composition across such interfaces.

The system comprising of the anionic surfactant, sodium dodecyl sulphate (SDS), and the cationic polymer, poly(diallyldimethylammonium chloride) (polyDADMAC), is of particular interest as it has been broadly explored in literature. These materials (Figure 2.1) are common ingredients found in haircare products, such as shampoos and conditioners. Thus, new insights gained into their equilibrium phase behaviour would be of great importance in the optimisation of formulations currently on the market or for exploitation in other industrial applications. For these reasons, the SDS and polyDADMAC system was used in developing these approaches.

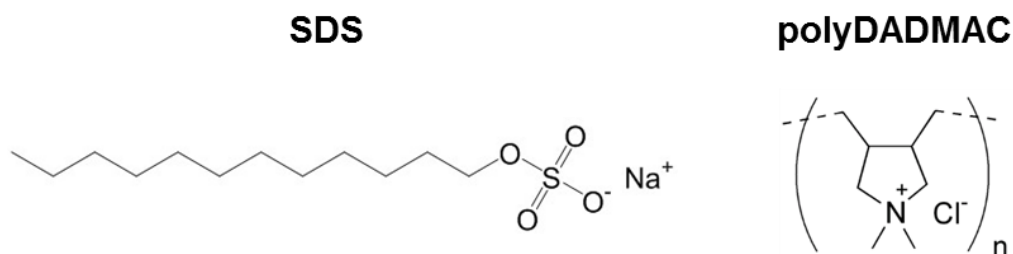


Figure 2.1 Chemical structures of sodium dodecyl sulphate (SDS) and poly(diallyldimethylammonium chloride) (polyDADMAC).

2.2 Hypothesis and Aims

Hypothesis

That structure and concentration gradients will arise across the interface created between oppositely charged solutions of surfactant and polymer.

Consequently, the following aims were undertaken in this chapter:

1. To develop an approach to spatially resolve the formation of liquid crystalline structures across surfactant–polymer interfaces.
2. To develop an approach to spatially resolve composition (surfactant, polymer, and water concentrations) across surfactant–polymer interfaces.
 - i. To generate calibration curves that can be employed to quantify the concentration of SDS, polyDADMAC, and water across SDS–polyDADMAC interfaces.

In order to achieve the aims stated above, it was important to develop an approach that allowed both structural and compositional detail at each point across the interface on the same sample to be determined. This chapter describes the successful developments of such an approach, together with some ‘lessons learned’.

2.3 Materials

Sodium dodecyl sulphate (SDS, BioXtra, $\geq 99.0\%$) and 1,4-dioxane (anhydrous, 99.8%) were purchased from Sigma–Aldrich (Sydney, Australia). Poly(diallyldimethylammonium chloride) (polyDADMAC, Merquat™ 100, molecular weight: 1.5×10^5 g/mol) was sourced from Nalco Company (Illinois, United States). The commercial polyDADMAC solution obtained contained 53.3% solid and 46.7% water (standard deviation: $\pm 0.3\%$) as determined by gravimetric analysis ($n = 10$). Merquat™ 100 was dried prior to preparation of polyDADMAC stock solutions to form a waxy solid.

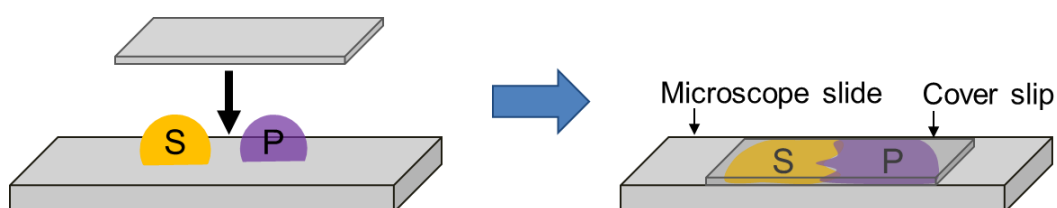
All materials were used without further purification. Milli-Q grade water purified through a Milli-pore system (Billerica, United States) was used throughout the studies.

2.4 Methods

2.4.1 Selecting the Sample Cell

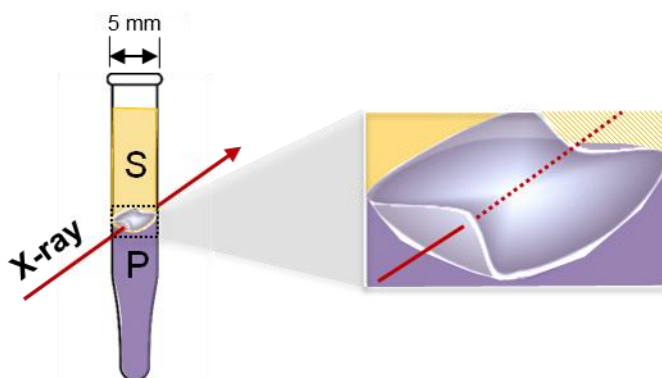
The primary goal in this chapter was to develop an approach to examine the kinetics of nanostructure formation across oppositely charged surfactant–polymer interfaces. To achieve this, an appropriate sample cell was essential. Some of the important requirements of the desired cell include (i) the ability to create a neat interface between the two solutions, (ii) openings where solutions can readily be removed and replaced, (iii) an inert material that allows transmittance of X-rays and light for analysis, and (iv) appropriate dimensions suitable for analysis by the particular techniques chosen to identify structures and determine the composition across surfactant–polymer interfaces. Before attaining the optimal sample cell, various systems were investigated.

Early method development stages involved placing a drop of surfactant and polymer solution onto a glass microscope slide within close proximity of each other and sandwiching them together with a glass cover slip (Schematic 2.1). Although an interface was formed between the flattened droplets, it was not well defined and difficult to reproduce.



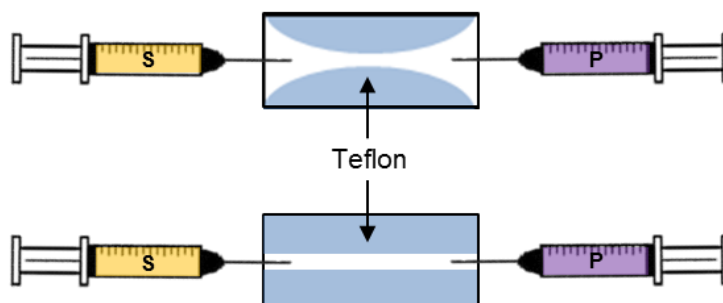
Schematic 2.1 Illustration of the initial approach to creating an interface between oppositely charged solutions of surfactant and polymer.

The next attempt entailed loading the more viscous polymer solution into the bottom half of a HPLC glass insert (~ 5 mm in diameter), while ensuring that the walls were not contaminated, then layering the surfactant solution above the existing solution (Schematic 2.2). Though a reasonably neat interface was formed upon contact of the two solutions, a much larger volume of the sample was required. Preliminary SAXS experiments conducted at the Australian Synchrotron demonstrated that scattering was obtained from this configuration. However, the diameter of the capillaries led to problems with the interface not being level in the direction perpendicular to the beam, which was approximately $100\ \mu\text{m}$ in height. Thus, the SAXS profiles acquired were a representative average of the material the X-ray beam passed through and would be an inaccurate characterisation of the actual mesophases formed at a given position across the surfactant–polymer interface (Schematic 2.2).



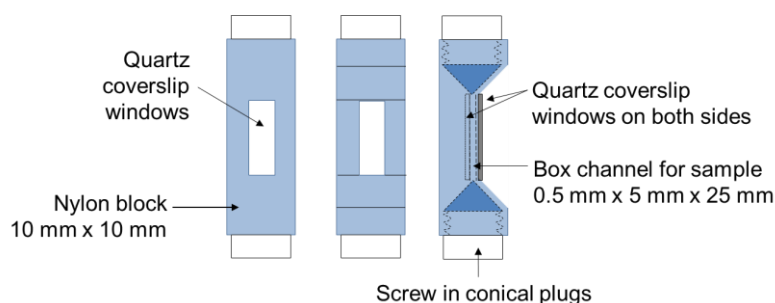
Schematic 2.2 Surfactant and polymer solutions loaded in a HPLC glass insert highlighting the issue involved when an X-ray beam is directed through a distorted meniscus (interface), which would produce scattering data non-representative of the true mesophases present at a particular position across the surfactant–polymer interface.

Following this endeavor, a simple cell comprised of Teflon cut precisely into shape, which either funneled or provided a more constricted route through which the opposing solutions could interact, was inserted between two glass cover slips and held together with superglue (Schematic 2.3). However, this prototype was not very successful because the design was prone to leaking and the formation of air bubbles.



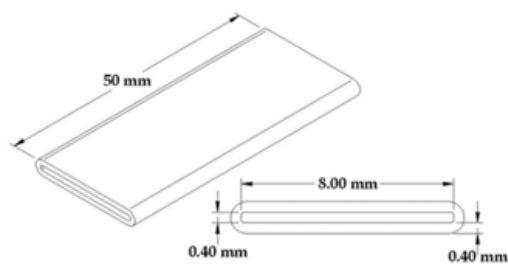
Schematic 2.3 One-dimensional representation of the ‘simple cell’ configuration for examining surfactant–polymer interfaces.

A more detailed alternative was a custom designed cell (Schematic 2.4). It featured (i) conical plugs that could be screwed into the chambers to prevent leakage and when opened could allow for delivery of the surfactant and polymer solutions, (ii) channels where the solutions could pass through to meet each other at midpoint, and (iii) quartz windows to view the small interface created. Considering the extreme detail encompassed in the proposed sample cell, assembly of the device envisaged would be costly, labour intensive, and time consuming, therefore actualisation of this design was not pursued.



Schematic 2.4 Custom designed sample cell for studying surfactant–polymer interfaces.

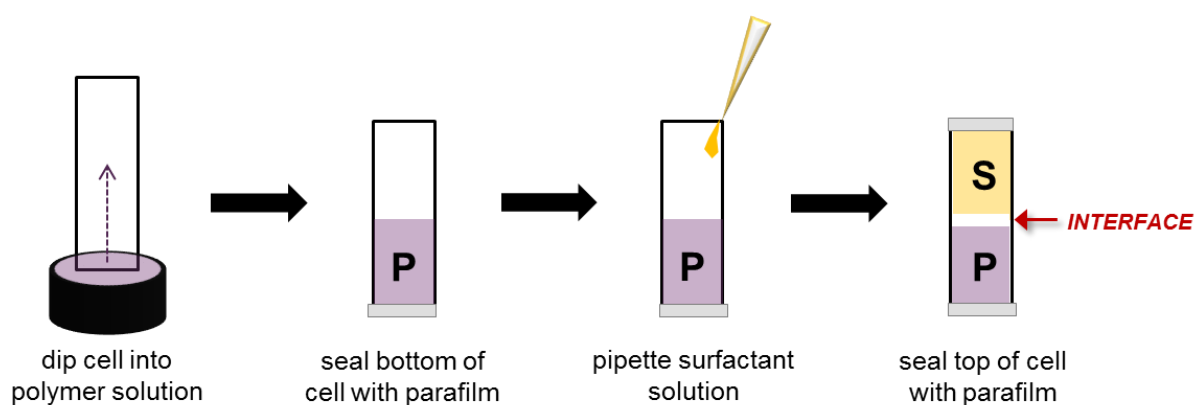
The commercially available rectangular borosilicate capillaries, VitroTubes™, sourced from VitroCom (New Jersey, United States) with dimensions: 0.4 x 8.0 x 50 mm were the ideal cells which fulfilled the prerequisites specified earlier (Schematic 2.5). Importantly, a reduction in the thickness of the material analysed by SAXS would yield a more accurate representation of the structures formed locally across the surfactant–polymer interfaces.



Schematic 2.5 Dimensions of the glass ‘flat cell’ selected to study the phase behaviour across surfactant–polymer interfaces. Reproduced from *www.vitrocom.com*.

2.4.2 Sample Preparation

In order to study the phase behaviour and distribution of molecules across oppositely charged surfactant and polymer interfaces, an appropriate preparation method was devised (Schematic 2.6). This entailed first loading the bottom half of the glass flat cell with the more viscous solution, in most cases by capillary action. In situations where the solution behaved more like semi-solids, they were loaded into the bottom of the empty flat cell via a syringe fitted with a 29G needle. The outer surface of the glass was wiped clean to ensure that the bottom of the cell was tightly sealed with parafilm. Afterwards, the less viscous solution was carefully pipetted into the remaining free volume within the flat cell via the top opening and sealed. This practice allowed a neat interface to be formed between surfactant and polymer solutions. The location of where the initial interface was created was marked on both edges of the cell to indicate the ‘point of origin’, which acts as a guide to monitoring the direction of growth and development of liquid crystalline structures across surfactant–polymer interfaces.



Schematic 2.6 The general method of preparing samples in flat cells for studying the phase behaviour and distribution of molecules across surfactant–polymer interfaces.

2.4.3 Characterisation of the Internal Structure of Liquid Crystalline Phases Across Surfactant–Polymer Interfaces

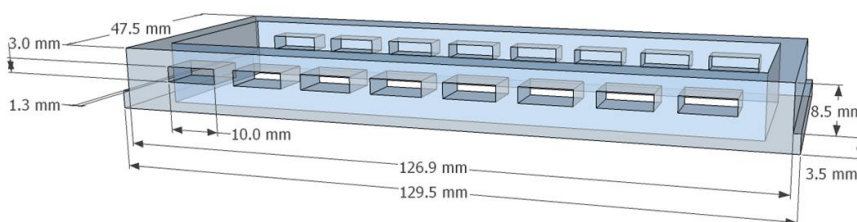
2.4.3.1 Crossed–Polarised Light Microscopy

Crossed–polarised light microscopy (CPLM) was used as a pre–screening step to visualise the growth of anisotropic liquid crystalline phases formed across oppositely charged surfactant–polymer interfaces. Images of samples loaded in flat cells were taken at various time intervals using a Nikon ECLIPSE Ni–U upright microscope fitted with crossed–polarising filters and a DS–U3 digital camera control unit (Nikon, Japan) at room temperature. This technique was employed complimentary to small angle X–ray scattering to identify the internal structure of self–assembled mesophases.

2.4.3.2 Synchrotron Small Angle X–ray Scattering

Synchrotron small angle X–ray scattering (SAXS) was utilised to spatially resolve the structural attributes of mesophases formed across surfactant–polymer interfaces.

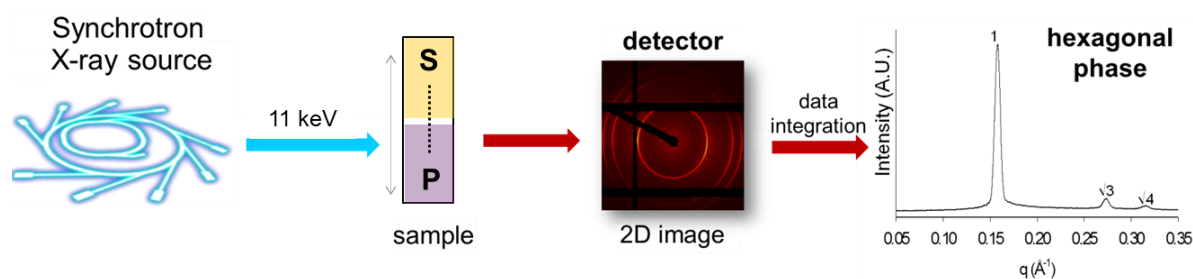
Samples prepared in flat cells were inserted into a custom built holder that was drawn on Google SketchUp and generated by the MakerBot Replicator 2 Desktop 3D Printer (Brooklyn, USA), where the external framework was identical to that of the dimensions of a standard 96–well plate (Schematic 2.7).



Schematic 2.7 2D drawing of the 3D printed flat cell holder employed when conducting line scans across multiple surfactant–polymer interfaces with synchrotron SAXS.

The sample holder was mounted up-right onto an appropriate fitting on the stage equipped with a motor that enabled automatic acquisition of sample while moving the sample through either the x- or y- direction. This set-up was used routinely to perform ‘line scans’ at the Australian Synchrotron SAXS/WAXS beamline.

A ‘line scan’ describes the approach that involved rastering across the interface created between solutions of oppositely charged surfactant and polymer molecules loaded in flat cells with spatial resolution (Schematic 2.8). 2D SAXS patterns were acquired for 1 s at each position the X-ray beam (beam size: 200 x 100 μm , horizontal x vertical) passed across the surfactant–polymer interface, at 100 μm increments several millimetres across the initial interface formed upon contact of both solutions. The scattering patterns at each position were acquired using a 1M Pilatus detector (active area 169 x 179 mm^2 with a pixel size of 172 μm). The energy or wavelength of the X-ray beam used (keV or \AA) and the distance between the sample and the detector (mm), which subsequently determined the q -range provided, varied slightly between each experiment conducted at the synchrotron depending on the experimental requirements during the allocated beamtime. These instrument specifications are specified in the methods section of each results chapter.



Schematic 2.8 Illustration of how a SAXS profile can be obtained spatially across surfactant–polymer interfaces by conducting a ‘line scan’ at 100 μm steps when the sample is placed in line with a synchrotron X-ray source.

The computer program ScatterBrain Analysis was used to reduce the 2D scattering patterns to the 1D scattering function, $I(q)$, for all data obtained at the synchrotron SAXS beamline. The Bragg peaks were indexed to confirm the nanostructure formed across surfactant–polymer interfaces, as correlated by the Miller indices (h, k, l) of known mesophases (Table 2.2). The absolute peak positions allow for the calculation of the mean lattice parameter, a , of the matrix from the corresponding interplanar distance, d ($d = 2\pi/q$), using the appropriate scattering law for the phase structure (Table 2.3).

Table 2.2 List of characteristic spacing ratios between lattice Bragg reflections for identification of common liquid crystalline phases.²⁸

Mesophase	Descriptor/symmetry (dimensionality)	Peak ratios
Lamellar	L_α, L_β	1:2:3:4...etc.
Bicontinuous cubics	Primitive $Im3m$	$\sqrt{2}:\sqrt{4}:\sqrt{6}:\sqrt{8}:\sqrt{10}$...etc.
	Diamond $Pn3m$	$\sqrt{2}:\sqrt{3}:\sqrt{4}:\sqrt{6}:\sqrt{8}$...etc.
	Gyroid $Ia3d$	$\sqrt{6}:\sqrt{8}:\sqrt{14}:\sqrt{16}:\sqrt{18}$...etc.
Hexagonal	p6m	1: $\sqrt{3}:\sqrt{4}:\sqrt{7}:\sqrt{12}$
Discrete cubic	$Fm3m$	$\sqrt{3}:\sqrt{4}:\sqrt{8}:\sqrt{11}:\sqrt{12}$...etc.
	$Pm3n$	$\sqrt{2}:\sqrt{4}:\sqrt{5}:\sqrt{6}:\sqrt{8}$...etc.
	$Fd3m$	$\sqrt{3}:\sqrt{8}:\sqrt{11}:\sqrt{12}:\sqrt{16}$

Table 2.3 List of equations used to calculate the mean lattice parameter, a , of common mesophases, where h, k , and l are the Miller indices for the corresponding structure.²⁸

Unit cell	Scattering law
Lamellar	$a = d$
Cubic	$a = d\sqrt{h^2 + k^2 + l^2}$
Hexagonal	$a = \frac{4d}{3}\sqrt{h^2 + k^2}$

2.4.4 Quantifying the Concentrations of Polymer, Surfactant, and Water Across SDS–PolyDADMAC Interfaces

Raman microscopy and small angle X-ray scattering were the primary techniques employed in combination to measure the concentrations of surfactant, polymer, and water across SDS–polyDADMAC interfaces as a function of time.

2.4.4.1 Raman Microscopy

The Raman microscopy experiments were performed on a Renishaw inVia confocal Raman microscope using a Nd:YAG 532 nm green laser (Gloucestershire, United Kingdom). An extended grating scan (10 s exposure, 1 accumulation, 50% laser power) was employed to acquire Raman spectra between 100–4000 cm^{-1} . The microscope was equipped with a long working distance objective lens (x20 magnification) providing a spectral resolution of ~ 10 μm . A depth scan in the z-direction of samples loaded in the flat cells was conducted to ensure that the solution was properly focused to achieve optimal Raman signal from the sample volume analysed.

Developing and Validating Standard Curves

PolyDADMAC/Water Binary Systems

A series of standard solutions comprised of polyDADMAC in Milli-Q water were prepared in triplicate between 2–50 wt%. The Raman spectrum (Figure 2.2) was collected for each solution and the area under the curve measured for the Raman signal at ~ 800 cm^{-1} (N-CH₂ stretch vibration)²⁹ was plotted as a function of the polymer concentration.

SDS/Water Binary Systems

Likewise, a series of standard solutions comprised of SDS in Milli-Q water were prepared in triplicate between 4–50 wt%. The Raman spectrum was collected for each solution (Figure 2.2) and the area under the curve measured for the Raman signal at ~ 1060 cm^{-1} (stretching vibration of two S–O bonds³⁰) representative of the sulphate moiety on the surfactant ion was plotted as a function of the surfactant concentration.

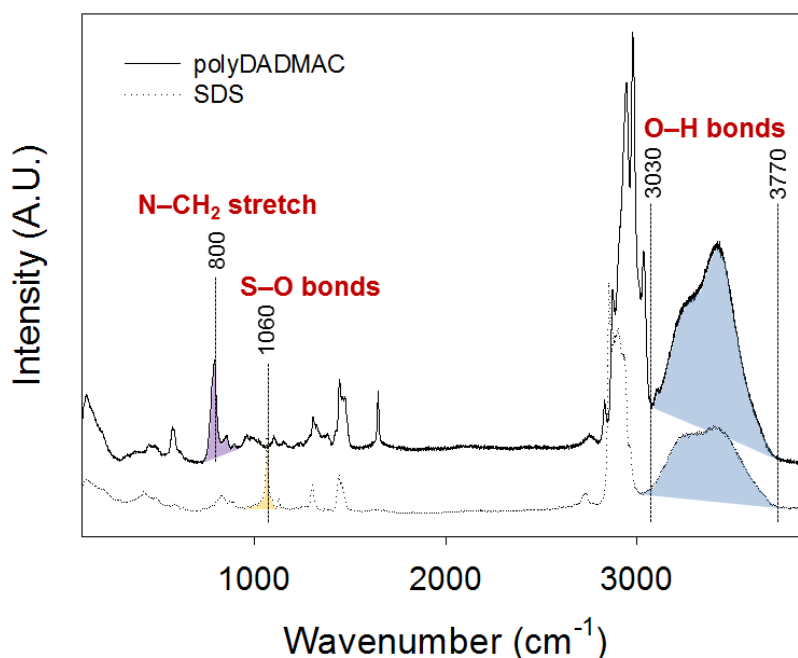


Figure 2.2 Raman spectra of polyDADMAC and SDS solutions loaded in flat cells highlighting the selected characteristic peaks, N–CH₂ stretch, S–O bonds, and O–H bonds for detection of the polymer, surfactant, and water molecules, respectively.

Water

The concentration of water was measured by probing the vibrational bonds existing between 3030–3770 cm^{-1} of the Raman spectrum (Figure 2.2).³¹ A calibration curve was generated from the area under the curve of the region representative of the O–H bond in the

Raman spectra obtained for the standard solutions of polyDADMAC and SDS. In addition, standard solutions of 1,4-dioxane, a solvent which is miscible in water, were also prepared and measured using the same approach to generate a calibration curve that would be valid for quantifying the concentration of water over a wider concentration range than is possible with solutions of polyDADMAC or SDS (Figure 2.3).

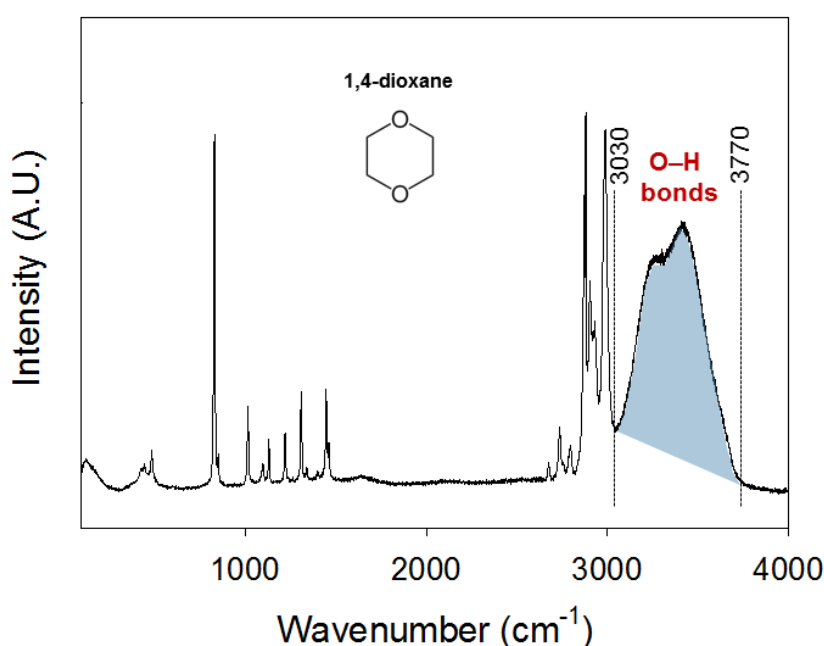


Figure 2.3 Raman spectrum of 1,4-dioxane prepared in Milli-Q water.

PolyDADMAC/SDS/Water Systems

It is known that hexagonal phases often arise upon mixing solutions of SDS and polyDADMAC,³²⁻³⁵ however the presence of anisotropic structures, as well white/opaque coacervates may have a significant impact on the ability of the laser light to pass through the sample and consequently fail to provide the true Raman signal for the existing molecular species analysed. In order to circumvent this problem, the relative Raman intensities (given as area under the curve) acquired for the peaks representative of SDS and polyDADMAC

(Figure 2.4) were used to determine the polyDADMAC-to-SDS molar charge ratio, expressed as $r = ([\text{polyDADMAC}] \times \text{charge per polymer molecule})/[\text{SDS}]$. Furthermore, the r value obtained can be compared to the approximate absolute concentrations measured for each component to rule out errors that may be associated with the variability in intensity or sensitivity of the Raman microscope. Deconvolution of Raman spectra collected for systems comprised of multiple components involves a methodology that has been widely accepted.³⁶ There were some assumptions made in the processing of data, including the disregard of the concentration of water in surfactant and polymer mixtures. More importantly, the refractive index of the mesophases formed was assumed to be the same across SDS–polyDADMAC interfaces.

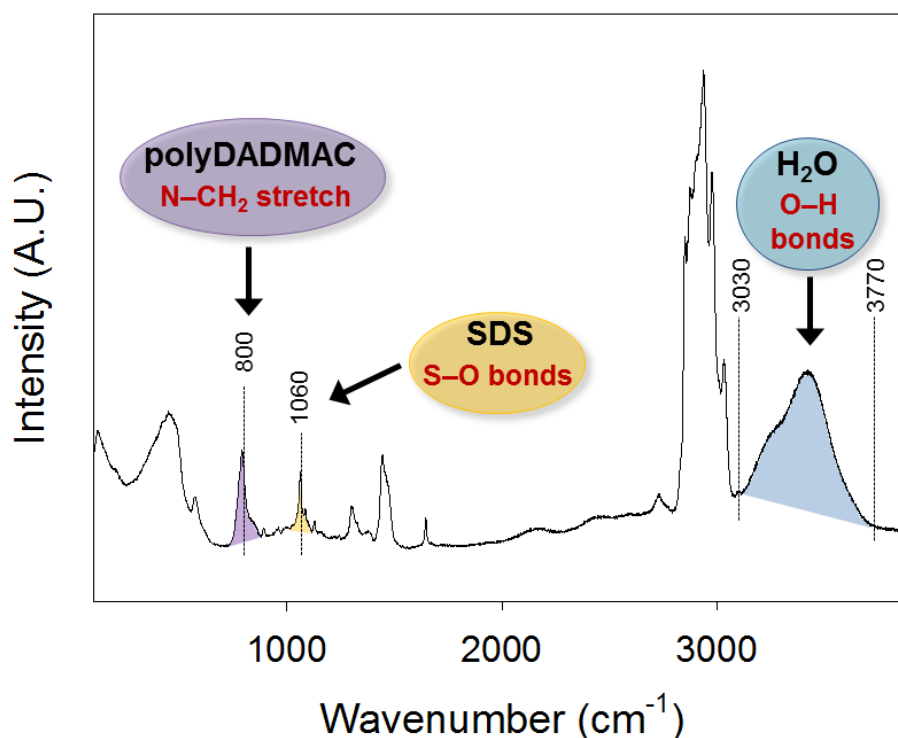


Figure 2.4 Raman spectrum of an aqueous mixture of SDS, polyDADMAC, and water highlighting the peaks characteristic of the corresponding molecules of interest.

Line Scans

Similar to the approach described for characterising the internal structure of mesophases formed across surfactant–polymer interfaces by synchrotron SAXS, line scans were also performed with a Raman microscope. Samples loaded in the flat cells were placed flat on top of the microscope stage. The position at which the initial interface was created was located and set as the ‘point of origin’. The stage was moved upwards (downwards in the z-direction of the sample) in order to focus on the sample material. Thereafter, a line scan was automated to collect Raman spectra every 100 μm steps from the bulk polymer solution, through the structured surfactant–polymer interface, and across the bulk surfactant region, using the same positions measured during the SAXS line scans.

2.4.4.2 Synchrotron Small Angle X-ray Scattering

In addition to Raman microscopy, synchrotron small angle X-ray scattering was also employed to quantify the concentrations of SDS and water in micellar solutions or hexagonal phases.

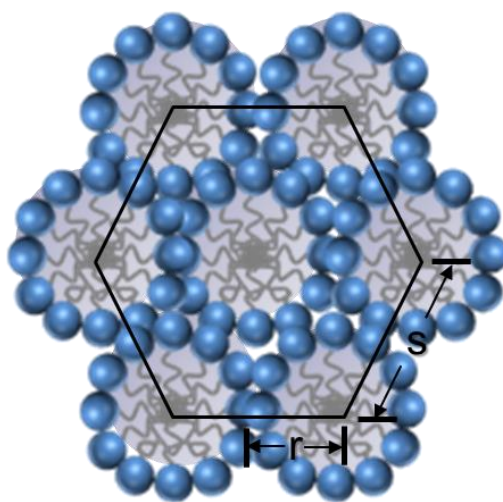
Developing Standard Curves for Quantifying SDS in Micellar Solutions or Hexagonal Phases

A series of SDS standard solutions in Milli-Q water prepared between 4–58 wt% were analysed by synchrotron SAXS. The area under the curve of the broad peak representative of micellar phase in the scattering curves obtained for the surfactant solutions were measured and plotted against concentration to generate a calibration curve for quantifying the concentration of SDS in regions across SDS–polyDADMAC interfaces comprising of micellar phase (in the absence of polymer molecules as determined by Raman microscopy). In contrast, the concentration of SDS present in regions containing hexagonal phase (35–58 wt%) was

determined from the lattice parameter calculated for the Bragg reflections with the spacing ratio of $1:\sqrt{3}:\sqrt{4}...$ present in the SAXS curves acquired.

Developing a Standard Curve for Measuring the Concentration of Water in Hexagonal Phases

The concentration of water can also be estimated from the lattice parameter of the hexagonal phases obtained by synchrotron SAXS. The lattice parameter given for a particular liquid crystalline structure describes the distance between each repeating unit cell within the nanostructure. Since hexagonal phases are composed of cylindrical micelles packed in a hexagonal lattice, the space between the polar head groups in the two-dimensional slice through the hexagonal phase was assumed to correlate to the amount of water present in the three-dimensional structures (Schematic 2.9).



Schematic 2.9 Illustration of how the concentration of water can be calculated based on the surface area occupied by the hydrophilic regions within a face of a model (normal, type 1) hexagonal phase, where s is the lattice parameter (nm), and r is the maximum radius of a micelle (nm).

The maximum radius, r , of each micelle was calculated from Tanford's law³⁷:

$$r (= l_{max}) \leq 0.154 + 0.1265n \quad [2.1]$$

where n is the number of carbon atoms on the alkyl surfactant tail. The surface area that represents the water content, A , was calculated by subtracting the area of three micelles from the area of a single hexagon, which is given by the following equation:

$$A = \frac{3\sqrt{3}}{2} s^2 - 3\pi r^2 \quad [2.2]$$

where s is the lattice parameter of the hexagonal phase (nm), and r is the radius of a micelle (nm).

It should be noted that there were various assumptions and limitations associated with the use of Tanford's law. Firstly, equation 2.1 gives an overestimation of the size of spherical micelles as it assumes the maximum extension of alkyl chains.³⁸ Secondly, the methyl group adjacent to polar headgroup lies within the hydration sphere of the headgroup, therefore do not possess hydrophobic properties.³⁷ Most importantly, repulsive surfaces created by charged headgroups, adsorption of ionic species, and/or Stern layers were ignored.³⁹ However, since the lattice parameter of hexagonal phases formed in aqueous mixtures of SDS and polyDADMAC accounts for the repulsive interactions resulting between the charged species in solution, the method of analysis presented here offers a realistic approximation of the local water concentration surrounding hexagonal phases formed across SDS–polyDADMAC interfaces.

2.5 Results

2.5.1 Visualisation of Anisotropic Liquid Crystalline Structures Across Surfactant–Polymer Interfaces

A preliminary contact study between a solution of polyDADMAC and a solution of SDS was initially viewed under a crossed-polarised light microscope. Several hours after the SDS–polyDADMAC interface was created within a flat cell, an isotropic region was observed in between two distinct bands exhibiting birefringence with different textures (Figure 2.5). It should be noted that the formation of the three distinct regions across the interface was highly reproducible, even by collaborators at P&G in Cincinnati.



Figure 2.5 CPLM image of the SDS–polyDADMAC interface ~32 hr after initial contact between solutions of 20 wt% polyDADMAC and 20 wt% SDS showing the formation of distinct bands with different optical properties.

In order to structurally resolve the bands displaying different optical properties across the SDS–polyDADMAC interface, a line scan was performed with synchrotron SAXS.

2.5.2 Spatially Resolved Structural Information Across Surfactant–Polymer Interfaces

A preliminary line scan with synchrotron small angle X-ray scattering was conducted across an aged SDS–polyDADMAC interface, where liquid crystalline structures were allowed to form over a week from initial contact between the oppositely charged bulk solutions.

The SAXS profiles obtained at 100 μm spatial resolution across this interface were presented as a waterfall plot as a function of distance from origin (Figure 2.6). Scattering from the polymer solution was poorly resolved as macromolecules do not often form periodic structures (Figure 2.6–A).⁴⁰ In contrast, micelles were present in the bulk SDS solution as indicated by the broad peak present at low q values (Figure 2.6–E). In addition, regions comprised of coexisting micellar and hexagonal phases (Figure 2.6–B and D) were found on either side of a region consisting of only hexagonal phases (Figure 2.6–C) across the interface. Moreover, the shape of the SAXS curve underlying the Bragg reflections from hexagonal phase were notably different between Figure 2.6–B and Figure 2.6–D.

Clearly a gradient of nanostructures were formed across the SDS–polyDADMAC interface, which was in agreement with the appearance of bands displaying different optical textures when examined under a crossed-polarised microscope (Figure 2.5). Interestingly, there were significant differences in the lattice parameter of hexagonal phases formed in different regions across the SDS–polyDADMAC interface.

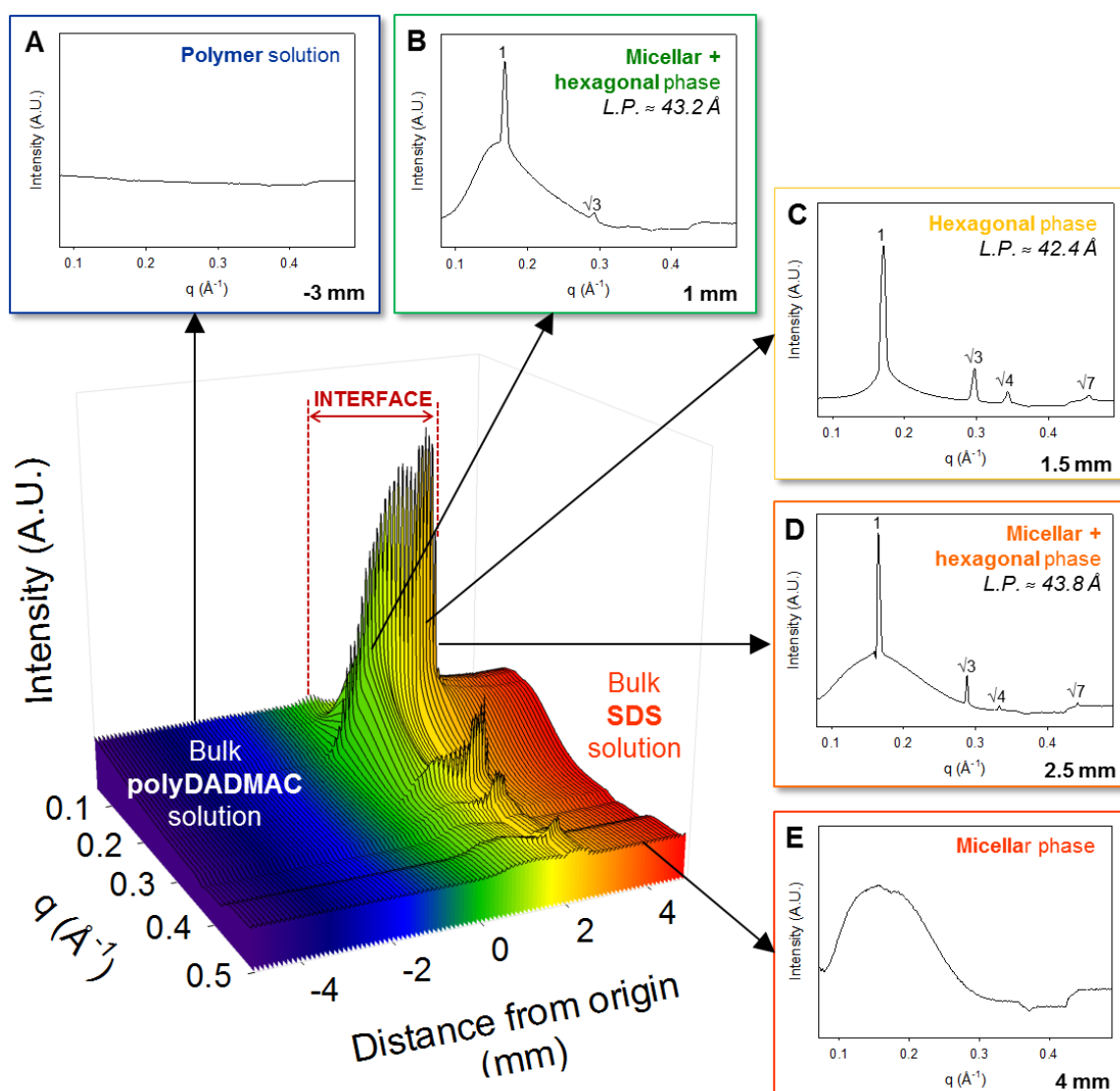


Figure 2.6 Waterfall plot of SAXS profiles acquired across the SDS–polyDADMAC interface illustrating a gradient of structures formed after a week from initial contact between solutions of 20 wt% polyDADMAC and 20 wt% SDS. Pertinent scattering curves obtained at different regions across the interface, given as distances from the origin (0 mm), are extracted to highlight the formation of different mesophases (A–E). Structured regions include SDS micellar (L_1) phases, coexisting micellar and hexagonal phases (L_1+H_1), or hexagonal phases only (H_1) which their calculated lattice parameters (L.P.) are presented.

2.5.3 Generation of Calibration Curves to Quantify the Concentrations of Surfactant, Polymer, and Water Across SDS–PolyDADMAC Interfaces

2.5.3.1 Use of Raman Microscopy for Composition Analysis

PolyDADMAC /Water Binary Systems

The area under the curve after background subtraction measured for the Raman signal at $\sim 800\text{ cm}^{-1}$ arising from the N-CH₂ stretch for polyDADMAC showed a linear relationship with increasing concentration (Figure 2.7-A) as might be expected from Beer's Law. The linear regression fitted for the data points generated will be used to quantify the concentration of polyDADMAC in aqueous solutions where SDS molecules are absent or undetectable, which is valid between 2–50 wt% polyDADMAC (Equation 2.3).

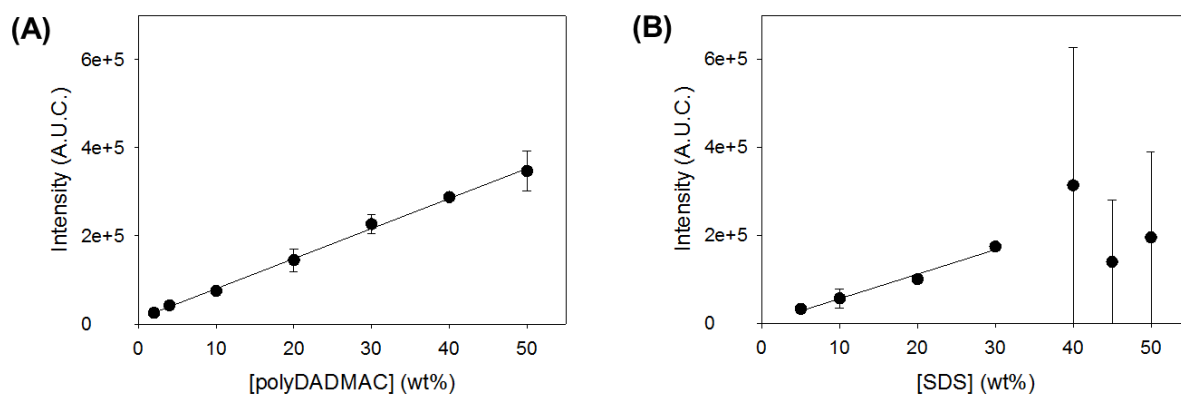


Figure 2.7 Standard curves generated to quantify the concentrations of polyDADMAC (A) and SDS (B) in Milli-Q water from the Raman intensity, as area under the curve, given by the characteristic peaks at $\sim 800\text{ cm}^{-1}$ and $\sim 1060\text{ cm}^{-1}$ of the corresponding molecules of interest.

SDS/Water Binary Systems

The Raman intensity (area under the curve) of the peak indicative of the S–O bonds present in the chemical structure of SDS increased linearly with surfactant concentration between 4–30 wt% SDS (Figure 2.7-B). However, the data points obtained above 40 wt% SDS did not follow the linear trend displayed at lower concentrations. The linear regression fitted for the data points generated at low SDS concentrations will be used to quantify the concentration of SDS in solutions where polyDADMAC molecules are absent or undetectable and is valid between 4–30 wt% SDS (Equation 2.4).

Water

The area under the curve of the region representative of water in the Raman spectra obtained for the standard solutions of polyDADMAC and SDS was found to increase with increasing water content. However, there were significant differences in the Raman intensity of water in solutions prepared with the same amount of water but with different additives (Figure 2.8).

The concentration of water in solutions of SDS or polyDADMAC became impractical to measure when prepared with high concentrations of the respective components due to a significant increase in their viscosity. Therefore, in order to access the Raman intensity for water at concentrations below 40 wt%, mixtures of water and 1,4-dioxane were used. Dioxane does not possess any O–H bonds but is fully miscible with water, allowing a series of solutions to be prepared at lower water concentrations to determine the changes in Raman intensity for water at these lower concentrations. The resulting calibration curve is also presented in Figure 2.8. The linear regression fitted for the data set obtained for the standard solutions of 1,4-dioxane is valid between 0–100 wt% water (Equation 2.9).

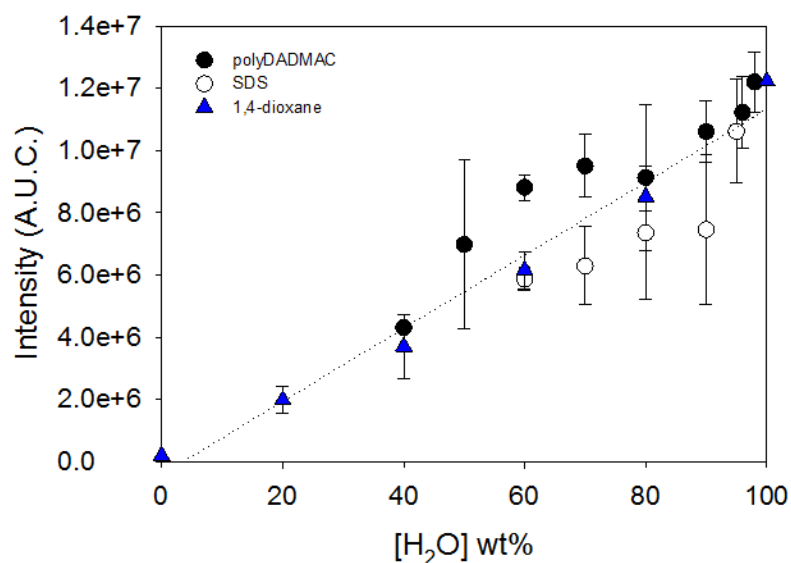


Figure 2.8 Calibration curve for measuring the concentration of water from either the Raman intensity (A.U.C.) determined between 3030–3770 cm^{-1} in solutions of polyDADMAC (filled circles), SDS (open circles), or 1,4-dioxane (triangles).

PolyDADMAC/SDS/Water Systems

When the Raman intensity of the peak indicative of SDS was given as a fraction of the sum of the Raman intensity measured for SDS and polyDADMAC, it displayed a positive correlation with increasing mass fraction of SDS in bulk aqueous mixtures of the surfactant and polymer (Figure 2.9). The polyDADMAC-to-SDS molar charge ratio can be determined from interpolating the mass fraction of SDS in bulk aqueous mixtures of SDS and polyDADMAC using the linear regression fitted for the scatter plot (Equation 2.11).

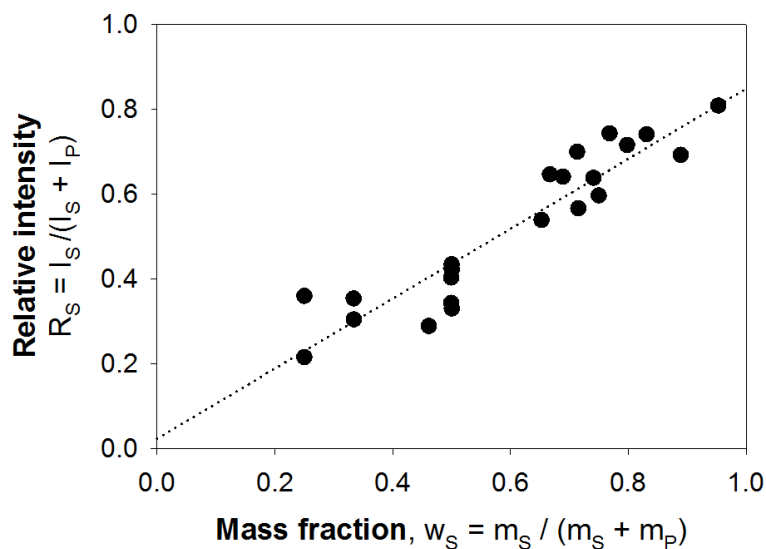


Figure 2.9 Calibration curve developed to determine the polyDADMAC-to-SDS molar charge ratio, expressed as $r = ([\text{polyDADMAC}] \times \text{charge per polymer molecule})/[\text{SDS}]$, across SDS–polyDADMAC interfaces by Raman microscopy.

2.5.3.2 Use of Synchrotron Small Angle X-ray Scattering for Composition Analysis

SDS/Water Binary Systems

Raman microscopy was able to resolve the quantity of SDS at low concentrations, but not at high concentrations due to the presence of hexagonal phase across the SDS–polyDADMAC interface. Therefore, a supplementary approach using the intensity scattering from micelles and the lattice parameter of hexagonal phase was developed to quantify the concentration of SDS in solutions where polyDADMAC is absent or undetectable.

A transformation in the broad peak observed in the low q -range of the SAXS profiles acquired for solutions of SDS, typically indicative of micellar phase, was evident with an increase in concentration (Figure 2.10–A). Specifically, a single broad peak was visible

between 4–10 wt% SDS. Above this concentration range, a second peak emerged on the left-hand side ‘shouldering’ the pre-existing broad peak, which grew in intensity with a further increase in the SDS concentration (12–32 wt%). The area under the curve measured for the scattering patterns of the SDS micellar solutions followed a linear trend (Figure 2.10-B), which can be used to validate the concentration of SDS determined by Raman microscopy in bulk solutions between 4–32 wt% SDS (Equation 2.5).

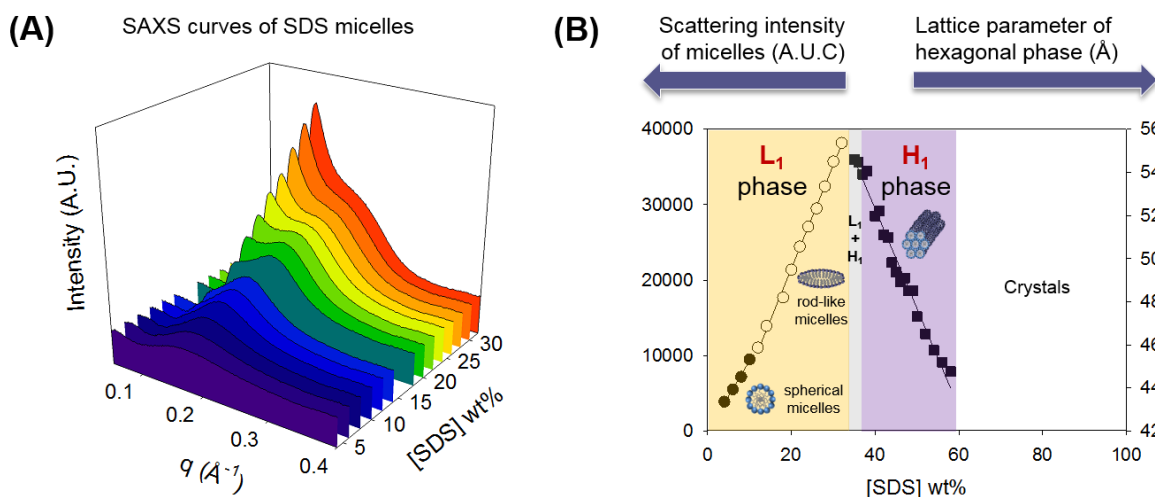


Figure 2.10 Quantifying the concentration of SDS by synchrotron SAXS in solutions where polyDADMAC is absent or undetectable. Scattering curves of micellar (L_1) phase present between 4–32 wt% SDS (A), where the area under the curve is plotted against concentration (B). In addition, the lattice parameter of hexagonal phases formed across SDS–polyDADMAC interfaces can be used to determine the concentration of SDS between 35–58 wt% in regions where polyDADMAC is absent or undetectable. Coloured regions highlight the presence of SDS micelles (L_1 –yellow), coexisting micellar and hexagonal phases (L_1+H_1 –grey), and hexagonal phases only (H_1 –purple) in the SDS/water binary phase diagram (B). The micellar-to-hexagonal phase boundary is superimposed on the SDS calibration curves to depict the phase behaviour of SDS with varying water content.

In contrast, the lattice parameter calculated for the hexagonal phases formed at higher SDS concentrations decreased proportionally with increasing surfactant concentration (Figure 2.10-B). The linear regression fitted for this data set can be employed to interpolate the concentration of SDS in bulk polymer-free regions where hexagonal phase exists (Equation 2.6).

Water

As previously mentioned, the area occupied by water in a cross-section of the hexagonal phase, which is assumed to correlate with the volume fraction of water in the hexagonal phase, can be calculated using the lattice parameter of the hexagonal phase, which varies systematically with water content when measured experimentally in Figure 2.10-B. Consequently, the concentration of water can be interpolated from the approximately linear calibration curve generated for the SDS solutions prepared between 35–58 wt% in Figure 2.11.

This method is valid to quantify the concentration of water for any hexagonal phase that may arise across surfactant–polymer interfaces in the absence or presence of polymer present between 42–65 wt% water (Equation 2.10). The one exception would be the existence of other mesophases, in which case the number of water molecules associated with the additional liquid crystalline structure would not be accounted for.

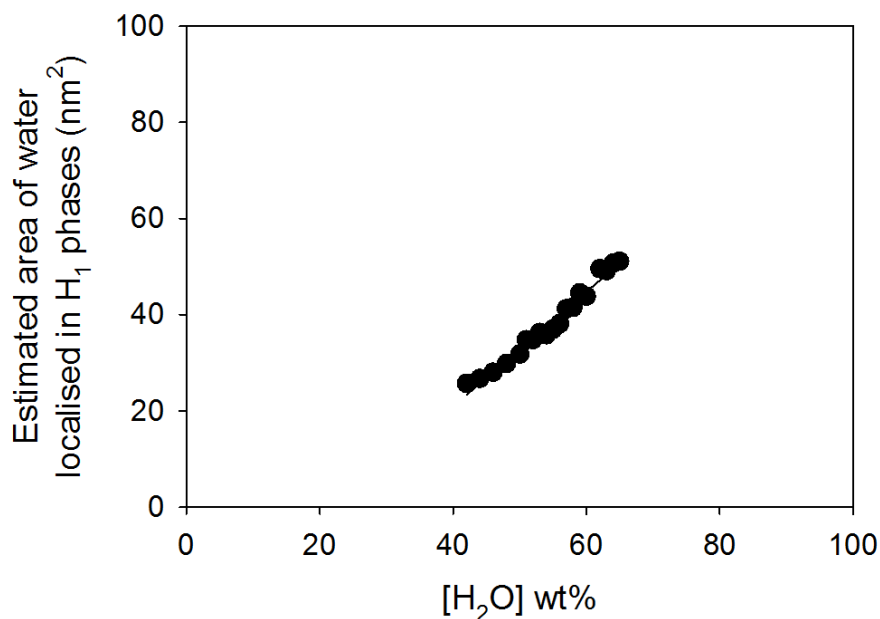


Figure 2.11 Quantifying the concentration of water from the lattice parameter of hexagonal phases formed across SDS–polyDADMAC interfaces based on the model depicted in Schematic 2.9. The calibration curve shown above was generated from the data acquired with synchrotron SAXS, which correlates the calculated area of water molecules contained in the liquid crystalline structure from the lattice parameter with the localised concentration of water within hexagonal (H₁) phases.

Table 2.4 Summary of the calibration curves generated to determine the concentrations of polyDADMAC, SDS, and water across SDS–polyDADMAC interfaces by Raman microscopy (n = 3) and synchrotron SAXS.

Standard curve	Technique	Related figure	Valid concentration range (wt%)	Equation No.	Linear regression	R ²
PolyDADMAC	Raman	Figure 2.7	2–50	2.3	$y = 6824.9x + 11986$	0.998
SDS	Raman	Figure 2.7	4–30	2.4	$y = 5565.7x + 613.47$	0.983
	SAXS	Figure 2.10	4–32	2.5	$y = 1251x + 2871.9$	0.993
	SAXS	Figure 2.10	35–58	2.6	$y = -0.4612x + 7.074$	0.981
Water	Raman	Figure 2.8 (polyDADMAC)	40–98	2.7	$y = 109957x + 1000000$	0.902
	Raman	Figure 2.8 (SDS)	60–95	2.8	$y = 111123x - 1000000$	0.732
	Raman	Figure 2.8 (1,4-dioxane)	0–100	2.9	$y = 117471x - 413603$	0.980
	SAXS	Figure 2.11	42–65	2.10	$y = 1.1924x + 26.765$	0.975
PolyDADMAC– to–SDS molar charge ratio	Raman	Figure 2.9	N/A	2.11	$y = 0.8254x + 0.0237$	0.870

2.6 Discussion

2.6.1 Probing Structures Across Surfactant–Polymer Interfaces

2.6.1.1 *Imaging Birefringent Materials*

Crossed-polarised light microscopy enabled visualisation of the growth of distinct bands across the SDS–polyDADMAC interface. The appearance of regions displaying dissimilar birefringent textures may indicate the presence of either different types of mesophases or the same nanostructure with varying internal dimensions.

A limitation of this technique is that the intensity of birefringence exhibited by anisotropic materials does not necessarily correlate with the amount of liquid crystalline structure formed. For example, a white coacervate (precipitate or complex salt) is often formed from the reaction between oppositely charged solutions of surfactant and polymer molecules.^{41, 42} The opacity or thickness of the resulting material formed may interfere with the amount of light transmitted, and consequently anisotropic mesophases may not appear to be particularly birefringent. This was demonstrated when the structures existing within the middle isotropic band visualised across the SDS–polyDADMAC interface (Figure 2.5) with CPLM was identified as hexagonal phase (Figure 2.6–C) with synchrotron SAXS. In addition, it is difficult to identify the presence of coexisting liquid crystalline structures with a crossed-polarised light microscope. Various mesophases that form across surfactant–polymer interfaces can be distinguished by performing line scans with synchrotron SAXS.

2.6.1.2 *Spatially Resolved SAXS Profiles with a Synchrotron Source*

Spatially resolved structural information across the surfactant–polymer interface was achieved through the functional capabilities of the Australian Synchrotron SAXS/WAXS

beamline.⁴³ We believe this to be the first time such an approach has been taken to study structure formation across surfactant–polymer interfaces. The spatial resolution (100 μm) was limited by the beam size, which depends on the type and size of pinholes and slits employed, while the high flux of X-rays allowed time–resolved collection of data with high resolution in comparison to a bench–top SAXS instrument.⁴³ While greater spatial resolution may be obtained on a microfocus beamline at a different synchrotron facility, the features studied here spanned millimetre dimensions, meant that it is unlikely that additional information about phase structures was missed as a result of the spatial resolution.

The evolution of structures developed across surfactant–polymer interfaces can be attributed to changes in composition, where the increase in the local concentrations of surfactant or polymer would dictate which mesophases are formed (Figure 2.6). Svensson *et al.* demonstrated that increasing the concentration of polyelectrolyte in a mixture of complex salt/water/polyelectrolyte lead to unstructured aggregates.⁴⁴ While increasing the concentration of surfactant resulted in the formation of more ordered and/or compact structures.⁴⁴ Thus, the phase behaviour displayed across such interfaces would be a reflection of the phase changes described on a ternary phase diagram as the composition changes.

2.6.2 Determining Composition Across SDS–PolyDADMAC Interfaces

2.6.2.1 Advantages and Disadvantages of Raman Microscopy

Raman microscopy was ideal for measurement of surfactant and polymer concentrations at low concentrations in isolation. The spot size for the Raman microscope was approximately 10 μm , meaning that the spatial resolution of the SAXS experiments was limiting in this regard, not the microscope. However, during the development and validation

of calibration curves by this technique several limitations were revealed as an approach to quantify the concentrations of polyDADMAC, SDS, and water across these interfaces.

Raman microscopy proved to be useful in measuring the concentration of polyDADMAC (in solutions where SDS is absent or undetectable) and SDS at low concentrations, however above 38 wt% SDS, the change in intensity with change in concentration of SDS did not follow Beer's Law due to the formation of hexagonal phase.⁴⁵ Since the packing of the SDS molecules differ significantly between the self-assembly of micellar aggregates to more highly ordered liquid crystalline structures with an increase in concentration, so too do their optical properties. A change in the polarisation of the sample in turn influences the Raman intensity measured by the spectrometer, which explains the randomness observed for anisotropic materials. Therefore, the values interpolated from the use of the linear regression generated for SDS (Equation 2.4) would be unreliable in the presence of hexagonal phase, which is one of the disadvantages of Raman microscopy. Further comments can be made in relation to the applicability of this method and other important factors that should be considered when interpreting the data obtained by this technique.

Firstly, a minor source of error in measuring the Raman intensity of samples could be associated with the thickness of the glass across each flat cell. The inVia confocal Raman microscope enables acquisition of cross-sections of materials, so the spatial resolution in the z-direction is very important. If thickness of the glass differs slightly across the flat cell, a true measurement of the components across the SDS–polyDADMAC interface may not be obtained during a line scan at a fixed z-position.

Secondly, it is well known that the counterions of the surfactant and polyelectrolyte are released as simple salts upon interaction between the oppositely charged species, where the increase in entropy of the systems favours the formation of highly ordered structures.^{8, 46-}

⁵⁰ It is assumed that the concentration of sodium chloride released upon contact of solutions of SDS and polyDADMAC is very small in comparison to the concentrations of SDS and polyDADMAC across the interface. Therefore, the concentration of salt produced as a result of structure formation at the interface was not measured because its quantity can be considered negligible when studying the phase behaviour across these interfaces.

Thirdly, it has been reported that the strength of hydrogen bonding of water molecules with ions in solution may cause shifts in the frequency of the characteristic stretching band for water in the Raman spectrum.^{51–55} As a result, a significant error may be associated with measuring the area under the curve of a peak if there are slight differences in the lower and upper limits of the Raman shift assigned for O–H bonds (i.e. if it deviates from 3030–3770 cm^{-1} , Figure 2.2 and Figure 2.3), which would be attributed to the presence of different ionic species or mesophases in solution. The calibration curve comparing the Raman intensities obtained for varying concentrations of water prepared with either polyDADMAC, SDS, or 1,4-dioxane clearly highlights the variance in the values generated by Raman microscopy for standard solutions with known water concentrations (Figure 2.8). As a guide to follow trends in the water content across SDS–polyDADMAC interfaces, the linear regression developed for quantifying the concentration of water (in solutions of 1,4-dioxane, Equation 2.9) will be employed to measure the content of water in the initial bulk solutions (distance furthest away from the origin). Moreover, since this technique has been demonstrated to deliver unreliable information pertaining to the amount of water found locally across nanostructured interfaces, data by this approach will intentionally be omitted when mapping the composition across SDS–polyDADMAC interfaces.

It has been established that it is possible to detect the vibrational bonds of certain chemical species present within a sample using Raman microscopy. However, it is still

uncertain as to whether the molecules exist freely in solution or associated with the oppositely charged counterpart. Certainly SAXS can provide information on the structures formed at corresponding positions across the interface, but it is unknown if the composition determined locally constitutes the entire mesophases identified or if the excess component is present concurrently with the existing nanostructure. Furthermore, it becomes even more difficult to discriminate how much of each component participates in the self-assembly of coexisting mesophases. Consequently in coming chapters, the focus will be on understanding (i) the relationship between structure and composition across SDS–polyDADMAC interfaces, (ii) the distribution of molecules across SDS–polyDADMAC interfaces, and (iii) determining whether equilibrium structures are formed across SDS–polyDADMAC interfaces.

Finally, as discussed earlier, the formation of hexagonal phase across the SDS–polyDADMAC interface may significantly change the Raman signal acquired resulting in an inaccurate measurement of the real concentration of the molecules of interest. Instead of using the absolute area under the curve measured for the peaks assigned to quantify the concentrations of SDS and polyDADMAC across the interface, the composition can alternatively be presented as the polyDADMAC-to-SDS molar charge ratio. Since the composition of bulk aqueous mixtures of SDS and polyDADMAC is known and can also be expressed in regards to their polyDADMAC-to-SDS molar charge ratio, the lattice parameter of the mesophases existing at apparent equilibrium can be compared to the hexagonal phases characterised across SDS–polyDADMAC interfaces with synchrotron SAXS (Flowchart 2.1).

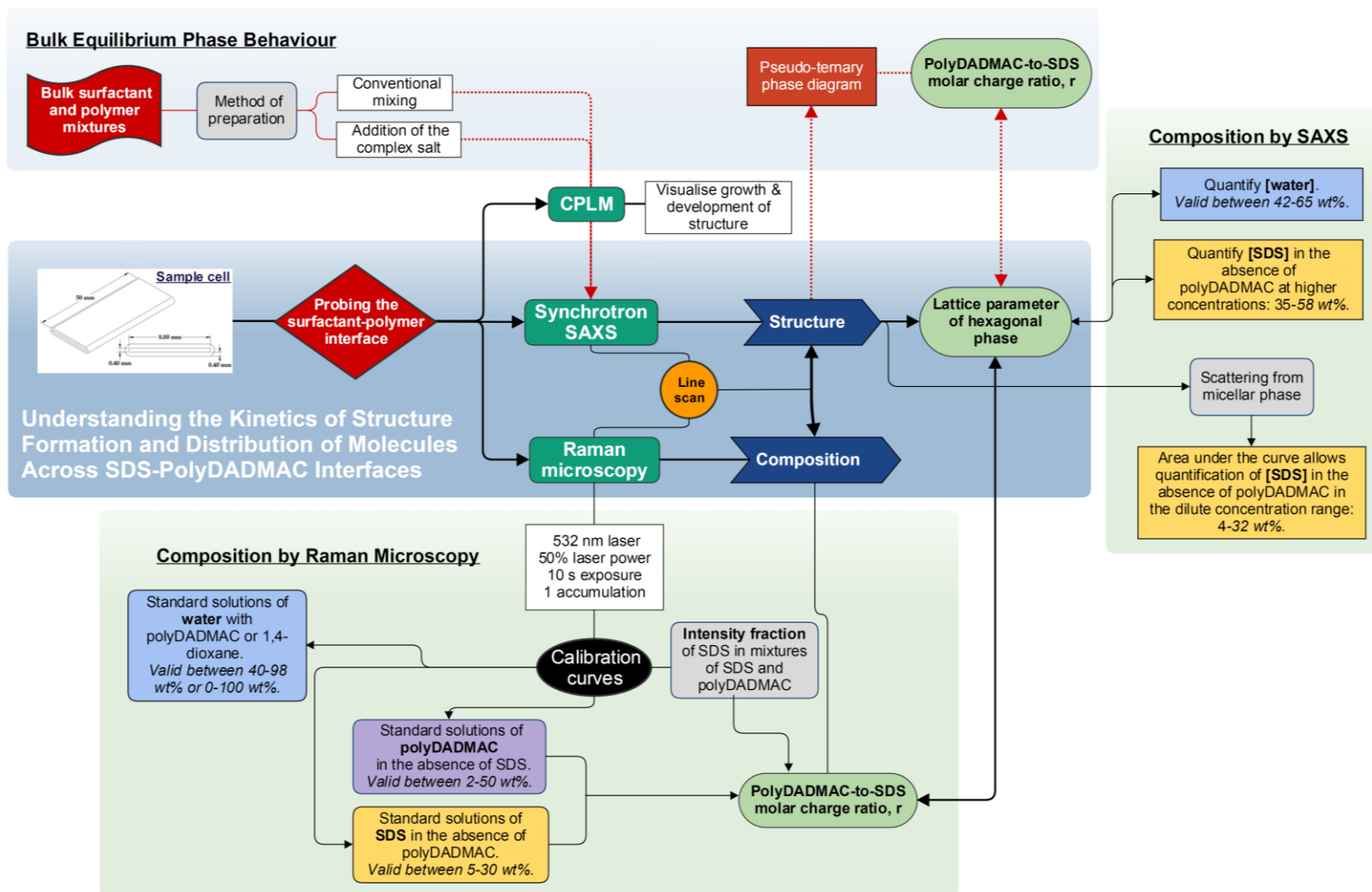
2.6.2.2 Using SAXS to Interpret Composition

The phase behaviour displayed at low concentrations of SDS was in agreement with the spherical-to-rod-like transition of SDS micelles induced by the addition of salt,⁵⁶⁻⁵⁹ where

spherical micelles exist between 4–10 wt% SDS and rod-like micelles formed between 12–32 wt% SDS (Figure 2.10). Furthermore, the shape of the SAXS curves can act as a guide to predict the concentration range of SDS present in solution and its preferred geometry in regions across the SDS–polyDADMAC interface where there is still some uncertainty from the data obtained with Raman microscopy (Flowchart 2.1).

In addition to enabling identification of nanostructures formed across surfactant–polymer interfaces, synchrotron SAXS also provides a means for quantifying the concentration of SDS in bulk binary micellar solutions and hexagonal phases, as well as the concentration of water in hexagonal phases. Essentially this technique can be utilised in combination with Raman microscopy to attain similar information. However, it should be noted that this approach assumes that all the surfactant molecules accounted for are either associated into micelles or participate in the formation of hexagonal phase. In other words, the method for analysing the SAXS data described in this chapter cannot distinguish between the different states SDS can exist as, namely free, micelles, or polymer-bound.

It has been demonstrated that the scattering data obtained from synchrotron SAXS can allow the composition across SDS–polyDADMAC interfaces to be determined. However, there are still limitations associated with the methodology described in this chapter. Firstly, as mentioned earlier, polymers scatter X-rays poorly, thus its concentration cannot be quantified by this approach. Secondly, slight differences in the energy of the X-ray beam employed during each beamtime may result in significant variances in the scattering intensities achieved. As a consequence, a less accurate concentration of surfactant present locally across the interface will be determined since the value is correlated with the area under the curve measured for micellar solutions. This error can also arise from poor background subtraction.



Flowchart 2.1 Summary of the methodology developed to study the equilibrium phase behaviour and the structure-composition relationship across SDS-polyDADMAC interfaces.

2.7 Conclusions

A novel approach was developed to study the kinetics of structure formation across oppositely charged surfactant–polymer interfaces. Line scans at 100 μm steps performed by synchrotron small angle X-ray scattering and Raman microscopy can spatially resolve information on the internal structure of mesophases formed and the concentrations of polyDADMAC, SDS, and water across surfactant–polymer interfaces. Together, these techniques will be employed to study changes in structure and composition across SDS–polyDADMAC interfaces over time as the nanostructures approach equilibrium or become kinetically trapped at nonequilibrium.

2.8 References

1. Thalberg, K.; Lindman, B.; Karlstroem, G., *Phase Behaviour of a System of Cationic Surfactant and Anionic Polyelectrolyte: The Effect of Salt*. J. Phys. Chem. 1991, 95, 6004–6011.
2. Goddard, E. D.; Leung, P. S., *Studies of Gel Formation, Phase Behaviour and Surface Tension in Mixtures of a Hydrophobically Modified Cationic Cellulose Polymer and Surfactant*. Colloid Surface. 1992, 65, 211–219.
3. Lindman, B.; Khan, A.; Marques, E.; Piculell, L.; Miguel, M. G.; Thalberg, K., *Phase Behaviour of Polymer–Surfactant Systems in Relation to Polymer–Polymer and Surfactant–Surfactant Mixtures*. Pure & Appl. Chem. 1993, 65, 953–956.
4. Hellebust, S.; Blokhuis, A. M.; Nilsson, S., *Associative and Segregative Phase Behaviour of a Mixed Aqueous Cationic Surfactant and Anionic Hydrophilic Polymer System*. Colloid Surface Physicochem. Eng. Aspect. 2004, 243, 133–138.
5. Li, D.; Kelkar, M. S.; Wagner, N. J., *Phase Behaviour and Molecular Thermodynamics of Coacervation in Oppositely Charged Polyelectrolyte/Surfactant Systems: A Cationic Polymer JR 400 and Anionic Surfactant SDS Mixture*. Langmuir. 2012, 28, 10348–10362.
6. Thalberg, K.; Lindman, B.; Karlstroem, G., *Phase Diagram of a System of Cationic Surfactant and Anionic Polyelectrolyte: Tetradecyltrimethylammonium Bromide–Hyaluronan–Water*. J. Phys. Chem. 1990, 94, 4289–4295.
7. Thalberg, K.; Lindman, B., *Segregation in Aqueous Systems of a Polyelectrolyte and an Ionic surfactant*. Colloid Surface Physicochem. Eng. Aspect. 1993, 76, 283–288.
8. Leonard, M. J.; Strey, H. H., *Phase Diagrams of Stoichiometric Polyelectrolyte–Surfactant Complexes*. Macromolecules. 2003, 36, 9549–9558.
9. Courtois, J.; Berret, J. F., *Probing Oppositely Charged Surfactant and Copolymer Interactions by Isothermal Titration Microcalorimetry*. Langmuir. 2010, 26, 11750–11758.
10. Lapitsky, Y.; Kaler, E. W., *Formation of Surfactant and Polyelectrolyte Gel Particles in Aqueous Solutions*. Colloids Surf., A. 2004, 250, 179–187.

11. Babak, V. G.; Merkovich, E. A.; Desbrières, J.; Rinaudo, M., *Formation of An Ordered Nanostructure in Surfactant–Polyelectrolyte Complexes Formed by Interfacial Diffusion*. *Polym. Bull.* 2000, 45, 77–81.
12. Babak, V. G.; Merkovich, E. A.; Galbraikh, L. S.; Shtykova, E. V.; Rinaudo, M., *Kinetics of Diffusionally Induced Gelation and Ordered Nanostructure Formation in Surfactant–Polyelectrolyte Complexes Formed at Water/Water Emulsion Type Interfaces*. *Mendeleev Commun.* 2000, 10, 94–95.
13. Lapitsky, Y.; Kaler, E. W., *Formation and Structural Control of Surfactant and Polyelectrolyte Gels*. *Colloids Surf., A.* 2006, 282–283, 118–128.
14. Lapitsky, Y.; Eskuchen, W. J.; Kaler, E. W., *Surfactant and Polyelectrolyte Gel Particles that Swell Reversibly*. *Langmuir.* 2006, 22, 6375–6379.
15. Mironov, A. V.; Starodoubtsev, S. G.; Khokhlov, A. R.; Dembo, A. T.; Dembo, K. A., *Effect of Chemical Nature of 1,1–Salt on Structure of Polyelectrolyte Gel–Surfactant Complexes*. *J. Phys. Chem. B.* 2001, 105, 5612–5617.
16. Mezei, A.; Mészáros, R.; Varga, I.; Gilányi, T., *Effect of Mixing on the Formation of Complexes of Hyperbranched Cationic Polyelectrolytes and Anionic Surfactants*. *Langmuir.* 2007, 23, 4237–4247.
17. Naderi, A.; Claesson, P. M.; Bergström, M.; Dédinaite, A., *Trapped Non–Equilibrium States in Aqueous Solutions of Oppositely Charged Polyelectrolytes and Surfactants: Effects of Mixing Protocol and Salt Concentration*. *Colloids and Surfaces A: Physicochem. Eng. Aspects.* 2005, 253, 83–93.
18. Naderi, A.; Claesson, P. M., *Association between Poly(vinylamine) and Sodium Dodecyl Sulfate: Effects of Mixing Protocol, Blending Procedure, and Salt Concentration*. *J. Dispersion Sci. Technol.* 2005, 26, 329–340.
19. Pojják, K.; Mészáros, R., *Novel Self–Assemblies of Oppositely Charged Polyelectrolytes and Surfactants in the Presence of Neutral Polymer*. *Langmuir.* 2009, 25, 13336–13339.
20. Hoffmann, I.; Heunemann, P.; Prévost, S.; Schweins, R.; Wagner, N. J.; Gradzielski, M., *Self–Aggregation of Mixtures of Oppositely Charged Polyelectrolytes and Surfactants*

- Studied by Rheology, Dynamic Light Scattering and Small-Angle Neutron Scattering.* Langmuir. 2011, 27, 4386–4396.
21. Caffrey, M., *A Lyotrope Gradient Method for Liquid Crystal Temperature–Composition–Mesomorph Diagram Construction using Time–Resolved X-ray Diffraction.* Biophys. J. 1989, 55, 47–52.
 22. Liu, C. K.; Warr, G. G., *Hexagonal Closest–Packed Spheres Liquid Crystalline Phases Stabilised by Strongly Hydrated Counterions.* Soft Matter. 2014, 10, 83–87.
 23. Boyd, B. J.; Dong, Y.–D.; Rades, T., *Nonlamellar Liquid Crystalline Nanostructured Particles: Advances in Materials and Structure Determination.* J. Liposome Res. 2009, 19, 12–28.
 24. Laughlin, R. G.; Lynch, M. L.; Marcott, C.; Munyon, R. L.; Marrer, A. M.; Kochvar, K. A., *Phase Studies by Diffusive Interfacial Transport Using Near–Infrared Analysis for Water (DIT–NIR).* J Phys Chem B. 2000, 104, 7354–7362.
 25. Laughlin, R. G.; Munyon, R. L., *Diffusive Interfacial Transport: A New Approach to Phase Studies.* J Phys Chem. 1987, 91, 3299–3305.
 26. Ricoul, F.; Dubois, M.; Zemb, T.; Heck, M.–P.; Vandais, A.; Plusquellec, D.; Rico–Lattes, I.; Diat, O., *An Efficient Method To Determine Isothermal Ternary Phase Diagrams Using Small–Angle X–ray Scattering.* J. Phys. Chem. B. 1998, 102, 2769–2775.
 27. Ferraro, J. R.; Nakamoto, K.; Brown, C. W., *Chapter 1 – Basic Theory.* In *Introductory Raman Spectroscopy (Second Edition)*, Brown, J. R. F. N. W., Ed. Academic Press: San Diego, 2003; pp 1–94.
 28. Hyde, S., *Chapter 16– Identification of Lyotropic Liquid Crystalline Mesophases.* In *Handbook of Applied Surface and Colloid Chemistry*, Holmberg, K., Ed. John Wiley & Sons, Ltd. 2001 pp 299–332.
 29. Park, S.–H.; Wei, S.; Mizaikoff, B.; Taylor, A. E.; Favero, C. d.; Huang, C.–H., *Degradation of Amine–Based Water Treatment Polymers During Chloramination as N–nitrosodimethylamine (NDMA) Precursors.* Environ. Sci. Technol. 2009, 43, 1360–1366.

30. Cazzolli, G.; Caponi, S.; Defant, A.; Gambi, C. M. C.; Marchetti, S.; Mattarelli, M.; Montagna, M.; Rossi, B.; Rossi, F.; Viliani, G., *Aggregation Processes in Micellar Solutions: A Raman Study*. J. Raman Spectrosc. 2012, 43, 1877–1883.
31. Cross, P. C.; Burnham, J.; Leighton, P. A., *The Raman Spectrum and the Structure of Water*. J. Am. Chem. Soc. 1937, 59, 1134–1147.
32. Nizri, G.; Magdassi, S.; Schmidt, J.; Cohen, Y.; Talmon, Y., *Microstructural Characterisation of Micro- and Nanoparticles Formed by Polymer–Surfactant Interactions*. Langmuir. 2004, 20, 4380–4385.
33. Sokolov, E.; Yeh, F.; Khokhlov, A.; Grinberg, V. Y.; Chu, B., *Nanostructure Formation in Polyelectrolyte–Surfactant Complexes*. J. Phys. Chem. B. 1998, 102, 7091–7098.
34. Chu, B.; Yeh, F.; Sokolov, E. L.; Starodoubtsev, S. G.; Khokhlov, A. R., *Interaction of Slightly Cross-Linked Gels of Poly(diallyldimethylammonium chloride) with Surfactants*. Macromolecules. 1995, 28, 8447–8449.
35. Sokolov, E. L.; Yeh, F.; Khokhlov, A.; Chu, B., *Nanoscale Supramolecular Ordering in Gel–Surfactant Complexes: Sodium Alkyl Sulfates in Poly(diallyldimethylammonium chloride)*. Langmuir. 1996, 12, 6229–6234.
36. Tsu, R.; Gonzalez–Hernandez, J.; Chao, S. S.; Lee, S. C.; Tanaka, K., *Critical Volume Fraction of Crystallinity for Conductivity Percolation in Phosphorus–Doped Si:F:H Alloys*. Appl. Phys. Lett. 1982, 40, 534–535.
37. Tanford, C., *Micelle Shape and Size*. J. Phys. Chem. 1972, 76, 3020–3024.
38. Tanford, C., *Theory of Micelle Formation in Aqueous Solutions*. J. Phys. Chem. 1974, 78, 2469–2479.
39. Israelachvili, J. N.; Mitchell, D. J.; Ninham, B. W., *Theory of Self-Assembly of Hydrocarbon Amphiphiles into Micelles and Bilayers*. J. Chem. Soc., Faraday Trans. 2. 1976, 72, 1525–1568.
40. Ridell, A. *Characterisation of Aqueous Solutions, Liquid Crystals and Solid State of Non-ionic Polymers in Association with Amphiphiles and Drugs*. Uppsala University, Uppsala, 2003.

41. Svensson, A.; Piculell, L.; Cabane, B.; Ilekli, P., *A New Approach to the Phase Behaviour of Oppositely Charged Polymers and Surfactants*. J. Phys. Chem. B. 2002, 106, 1013–1018.
42. Ilekli, P.; Piculell, L.; Tournilhac, F.; Cabane, B., *How to Concentrate an Aqueous Polyelectrolyte/Surfactant Mixture by Adding Water*. J. Phys. Chem. B. 1998, 102, 344–351.
43. Kirby, N. M.; Mudie, S. T.; Hawley, A. M.; Cookson, D. J.; Mertens, H. D. T.; Cowieson, N.; Samardzic-Boban, V., *A Low-Background-Intensity Focusing Small-Angle X-ray Scattering Undulator Beamline*. J Appl. Crystallogr. 2013, 46, 1670–1680.
44. Svensson, A.; Norrman, J.; Piculell, L., *Phase Behaviour of Polyion–Surfactant Ion Complex Salts: Effects of Surfactant Chain Length and Polyion Length*. J. Phys. Chem. B. 2006, 110, 10332–10340.
45. Kékicheff, P., *Phase Diagram of Sodium Dodecyl Sulfate–Water System. 2. Complementary Isoplethal and Isothermal Phase Studies*. J. Colloid Interface Sci. 1989, 131, 133–152.
46. Wagner, K.; Harries, D.; May, S.; Kahl, V.; Rädler, J. O.; Ben-Shaul, A., *Direct Evidence for Counterion Release Upon Cationic Lipid–DNA Condensation*. Langmuir. 1999, 16, 303–306.
47. Hsu, W.-L.; Li, Y.-C.; Chen, H.-L.; Liou, W.; Jeng, U. S.; Lin, H.-K.; Liu, W.-L.; Hsu, C.-S., *Thermally-Induced Order–Order Transition of DNA–Cationic Surfactant Complexes*. Langmuir. 2006, 22, 7521–7527.
48. Wang, H.; Wang, Y.; Yan, H.; Zhang, J.; Thomas, R. K., *Binding of Sodium Dodecyl Sulfate with Linear and Branched Polyethyleneimines in Aqueous Solution at Different pH Values*. Langmuir. 2006, 22, 1526–1533.
49. Ranganathan, S.; Kwak, J. C. T., *Effect of Polymer Charge Density on the Phase Behavior of Sodium Poly(acrylate-co-acrylamide)–DTAB Systems*. Langmuir. 1996, 12, 1381–1390.
50. Merta, J.; Torkkeli, M.; Ikonen, T.; Serimaa, R.; Stenius, P., *Structure of Cationic Starch (CS)/Anionic Surfactant Complexes Studied by Small-Angle X-ray Scattering (SAXS)*. Macromolecules. 2001, 34, 2937–2946.

51. Ohno, K.; Okimura, M.; Akai, N.; Katsumoto, Y., *The Effect of Cooperative Hydrogen Bonding on the OH Stretching–Band Shift for Water Clusters Studied by Matrix–Isolation Infrared Spectroscopy and Density Functional Theory*. Phys. Chem. Chem. Phys. 2005, 7, 3005–3014.
52. Leikin, S.; Parsegian, V. A.; Yang, W. H.; Walrafen, G. E., *Raman Spectral Evidence for Hydration Forces between Collagen Triple Helices*. Proc. Natl. Acad. Sci. U. S. A. 1997, 94, 11312–11317.
53. Eisenberg, D.; Kauzmann, W., *The Structure and Properties of Water (Oxford Classic Texts in the Physical Sciences)*. Oxford University Press: 2005.
54. Ahmed, M.; Namboodiri, V.; Singh, A. K.; Mondal, J. A.; Sarkar, S. K., *How Ions Affect the Structure of Water: A Combined Raman Spectroscopy and Multivariate Curve Resolution Study*. J Phys. Chem. B. 2013, 117, 16479–16485.
55. Ahmed, M.; Namboodiri, V.; Singh, A. K.; Mondal, J. A., *On the Intermolecular Vibrational Coupling, Hydrogen Bonding, and Librational Freedom of Water in the Hydration Shell of Mono– and Bivalent Anions*. J. Chem. Phys. 2014, 141, 164708.
56. Zhang, J.; Ge, Z.; Jiang, X.; Hassan, P. A.; Liu, S., *Stopped–Flow Kinetic Studies of Sphere–to–Rod Transitions of Sodium Alkyl Sulfate Micelles Induced by Hydrotropic Salt*. J. Colloid Interface Sci. 2007, 316, 796–802.
57. Hassan, P. A.; Raghavan, S. R.; Kaler, E. W., *Microstructural Changes in SDS Micelles Induced by Hydrotropic Salt*. Langmuir. 2002, 18, 2543–2548.
58. Hassan, P. A.; Sawant, S. N.; Bagkar, N. C.; Yakhmi, J. V., *Polyaniline Nanoparticles Prepared in Rodlike Micelles*. Langmuir. 2004, 20, 4874–4880.
59. Hassan, P. A.; Fritz, G.; Kaler, E. W., *Small Angle Neutron Scattering Study of Sodium Dodecyl Sulfate Micellar Growth Driven by Addition of a Hydrotropic Salt*. J. Colloid Interface Sci. 2003, 257, 154–162.

Chapter 3: *Investigation of Structure Formation
Across the SDS–PolyDADMAC Interface*

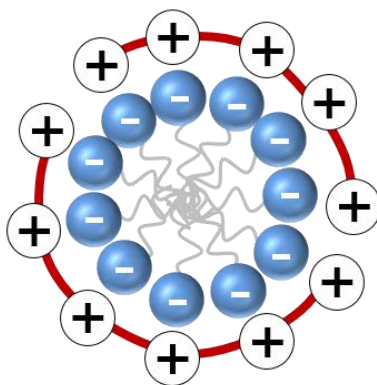
3. Investigation of Structure Formation Across the SDS–PolyDADMAC Interface

3.1 Introduction

Oppositely charged surfactant and polymer systems have been a growing field of research since their emergence in the late 1970s.¹ Early studies revolved around understanding their mechanism of interaction in bulk aqueous mixtures by measuring changes in surface tension,³⁻⁶ rheology,^{7,8} enthalpy,⁹⁻¹¹ particle size,¹²⁻¹⁴ zeta potential,¹⁵ and conductivity^{16, 17} as a function of concentration. Moreover, factors influencing the equilibrium phase behaviour of nanostructures formed in such systems have also been studied for exploitation in various industrial¹⁸⁻²² and pharmaceutical²³⁻²⁷ applications.

The phase behaviour demonstrated by bulk aqueous mixtures of oppositely charged surfactants and polymers are generally illustrated as ternary phase diagrams, however a more recent approach has been developed to account for the presence of four components within the system. Specifically, these consist of the surfactant ion and polyion, and their corresponding counterions. In order to study the phase behaviour of a true ternary system Piculell *et al.* examined the ‘complex salt’.^{28, 29} The complex salt is the solid precipitate formed from the reaction between the surfactant ion and the polyion (Schematic 3.1). Copious washing of the product ensures removal of the simple salts released after complexation. There is an assumption that the mesophases formed with the complex salt are at equilibrium, therefore, this approach allows for a more accurate investigation into how the addition of either the surfactant ion or polyion influences the equilibrium phase behaviour of the complex salt in aqueous mixtures. It would be impractical to introduce the complex salt as an

additional component into formulations as a means to favour the formation of kinetically stable equilibrium structures. However, it is unknown if the complex salt is formed *in situ* when bulk aqueous mixtures of surfactant and polymer are prepared employing the conventional method, which typically involves dropwise addition of one solution into the other followed by some form of mixing. Thus, it is hypothesised that employing different methods of preparing samples with the same final composition will yield comparable structures at equilibrium.



Schematic 3.1 Illustration of an oppositely charged surfactant/polymer complex salt which is comprised of a single surfactant ion per polyion charge and the absence of other ions. Adapted from Svensson *et al.*²

Although equilibrium structures often arise upon mixing of oppositely charged surfactant and polymer solutions, the existence of kinetically trapped nonequilibrium structures have also been reported.³⁰⁻³³ The order of addition and the rate of mixing of the two components have been shown to significantly influence the structural characteristics of the complexes formed in solution.^{31, 34-36} Furthermore, the molar concentration of molecules in solution is known to dictate its viscosity,^{7, 17} which can impact the diffusivity of the molecules through the mixture and the number of associations formed between the oppositely

charged species in solution. The mesophase existing in solution also creates a barrier through which the molecules must pass in order to form further interactions, which is determined by the degree of order and rheology of the mesophases formed.³⁷ All of these factors are important in rationalising the formation of equilibrium or nonequilibrium structures in aqueous mixtures of oppositely charged surfactants and polymers.

Extensive research has been performed on bulk aqueous mixtures of oppositely charged surfactants and polymers, however little is known about the kinetics of structure formation across surfactant–polymer interfaces. Babak *et al.* were one of the earliest to examine the formation of an ordered structure at the interface between solutions of an anionic surfactant and a cationic polymer.³⁸ Babak *et al.* showed the formation of bead-like gels after the dropwise addition of chitosan into a solution of SDS. Over time, a lamellar phase evolved from the outer surface of the gel beads towards the inner core. The rate of structure formation was limited by the frontal diffusion of SDS molecules, which was calculated based on measuring the thickness of the structure formed at the interface as a function of time. It was indicated that the movement of SDS molecules into the chitosan gel resulted in the self-assembly of an ordered structure at the interface. The diffusion of chitosan within the gel beads was not measured. However, since the final thickness of the structured layer within the beads was found to correlate with the total mass of chitosan present in the droplet, it can be assumed that the polymer molecules must have diffused toward the outer surface of the bead to complex with the incoming SDS molecules, thus resulting in gel beads with a water rich or hollow core. Lapitsky *et al.* also reported the formation of gel particles upon dropwise addition of a solution of the partially cross-linked cationic polymer, JR-400, into a bath of mixed surfactant solution, where the structures formed across the surfactant–polymer interface comprised of a dense shell, a porous interstitial layer, and a homogeneous core.³⁹ Overall,

these findings demonstrate that the diffusivity of molecules within the initial bulk solutions can limit the rate of structure formation at the interface. The local interfacial composition and inherent viscosity of the existing nanostructures is hypothesised to significantly influence the diffusion of these molecules across the surfactant–polymer interface, and if the structures reach equilibrium or become trapped in a nonequilibrium state.

Many combinations of oppositely charged surfactants and polymers have been studied. One example is the industrially relevant system comprising of the anionic surfactant, sodium dodecyl sulphate (SDS), and the cationic polymer, poly(diallyldimethylammonium chloride) (polyDADMAC) (Figure 3.1). Both are commonly employed in hair care products.

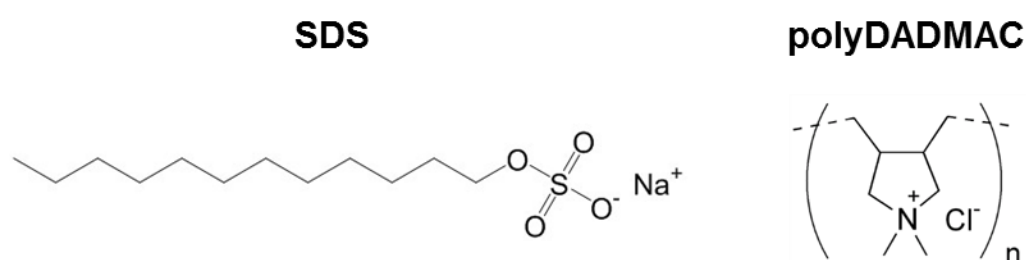
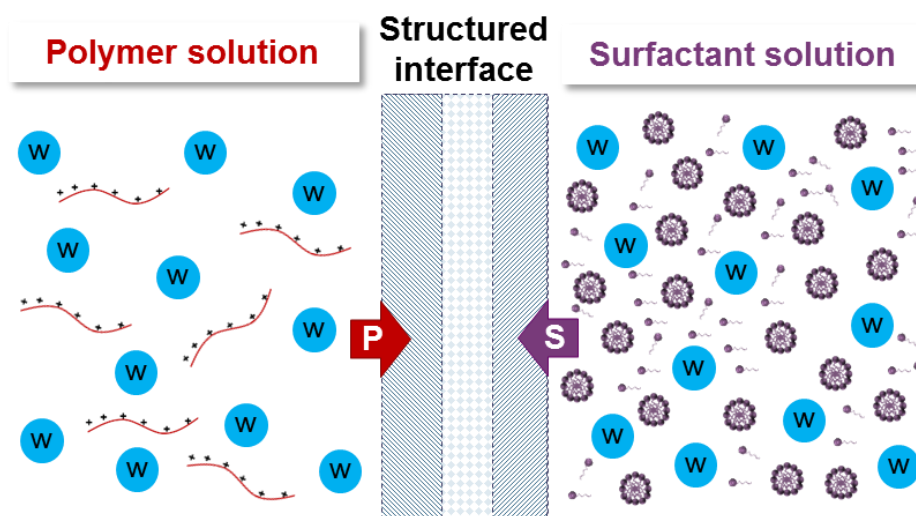


Figure 3.1 Chemical structures of sodium dodecyl sulphate (SDS) and poly(diallyldimethylammonium chloride) (polyDADMAC).

Formation of highly ordered structures, specifically hexagonal phase, has been identified in bulk aqueous mixtures of SDS and polyDADMAC by small angle X-ray scattering, where the scattering intensity of the Bragg reflections at $1:\sqrt{3}:\sqrt{4}:\sqrt{7}\dots$ increased with increasing surfactant concentration.⁴⁰ It has been demonstrated that the melting temperature and the lattice parameter of the nanostructures formed were dependent on the length of the surfactant chain, where the internal dimensions increased proportionally to the number of carbon atoms on the surfactant alkyl chain for similar lattice types.⁴¹ Khokhlov *et al.* studied

the effect of the chemical structure of salts on the structural integrity of the highly ordered structures formed. The complexes Khokhlov *et al.* studied were destroyed when salt ions competed with the surfactant ion. Whereas, the formation of ordered structures was more favourable at intermediate salt concentrations comprised of weakly competitive anions.⁴² The surfactant-to-polymer molar charge ratio has been shown to control the size and zeta potential of SDS and polyDADMAC nanoparticles,⁴³ which in turn was found to dictate the viscosity of the system at a given composition.^{7, 17}

The phase behaviour of systems comprised of SDS and polyDADMAC have been well reported for dispersions and bulk aqueous mixtures, however there is little understanding of the dynamics involved across the SDS–polyDADMAC interface as the system approaches equilibrium. It is anticipated that hexagonal and/or micellar phases will form across the interface when solutions of SDS and polyDADMAC come in to contact as illustrated in Schematic 3.2. The charged species in respective solutions will continue to diffuse across the SDS–polyDADMAC interface as mixing occurs, forming more mesophases until the composition and/or the degree of order within nanostructures existing locally across the interface no longer permits the diffusion of molecules through a given region of material. In other words, the distribution of surfactant, polymer, and water molecules, as well the structures formed across the SDS–polyDADMAC interface are expected to change over time until equilibrium structures form or when they are kinetically trapped in a metastable state.



Schematic 3.2 A model depicting the possible movement of surfactant (S), polymer (P), and water (w) molecules, and the formation of nanostructures across an interface created between a solution of polyDADMAC (left) and a micellar solution of SDS (right).

This chapter studies the equilibrium phase behaviour of systems comprising of SDS and polyDADMAC in concentrated aqueous mixtures and how the method of preparation influences the nanostructures formed, as well as the kinetics of structure formation across the SDS–polyDADMAC interface. The methods previously developed in Chapter 2 were employed to examine changes in structure and composition across the interface over time, and the mesophases formed will be compared to those existing in bulk mixtures at the same composition to determine the presence of equilibrium or nonequilibrium structures across the SDS–polyDADMAC interface.

3.2 Hypotheses and Aims

Hypothesis 1

That the phase behaviour demonstrated by aqueous mixtures of SDS and polyDADMAC will be similar to those prepared with the complex salt.

Hypothesis 2

That the diffusion of surfactant, polymer, and water molecules across the SDS–polyDADMAC interface will occur in both directions.

Hypothesis 3

That the rate of structure formation across the SDS–polyDADMAC interface is dictated by the existing concentration and structure gradients and is diffusion–controlled.

Hypothesis 4

That nanostructures at equilibrium are formed locally across the SDS–polyDADMAC interface.

In order to investigate these hypotheses, the following aims were undertaken:

1. To generate ternary phase diagrams of mixtures of SDS, polyDADMAC, and water prepared by the conventional mixing method or with the complex salt.
2. To identify mesophases formed across the SDS–polyDADMAC interface.
3. To study the rate of structure formation across the SDS–polyDADMAC interface.
4. To quantify the concentrations of SDS, polyDADMAC, and water across the SDS–polyDADMAC interface.
5. To establish the existence of equilibrium and/or nonequilibrium structures across the SDS–polyDADMAC interface.

3.3 Materials

Sodium dodecyl sulphate (SDS, BioXtra, $\geq 99.0\%$) was purchased from Sigma–Aldrich (Sydney, Australia). Poly(diallyldimethylammonium chloride) (polyDADMAC, Merquat™ 100, molecular weight: 1.5×10^5 g/mol) was sourced from Nalco Company (Illinois, United States) and comprised 53.3 % solid and 46.7 % water (standard deviation: $\pm 0.3\%$) as determined by gravimetric analysis ($n = 10$). Merquat™ 100 was dried prior to preparation of polyDADMAC stock solutions to form a waxy solid.

All materials were used without further purification. Milli–Q grade water purified through a Milli–pore system (Billerica, United States) was used throughout the studies.

3.4 Methods

3.4.1 Synthesis of the Complex Salt, PolyDADMADS

The complex salt of SDS and polyDADMAC, poly(diallyldimethylammonium–dodecyl sulphate) (polyDADMADS), was synthesised by utilising the method described by Svensson *et al.*⁴⁴ Briefly, a solution of the polymer (8 g of 0.03 mM polyDADMAC) was added dropwise to a stirred solution of surfactant, which was in excess (992 g of 44 mM SDS), in a plastic beaker. Under these conditions a cloudy homogeneous solution formed, which became clear after 4 hr. Milli–Q water (4.2 L) was added dropwise to the solution whilst stirring which resulted in precipitation of the complex. The gel–like milky dispersion was allowed to sediment overnight, after which the solution was decanted to separate the precipitate from the supernatant. This involved vacuum filtration and centrifugation of the suspension to remove the complex salt from the excess solution. The white precipitate collected was washed with fresh Milli–Q water (3 x 1 L). After the last washing step, the supernatant was removed

and the precipitate was freeze-dried to yield a white gum-like material (4.89 g, ~49 %), which was pulverised to allow ease of handling.

3.4.2 Preparation of Bulk Mixtures

3.4.2.1 Conventional Mixing Protocol

Bulk aqueous mixtures of SDS and polyDADMAC were prepared by weight by utilising the conventional mixing protocol. This involved dropwise addition of the surfactant solution into a solution of polymer to reach the desired sample composition.

3.4.2.2 Employing the Complex Salt, PolyDADMADS

Samples comprising of the complex salt were prepared by dropwise addition of either SDS or polyDADMAC solution of known concentration (wt%) into a glass vial (2 mL) containing the solid polyDADMADS. The total concentration of surfactant, polymer, and water in these mixtures were calculated based on the theoretical moles of surfactant ion and polyion present in the known mass of polyDADMADS incorporated in the system assuming 1:1 charge stoichiometry of the complex salt. Only a selected number of sample mixtures were studied. These compositions represent a region within the ternary phase diagram where interesting structures form *in situ*, hence there would be greater sensitivity in detecting the presences of mesophases in systems comprising of polyDADMADS.

All the samples were mixed with a vortex mixer then manually stirred and left to equilibrate on rollers in a 37 °C incubator oven approximately a month prior to analysis by small angle X-ray scattering to promote homogeneous mixing of the materials and to prevent the formation of hydrated SDS crystals at lower temperatures.⁴⁵⁻⁴⁸

3.4.3 Characterisation of Mesophases in Bulk Mixtures

Identification of the mesophases existing in the bulk mixtures prepared by the conventional mixing method (150 samples) enabled the generation of the SDS/water/polyDADMAC ternary phase diagram for comparison with the phase behaviour exhibited by mixtures prepared with the complex salt (23 samples).

Bulk mixtures were loaded into Nunc™ MicroWell™ 96-Well Microplates from Thermo Scientific (Roskilde, Denmark) and structurally characterised on the SAXS/WAXS beamline at the Australian Synchrotron. Automated static scans were performed with 1 s exposure to an X-ray beam with a wavelength of 1.127 Å (11 keV), with a sample to detector distance of 1431 mm providing a q -range between $0.011 < q < 0.63 \text{ \AA}^{-1}$. The two-dimensional SAXS patterns were acquired using a Pilatus 1M detector (active area 169 x 179 mm² with a pixel size of 172 μm) and integrated into the one-dimensional scattering function $I(q)$ using ScatterBrain.

3.4.4 Studying the Phase Behaviour Across the SDS–PolyDADMAC Interface

The equilibrium phase behaviour displayed across the SDS–polyDADMAC solution interface was examined in this chapter. The concentrations of the bulk solutions were selected based on the phase behaviour exhibited by an industrially relevant oppositely charged surfactant and polymer system studied by Procter and Gamble, which comprised of alkyl ethoxysulphates (AES) and polyDADMAC (Appendix–Figure A3.1). Since the chemical structure of AES closely resembles that of SDS, the composition at which a rich pool of mesophases were identified in a mixture of polyDADMAC, water, and AES was viewed as a suitable starting point. The formation of highly ordered structures was anticipated upon

contact between solutions of 20 wt% SDS and 20 wt% polyDADMAC, therefore the phase behaviour across the SDS–polyDADMAC interface was studied at this composition.

3.4.4.1 Preparation of SDS–PolyDADMAC Interfaces

Samples were prepared as described in Section 2.4.2 (Schematic 2.6). Briefly, the solution of polyDADMAC was drawn half way up from the bottom end of the flat cell by capillary action, after which the surface of the glass was cleaned to ensure a tight seal of the opening with parafilm. The SDS solution was then carefully pipetted into the top opening of the flat cell to create a neat interface, which was marked as the ‘point of origin’. The top was also sealed with parafilm to prevent evaporation and the formation of bubbles.

3.4.4.2 Characterisation of Nanostructures Formed Across the SDS–PolyDADMAC Interface

The growth and development of nanostructures exhibiting birefringence across the SDS–polyDADMAC interface were visualised under a crossed–polarised light microscope (CPLM). For more details, see Section 2.4.3.1.

The mesophases formed across the SDS–polyDADMAC interface at various time points were spatially characterised by small angle X–ray scattering (SAXS) at the Australian Synchrotron. Line scans were performed, collecting SAXS patterns for 1 s at every $100 \mu\text{m} \pm 5 \text{ mm}$ from where the initial interface was created at time zero employing an X–ray beam with a wavelength of 1.13 \AA (11 keV) and a sample to detector distance of 1650 mm providing a q -range between $0.01 < q < 0.65 \text{ \AA}^{-1}$. The lattice parameter of hexagonal phases identified across the SDS–polyDADMAC interface was calculated by using the equation listed in Chapter 2 (Table 2.3).

3.4.4.3 Quantifying the Concentrations of PolyDADMAC, SDS, and Water Across the SDS–PolyDADMAC Interface

Line scans were also performed with a Raman microscope to acquire Raman spectra at 100 μm steps across the SDS–polyDADMAC interface. The calibration curves generated in Chapter 2 (Table 2.4) were employed to determine the concentrations of polyDADMAC, SDS, and water from the area under the curve measured for the corresponding peaks present in the Raman spectra. However, it was revealed that this method resulted in significant error in quantifying the concentrations of water and SDS especially where hexagonal phases formed.

Additional approaches described in Chapter 2 in greater detail (Section 2.5.3.2) were developed which enabled a reliable approximation of the amount of SDS and water molecules associated within the hexagonal phases existing locally across the SDS–polyDADMAC interface, as well as the concentration of SDS in micellar regions (where polyDADMAC is absent or undetectable). Briefly, the scattering curves obtained from line scans conducted with synchrotron SAXS not only allowed identification of the mesophases formed at a particular positions across the interface, but also the determination of the lattice parameter of the nanostructures analysed, namely hexagonal phases. The calculated lattice parameter can be used to interpolate the concentrations of SDS and water from the linear regressions fitted for the corresponding molecules of interest, Equation 2.6 and Equation 2.10, respectively (Table 2.4). Furthermore, the shape of the scattering curve of micellar phases can also give an indication of the concentration range of SDS. Specifically, a single symmetric peak at low q values is indicative of spherical micelles existing between 4–10 wt% SDS, while two broad peaks within an asymmetric peak suggests the presence of rod-like micelles between 12–32 wt% SDS (Figure 2.10–A).

3.5 Results

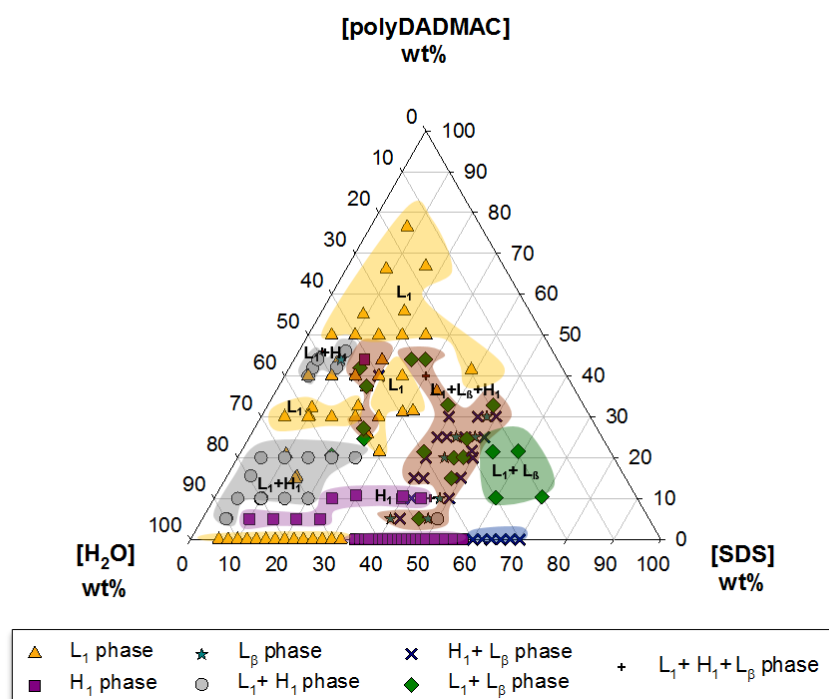
3.5.1 Phase Behaviour of SDS/PolyDADMAC Homogeneous Aqueous Mixtures

Ternary phase diagrams were generated for aqueous mixtures of SDS and polyDADMAC that were prepared using two different approaches.

Samples prepared by the conventional mixing protocol showed the appearance of multiple phase regions (Figure 3.2-A). Single-phase regions comprised of either purely hexagonal phases or SDS micelles in the presence or absence of polymer, whereas two-phase regions were composed of either mixed micellar and hexagonal phases, or mixed hexagonal and lamellar phases. Lastly, three-phase regions consisted of coexisting micellar, hexagonal, and lamellar phases. Phase boundaries drawn highlight the approximate compositions over which these liquid crystalline phases exist.

In order to directly compare the phase behaviour resulting from the different methods of preparation, the theoretical mass of dodecyl sulphate and poly(diallyldimethylammonium) present in the complex salt were summed with the concentration (wt%) of SDS or polyDADMAC added to produce the final mixture. The total composition was then plotted on the corresponding apex of the ternary phase diagram as denoted by an asterisk (Figure 3.2-B). This methodology assumed that the content of the surfactant ion and polyion within the solid polyDADMADS were at molar charge equivalence. The ternary phase diagram of samples prepared with the complex salt, polyDADMADS, revealed similar phase behaviour with bulk mixtures prepared by the conventional mixing approach. However, lamellar phases did not arise in mixtures prepared with the complex salt at high concentrations of SDS or polyDADMAC.

(A) Addition of SDS solution to polyDADMAC solution



(B) Addition of SDS or polyDADMAC solution to the complex salt

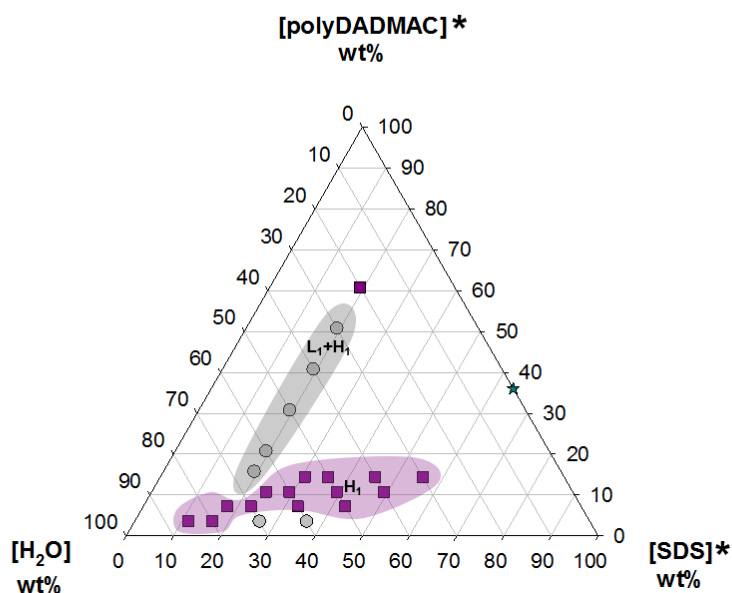


Figure 3.2 Ternary phase diagrams of aqueous mixtures of SDS and polyDADMAC prepared by the conventional mixing protocol (A) or with the complex salt (B). Coloured regions highlight approximate phase boundaries. Asterisks denote the estimated total concentration of surfactant ion or polyion in mixtures prepared with the complex salt.

To better understand the relationship between structure and composition, the lattice parameter of hexagonal phases formed in samples containing these structures were plotted as a function of the polyDADMAC-to-SDS molar charge ratio, expressed as $r = ([\text{polyDADMAC}] \times \text{charge per polymer molecule})/[\text{SDS}]$ (Figure 3.3). Below molar charge equivalence, only hexagonal phases were formed, whereas above this value, micellar phases coexisted with the hexagonal phases (Figure 3.3–A). Furthermore, the lattice parameter of the hexagonal phases was found to increase with increasing number of moles of SDS at a fixed molar concentration of polyDADMAC. Similarly, with increasing number of moles of polyDADMAC at a fixed molar concentration of SDS, the lattice parameter of the hexagonal phases increased (Figure 3.3–A). These trends were also demonstrated by bulk aqueous mixtures prepared with polyDADMADS (Figure 3.3–B), suggesting that equilibrium structures can form upon mixing of oppositely charged solutions of surfactant and polymer without inclusion of the complex salt.

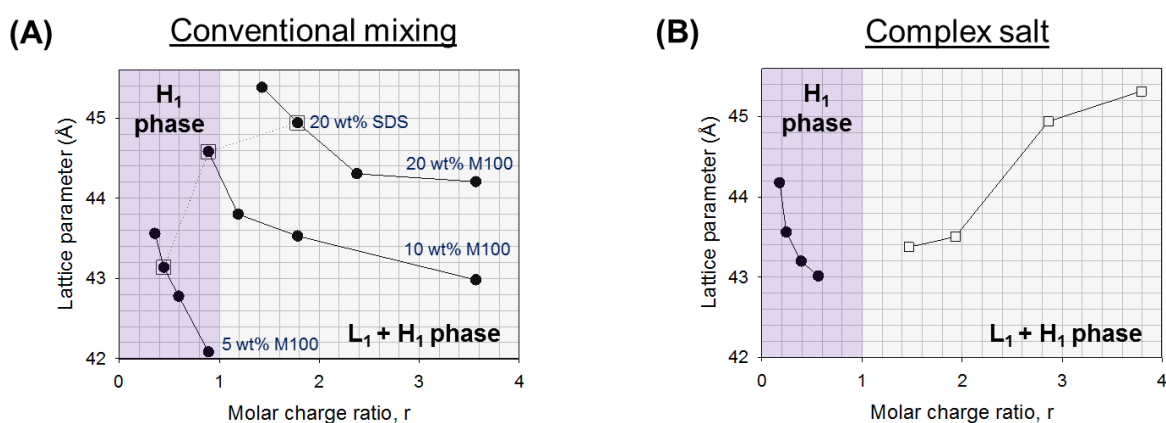


Figure 3.3 Trends in the lattice parameter of hexagonal phases existing in bulk aqueous mixtures of SDS and polyDADMAC (M100) prepared by the conventional mixing protocol (A) or inclusion of the complex salt, (B) with varying polyDADMAC-to-SDS molar charge ratios, r .

3.5.2 Structure Formation Across the SDS–PolyDADMAC Interface

When solutions of 20 wt% SDS and 20 wt% polyDADMAC were brought into contact, a band exhibiting birefringence was visualised under a crossed-polarised light microscope (Figure 3.4). The growth and development of the anisotropic structure was directed predominantly towards the bulk SDS solution and the area over which the newly formed material occupied the SDS–polyDADMAC interface increased over time. Notably, three bands with distinct optical properties were observed after 32 hr from initial contact. The intensity and texture displayed by the material continued to change subtly as time progressed (Figure 3.4).

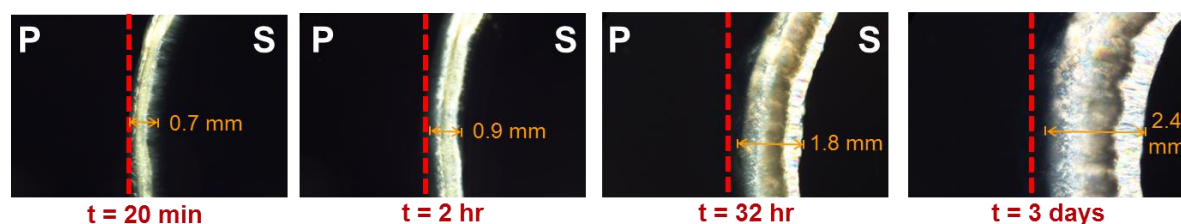


Figure 3.4 The growth and development of bands exhibiting birefringence across the interface created between solutions of 20 wt% polyDADMAC (P) and 20 wt% SDS (S) viewed under a crossed-polarised light microscope. The dashed line marks the point of origin.

When the measured total width of the birefringent nanostructures was plotted as a function of square root of time, an approximate linear relationship was evident up to ~3 days after initial contact between the solutions of SDS and polyDADMAC (Figure 3.5). After this point, the rate of structure formation significantly slowed as marked by a plateau in the width vs. time^{1/2} plot (Figure 3.5).

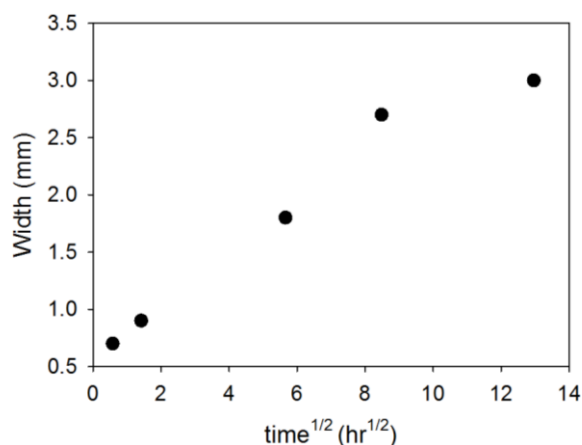


Figure 3.5 Rate of structure growth across the SDS–polyDADMAC interface, where the width of the anisotropic bands is plotted against the square root of time.

The internal structure of the liquid crystalline phases formed across the SDS–polyDADMAC interface was further characterised by synchrotron SAXS. Spatially resolved scattering curves were obtained in steps, every 100 μm , from the bulk polyDAMAC solution, through the structured interface, and across to the bulk SDS solution. These are illustrated as function of the distance from origin (0 mm) on three-dimensional SAXS waterfall plots (Figure 3.6).

Before contact of the SDS solution with the polyDADMAC solution, SDS existed as micelles as indicated by the broad peak at low q values (Figure 3.6). In contrast, scattering from the polyDADMAC solution was not easily resolved in the flat cell configuration as the polymeric solution scattered the X-rays poorly.⁴⁹ The absence of any birefringence within the bulk polymer and surfactant solutions which occupied both ends of the flat cell when visualised under a crossed-polarised light microscope confirmed the presence of unstructured or isotropic materials, respectively (Figure 3.4).

After 2 hr from initial contact between the two solutions, Bragg reflections indexed as hexagonal phase emerged at the SDS–polyDADMAC interface (Figure 3.6–A). In agreement

with the CPLM images, hexagonal phases continued to form across the interface, which grew progressively in the direction of the bulk SDS micellar region at 36 hr (Figure 3.6-B), 3 days (Figure 3.6-C), and 7 days (Figure 3.6-D) after time zero.

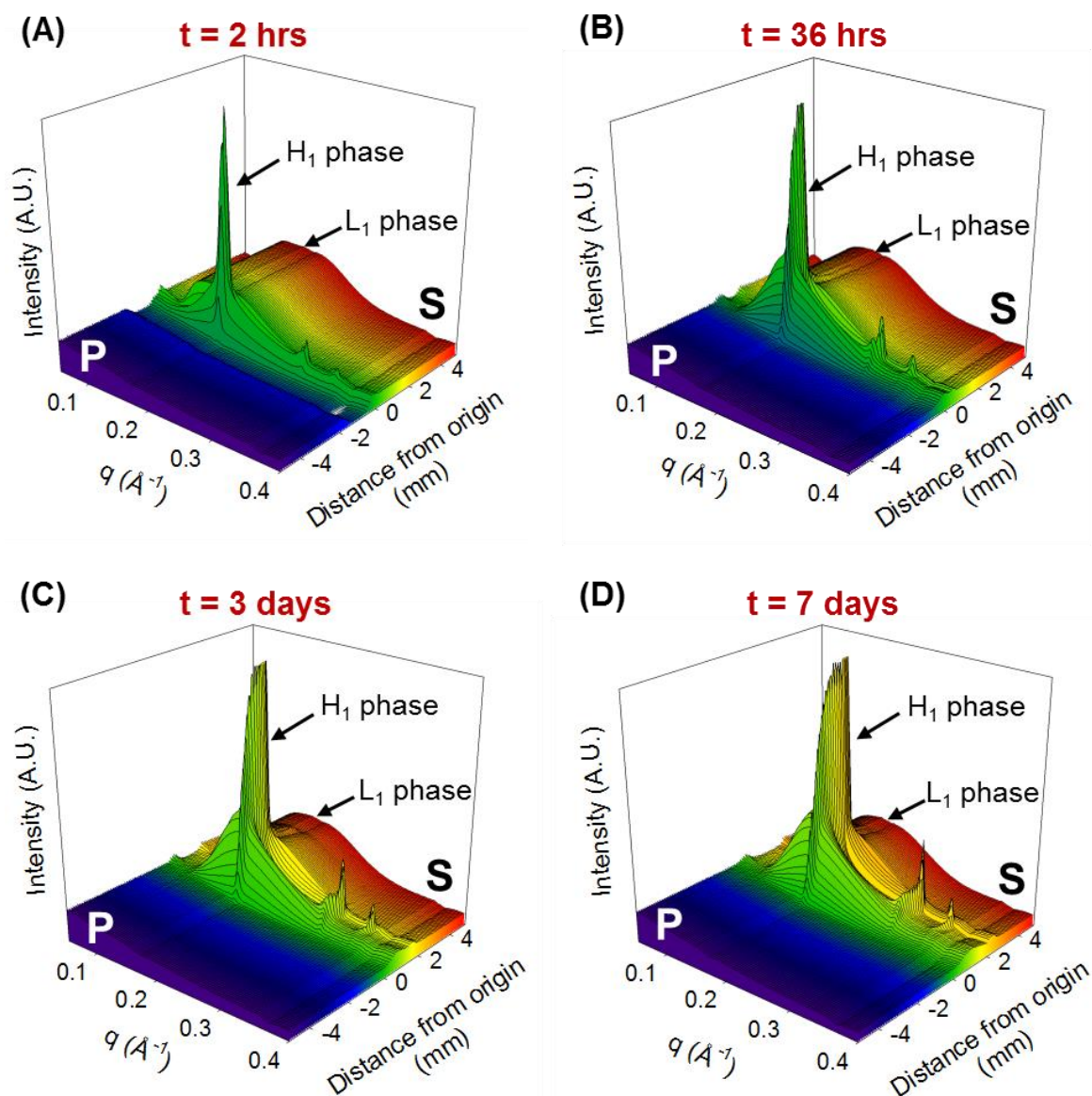


Figure 3.6 Spatially resolved SAXS waterfall plots showing the formation of hexagonal (H_1) and coexisting micellar (L_1) phases upon contact between 20 wt% polyDADMAC (P) and 20 wt% SDS (S), which grew predominantly towards the bulk SDS region from where the initial interface was created (0 mm) over time.

Slight shifts in the peaks identified as hexagonal phase were also noted. Since the absolute peak positions convey information on the internal size of the mesophases formed, it was of interest to further process the data by calculating the lattice dimensions to interrogate the structural attributes over different regions across the SDS–polyDADMAC interface over time.

The lattice parameter of the hexagonal phases mapped across the SDS–polyDADMAC interface differed significantly between different regions and time points (Figure 3.7). As depicted in the SDS/polyDADMAC/water ternary phase diagrams (Figure 3.2), regions comprised of coexisting micellar and hexagonal phases or just hexagonal phase were also formed across the SDS–polyDADMAC interface. The distance over which these different phase regions spanned across the interface changed over time, however the order at which they appeared remained constant. These observations were in accordance with the images taken under a crossed-polarised light microscope which revealed the formation of bands possessing dissimilar optical properties (Figure 3.4).

At the earliest time point studied, 2 hr after initial contact between the SDS and polyDADMAC solutions, hexagonal phase was present directly at the interface, with a small portion of coexisting micellar phase on the side closest to the bulk surfactant region (Figure 3.7-A). This hexagonal phase was found to be the most compact nanostructure with a lattice parameter of $\sim 42.1 \text{ \AA}$, which existed across the interface throughout duration of the study.

After 36 hr, regions of coexisting micellar and hexagonal phases appeared on both sides of the original band of hexagonal phase (Figure 3.7-B).

After 3 days, the entire cluster of mesophases that had already formed across the interface moved in the direction of the bulk SDS micellar phase (Figure 3.7-C). The trend in

the lattice parameter of the hexagonal phases formed across the SDS–polyDADMAC interface persisted even after approximately a week following the primary growth of hexagonal phase at the interface. Interestingly, the area comprised of purely hexagonal phase significantly increased with time.

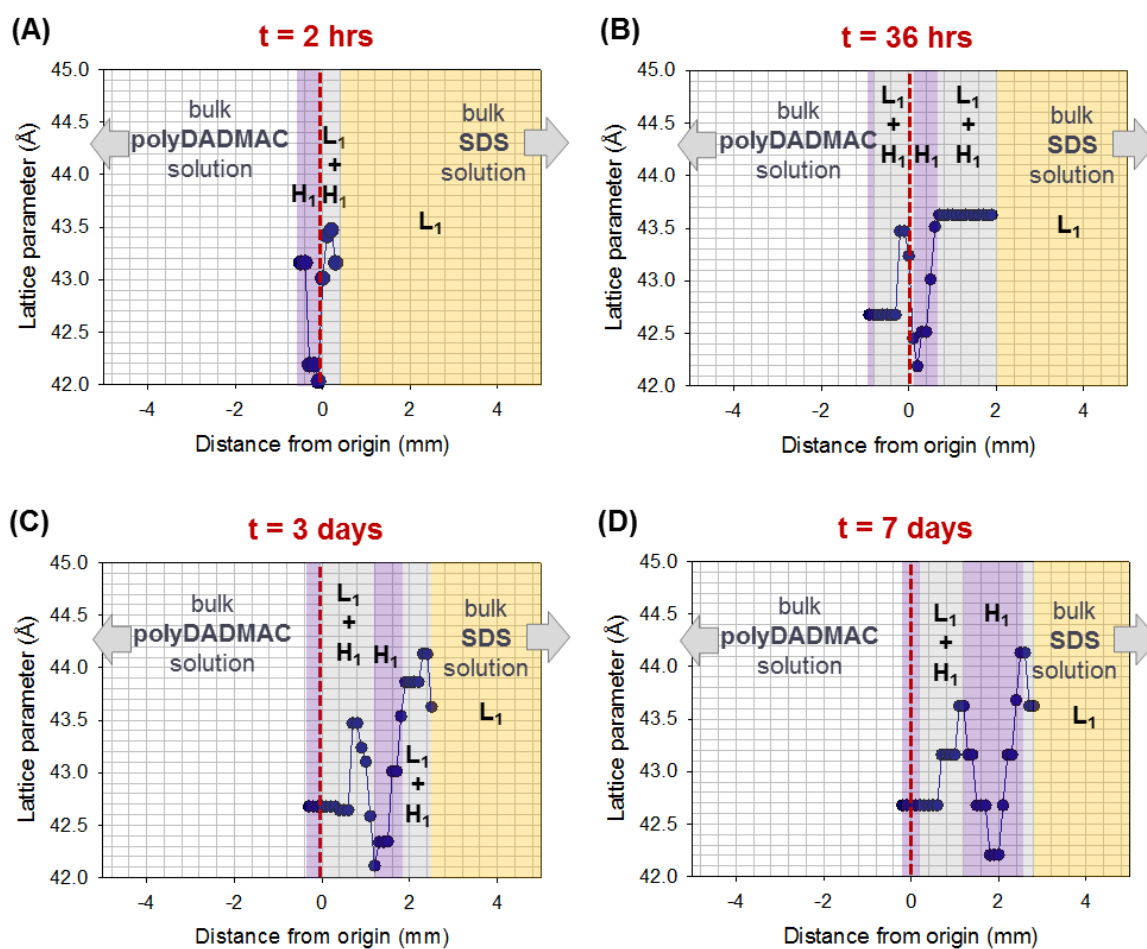


Figure 3.7 Differences in the lattice parameter of hexagonal phases formed across the SDS–polyDADMAC interface over time. Coloured regions highlight the presence of SDS micelles (L₁–yellow), coexisting micellar and hexagonal phases (L₁+H₁–grey), and hexagonal phases only (H₁–purple).

This data set was further used to determine the concentrations of SDS and water existing locally where hexagonal phases formed across the SDS–polyDADMAC interface.

3.5.3 Mapping Composition Across the SDS–PolyDADMAC Interface

Raman microscopy was the primary technique employed to determine the composition across the SDS–polyDADMAC interface, as described in Chapter 2. One of the limitations of performing a line scan with a Raman microscope was the length scale associated with acquiring spatially resolved Raman spectra across the sample. Typically, lines scans at 100 μm increments require several hours to collect data depending on the distance across the surfactant–polymer interface to be measured. Since it was recognised earlier that the rate of structure formation was retarded after ~ 3 days from initial contact between the two solutions (Figure 3.5), it was feasible for these experiments to run automatically overnight once this time point was surpassed. Any measurements taken at an earlier time point could be confounded by changes in the actual composition present during the measurement. For these reasons, information pertaining to the distribution of molecules across the SDS–polyDADMAC interface was only obtained for the corresponding structural data at approximately three and seven days after contact (Figure 3.8). The concentrations of SDS and water across the SDS–polyDADMAC interface were also determined from the lattice parameters of hexagonal phases identified from line scans performed with synchrotron SAXS. The data obtained from both methods were plotted as a function of distance across the interface to produce a map of the distribution of molecules across the SDS–polyDADMAC interface at these two time points (Figure 3.8).

Prior to contact and mixing of the two solutions, the measured concentrations of SDS and polyDADMAC in their respective bulk solutions (± 15 mm from origin) were both close to 20 wt%, which functioned as an indicator of the validity of the measurements across the SDS–polyDADMAC interface.

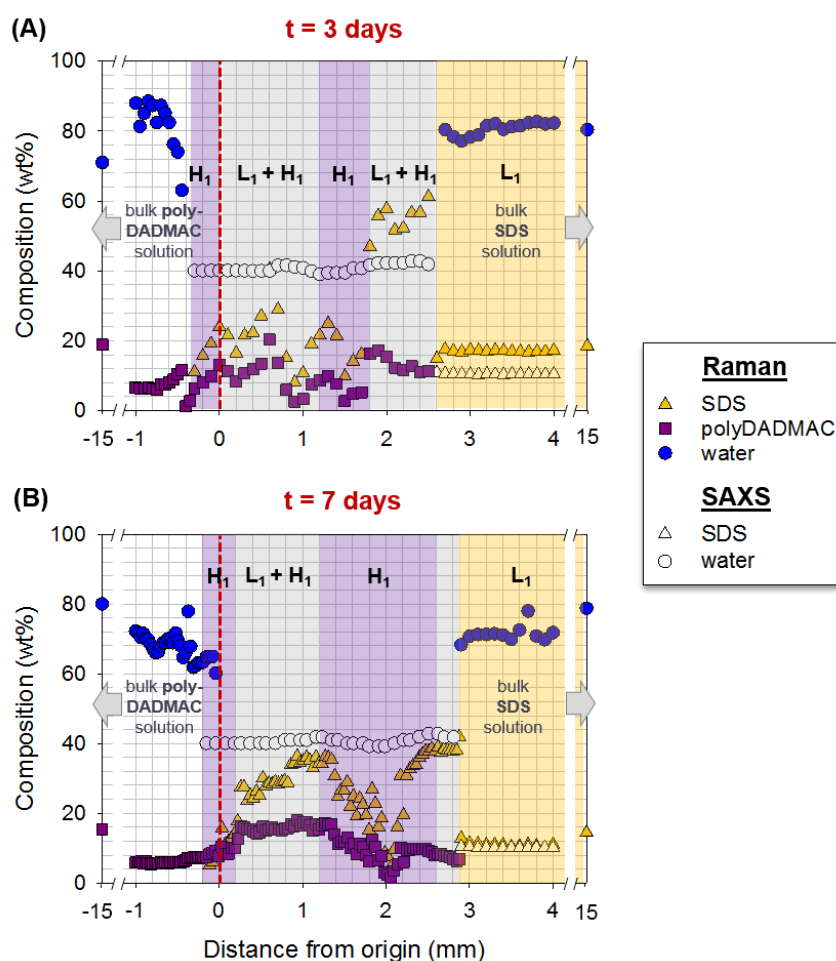


Figure 3.8 Mapping the concentrations of polyDADMAC (squares), SDS (triangles), and water (circles) across the SDS–polyDADMAC interface 3 days (A) and 7 days (B) after initial contact between solutions of 20 wt% SDS and 20 wt% polyDADMAC measured by Raman microscopy (filled) and synchrotron SAXS (unfilled). Coloured regions highlight the presence of SDS micelles (L₁–yellow), coexisting micellar and hexagonal phases (L₁+H₁–grey), and hexagonal phases only (H₁–purple).

After contact of the solutions of oppositely charged surfactant and polymer, both SDS and polyDADMAC molecules were detected across the SDS–polyDADMAC interface where liquid crystalline structures had formed. The distribution of these molecules across the structured interface varied slightly over the regions comprised of different mesophases at $t \approx 3$ days (Figure 3.8–A). However, the concentration of water existing locally where hexagonal phases were present remained constant. The water content at the interface decreased significantly, almost by half the amount in comparison to the initial concentration measured in the bulk solutions. Hexagonal phases are characteristically viscous materials,³⁷ so the presence of a large water depleted region further supports the formation of highly ordered structures across the SDS–polyDADMAC interface as the complexation process generally involves the release of counterions into the bulk solution and the dehydration of the polymer structure upon adsorption of surfactant micelles onto its surface.^{7, 25, 50–52}

The concentration gradient, particularly for SDS and polyDADMAC, across the structured interface, changed significantly at $t \approx 7$ days in comparison to the measured composition at the previous time point (Figure 3.8–B). Specifically, the concentration of both molecules across the interface increased considerably suggesting the continual influx of SDS micelles and polyDADMAC from their respective bulk solutions into the interface. However, the local concentration of water did not differ greatly between the hexagonal phases existing across the SDS–polyDADMAC interface.

Interestingly, there was also a concentration gradient formed across the bulk polyDADMAC region. The concentration of polyDADMAC at a position furthest away from the interface was significantly higher (~ 20 wt%) in comparison with the number of uncomplexed polymer molecules detected near the interface (Figure 3.8–A). The polymer concentration gradient decreased over time, as evident with a decrease in the number of

polyDADMAC molecules in the bulk region at -15 mm, which was a consequence of the diffusion of more polymer molecules into the interfacial region (Figure 3.8-B). Conversely, there was no obvious concentration gradient existing in the bulk SDS solution, which indicates that polyDADMAC was able to diffuse more efficiently across the interface into the micellar region than the ability of SDS micelles to move in the opposite direction.

Line scans with the Raman microscope demonstrated that there are certainly some difficulties associated with the capability of the technique in quantifying the composition across surfactant–polymer interfaces with a high degree of confidence. One of the major issues is the formation of a thick anisotropic material at the interface, which interferes with the amount of light transmitted through the sample and as a result may give a false representation of the actual composition. This was revealed when the sum of the concentrations of SDS, polyDADMAC, and water measured across structured interface was either well below or above the expected 100%. Therefore, an alternative approach was sought in order to more accurately describe the distribution of molecules across the SDS–polyDADMAC interface. This entailed a different means of interpretation of the data already obtained. Instead of treating the data in absolute concentrations, a relative comparison between the concentrations of surfactant and polymer, given as the polyDADMAC-to-SDS molar charge ratio, r , would potentially be more informative. Since the phase behaviour of bulk aqueous mixtures of SDS and polyDADMAC was already determined and presented as the lattice parameter of hexagonal phases as a function of r (Figure 3.3-A), the mesophases identified across the SDS–polyDADMAC interface (Figure 3.7) can be compared to those existing in bulk mixtures at the same composition. This methodology was introduced in Chapter 2 (Flowchart 2.1) as an approach for determining the existence of equilibrium or nonequilibrium structures across the SDS–polyDADMAC interface.

3.5.4 Correlating Changes in Structure and Composition Across the SDS–PolyDADMAC Interface Over Time

The aforementioned results acknowledged the structural and compositional data obtained spatially across the SDS–polyDADMAC interface by synchrotron SAXS and Raman microscopy as separate components. Studying the correlations between them and how these parameters change over time will help explain the formation of equilibrium or nonequilibrium structures locally across the SDS–polyDADMAC interface.

As mentioned, the composition across the interface can be given as the polyDADMAC–to–SDS molar charge ratio by using the calibration plot developed in earlier (Figure 2.9). The formula describes the relationship between the relative intensity of the peaks representative of SDS and polyDADMAC that appear in the Raman spectra with the known fraction of SDS in bulk aqueous mixtures of SDS and polyDADMAC (Figure 2.9, Equation 2.11). Therefore, the polyDADMAC–to–SDS molar charge ratio determined by this approach can be superimposed over the map of liquid crystalline phases resolved across the SDS–polyDADMAC interface (Figure 3.9).

If it was found that there was a difference between the nanostructures present in bulk mixtures and across the interface at a comparable composition, it was concluded that mesophases formed at that particular region across the interface had not yet reached equilibrium. On the other hand, if the structures did match then they were regarded as being locally at equilibrium. Regions containing equilibrium or nonequilibrium structures formed across the interface were annotated on the phase map in Figure 3.9. These findings demonstrate that the distance over which the hexagonal phase exists at apparent equilibrium grew overtime. Whereas, the regions comprising of nonequilibrium structures across the SDS–polyDADMAC interface slowly became smaller as time progressed.

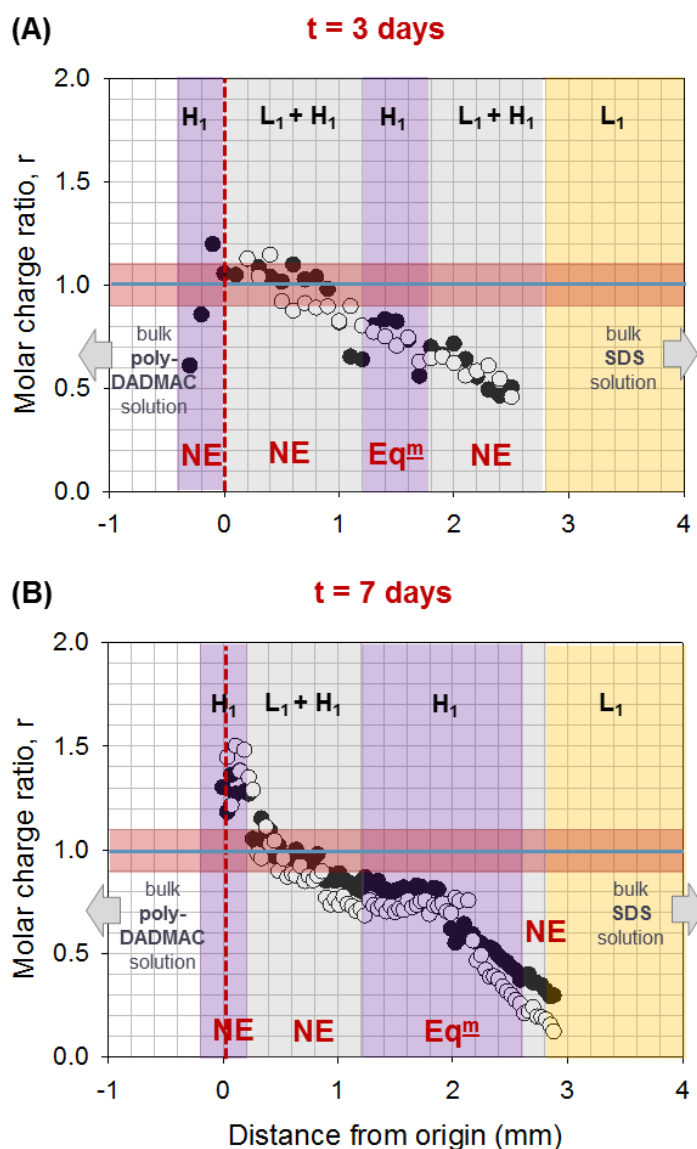


Figure 3.9 Mapping the polyDADMAC-to-SDS molar charge ratio across the surfactant–polymer interface 3 days (A) and 7 days (B) after initial contact between solutions of 20 wt% SDS and 20 wt% polyDADMAC interpolated from the Raman intensity calibration plots for bulk polyDADMAC and SDS standard solutions (filled circles) or from the relative intensity vs. mass fraction calibration plot (open circles). Coloured regions highlight the presence of SDS micelles (L_1 –yellow), coexisting micellar and hexagonal phases (L_1+H_1 –grey), and hexagonal phases only (H_1 –purple). Annotations indicate structures existing at equilibrium (Eq^m) or nonequilibrium (NE).

3.6 Discussion

3.6.1 Formation of the Complex Salt in Bulk Mixtures

It was hypothesised that similar liquid crystalline phases would arise in samples prepared with or without use of the complex salt as a specific component but with the same final SDS and polyDADMAC molar content. This statement was somewhat proven true since the small area of the ternary phase diagram generated for aqueous mixtures of SDS and polyDADMAC comprising of the complex salt was comparable to that produced for the systems formulated using the conventional mixing protocol. It is acknowledged in the literature that the complex salt is the coacervate produced after complete reaction between the surfactant and polyelectrolyte,^{28, 29} in this case it was SDS and polyDADMAC. Furthermore, the existence of the complex salt, polyDADMADS, exemplifies the system having reached equilibrium. Thus, it was concluded that the complex salt was most likely formed upon mixing of separate solutions of SDS and polyDADMAC, resulting in mesophases at apparent equilibrium. This is advantageous in product formulation where additional processes involved in the formation of equilibrium structures *via* synthesis of the complex salt becomes unnecessary, which can be avoided by employing the conventional mixing protocol instead.

A major discrepancy that resulted from this study was the appearance of lamellar phases when mixtures of SDS and polyDADMAC were prepared using the conventional method (Figure 3.2–A). The lamellar phases may be an artifact from the formation of crystals due to the release of the counterions into the bulk mixture as sodium chloride, particularly at high SDS and polyDADMAC concentrations (Appendix–Figure A4.2), or more likely, the hydration of SDS crystals at high surfactant concentrations (Appendix–Figure A3.3 and Figure

A3.4) either at or below room temperature.⁴⁵⁻⁴⁸ These lamellar structures are probably L_{β} phases as they have been known to arise in surfactant/water binary systems at high surfactant concentrations.⁵³ The alkyl chains in these types of systems are in a ‘solid state’ resulting in a rigid bilayer structure with restricted molecular motion. Consequently, L_{β} phases can be characterised with sharp Bragg peaks, while L_{α} phases display broader peaks which appear equidistant in their corresponding SAXS profiles. Interestingly, L_{β} phases have not yet been reported for C_{12} surfactants at room temperature.

On the other hand, lamellar phase was absent in the ternary phase diagram that represented the phase behaviour exhibited by mixtures prepared with the complex salt as the concentration of either the surfactant ion or polyion was varied (Figure 3.2-B). Many researchers exploit the complex salt as it removes the simple salt from the picture and allows the study of a true ternary system. Nevertheless, an appropriate trajectory to attain the desired end point can be selected to bypass this instability issue without the inclusion of the complex salt.

3.6.2 Self-Assembly of Nanostructures Across the SDS–PolyDADMAC Interface

The formation of hexagonal phase in aqueous mixtures of SDS and polyDADMAC has been extensively reported in the literature,⁴⁰⁻⁴³ however, this is the first known study of the kinetics of structure formation across liquid–liquid interfaces. Examining the SDS–polyDADMAC interface by the novel approaches developed in this thesis provides a new insight into the phase behaviour of oppositely charged surfactant and polymer systems that would not otherwise be achieved when studied as a bulk mixture.

3.6.2.1 Development of Micellar and Hexagonal Phases Towards the Bulk SDS Region

The growth and development of mesophases across the SDS–polyDADMAC interface predominantly toward the bulk SDS micellar region was an unexpected outcome. Movement of the nanostructures toward the bulk SDS micellar region was not a random event as the same behaviour was observed during experiments employing CPLM, synchrotron SAXS, and Raman microscopy regardless of the orientation of the sample cell; whether it was propped up vertically within the flat cell holder or lying flat whilst examined under the microscope. A possible explanation could be that the structure of the polymer, being relatively long and flexible, allows it to traverse through the tightly packed internal structure of hexagonal phases formed across the SDS–polyDADMAC interface more easily than spherical or rod-like SDS micelles. Upon contact of the two solutions, an entropically driven mixing process initially occurs at the interface. After the initial hexagonal phase was formed, polymer molecules diffused in the opposite direction at a greater extent across the structured interface, which led to the formation of more liquid crystalline phases toward the bulk SDS micellar region. This proposed model for rationalising the growth and development of nanostructures toward the bulk surfactant solution was supported by a distinct concentration gradient created in the bulk polymer solution as the interface was approached, where it decreased over time (Figure 3.8). In contrast, there was no obvious concentration gradient existing within the bulk SDS solution, however this did not mean that SDS micelles were not involved in the formation of mesophases across the interface through interactions with polyDADMAC molecules.

An understanding of the distribution of surfactant, polymer, and water molecules across the SDS–polyDADMAC interface would support the postulations gathered to rationalise this phenomenon.

3.6.2.2 Diffusion–Controlled Rate of Structure Formation Across the SDS–PolyDADMAC Interface

Changes in the relative concentrations of surfactant, polymer, and water across the SDS–polyDADMAC interface at different time points suggest that the self-assembly of mesophases did not hinder the diffusion of the system components through the nanostructured complexes across the interface.

The width of the band of nanostructures formed across the interface seemed to increase approximately linearly with the square root of time during the first ~3 days from initial contact between the solutions of SDS and polyDADMAC. This behaviour is similar to what is often used to describe the passive release of drugs into bulk solutions which is a diffusion–controlled process.⁵⁴ After this time, the presence of more hexagonal phases across the interface introduced a thicker and more highly viscous material³⁷ which molecules had to diffuse through in order for new associations or nanostructures to form. This water deprived region created a difficult pathway for the molecules to overcome and redistribute across the interface, which was apparent when the rate of structure formation across the interface slowed down. Furthermore, since the bulk solutions still contained detectable amounts of SDS and polyDADMAC at the end of the study, the formation of hexagonal and micellar phases across the interface did partially restrict the diffusion of more molecules into the structured region.

Significant changes in the rate of transport of molecules across the SDS–polyDADMAC interface were observed since the diffusion of molecules is inversely proportional to the viscosity of the material formed.^{7, 17, 37, 55} The formation of rod–like micelles across the interface demonstrates the importance of not just the type of mesophase formed, but also its specific structure. It should be emphasised that the micellar phases present across the

structured interface is very different from the spherical micelles in the bulk SDS solution,⁵⁶
⁵⁷ which further impacts the diffusivity molecules across the SDS–polyDADMAC interface.

3.6.2.3 The Slow Kinetics Involved in the Formation of Equilibrium Structures Across the SDS–PolyDADMAC Interface

Examination of the phase behaviour demonstrated in bulk aqueous mixtures of SDS and polyDADMAC, as well as at the SDS–polyDADMAC interface provided a new perspective on the existence of equilibrium and nonequilibrium structures in this system.

There is often a misconception that the liquid crystalline structures identified in aqueous mixtures of oppositely charged surfactant and polymer systems are present at equilibrium when left to ‘equilibrate’ for a substantial period of time, a month for example, prior to analysis. It should be clarified that the mesophases characterised for bulk mixtures presented in the form of ternary phase diagrams were a representation of the system as a whole. In other words, globally they may appear to be comprised of particular coexisting phases when actually there may have been regions in the mixture that contain a single equilibrium phase and others with multiple self-assembled structures at nonequilibrium. There is, however, a high probability that inhomogeneities would arise in mixtures with high concentrations surfactant and/or polymer, where some regions in the mixture are at equilibrium and others not.

A major advantage of employing the novel approach developed for studying the phase behaviour across liquid–liquid interfaces is the ability to examine the formation of different bands of equilibrium and/or nonequilibrium nanostructures across the SDS–polyDADMAC interface. Coexisting micellar and hexagonal phases were identified in a sample prepared by vigorous mixing of equal volumes of 20 wt% SDS and 20 wt% polyDADMAC solutions

(Appendix–Figure A3.2). While regions of only hexagonal phase or coexisting hexagonal and micellar phases were evident across the SDS–polyDADMAC interface when studied at a comparable composition. This may justify the existence of both equilibrium and nonequilibrium structures in the bulk mixtures. This subject will be discussed in greater detail in Chapter 5 where the phase behaviour exhibited by dilute dispersions and concentrated bulk mixtures, as well as structures formed across solution interfaces of SDS and polyDADMAC will be compared to understand the formation of equilibrium and/or nonequilibrium structures in these systems.

The hexagonal phase initially formed at the SDS–polyDADMAC interface was at apparent equilibrium. The lattice parameter and polyDADMAC–to–SDS molar charge ratio remained constant at $\sim 42.1 \text{ \AA}$ and $r \approx 0.8$, respectively, even though the group of mesophases shifted toward the bulk SDS solutions at three and seven days after initial contact of the solutions. In contrast, the structure and composition in regions comprising of coexisting micellar and hexagonal phases continued to change over time. Interestingly as time passed, more and more of these two–phase regions transitioned to purely hexagonal phase once a specific composition was reached, suggesting that the micelles acted as a mechanism of transport on both sides of the structured interface.

In summary, these kinetic studies have demonstrated that nanostructures apparently at equilibrium were formed locally across the SDS–polyDADMAC interface. Furthermore, the area over which the equilibrium hexagonal phases spans across the interface is predicted to increase until complete complexation of the molecules in the system occurs or when the diffusion of molecules through the structured interface is no longer possible. These findings shed light on how true equilibrium can be reached after very long time scales as described by Dedinaite *et al.*⁵⁸

3.7 Conclusions

This chapter presented new insights into the equilibrium phase behaviour across the interface created between solutions of the anionic surfactant, sodium dodecyl sulphate (SDS), and the cationic polymer, poly(diallyldimethylammonium chloride) (polyDADMAC).

Comparison of the ternary phase diagrams generated for bulk aqueous mixtures of SDS and polyDADMAC prepared by the conventional mixing protocol or by incorporation of the complex salt demonstrated that the method of sample preparation did not significantly influence the resulting mesophases formed, suggesting that the complex salt may be formed *in situ* during the reaction between surfactant ions and polyions.

Information acquired from line scans performed with synchrotron SAXS and Raman microscopy enabled the study of the kinetics of structure formation across the SDS–polyDADMAC interface. Regions comprised of different mesophases developed across the SDS–polyDADMAC, where the distribution of molecules continued to change until equilibrium hexagonal phases were formed. Diffusion of surfactant, polymer, and water molecules occurred in both directions across the structured interface, where the rate of self-assembly of mesophases was substantially reduced as more hexagonal phases formed across the SDS–polyDADMAC interface. This, to some extent, hindered the passage of molecules to participate in associations with existing structured complexes or unbound molecules and subsequent formation of more equilibrium structures, which resulted in the existence of kinetically trapped nonequilibrium nanostructures.

It is still unclear as to why these mesophases grew predominantly towards the bulk SDS micellar region across the SDS–polyDADMAC interface, thus it will be addressed in the following chapter.

3.8 References

1. Goddard, E. D.; Hannan, R. B., *Cationic Polymer/Anionic Surfactant Interactions*. J. Colloid Interface Sci. 1976, 55, 73–79.
2. Svensson, A.; Norrman, J.; Piculell, L., *Phase Behaviour of Polyion–Surfactant Ion Complex Salts: Effects of Surfactant Chain Length and Polyion Length*. J. Phys. Chem. B. 2006, 110, 10332–10340.
3. Zhao, X.; Shang, Y.; Hu, J.; Liu, H.; Hu, Y., *Biophysical Characterisation of Complexation of DNA with Oppositely Charged Gemini Surfactant 12-3-12*. Biophys. Chem. 2008, 138, 144–149.
4. Campbell, R. A.; Angus–Smyth, A.; Yanez Arteta, M.; Tonigold, K.; Nylander, T.; Varga, I., *New Perspective on the Cliff Edge Peak in the Surface Tension of Oppositely Charged Polyelectrolyte/Surfactant Mixtures*. J. Phys. Chem. Letters. 2010, 1, 3021–3026.
5. Goddard, E. D.; Leung, P. S., *Studies of Gel Formation, Phase Behaviour and Surface Tension in Mixtures of a Hydrophobically Modified Cationic Cellulose Polymer and Surfactant*. Colloid Surface. 1992, 65, 211–219.
6. Onésippe, C.; Lagerge, S., *Studies of the Association of Chitosan and Alkylated Chitosan with Oppositely Charged Sodium Dodecyl Sulfate*. Colloid Surface Physicochem. Eng. Aspect. 2008, 330, 201–206.
7. Mukherjee, S.; Dan, A.; Bhattacharya, S. C.; Panda, A. K.; Moulik, S. P., *Physicochemistry of Interaction between the Cationic Polymer Poly(diallyldimethylammonium chloride) and the Anionic Surfactants Sodium Dodecyl Sulfate, Sodium Dodecylbenzenesulfonate, and Sodium N-Dodecanoylsarcosinate in Water and Isopropyl Alcohol– Water Media*. Langmuir. 2011, 27, 5222–5233.
8. Bhattacharyya, A.; Monroy, F.; Langevin, D.; Argillier, J.–F., *Surface Rheology and Foam Stability of Mixed Surfactant– Polyelectrolyte Solutions*. Langmuir. 2000, 16, 8727–8732.
9. Courtois, J.; Berret, J. F., *Probing Oppositely Charged Surfactant and Copolymer Interactions by Isothermal Titration Microcalorimetry*. Langmuir. 2010, 26, 11750–11758.

10. Thongngam, M.; McClements, D. J., *Isothermal Titration Calorimetry Study of the Interactions between Chitosan and a Bile Salt (Sodium Taurocholate)*. Food Hydrocolloids. 2005, 19, 813–819.
11. Li, Y.; Xu, R.; Couderc, S.; Bloor, D. M.; Warr, J.; Penfold, J.; Holzwarth, J. F.; Wyn-Jones, E., *Structure of the Complexes Formed between Sodium Dodecyl Sulfate and a Charged and Uncharged Ethoxylated Polyethyleneimine. Small-Angle Neutron Scattering, Electromotive Force, and Isothermal Titration Calorimetry Measurements*. Langmuir. 2001, 17, 5657–5665.
12. Samuel, G.; Daragh, M.; Nirmesh, J.; Michel, D.; Dominique, L., *Polyelectrolyte–Surfactant Complexes at Interfaces and in Bulk*. J. Phys.: Condens. Matter. 2003, 15, S219.
13. Ikonen, M.; Murtomäki, L.; Kontturi, K., *Controlled Complexation of Plasmid DNA with Cationic polymers. Effect of Surfactant on the Complexation and Stability of the Complexes*. Colloids Surf, B. 2008, 66, 77–83.
14. Bastardo, L. A.; Iruthayaraj, J.; Lundin, M.; Dedinaite, A.; Vareikis, A.; Makuška, R.; van der Wal, A.; Furó, I.; Garamus, V. M.; Claesson, P. M., *Soluble Complexes in Aqueous Mixtures of Low Charge Density Comb Polyelectrolyte and Oppositely Charged Surfactant Probed by Scattering and NMR*. J. Colloid Interface Sci. 2007, 312, 21–33.
15. Nizri, G.; Makarsky, A.; Magdassi, S.; Talmon, Y., *Nanostructures Formed by Self-Assembly of Negatively Charged Polymer and Cationic Surfactants*. Langmuir. 2009, 25, 1980–1985.
16. Nizri, G.; Lagerge, S.; Kamyshny, A.; Major, D. T.; Magdassi, S., *Polymer–Surfactant Interactions: Binding Mechanism of Sodium Dodecyl Sulfate to Poly(diallyldimethylammonium chloride)*. J. Colloid Interface Sci. 2008, 320, 74–81.
17. Kong, L.; Cao, M.; Hai, M., *Investigation on the Interaction between Sodium Dodecyl Sulfate and Cationic Polymer by Dynamic Light Scattering, Rheological, and Conductivity Measurements*. J. Chem. Eng. Data. 2007, 52, 721–726.
18. Somasundaran, P.; Chakraborty, S.; Qiang, Q.; Deo, P.; Wang, J.; Zhang, R., *Surfactants, Polymers and their Nanoparticles for Personal Care Applications*. J Cosmet Sci. 2004, 55.

19. Miyake, M.; Kakizawa, Y., *Morphological Study of Cationic Polymer–Anionic Surfactant Complex Precipitated in Solution during the Dilution Process*. *J. Cosmet. Sci.* 2010, 61, 289–301.
20. Svensson, A. V.; Johnson, E. S.; Nylander, T.; Piculell, L., *Surface Deposition and Phase Behavior of Oppositely Charged Polyion–Surfactant Ion Complexes. 2. A Means to Deliver Silicone Oil to Hydrophilic Surfaces*. *ACS Appl Mater Interfaces*. 2010, 2, 143–156.
21. Clauzel, M.; Johnson, E. S.; Nylander, T.; Panandiker, R. K.; Sivik, M. R.; Piculell, L., *Surface Deposition and Phase Behavior of Oppositely Charged Polyion–Surfactant Ion Complexes. Delivery of Silicone Oil Emulsions to Hydrophobic and Hydrophilic Surfaces*. *ACS Appl Mater Interfaces*. 2011, 3, 2451–2462.
22. Lochhaas, K. H.; Thünemann, A. F.; Antonietti, M., *Polyelectrolyte–Surfactant Complexes with Fluorinated Surfactants. A New Type of Material for Coatings*. *Surface Coatings International*. 1999, 82, 451–455.
23. Liu, W.; Sun, S.; Cao, Z.; Zhang, X.; Yao, K.; Lu, W. W.; Luk, K. D. K., *An Investigation on the Physicochemical Properties of Chitosan/DNA Polyelectrolyte Complexes*. *Biomaterials*. 2005, 26, 2705–2711.
24. Amar–Yuli, I.; Adamcik, J.; Blau, S.; Aserin, A.; Garti, N.; Mezzenga, R., *Controlled Embedment and Release of DNA from Lipidic Reverse Columnar Hexagonal Mesophases*. *Soft Matter*. 2011, 7, 8162–8168.
25. Hsu, W.-L.; Chen, H.-L.; Liou, W.; Lin, H.-K.; Liu, W.-L., *Mesomorphic Complexes of DNA with the Mixtures of a Cationic Surfactant and a Neutral lipid*. *Langmuir*. 2005, 21, 9426–9431.
26. Morán, M. C.; Miguel, M. G.; Lindman, B., *Surfactant–DNA Gel Particles: Formation and Release Characteristics*. *Biomacromolecules*. 2007, 8, 3886–3892.
27. Lin, H.; Zhu, G.; Xing, J.; Gao, B.; Qiu, S., *Polymer–Mesoporous Silica Materials Templated with an Oppositely Charged Surfactant/Polymer System for Drug Delivery*. *Langmuir*. 2009, 25, 10159–10164.

28. Ilekli, P.; Piculell, L.; Tournilhac, F.; Cabane, B., *How to Concentrate an Aqueous Polyelectrolyte/Surfactant Mixture by Adding Water*. J. Phys. Chem. B. 1998, 102, 344–351.
29. Svensson, A.; Piculell, L.; Cabane, B.; Ilekli, P., *A New Approach to the Phase Behaviour of Oppositely Charged Polymers and Surfactants*. J. Phys. Chem. B. 2002, 106, 1013–1018.
30. Braem, A. D.; Biggs, S.; Prieve, D. C.; Tilton, R. D., *Control of Persistent Nonequilibrium Adsorbed Polymer Layer Structure by Transient Exposure to Surfactants*. Langmuir. 2003, 19, 2736–2744.
31. Pojják, K.; Bertalanits, E.; Mészáros, R., *Effect of Salt on the Equilibrium and Nonequilibrium Features of Polyelectrolyte/Surfactant Association*. Langmuir. 2011, 27, 9139–9147.
32. Fegyver, E.; Meszaros, R., *Fine-Tuning the Nonequilibrium Behavior of Oppositely Charged Macromolecule/Surfactant Mixtures via the Addition of Nonionic Amphiphiles*. Langmuir. 2014.
33. Mezei, A. I.; Pojják, K.; Mészáros, R. b., *Nonequilibrium Features of the Association between Poly(vinylamine) and Sodium Dodecyl Sulfate. The Validity of the Colloid Dispersion Concept*. J. Phys. Chem. B. 2008, 112, 9693–9699.
34. Mezei, A.; Mészáros, R.; Varga, I.; Gilányi, T., *Effect of Mixing on the Formation of Complexes of Hyperbranched Cationic Polyelectrolytes and Anionic Surfactants*. Langmuir. 2007, 23, 4237–4247.
35. Naderi, A.; Claesson, P. M.; Bergström, M.; Dédinaite, A., *Trapped Non-Equilibrium States in Aqueous Solutions of Oppositely Charged Polyelectrolytes and Surfactants: Effects of Mixing Protocol and Salt Concentration*. Colloids and Surfaces A: Physicochem. Eng. Aspects. 2005, 253, 83–93.
36. Naderi, A.; Claesson, P. M., *Association between Poly(vinylamine) and Sodium Dodecyl Sulfate. Effects of Mixing Protocol, Blending Procedure, and Salt Concentration*. J. Dispersion Sci. Technol. 2005, 26, 329–340.

37. Mezzenga, R.; Meyer, C.; Servais, C.; Romoscanu, A. I.; Sagalowicz, L.; Hayward, R. C., *Shear Rheology of Lyotropic Liquid Crystals: A Case Study*. Langmuir. 2005, 21, 3322–3333.
38. Babak, V. G.; Merkovich, E. A.; Galbraikh, L. S.; Shtykova, E. V.; Rinaudo, M., *Kinetics of Diffusionally Induced Gelation and Ordered Nanostructure Formation in Surfactant–Polyelectrolyte Complexes Formed at Water/Water Emulsion Type Interfaces*. Mendeleev Commun. 2000, 10, 94–95.
39. Lapitsky, Y.; Eskuchen, W. J.; Kaler, E. W., *Surfactant and Polyelectrolyte Gel Particles that Swell Reversibly*. Langmuir. 2006, 22, 6375–6379.
40. Yeh, F.; Sokolov, E. L.; Khokhlov, A. R.; Chu, B., *Nanoscale Supramolecular Structures in the Gels of Poly(diallyldimethylammonium chloride) Interacting with Sodium Dodecyl Sulfate*. J. Am. Chem. Soc. 1996, 118, 6615–6618.
41. Sokolov, E.; Yeh, F.; Khokhlov, A.; Grinberg, V. Y.; Chu, B., *Nanostructure Formation in Polyelectrolyte–Surfactant Complexes*. J. Phys. Chem. B. 1998, 102, 7091–7098.
42. Mironov, A. V.; Starodoubtsev, S. G.; Khokhlov, A. R.; Dembo, A. T.; Dembo, K. A., *Effect of Chemical Nature of 1,1–Salt on Structure of Polyelectrolyte Gel–Surfactant Complexes*. J. Phys. Chem. B. 2001, 105, 5612–5617.
43. Nizri, G.; Magdassi, S.; Schmidt, J.; Cohen, Y.; Talmon, Y., *Microstructural Characterisation of Micro- and Nanoparticles Formed by Polymer–Surfactant Interactions*. Langmuir. 2004, 20, 4380–4385.
44. Svensson, A.; Sjöström, J.; Scheel, T.; Piculell, L., *Phases and Structures of a Polyion–Surfactant Ion Complex Salt in Aqueous Mixtures: Cationic Hydroxyethyl Cellulose with Dodecylsulfate Counterions*. Colloid Surface Physicochem. Eng. Aspect. 2003, 228, 91–106.
45. Hammouda, B., *Temperature Effect on the Nanostructure of SDS Micelles in Water*. J. Res. Natl. Inst. Stand. Technol. 2013, 118, 151–167.
46. Kékicheff, P.; Grabielle–Madelmont, C.; Ollivon, M., *Phase Diagram of Sodium Dodecyl Sulfate–Water System*. J. Colloid Interface Sci. 1989, 131, 112–132.

47. Kékicheff, P., *Phase Diagram of Sodium Dodecyl Sulfate–Water System. 2. Complementary Isolethal and Isothermal Phase Studies*. J. Colloid Interface Sci. 1989, 131, 133–152.
48. Kékicheff, P.; Cabane, B., *Crystallography of Systems with Long Periods. A Neutron-Scattering Study of Sodium Dodecyl Sulfate/Water Mesophases*. Acta Cryst. 1988, 44, 395–406.
49. Ridell, A. *Characterisation of Aqueous Solutions, Liquid Crystals and Solid State of Non-ionic Polymers in Association with Amphiphiles and Drugs*. Uppsala University, Uppsala, 2003.
50. Loh, W.; Teixeira, L. A. C.; Lee, L.-T., *Isothermal Calorimetric Investigation of the Interaction of Poly(N-isopropylacrylamide) and Ionic Surfactants*. J. Phys. Chem. B. 2004, 108, 3196–3201.
51. Wagner, K.; Harries, D.; May, S.; Kahl, V.; Rädler, J. O.; Ben-Shaul, A., *Direct Evidence for Counterion Release Upon Cationic Lipid–DNA Condensation*. Langmuir. 1999, 16, 303–306.
52. Hsu, W.-L.; Li, Y.-C.; Chen, H.-L.; Liou, W.; Jeng, U. S.; Lin, H.-K.; Liu, W.-L.; Hsu, C.-S., *Thermally-Induced Order–Order Transition of DNA–Cationic Surfactant Complexes*. Langmuir. 2006, 22, 7521–7527.
53. Ferreira, G. A.; Loh, W., *Structural Parameters of Lamellar Phases Formed by the Self-Assembly of Dialkyldimethylammonium Bromides in Aqueous Solution*. J. Braz. Chem. Soc. 2016, 27, 392–401.
54. Higuchi, W. I., *Diffusional Models Useful in Biopharmaceutics. Drug Release Rate Processes*. J. Pharm. Sci. 1967, 56, 315–324.
55. Philippova, O. E.; Starodoubtzev, S. G., *Interaction of Slightly Cross-linked Gels of Poly(diallyldimethylammonium bromide) with Sodium Dodecyl Sulfate. Diffusion of Surfactant Ions in Gel*. J. Polym. Sci., Part B: Polym. Phys. 1993, 31, 1471–1476.
56. Hassan, P. A.; Raghavan, S. R.; Kaler, E. W., *Microstructural Changes in SDS Micelles Induced by Hydrotropic Salt*. Langmuir. 2002, 18, 2543–2548.

57. Christov, N. C.; Denkov, N. D.; Kralchevsky, P. A.; Ananthapadmanabhan, K. P.; Lips, A., *Synergistic Sphere-to-Rod Micelle Transition in Mixed Solutions of Sodium Dodecyl Sulfate and Cocoamidopropyl Betaine*. *Langmuir*. 2004, 20, 565–571.
58. Dedinaite, A.; Claesson, P. M.; Bergström, M., *Polyelectrolyte–Surfactant Layers: Adsorption of Preformed Aggregates versus Adsorption of Surfactant to Preadsorbed Polyelectrolyte*. *Langmuir*. 2000, 16, 5257–5266.

3.9 Appendix

A3.1 Phase Behaviour of an Industrially Relevant Surfactant/Polymer System

A ternary phase diagram (Figure A3.1) was developed for an industrially relevant system comprised of poly(diallyldimethylammonium chloride) (polyDADMAC), water, and an undisclosed mixture of alkyl ethoxysulphates (identity AES paste). Since the chemical structure of alkyl ethoxysulphates (AES) is similar to that of sodium dodecyl sulphate, the phase behaviour exhibited by this system was used as a basis to select the most suitable composition to study the phase behaviour across the SDS–polyDADMAC interface.

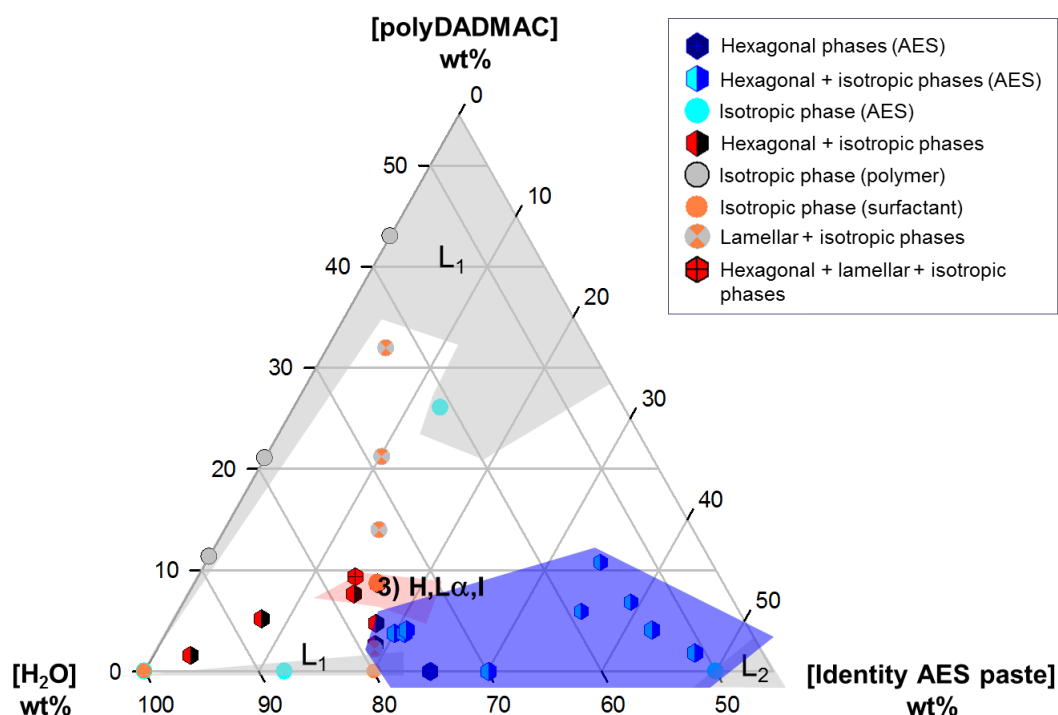


Figure A3.1 Ternary phase diagram developed by Procter and Gamble for systems comprised of poly(diallyldimethylammonium chloride), water, and a mixture of alkyl ethoxysulphates (AES) by visual observation with CPLM. Unpublished data.

A3.2 Equilibrium Structure of the 20 wt% SDS: 20 wt% PolyDADMAC System as a Bulk Mixture

This chapter studies the phase behaviour across the interface between solutions of 20 wt% SDS and 20 wt% polyDADMAC. Since approximately equal volumes of both components were loaded into the sample flat cells, the final composition of the overall system would be comprised of 10 wt% SDS, 10 wt% polyDADMAC, and 80 wt% water. The liquid crystalline structures present in this surfactant/polymer/water mixture is representative of the system that has reached apparent equilibrium, which can act as a guide to what is the expected to exist across the SDS–polyDADMAC interface if a complete reaction has occurred. Characterisation of the sample mixture by SAXS showed the presence of micelles from the broad peak at low q values coexisting with hexagonal phase (Figure A3.2).

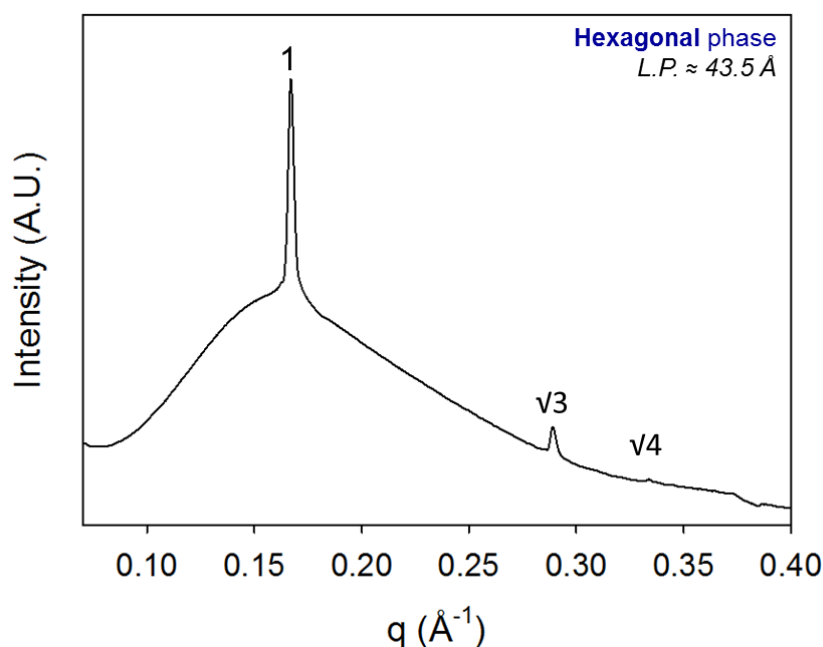


Figure A3.2 SAXS profile shows coexisting micellar and hexagonal phases in a mixture comprised of 10 wt% SDS, 10 wt% polyDADMAC, and 80 wt% water.

A3.3 Structural Characterisation of a Concentrated Aqueous Mixture of SDS and Water by SAXS

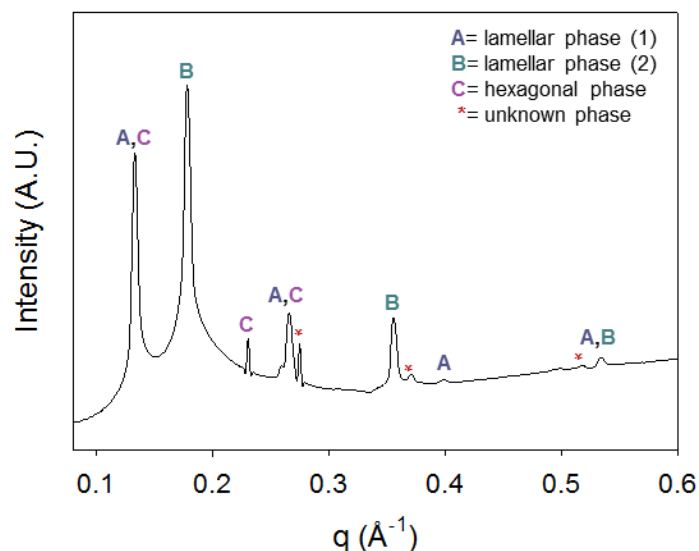


Figure A3.3 SAXS profile of 62 wt% SDS prepared in Milli-Q water showing a mixture of liquid crystalline structures. The Bragg peaks were indexed as lamellar (A, B) and hexagonal (C) phases. Unknown mesophases are marked with an asterisk (*).

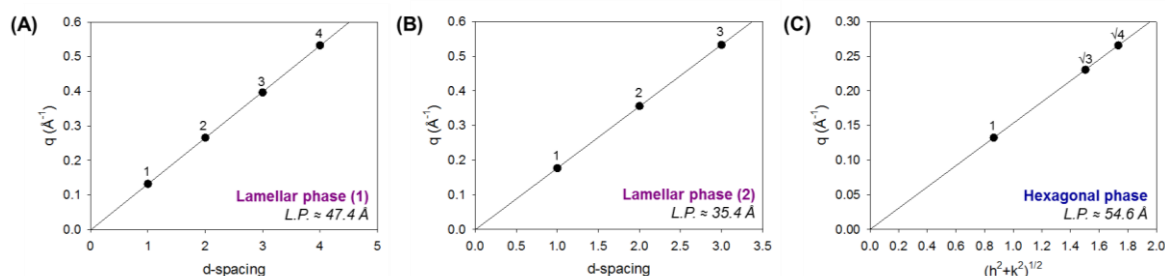


Figure A3.4 Graphs of d-spacing vs. Miller indices generated from the corresponding Bragg reflections observed in the SAXS profile (Figure A3.3) in an aqueous mixture of 62 wt% SDS prepared in Milli-Q water indicating the coexistence of two lamellar phases with differing lattice parameters (A, B), and a hexagonal phase (C).

Chapter 4: *Controlling the Mobility of System
Components Across Surfactant–Polymer
Interfaces*

4. Controlling the Mobility of System Components Across Surfactant–Polymer Interfaces

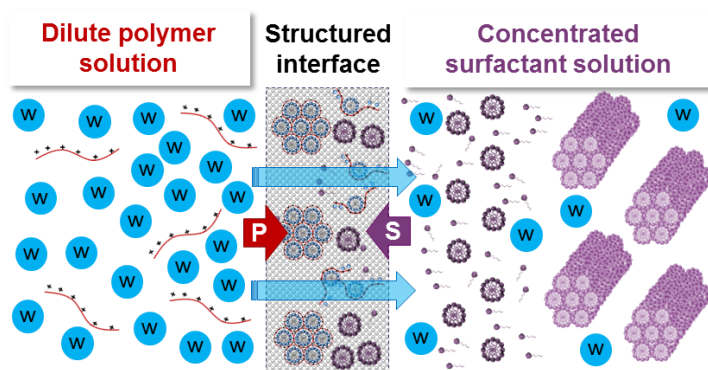
4.1 Introduction

An unforeseen phenomenon discovered during the study of the equilibrium phase behaviour across the SDS–polyDADMAC interface in Chapter 3 was the growth and development of hexagonal and micellar phase structures toward the bulk SDS solution. In order to understand such phenomena it is necessary to understand the relative diffusivity of surfactant, polymer, and water within and across the surfactant–polymer solution interface under nonequilibrium conditions.

It is known that the strength of interactions and geometric packing between oppositely charged surfactant and polymer molecules in solution dictates the self-assembly of colloidal structures in dispersions, which in turn can influence the viscosity of the system.¹⁻⁹ Thalberg *et al.* demonstrated that the self-diffusion of surfactant in a solution of polymer significantly decreased with increasing concentrations due to intermolecular interactions formed between the polymer chains and the micelles in solution.¹⁰ Furthermore, the type of liquid crystalline phase formed in these systems may also be important in determining the diffusivity of molecules through these complex structures as the rheological behaviour has been shown to differ between lamellar, cubic, and hexagonal phases.¹¹⁻¹⁴ Generally, an increase in the diffusivity of molecules in solution is expected to occur with a decrease in viscosity, while a decrease in the rate of diffusion of molecules in solution would correlate to an increase in viscosity of the system. An example that highlights the relationship between the rate of diffusion of molecules and the formation of inherently viscous nanostructures across

surfactant–polymer interface is given by Lapitsky *et al.* and Babak *et al.* Their studies showed the formation of a ‘structured shell’ within gel capsules upon dropwise addition of polymer solution into a pool of surfactant solution. It was revealed that the rate of structure formation depended on the frontal diffusion of surfactant across the interface between the surfactant solution and the polymer droplet, which was also limited by the thickness and permeability of the material formed.¹⁵⁻¹⁸ Clearly, the ability of the molecules to diffuse through the bulk surfactant or polymer solution and across ordered structures is critical in determining the rate and extent to which mixing occurs across surfactant–polymer solution interfaces.

One means of controlling the distribution of molecules and formation of mesophases across surfactant–polymer interfaces may involve employing an immobilised or highly viscous phase as one of the initial structures in the system to essentially constrain the movement of one or more components and enable study of the movement of other components. Some surfactants, such as SDS and CTAB, are known to often form highly ordered structures, such as hexagonal phases, when prepared at high concentrations.^{19, 20} It is anticipated that when a dilute solution of polymer is placed into contact with a gel of hexagonal phase, the polymer molecules would have difficulties penetrating the very compact structure of the bulk surfactant region, therefore driving the formation of new nanostructures toward the opposite direction (Schematic 4.1). In chapter 3, the SDS–polyDADMAC interface was studied with micellar SDS solution as the ‘donor’ phase, where surfactant has high mobility. Hexagonal phase has been shown to form at concentrations in excess of 38 wt% SDS in water (Figure 2.10-B).²⁰ Thus, using a hexagonal phase as the donor phase would impart restricted mobility of the surfactant in the system and may enable investigation of polymer mobility somewhat decoupled from surfactant movement, or at least with significant hindrance of polymer movement into the surfactant phase.



Schematic 4.1 A model depicting the possible movement of surfactant (S), polymer (P), and water (w) molecules and the formation of nanostructures across an interface created between a dilute polymer solution (left) and a surfactant hexagonal phase (right).

Another approach to direct the growth of nanostructures across surfactant–polymer interfaces could be achieved by immobilising the polymer through cross-linkings. Cross-linked polymers are commonly exploited as hydrogels for their swelling behaviour in certain conditions, such as changes in pH.^{21–23} The rate of diffusion of surfactant micelles measured within the core of these gels was considerably slower than in the external surfactant solution, which was found to increase with an increased swelling of the network.^{24, 25} Nilsson *et al* demonstrated that the formation of nanostructures within the core of the gel can be manipulated by effectively rendering the polymer immobile.^{26, 27} The kinetics of deswelling of a cross-linked polyacrylate gel with a series of alkyltrimethylammonium bromide surfactants were studied by the use of a micromanipulator.²⁶ The deswelling process was governed by the ion–exchange kinetics for the transport of surfactant from the bulk solution to inside the gel core, where the concentration of the surfactant was measured by steady–state fluorescence.²⁶ The rate of diffusion of surfactant molecules into the core of the gel was driven greatly by the free energy gained by the system due to the association between the charged

cross-linked polymer gel and the oppositely charged surfactant molecules, and the subsequent formation of complexes.²⁶ Therefore, it is anticipated that an increase in the initial concentration gradient existing across the CTAB–PA gel interface by introducing more concentrated CTAB micellar solution would accelerate the rate of structure formation within the macrogel more than if the gel was in contact with a solution of surfactant prepared at lower concentrations. Nilsson *et al.* also showed that the adsorption of CTAB micelles onto the surface of the gel caused an initial collapse of the polymer due to the formation of *Pm3n* cubic phase within the surface layer of the gel.²⁸ As increasing amounts of micelles diffused into the gel, the surface layer now comprised of densely packed hexagonal phase structures with a reduced water content continued to exert pressure toward the core until it fully collapsed.^{26, 28, 29} The global phase behaviour of the system was examined, as well as the distribution of the cationic surfactant molecules from the aqueous solution to inside the gel, however, spatially resolved information on structure and composition across the surfactant–polymer interface was not determined. Thus, the interface formed between a cross-linked polyacrylate gel and solution of alkyltrimethylammonium bromide surfactants provides a means of constraining diffusion of the polymer phase, to enable insight into surfactant mobility in these systems, and is therefore complementary to the SDS hexagonal phase approach for restricting the movement of surfactant molecules. It was shown previously that both concentration and structure gradients were formed across the interface created between 20 wt% SDS and 20 wt% polyDADMAC. Hence, it is expected that a gradient of surfactant concentration will be established across the CTAB–PA macrogel interface, leading to a gradient of different structures also formed over time.

In this chapter, synchrotron SAXS and Raman microscopy were again used to spatially resolve the structure and composition across surfactant–polymer interfaces where one

component has been constrained using the aforementioned approaches of constraining the movement of materials in the system. Specifically, the constraint of the surfactant in the SDS and polyDADMAC system by formation of the hexagonal phase as the donor phase for surfactant has been studied in contact with a low concentration polyDADMAC solution, as has the constraint of the polymer component by cross-linking the polyacrylate gel and introducing cetyltrimethylammonium bromide (CTAB) as the surfactant phase. In addition, the rate and direction of structure formation and diffusion of components across these oppositely charged surfactant–polymer interfaces has been elucidated.

4.2 Hypotheses and Aims

Hypothesis 1

That constraining the mobility of a system component will influence the direction in which structures are formed across surfactant–polymer interfaces. Specifically:

- i. That cross-linking of polyacrylate will direct the formation of liquid crystalline structures toward the core of the macrogel upon contact with CTAB solution.
- ii. That an SDS hexagonal phase will serve as a ‘donor’ for the release and diffusion of SDS micelles across the SDS–polyDADMAC interface into a dilute polymer solution where a gradient of different mesophases will form over time.

Hypothesis 2

That a gradient of surfactant concentration will be established across the CTAB–polyacrylate macrogel interface, leading to a gradient in different structures over time.

Hypothesis 3

That the diffusion of mobile components from their initial phase regions and across the CTAB–polyacrylate macrogel or SDS–polyDADMAC interface will determine the rate of structure formation.

In order to investigate these hypotheses, the following aims were achieved.

1. To study the phase behaviour and distribution of molecules across the SDS–polyDADMAC interface where the surfactant region exists as a highly viscous hexagonal phase.
 - i. To spatially characterise the nanostructures formed across the SDS–polyDADMAC interface at different time points.
 - ii. To map the distribution of SDS, polyDADMAC, and water molecules across the SDS–polyDADMAC interface at different time points.
2. To study the kinetics of structure of formation across the CTAB–polyacrylate macrogel interface.
 - i. To spatially characterise the nanostructures formed across the CTAB–polyacrylate macrogel at different time points.
 - ii. To spatially map the relative concentrations of CTAB and water across the CTAB–polyacrylate macrogel interface at different time points.
 - iii. To determine how the CTAB concentration influences the rate of structure formation toward the core of the polyacrylate macrogel.

4.3 Materials

Sodium dodecyl sulphate (SDS, BioXtra, ≥ 99.0 %), acrylic acid anhydrous (contains 180–200 ppm MEHQ as inhibitor, 99 %), N,N'-methylenebis(acrylamide) (NMBA, 99%), ammonium persulphate (AP, reagent grade, 98 %), and N,N,N',N'-tetramethylethylenediamine (TEMED, ReagentPlus[®], 99 %) were purchased from Sigma-Aldrich (Sydney, Australia). Potassium hydroxide (KOH, Emsure) was obtained from Merck Millipore (Darmstadt, Germany). Poly(diallyldimethylammonium chloride)(polyDADMAC, Merquat[™] 100, molecular weight: 1.5×10^5 g/mol) was sourced from Nalco Company (Illinois, United States). The commercial solution of polyDADMAC obtained contained 53.3 % solid and 46.7 % water (standard deviation: ± 0.3 %) as determined by gravimetric analysis ($n = 10$). Merquat[™] 100 was dried prior to preparation of polyDADMAC stock solutions to form a waxy solid.

All materials were used without further purification. Milli-Q grade water purified through a Milli-pore system (Billerica, United States) was used throughout the studies.

4.4 Methods

4.4.1 Synthesis of the Cross-linked Polyacrylate Macrogel

Cross-linking of polyacrylate effectively produces a macrogel that is immobile. Constraining the polymer by this approach provides a means of directing the diffusion of CTAB molecules and growth of nanostructures toward the core of the PA macrogel.

The synthesis of the PA macrogel was based on the procedure outlined by Nilsson *et al.*²⁶ Briefly, a solution of 1.6 M acrylic acid, 14 mM NMBA (cross-linker), and 6 mM TEMED (initiator) was prepared and degassed under vacuum. The solution was transferred into a glass

beaker and heated to 65 °C for 3 hr. The gel was transferred to a 0.5 M KOH solution overnight. After washing (3 x 12 hr) in large excess of Milli-Q water the fully swollen gel was dehydrated in a vacuum oven to prevent degradation. The PA macrogel contained ~98 % water content as determined by gravimetric analysis (n = 10). The cross-linked polyacrylate crystals were rehydrated prior to sample preparation.

4.4.2 Preparation of the Surfactant–Polymer Interfaces

4.4.2.1 CTAB/Polyacrylate Macrogel System

To closely compare the phase behaviour across the CTAB–polyacrylate macrogel interface with the system investigated by Nilsson *et al.*, the concentration of CTAB was prepared at 0.2 wt% (5 mM). In addition, CTAB was also prepared at a concentration 5-fold greater than the control system at 1 wt% (~27 mM) to study the effect of surfactant concentration on the kinetics of structure formation across the CTAB–PA macrogel interface.

The polyacrylate macrogel was loaded into the flat cell in its swollen state. This was achieved by delivering the gel by a syringe fitted with a 29G needle to produce a disk ~2 mm in diameter. The bottom end of the flat cell was sealed with parafilm, and then CTAB solution was carefully pipetted into the free volume to ensure complete contact with the polymer gel disk. The centre of the disk was marked as a reference to determine the extent of which the gel swelled upon contact with the surfactant solution.

4.4.2.2 SDS_{H₂O}/PolyDADMAC System

The SDS component was prepared at 40 wt% where it exists as a hexagonal phase at room temperature,³⁰ while a comparatively dilute polymer solution was prepared with 4 wt% polyDADMAC.

Due to the high viscosity of the hexagonal phase, the surfactant ‘gel’ component was delivered into the bottom end of the flat cell also via a syringe fitted with a 29G needle. Once the material occupied half the volume of the flat cell, the bottom was then wiped clean and sealed with parafilm. The firm boundary residing at the interface was marked as the point of origin, above which the polyDADMAC solution was added carefully by pipette and the top end of the flat cell was sealed with parafilm.

4.4.3 Characterisation of Nanostructures Across Surfactant–Polymer Interfaces

The growth and development of liquid crystalline structures across the surfactant–polymer interfaces studied in this chapter were viewed under a crossed–polarised microscope and spatially resolved at 100 μm steps with synchrotron small angle X–ray scattering as described in Chapter 2 (Section 2.4.3). Line scans across the CTAB–PA macrogel interfaces were conducted from the centre of the polymer disk to the outer surfactant solution (see Appendix A4.1 for details on the instrument specifications).

4.4.4 Determining the Distribution of System Components Across Surfactant–Polymer Interfaces

4.4.4.1 *CTAB/Polyacrylate Macrogel System*

Raman microscopy was employed to measure changes in the relative concentrations of CTAB and water within the PA macrogel over time. A Raman signal was not detectable for the polyacrylate gel itself since it only contained 2 wt% dry crystal granules. However, the Raman intensity (measured as area under the curve) of the C–H bending energy exhibited at

$\sim 1440\text{ cm}^{-1}$ for CTAB was used to map its relative concentration across the PA macrogel in comparison to the bulk surfactant solution (Figure 4.1). In addition, the relative water content across the interface was determined from the vibrations between 3000 and 3760 cm^{-1} (Figure 4.1).

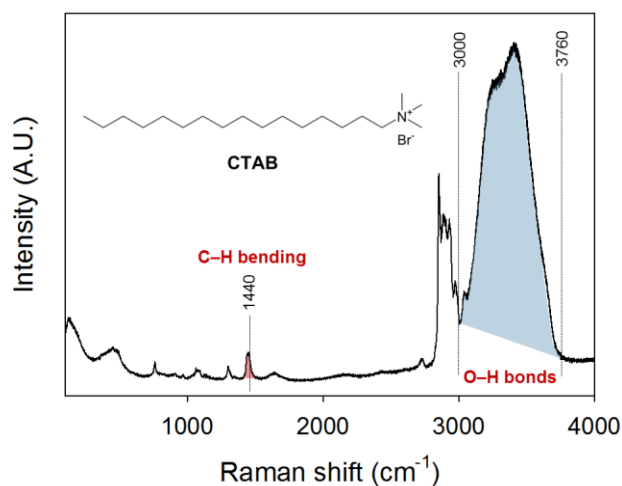


Figure 4.1 Raman spectrum of CTAB prepared in Milli-Q water. The Raman intensity (area under the curve) obtained for the peaks at $\sim 1440\text{ cm}^{-1}$ and between $3000\text{--}3760\text{ cm}^{-1}$ were used to map the relative concentrations of CTAB and water across CTAB–PA gel interfaces.

4.4.4.2 *SDS_{HI}/PolyDADMAC System*

Line scans were performed with Raman microscopy across SDS–polyDADMAC interfaces using the same approach described in Chapter 2. The area under the curve calculated for the peaks representative of the SDS and polyDADMAC molecules in the Raman spectra were used to interpolate the concentration present from the calibration curves generated for the corresponding constituents (Table 2.4). The concentrations of water and SDS across SDS–polyDADMAC interfaces were determined from the lattice parameter of the hexagonal phases characterised by synchrotron SAXS as described in Chapter 2 (Section 2.4.4.2).

4.5 Results

4.5.1 Kinetics of Structure Formation Across the CTAB–Polyacrylate Macrogel Interface

4.5.1.1 Growth of Mesophases Within the Polyacrylate Macrogel

A gradient of structures formed across the CTAB–PA macrogel interface was visualised with crossed–polarised light microscopy (Figure 4.2) and spatially resolved with synchrotron SAXS (Figure 4.3 to Figure 4.6). Isotropic $Pm3n$ cubic phase (Figure 4.3 and Figure 4.5) was the earliest structure to form within the gel. Almost immediately after initial contact between the two components, a birefringent band of hexagonal phase appeared within the outer circumference of the gel disk, which subsequently developed toward the core of the gel over time (Appendix–Figure A4.1). The kinetics involved in the complete transition from $Pm3n$ cubic to hexagonal phases existing within the PA gel was significantly influenced by the initial concentration of CTAB in the bulk solution.

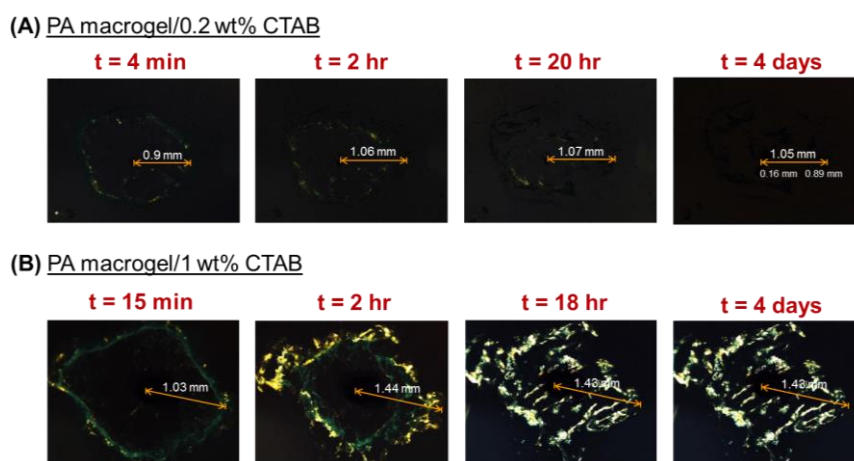


Figure 4.2 CPLM images of the growth of anisotropic structures across a disk of polyacrylate macrogel after contact with a solution of CTAB at 0.2 wt% (A) and 1 wt% (B). The approximate radius (mm) of the polymer disk at the various time points are annotated on the images.

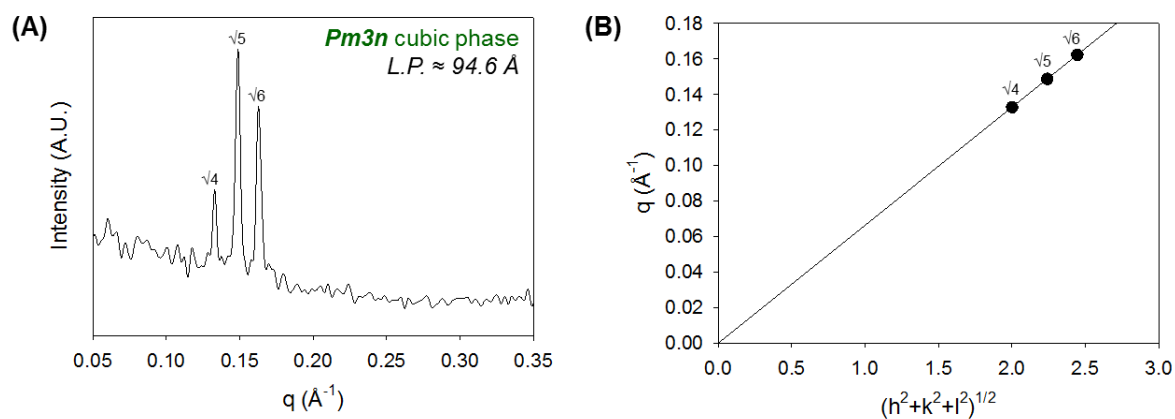


Figure 4.3 Representative SAXS profile of $Pm3n$ cubic phase formed within the polyacrylate macrogel at $t = 3$ days after initial contact with 0.2 wt% CTAB solution (A) and the corresponding Miller indices vs. q (\AA^{-1}) plot (B).

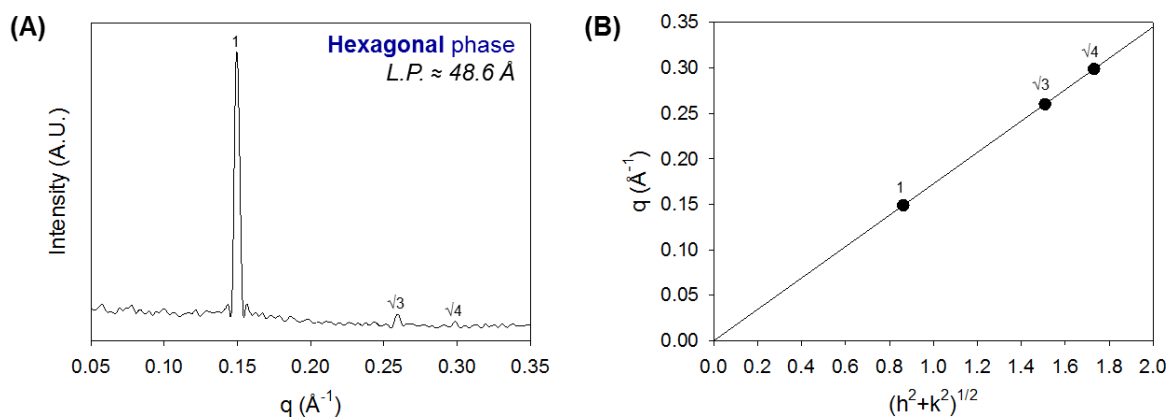


Figure 4.4 Representative SAXS profile of hexagonal phase formed within the polyacrylate macrogel at $t = 7$ days after initial contact with 0.2 wt% CTAB solution (A) and the corresponding Miller indices vs. q (\AA^{-1}) plot (B).

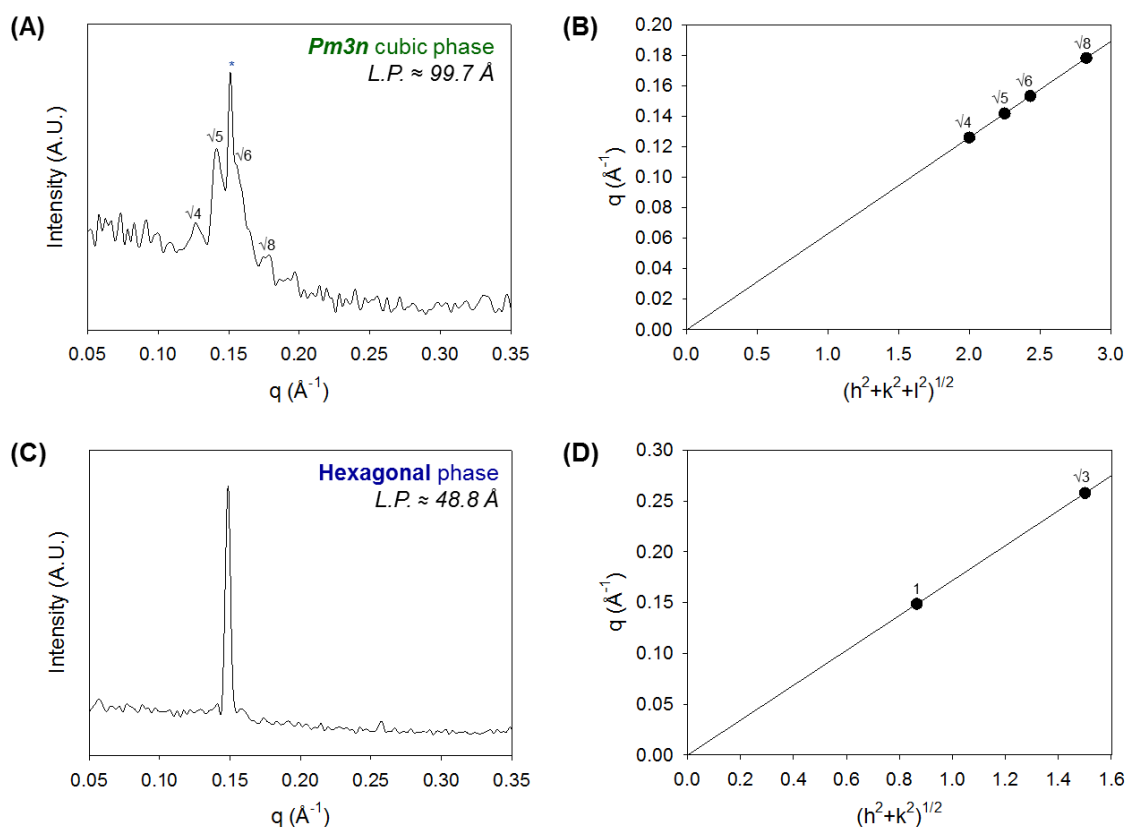


Figure 4.5 Representative SAXS profiles $Pm3n$ cubic phase (A) and hexagonal phase (C) existing across the polyacrylate macrogel at $t = 2$ hr after initial contact with 1 wt% CTAB solution, and the corresponding Miller indices vs. q (\AA^{-1}) plots (B, D).

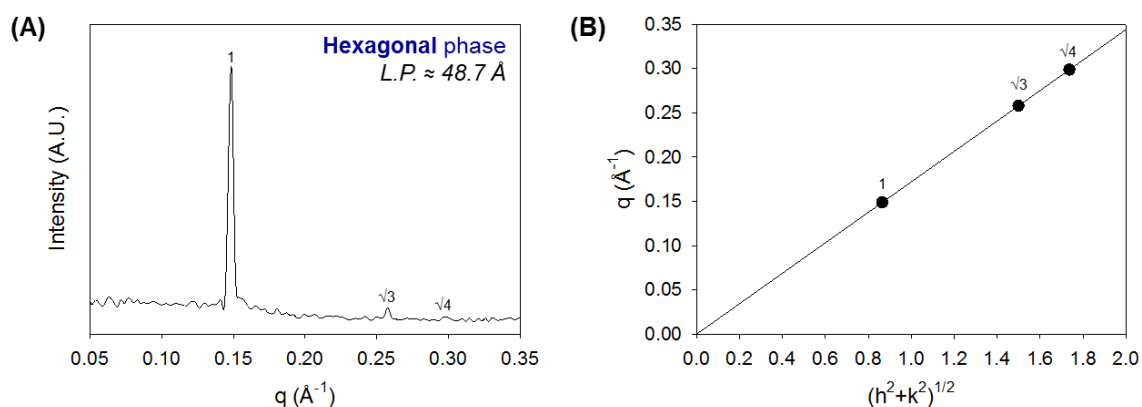


Figure 4.6 Representative SAXS profile of hexagonal phase formed within the polyacrylate macrogel at $t = 3$ days after initial contact with 1 wt% CTAB solution and the corresponding Miller indices vs. q (\AA^{-1}) plot (B).

4.5.1.2 Frontal Diffusion of CTAB Molecules into the PA Macrogel

The growth of mesophases toward the centre of the PA macrogel was supported by the diffusion of CTAB molecules into the polymer disk. The local relative concentration of CTAB was initially highest in the outermost regions of the gel at early time points (Figure 4.7-A). Over time, the CTAB molecules became well distributed throughout the gel with formation of ordered structures (Figure 4.7-B, C). A reduction in the water content within the gel was also observed. The rate at which the composition changed across the interface greatly depended on the initial CTAB concentration in the bulk solution, which was in agreement with rate of structure formation determined by CPLM and synchrotron SAXS.

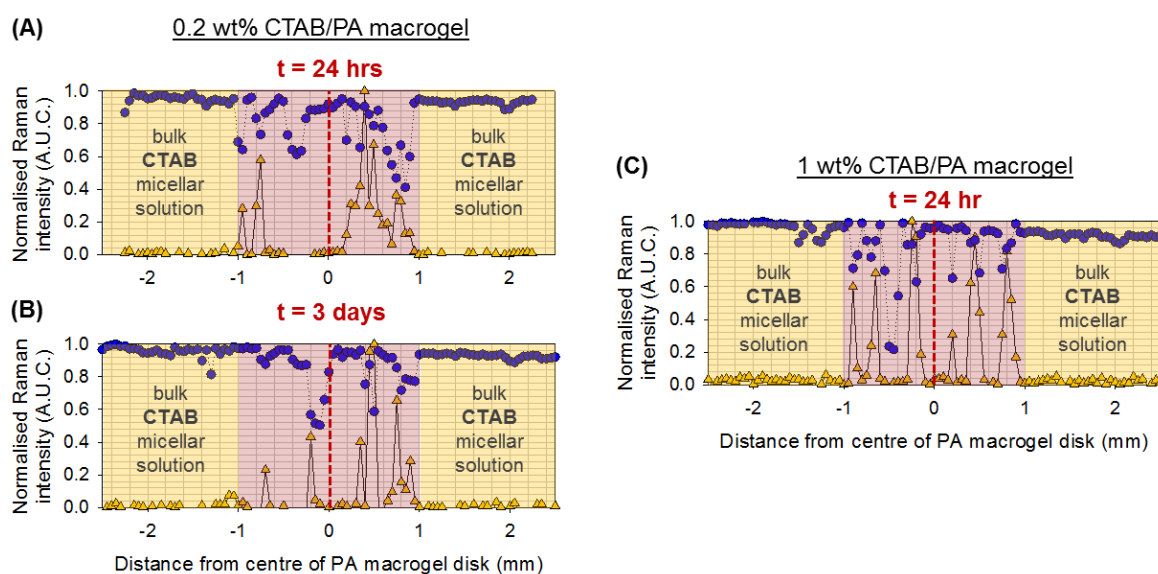


Figure 4.7 Normalised Raman intensity of CTAB (yellow triangles) and water (blue circles) molecules mapped across the PA macrogel disk over time after contact with low (A, B) or high (C) concentration of surfactant solution. This enables trends in the relative concentrations of surfactant and water to be followed rather than their absolute concentrations.

4.5.2 Dynamics of Structure Formation Upon Contact of SDS Hexagonal Phase with Dilute PolyDADMAC Solution

4.5.2.1 Mesophases Formed Across the SDS_{HI}–PolyDADMAC Interface

Constraining the mobility of surfactant molecules or micelles across this SDS–polyDADMAC interface by introducing SDS in the form of hexagonal phase led to the formation of new hexagonal and micellar phases predominantly towards the dilute polyDADMAC solution (Figure 4.8 and Figure 4.10).

Micrographs obtained with CPLM showed that the optical texture displayed by the birefringent structures formed across the interface a week after initial contact (Figure 4.8, $t = 6$ days) differed from those originally existing in the bulk SDS region (Figure 4.8, $t = 9$ hr).

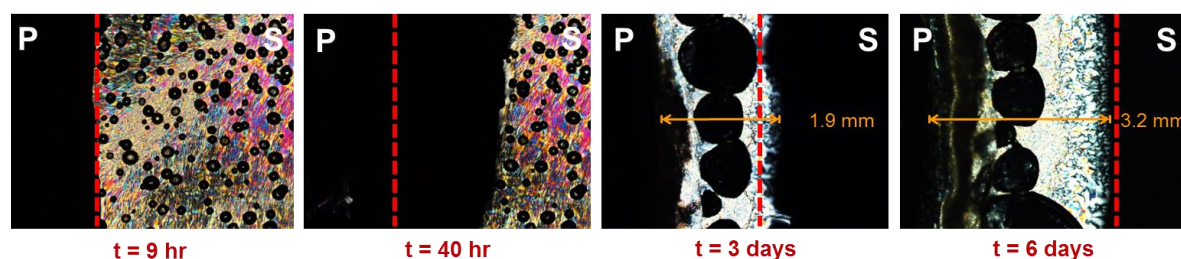


Figure 4.8 The growth of structures exhibiting birefringence across the interface between solutions of 4 wt% polyDADMAC (P) and 40 wt% SDS (S) viewed under crossed-polarisers. The dashed line marks the point of origin. *Note: black circles represent bubbles.*

The rate of structure formation across the SDS–polyDADMAC interface when studied at this composition was significantly slower in comparison with the 20 wt% SDS: 20 wt% polyDADMAC system described in Chapter 3. Here, the width of the band comprising of hexagonal phase increased approximately linearly with the square root of time throughout

the duration of the kinetic study at a rate of ~ 0.02 mm/hr, also indicating diffusion-controlled transfer of material (Figure 4.9). Whereas the mesophases formed across the SDS–polyDADMAC interface studied at the other composition grew at a rate of ~ 0.06 mm/hr, which slowed down after ~ 3 days from initial contact.

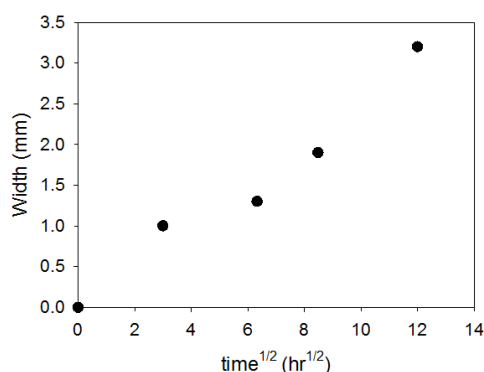


Figure 4.9 Rate of structure growth across the 40 wt % SDS–4 wt % polyDADMAC interface.

Characterisation of these anisotropic structures by synchrotron SAXS revealed that both were hexagonal phases (Figure 4.10). However, the absolute positions of the Bragg reflections varied significantly, indicating differences between their internal dimensions. Specifically, the lattice parameter of hexagonal phase present in the bulk SDS region was ~ 53 Å (Figure 4.11-A), while those formed across the interface were ~ 41 Å (Figure 4.11-D).

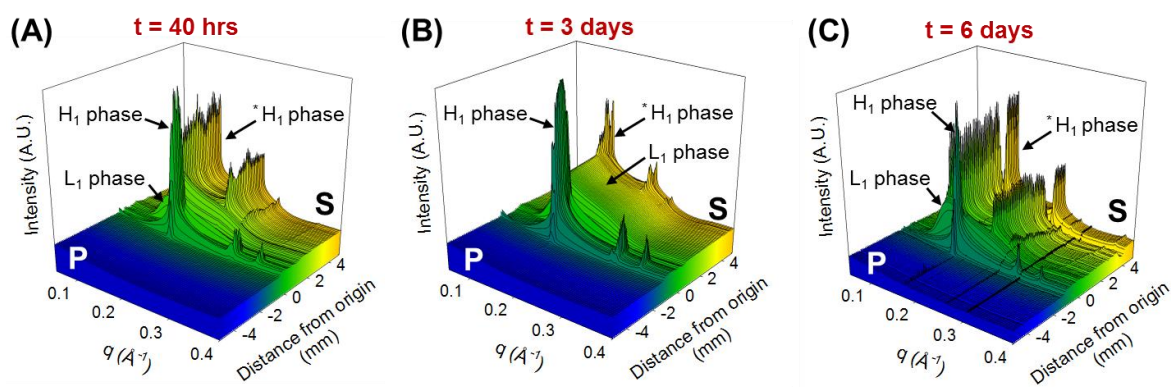


Figure 4.10 SAXS waterfall plots of the formation of hexagonal (H_1) phase upon contact between a 4 wt% polyDADMAC solution (P) and a 40 wt% SDS hexagonal ($*H_1$) phase (S).

Interestingly at $t = 3$ days, a large isotropic region existed in between the two regions consisting of hexagonal phase (Figure 4.8), suggesting the growth of new hexagonal and micellar phases (Figure 4.11-B, C, D) simultaneously across the interface (Figure 4.10-B). Over time, more hexagonal phase formed where rod-like micelles existed previously (Figure 4.10-C).

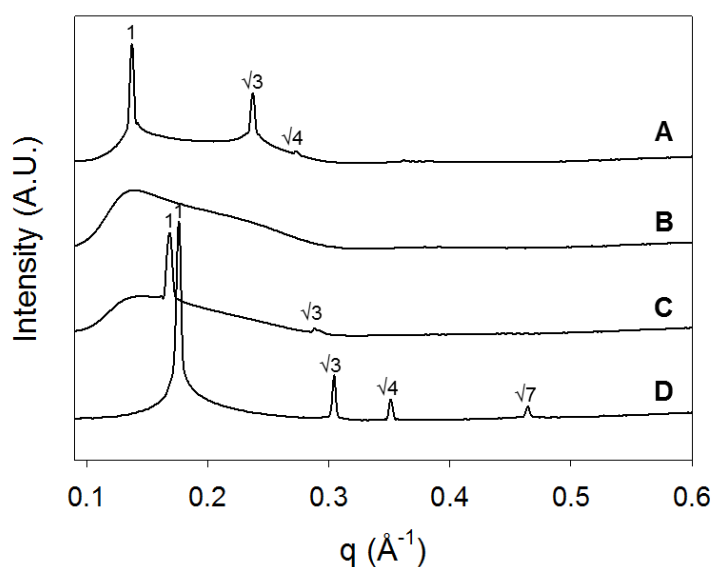


Figure 4.11 Selected SAXS profiles across the SDS–polyDADMAC interface at $t = 3$ days. Bulk SDS hexagonal phase (A), micellar phases (B), coexisting hexagonal and micellar phases (C), and regions of only hexagonal phase (D) were present across the interface.

A gradient of structures were not only formed across the SDS–polyDADMAC interface, but gradients in the lattice parameter of hexagonal phase were also evident (Figure 4.12). As established during method development, the lattice parameter of hexagonal phases can be correlated within the approximate amount of SDS and water molecules present locally across the interface. Therefore, following trends in the internal size of mesophases formed across the SDS–polyDADMAC interface enabled changes in the local composition and distribution of molecules to be determined over time.

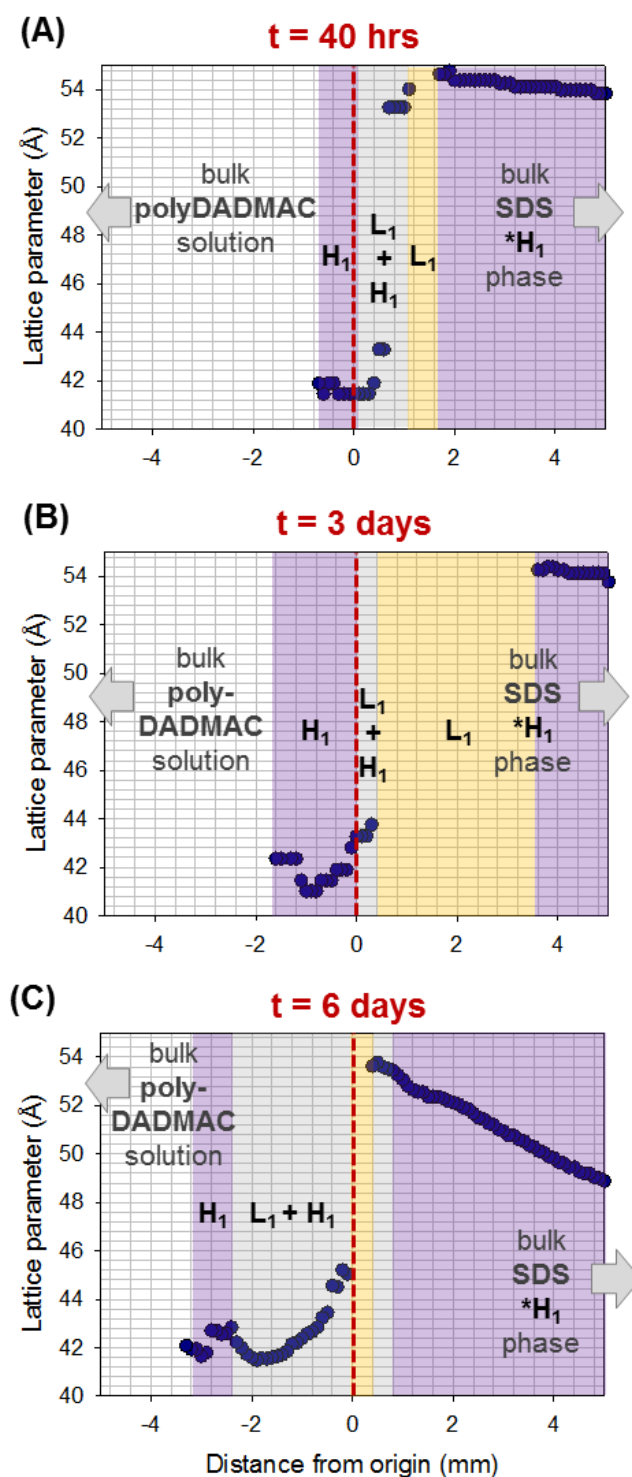


Figure 4.12 Changes in the lattice parameter of hexagonal phases formed across the 40 wt% SDS ($*H_1$ phase)–4 wt% polyDADMAC interface over time. Coloured regions highlight the presence of SDS micelles (L_1 –yellow), coexisting micellar and hexagonal phases (L_1+H_1 – grey), and hexagonal phases only (H_1 –purple).

4.5.2.2 Correlating Changes in Composition with the Formation of Mesophases Across the SDS_{HI}–PolyDADMAC Interface

Raman microscopy and synchrotron small angle X-ray scattering were both employed to map changes in the local composition across the SDS–polyDADMAC interface over time (Figure 4.13).

At $t = 40$ hr, the concentrations of SDS and polyDADMAC in their respective bulk regions were comparable to the initial known composition present prior to contact with each other, however were significantly higher across the interface (Figure 4.13-A).

At $t = 3$ days, there was a further increase in the polymer concentration across the interface, which resulted in values that were below the limit of quantification with Raman microscopy in the bulk polyDADMAC solution (Figure 4.13-B). On the other hand, the concentration of SDS where hexagonal phases were formed across the interface did not differ greatly to the amount measured at the previous time point. However, there was a significant decrease in the surfactant concentration in the region in between the new hexagonal phases formed and the initial hexagonal phase present in the bulk SDS region, which corresponded to the formation of SDS micelles. Moreover, the decrease in the concentration of SDS as the interface was approached from the bulk SDS region suggests that the SDS micelles diffused across the interface to participate in the formation of new hexagonal phase or coexist as free or bound micelles within that region.

The diffusion of SDS micelles from the bulk SDS hexagonal phase and across the SDS–polyDADMAC interface was proposed to be the main factor driving the growth of mesophases toward the bulk polymer solution. In addition, the redistribution of polyDADMAC molecules across the interface at $t = 6$ days highlights the large degree of mobility polyDADMAC has in solution and across viscous materials formed (Figure 4.13-C).

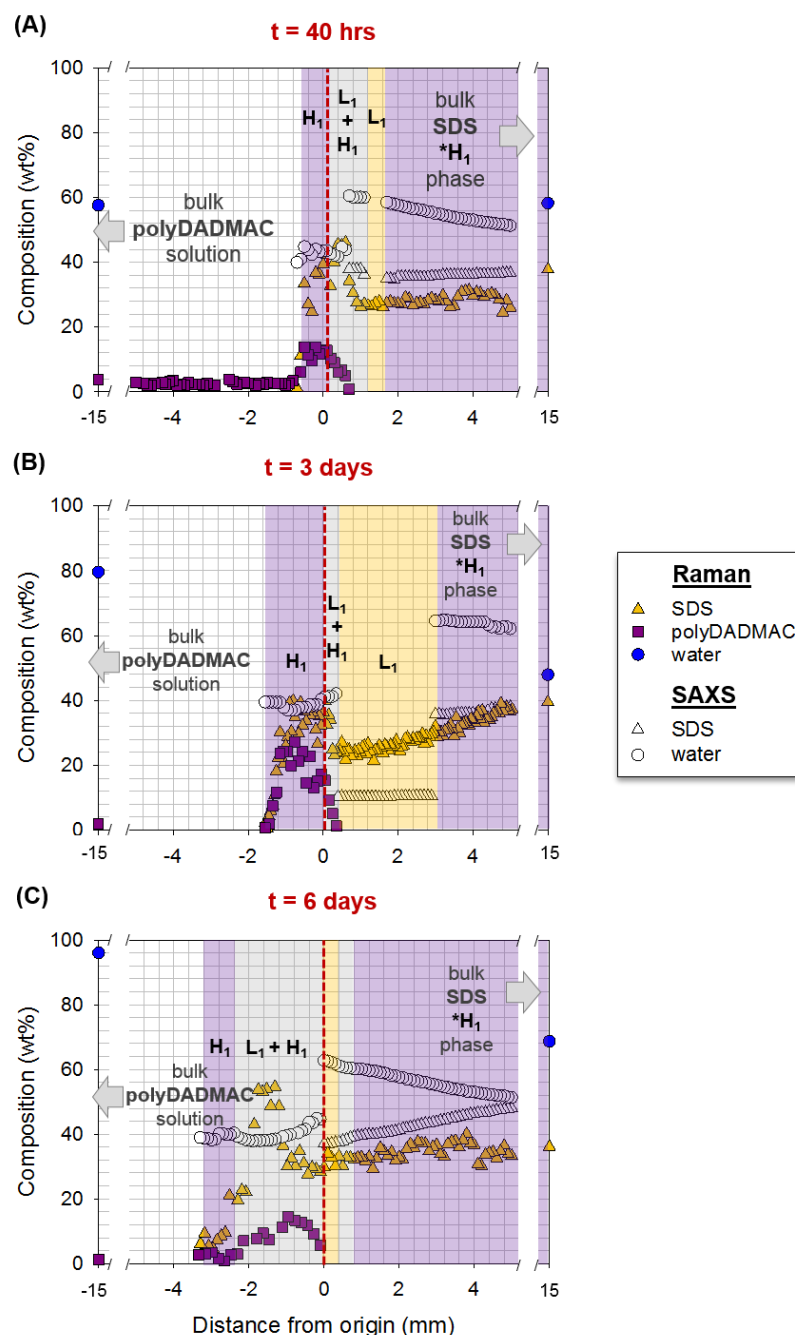


Figure 4.13 Mapping the concentrations of polyDADMAC (squares), SDS (triangles), and water (circles) across the SDS–polyDADMAC interface at 40 hr (A), 3 days (B), and 6 days (C) after initial contact between 40 wt% SDS (*H₁ phase) and 4 wt% polyDADMAC measured by Raman microscopy (filled symbols) or synchrotron SAXS (open symbols). Coloured regions highlight the presence of SDS micelles (L₁–yellow), coexisting micellar and hexagonal phases (L₁+H₁–grey), and hexagonal phases only (H₁–purple).

It should be noted that the measured Raman intensities for water in the bulk surfactant and polymer regions at $t = 40$ hr (60 wt %) and 3 days (80 wt%) disagreed with their known starting concentrations (> 95 wt%), which is a major limitation of Raman microscopy for providing quantitative analysis of materials. Nevertheless, the findings presented in Figure 4.13 demonstrate that the dilution of the SDS hexagonal phase with water triggered the release and facilitated the transport of SDS micelles across the SDS–polyDADMAC interface. Therefore, it was proven that the SDS hexagonal phase acted as a donor site of SDS micelles and structures evolved towards the polymer solution when the mobility of the surfactant was no longer restricted after contact with the dilute solution of polyDADMAC.

4.6 Discussion

4.6.1 Dynamic Phase Behaviour Across the Cross-linked Polyacrylate Gel Upon Contact with CTAB Solution

Exploiting the cross-linked polyacrylate macrogel directed the diffusion of CTAB molecules and the formation of nanostructures toward the core of the polymer network.

Upon contact of the polyacrylate macrogel with a solution of CTAB, a layer of liquid crystalline structure was formed on the ‘surface phase’ of the polymer disk as described by Nilsson *et al.*²⁶ Under crossed-polarisers, this layer appeared to be primarily birefringent, however characterisation with SAXS showed the existence of $Pm3n$ cubic phase prior to the formation of the anisotropic hexagonal phase (Figure 4.3). It is possible that the number of anionic charges presented by the polymer chains within the cross-linked polyacrylate gel strongly attracted the oppositely charged surfactant molecules from the bulk solution to cause the immediate diffusion of CTAB into the gel.^{31, 32} Subsequently, the cooperative binding of

CTAB with the polyacrylate chains led to the formation of ordered structures, as is often demonstrated by similar oppositely charged surfactant and cross-linked polymer systems.²⁷

33, 34

The molar concentration of CTAB within the gel determined the type of mesophase formed. *Pm3n* cubic phase developed toward the core of the polymer gel as a consequence of the frontal diffusion of CTAB towards the core of the polymer gel, across which a surfactant concentration gradient was created over time. The immediate formation of cubic phase within the gel also suggests that CTAB molecules were highly permeable across the gel surface. Afterwards, the diffusion of more surfactant molecules inside the gel resulted in the self-assembly of hexagonal phase, which was not surprising as literature has shown that discrete *Pm3n* cubic phases can transition into hexagonal phases at higher surfactant concentrations.^{35, 36} Specifically, as the concentration of the bromide ions increased inside the gel, there was a greater tendency for more dense and highly ordered structures to form.²⁶ Therefore, further diffusion of CTAB toward the core of the gel resulted in the gradual appearance of anisotropic structures towards the core. Aside from the diffusional barrier created by the nanostructured complexes formed in the PA macrogel, the ability of the matrix to expand and collapse upon changes in composition may also contribute to the rate-determining step of structure formation within the cross-linked polyacrylate gel.

Contact of the polyacrylate gel with a higher concentration of CTAB initially in the bulk solution increased the driving force for the diffusion of CTAB into the gel resulting in the earlier formation of hexagonal phase. Lapitsky *et al.* also demonstrated that dropwise addition of a solution of a cationic polymer into higher concentrations of mixed micellar solutions was favourable toward the efficient production of structured gel particles.¹⁸ When a critical concentration of CTAB was reached inside the polyacrylate gel, reorganisation of micellar

aggregates from discrete cubic assemblies into hexagonal lattices occurred. In other words, the concentration of surfactant present inside the polyacrylate macrogel increased progressively with the diffusion of CTAB into the gel until the system composition ceased to change. Since the concentration of polyion within the cross-linked gel network remained constant throughout the study, the key rate-limiting step to the evolution of different structures across the CTAB–PA macrogel interface was the diffusion of surfactant molecules inside the polymer gel, which was accelerated when a higher concentration gradient was created between the bulk CTAB solution and the stagnant polymer gel.

It was evident in the CPLM images that formation of birefringent material within the cross-linked gel was not evenly distributed. The heterogeneity of charged ions displayed within a polymer network has been described to possibly cause the non-uniform distribution of surfactant molecules across cross-linked gels.^{23, 27} Hence, this theory could also rationalise the appearance of random bright textures of hexagonal phases formed throughout the PA macrogel studied here. It is also worth mentioning that the degree of cross-linking within the polymer gel could influence the porosity of the matrix through which surfactant molecules must diffuse into from the bulk solution. This could also affect the distribution of CTAB molecules inside the PA gel disk that are most likely to exist as micelles and subsequently how compact or dense the resulting polyacrylate macrogel becomes due to the formation of complexes comprised of ordered mesophases.

In summary, the apparent surfactant-to-polymer molar charge ratio within the polyacrylate macrogel determined the mesophases formed. Furthermore, the concentration gradient created between the cross-linked polymer and the surrounding surfactant solution dictated the rate of diffusion of CTAB molecules and the self-assembly of mesophases toward the centre of the gel. The findings presented here are in agreement with the system studied by

Nilsson *et al.* demonstrating the adaptability of synchrotron SAXS and Raman microscopy to study the kinetics of structure formation across interfaces created not only between two solutions, but also solutions and gel disks.

4.6.2 Implications of Cross-linked Polymers and Oppositely Charged Molecules in Drug Delivery

The high swelling capacity of cross-linked polymer gels demonstrated upon absorption of large volumes of water and responsiveness to certain stimuli render hydrogels desirable as a means of controlling the release of drugs from such matrices.³⁷⁻⁴⁷

Generally, when charged cross-linked polymer gels are surrounded by a solution of oppositely charged surfactant deswelling occurs.^{23, 26, 27, 33} This phenomenon can be described by the neutralisation of charges and the formation of dense ordered structures within the gel, which causes the collapse of the polymer network and expulsion of water molecules into the surrounding solution.²⁶ However, slight swelling of the cross-linked polyacrylate gel resulted upon its contact with the CTAB solution, which contradicts the behaviour often exhibited by these systems. The extent of swelling demonstrated by hydrogels in aqueous solutions depends highly on the osmotic pressure difference existing between the bulk solution and the interior of the gel.^{43, 48} Given that only mobile ions present across the system contribute to the osmotic pressure, it was expected that water molecules would be transported out of the gel to compensate for the osmotic pressure difference. The measured relative content of water inside the gel was considerably lower than in the bulk solution after the formation of liquid crystalline structures within the polyacrylate macrogel, which supports the theory that the diffusion of water into the bulk surfactant solution was osmotically driven. Therefore, there must be a different mechanism responsible for the swelling of this gel upon contact with the

solution of surfactant. Perhaps the increase in ionic strength or rather the concentrations of charged surfactant ion and its counterion inside the gel led to an increase in the electrostatic repulsion experienced between the structured complexes, thus causing the gel to swell.

The formation of ordered structures within a cationic cross-linked polymer gel upon the inward diffusion of anionic surfactants provides a platform for the encapsulation of oppositely charged therapeutics within such polymer networks. The study of the diffusion kinetics and distribution of proteins and peptides within oppositely charged cross-linked polymer gels have received increasing interest over the decades.^{32, 49–52} Bysell *et al.* demonstrated the formation of a thin surface layer upon interaction of poly-L-lysine with polyacrylic acid macroscopic gel networks, which propagated inwards at the expense of the swollen gel core.²³ Furthermore, the rate of diffusion of protein into the gel was determined by the peptide concentration adsorbed onto the surface, as well as the molecular weight of the peptide.²³ As described earlier, the degree of cross-linking within a polymer gel greatly influences the extent of swelling in aqueous media, which in turn controls the release behaviour of payload from these systems. Therefore, studying the structural attributes of mesophases formed across such surface layers and their response to certain stimuli, such as changes in temperature, salt concentration, or solution pH, would be advantageous in the design and delivery of charged drugs from stimuli-responsive cross-linked biomaterials.

4.6.3 The Importance of SDS Concentration in the Formation of Micellar-like Ordered Structures Upon Contact with Solutions of Mobile PolyDADMAC Molecules

The formation of coexisting micellar and hexagonal phases was evident across the SDS–polyDADMAC interfaces studied in Chapter 3 and Chapter 4, which demonstrates that

constraining the mobility of SDS by introducing the surfactant component as hexagonal phase did not inhibit the development of concentration gradients across such interfaces. More so, the initial concentrations within the respective bulk regions did not influence the type of mesophases formed across the interface, but rather the local composition.

In both systems, polyDADMAC molecules in the bulk solutions were relatively mobile where its intrinsic viscosity was dictated by the degree of entanglements present, which depended mainly on the packing of the polymer chains.⁵³⁻⁵⁷ Polymers have been described to move in a snake-like motion in solution,^{58, 59} so it was not surprising that diffusion of polyDADMAC was greater across solutions of spherical micelles than through more compact structures. Essentially, the presence of hexagonal phase in the bulk SDS region hindered the penetration of polyDADMAC into this phase. Svensson *et al.* have also reported of the obstruction effects of polymer having to diffuse through stationary micelles within a concentrated matrix.³⁵ Thus, the diffusivity of polyDADMAC across the interface immediately after initial contact of the two components was an early factor in determining the direction in which mesophases would form across the SDS–polyDADMAC interface.

As established in this chapter, the hexagonal phase existing in the bulk 40 wt% SDS region represented a source of SDS micelles. Upon contact with the dilute polyDADMAC solution, the SDS micelles were expelled from this constrained region and temporarily attained greater mobility. Subsequent diffusion of these SDS micelles into the polymer solution resulted in the formation of hexagonal phase and rod-like micelles simultaneously, which constituted the initial interfacial region. Laurati *et al.* demonstrated a similar process where the breaking of bonds must occur prior to the creation of a gelation boundary upon interaction between solutions of colloids and polymer.⁶⁰ Therefore, it is recognised that the time associated with the dissociation of SDS micelles to form the SDS hexagonal phase is an

additional rate-determining step in the formation of mesophases across the SDS–polyDADMAC interface. As a result, the kinetics of structure formation was faster upon contact of polyDADMAC with SDS initially existing as spherical micelles in solution.

Different concentration gradients existed across the SDS–polyDADMAC interface over time. Importantly, hexagonal phases with smaller internal dimensions were formed at the interface in comparison with those existing in the bulk SDS region. The increase in concentration of polymer at the interface and its subsequent association with the oppositely charged SDS micelles could explain the formation of more compact structures at the interface. More so, the rate of diffusion of molecules across the bulk and interfacial regions was controlled by the local viscosity across the system, which in turn determined the local composition of structures formed across the interface. While the viscosity across the SDS–polyDADMAC interface was not measured, the diffusion behaviour of key components in the system was inferred from studying both the structural and compositional changes over time. Furthermore, the Stokes–Einstein law for diffusion in solution (Equation 1.2) describes that viscosity and diffusion are inversely proportional. Thus, they are not only important in governing the mixing kinetics in such systems, but they may also become barriers in the formation of equilibrium structures as discussed previously in Chapter 3.

The formation of lamellar phase in a mixture of SDS and polyDADMAC with a similar composition to the system studied in this chapter is a potential instability issue in formulations (Appendix–Figure A4.2), which may be due to crystallisation of SDS at high concentrations (Appendix–Figure A3.3).⁶¹ Interestingly, similar hexagonal phases were formed across SDS–polyDADMAC interfaces regardless of the initial surfactant concentration, suggesting that SDS hexagonal phases may be exploited as a SDS micelle–releasing film or within formulations to reduce the use of high volumes of water.

4.7 Conclusions

Constraining the mobility of system components across surfactant–polymer interfaces was an approach to control the direction and rate of structure formation across the interface which was achieved in two ways.

Firstly, cross-linking of polyacrylate resulted in the diffusion of CTAB molecules into the macrogel. A gradient of $Pm3n$ cubic and hexagonal phases were formed across the CTAB–PA macrogel interface. The rate at which cubic phases transitioned into hexagonal phase was significantly influenced by the surfactant concentration gradient existing across the interface after initial contact between the oppositely charged components. The phase behaviour demonstrated by this system was in agreement with analogous experiments performed by Nilsson *et al.*, highlighting the versatility of the methods developed with synchrotron SAXS and Raman microscopy for examining the kinetics of structure formation across the interface created between other types of materials.

Secondly, contact of a SDS hexagonal phase with a dilute solution of polyDADMAC led to the formation of new hexagonal phases with smaller lattice parameters and coexisting micellar phases, which grew predominantly toward the bulk polymer solution. It was proposed that the dilution of the hexagonal phase initially existing in the bulk SDS region with water triggered the diffusion of SDS micelles across the SDS–polyDADMAC interface to interact with the relatively mobile polyDADMAC molecules and the formation of ordered structures. Effectively, the mobility of surfactant molecules became less restricted for some time until they once again participated in the self-assembly of ordered structures. Therefore, the diffusion of SDS micelles across the SDS–polyDADMAC interface was the main rate-determining step toward the formation of nanostructures.

4.8 References

1. Plucktaveesak, N.; Konop, A. J.; Colby, R. H., *Viscosity of Polyelectrolyte Solutions with Oppositely Charged Surfactant*. *J. Phys. Chem. B*. 2003, 107, 8166–8171.
2. Samuel, G.; Daragh, M.; Nirmesh, J.; Michel, D.; Dominique, L., *Polyelectrolyte–Surfactant Complexes at Interfaces and in Bulk*. *J. Phys.: Condens. Matter*. 2003, 15, S219.
3. Beheshti, N.; Zhu, K.; Kjøniksen, A.–L.; Nyström, B., *Interaction Behaviors in Aqueous Solutions of Negatively and Positively Charged Hydrophobically Modified Hydroxyethylcellulose in the Presence of an Anionic Surfactant*. *Colloid Surface Physicochem. Eng. Aspect*. 2008, 328, 79–89.
4. Hoffmann, I.; Heunemann, P.; Prévost, S.; Schweins, R.; Wagner, N. J.; Gradzielski, M., *Self-Aggregation of Mixtures of Oppositely Charged Polyelectrolytes and Surfactants Studied by Rheology, Dynamic Light Scattering and Small-Angle Neutron Scattering*. *Langmuir*. 2011, 27, 4386–4396.
5. Leung, P. S.; Goddard, E. D.; Han, C.; Glinka, C. J., *A Study of Polycation—Anionic-Surfactant Systems*. *Colloid Surface*. 1985, 13, 47–62.
6. Shrestha, R. G.; Shrestha, L. K.; Aramaki, K., *Formation of Wormlike Micelle in a Mixed Amino-Acid Based Anionic Surfactant and Cationic Surfactant Systems*. *J. Colloid Interface Sci*. 2007, 311, 276–284.
7. Thalberg, K.; Lindman, B.; Bergfeldt, K., *Phase Behavior of Systems of Polyacrylate and Cationic Surfactants*. *Langmuir*. 1991, 7, 2893–2898.
8. Mukherjee, S.; Dan, A.; Bhattacharya, S. C.; Panda, A. K.; Moulik, S. P., *Physicochemistry of Interaction between the Cationic Polymer Poly(diallyldimethylammonium chloride) and the Anionic Surfactants Sodium Dodecyl Sulfate, Sodium Dodecylbenzenesulfonate, and Sodium N-Dodecanoylsarcosinate in Water and Isopropyl Alcohol–Water Media*. *Langmuir*. 2011, 27, 5222–5233.
9. Katona, J. M.; Sovilj, V. J.; Petrović, L. B., *Rheological Investigation on Dynamic and Structure of Separated Phases in Polymer Mixture–Ionic Surfactant Ternary System*. *Carbohydr. Polymer*. 2008, 74, 193–200.

10. Thalberg, K.; Van Stam, J.; Lindblad, C.; Almgren, M.; Lindman, B., *Time-Resolved Fluorescence and Self-Diffusion Studies in Systems of a Cationic Surfactant and an Anionic Polyelectrolyte*. J. Phys. Chem. 1991, 95, 8975–8982.
11. Alam, M. M.; Mezzenga, R., *Particle Tracking Microrheology of Lyotropic Liquid Crystals*. Langmuir. 2011, 27, 6171–6178.
12. Rodriguez–Abreu, C.; Acharya, D. P.; Aramaki, K.; Kunieda, H., *Structure and Rheology of Direct and Reverse Liquid-Crystal Phases in a Block Copolymer/Water/Oil System*. Colloids Surf., A. 2005, 269, 59–66.
13. Alam, M. M.; Aramaki, K., *Hexagonal Phase Based Gel-Emulsion (O/H1 Gel-Emulsion): Formation and Rheology*. Langmuir. 2008, 24, 12253–12259.
14. Mezzenga, R.; Meyer, C.; Servais, C.; Romoscanu, A. I.; Sagalowicz, L.; Hayward, R. C., *Shear Rheology of Lyotropic Liquid Crystals. A Case Study*. Langmuir. 2005, 21, 3322–3333.
15. Lapitsky, Y.; Kaler, E. W., *Formation and Structural Control of Surfactant and Polyelectrolyte Gels*. Colloids Surf., A. 2006, 282–283, 118–128.
16. Babak, V. G.; Merkovich, E. A.; Galbraikh, L. S.; Shtykova, E. V.; Rinaudo, M., *Kinetics of Diffusionally Induced Gelation and Ordered Nanostructure Formation in Surfactant–Polyelectrolyte Complexes Formed at Water/Water Emulsion Type Interfaces*. Mendeleev Commun. 2000, 10, 94–95.
17. Babak, V. G.; Merkovich, E. A.; Desbrières, J.; Rinaudo, M., *Formation of An Ordered Nanostructure in Surfactant–Polyelectrolyte Complexes Formed by Interfacial Diffusion*. Polym. Bull. 2000, 45, 77–81.
18. Lapitsky, Y.; Kaler, E. W., *Formation of Surfactant and Polyelectrolyte Gel Particles in Aqueous Solutions*. Colloids Surf., A. 2004, 250, 179–187.
19. Auvray, X.; Petipas, C.; Anthore, R.; Rico, I.; Lattes, A., *X-ray Diffraction Study of Mesophases of Cetyltrimethylammonium Bromide in Water, Formamide, and Glycerol*. J. Phys. Chem. 1989, 93, 7458–7464.
20. Kékicheff, P.; Grabielle–Madelmont, C.; Ollivon, M., *Phase Diagram of Sodium Dodecyl Sulfate–Water System*. J. Colloid Interface Sci. 1989, 131, 112–132.

21. Jabbari, E.; Nozari, S., *Swelling Behavior of Acrylic Acid Hydrogels Prepared by γ -radiation Crosslinking of Polyacrylic Acid in Aqueous Solution*. Eur. Polym. J. 2000, 36, 2685-2692.
22. Bonina, P.; Petrova, T.; Manolova, N., *pH-Sensitive Hydrogels Composed of Chitosan and Polyacrylamide - Preparation and Properties*. J. Bioact. Compat. Polym. 2004, 19, 101-116.
23. Bysell, H.; Hansson, P.; Malmsten, M., *Transport of Poly-L-lysine into Oppositely Charged Poly(acrylic acid) Microgels and Its Effect on Gel Deswelling*. J. Colloid Interface Sci. 2008, 323, 60-69.
24. Philippova, O. E.; Starodoubtzev, S. G., *Interaction of Slightly Cross-linked Gels of Poly(diallyldimethylammonium bromide) with Sodium Dodecyl Sulfate. Diffusion of Surfactant Ions in Gel*. J. Polym. Sci., Part B: Polym. Phys. 1993, 31, 1471-1476.
25. Chu, B.; Yeh, F.; Sokolov, E. L.; Starodoubtsev, S. G.; Khokhlov, A. R., *Interaction of Slightly Cross-Linked Gels of Poly(diallyldimethylammonium chloride) with Surfactants*. Macromolecules. 1995, 28, 8447-8449.
26. Nilsson, P.; Hansson, P., *Regular and Irregular Deswelling of Polyacrylate and Hyaluronate Gels Induced by Oppositely Charged Surfactants*. J. Colloid Interface Sci. 2008, 325, 316-323.
27. Hansson, P., *Self-Assembly of Ionic Surfactant in Cross-Linked Polyelectrolyte Gel of Opposite Charge. A Physical Model for Highly Charged Systems*. Langmuir. 1998, 14, 2269-2277.
28. Hansson, P.; Schneider, S.; Lindman, B., *Phase Separation in Polyelectrolyte Gels Interacting with Surfactants of Opposite Charge*. J. Phys. Chem. B. 2002, 106, 9777-9793.
29. Svensson, A.; Piculell, L.; Cabane, B.; Iliekti, P., *A New Approach to the Phase Behavior of Oppositely Charged Polymers and Surfactants*. J. Phys. Chem. B. 2002, 106, 1013-1018.
30. Kékicheff, P., *Phase Diagram of Sodium Dodecyl Sulfate-Water System. 2. Complementary Isoplethal and Isothermal Phase Studies*. J. Colloid Interface Sci. 1989, 131, 133-152.

31. Narita, T.; Gong, J.; Osada, Y., *Enhanced Velocity of Surfactant Binding after the Volume Collapse of an Oppositely Charged Gel*. *Macromol. Rapid Commun.* 1997, 18, 853–857.
32. Gong, J. P.; Mizutani, T.; Osada, Y., *A Comparative Study on the Cooperative Binding of Surfactants with Solubilized Polymers and Networks*. *Polym. Adv. Technol.* 1996, 7, 797–804.
33. Okuzaki, H.; Osada, Y., *Ordered-Aggregate Formation by Surfactant-Charged Gel Interaction*. *Macromolecules.* 1995, 28, 380–382.
34. Ilekli, P.; Piculell, L.; Tournilhac, F.; Cabane, B., *How to Concentrate an Aqueous Polyelectrolyte/Surfactant Mixture by Adding Water*. *J. Phys. Chem. B.* 1998, 102, 344–351.
35. Svensson, A.; Piculell, L.; Karlsson, L.; Cabane, B.; Jönsson, B., *Phase Behaviour of an Ionic Surfactant with Mixed Monovalent/Polymeric Counterions*. *J. Phys. Chem. B.* 2003, 107, 8119–8130.
36. Svensson, A.; Piculell, L.; Cabane, B.; Ilekli, P., *A New Approach to the Phase Behaviour of Oppositely Charged Polymers and Surfactants*. *J. Phys. Chem. B.* 2002, 106, 1013–1018.
37. Liu, M.; Guo, T., *Preparation and Swelling Properties of Crosslinked Sodium Polyacrylate*. *J. Appl. Polym. Sci.* 2001, 82, 1515–1520.
38. Jankaew, R.; Rodkate, N.; Lamlertthon, S.; Rutnakornpituk, B.; Wichai, U.; Ross, G.; Rutnakornpituk, M., *“Smart” Carboxymethylchitosan Hydrogels Crosslinked with Poly(N-isopropylacrylamide) and Poly(acrylic acid) for Controlled Drug Release*. *Polym. Test.* 2015, 42, 26–36.
39. Soppirnath, K. S.; Aminabhavi, T. M., *Water Transport and Drug Release Study from Cross-linked Polyacrylamide Grafted Guar Gum Hydrogel Microspheres for the Controlled Release Application*. *Eur. J. Pharm. Biopharm.* 2002, 53, 87–98.
40. Korsmeyer, R. W.; Peppas, N. A., *Effect of the Morphology of Hydrophilic Polymeric Matrices on the Diffusion and Release of Water Soluble Drugs*. *J. Membr. Sci.* 1981, 9, 211–227.

41. Luo, Y.; Kirker, K. R.; Prestwich, G. D., *Cross-linked Hyaluronic Acid Hydrogel Films: New Biomaterials for Drug Delivery*. *J. Controlled Release*. 2000, 69, 169–184.
42. Zhang, X.-Z.; Wu, D.-Q.; Chu, C.-C., *Synthesis, Characterization and Controlled Drug Release of Thermosensitive IPN–PNIPAAm Hydrogels*. *Biomaterials*. 2004, 25, 3793–3805.
43. Yao, K. D.; Peng, T.; Feng, H. B.; He, Y. Y., *Swelling Kinetics and Release Characteristic of Crosslinked Chitosan: Polyether Polymer Network (Semi-IPN) Hydrogels*. *J. Polym. Sci., Part A: Polym. Chem.* 1994, 32, 1213–1223.
44. Yu, Y.; Lau, L. C. M.; Lo, A. C.-y.; Chau, Y., *Injectable Chemically Crosslinked Hydrogel for the Controlled Release of Bevacizumab in Vitreous: A 6-Month In Vivo Study*. *Transl. Vis. Sci. Technol.* 2015, 4, 5.
45. Carbinatto, F. M.; de Castro, A. D.; Evangelista, R. C.; Cury, B. S. F., *Insights into the Swelling Process and Drug Release Mechanisms from Cross-linked Pectin/High Amylose Starch Matrices*. *Asian J. Pharm. Sci.* 2014, 9, 27–34.
46. Varshosaz, J.; Koopaie, N., *Cross-linked Poly(vinyl alcohol) Hydrogel: Study of Swelling and Drug Release Behaviour*. *Iran. Polym. J.* 2002, 11, 123–131.
47. Shu, X. Z.; Zhu, K. J.; Song, W., *Novel pH-Sensitive Citrate Cross-linked Chitosan Film for Drug Controlled Release*. *Int. J. Pharm.* 2001, 212, 19–28.
48. Horkay, F.; Tasaki, I.; Basser, P. J., *Osmotic Swelling of Polyacrylate Hydrogels in Physiological Salt Solutions*. *Biomacromolecules*. 2000, 1, 84–90.
49. Kabanov, V. A.; Skobeleva, V. B.; Rogacheva, V. B.; Zezin, A. B., *Sorption of Proteins by Slightly Cross-Linked Polyelectrolyte Hydrogels: Kinetics and Mechanism*. *J. Phys. Chem. B*. 2004, 108, 1485–1490.
50. Van Tomme, S. R.; De Geest, B. G.; Braeckmans, K.; De Smedt, S. C.; Siepmann, F.; Siepmann, J.; van Nostrum, C. F.; Hennink, W. E., *Mobility of Model Proteins in Hydrogels Composed of Oppositely Charged Dextran Microspheres Studied by Protein Release and Fluorescence Recovery After Photobleaching*. *J. Controlled Release*. 2005, 110, 67–78.
51. Smith, M. H.; Lyon, L. A., *Tunable Encapsulation of Proteins within Charged Microgels*. *Macromolecules*. 2011, 44, 8154–8160.

52. Bysell, H.; Schmidtchen, A.; Malmsten, M., *Binding and Release of Consensus Peptides by Poly(acrylic acid) Microgels*. *Biomacromolecules*. 2009, 10, 2162–2168.
53. Ronca, G., *Frequency Spectrum and Dynamic Correlations of Concentrated Polymer Liquids*. *J. Chem. Phys.* 1983, 79, 1031–1043.
54. Lin, Y. H., *Number of Entanglement Strands Per Cubed Tube Diameter, A Fundamental Aspect of Topological Universality in Polymer Viscoelasticity*. *Macromolecules*. 1987, 20, 3080–3083.
55. Kavassalis, T. A.; Noolandi, J., *New View of Entanglements in Dense Polymer Systems*. *Phys. Rev. Lett.* 1987, 59, 2674–2677.
56. Kavassalis, T. A.; Noolandi, J., *A New Theory of Entanglements and Dynamics in Dense Polymer Systems*. *Macromolecules*. 1988, 21, 2869–2879.
57. King, M.; Eisenberg, A., *Dilute Solution Viscoelasticity of Simple Ionic Polymers—A Theory for Charged Bead - Spring Models*. *J. Chem. Phys.* 1972, 57, 482–491.
58. Doi, M.; Edwards, S. F., *The Theory of Polymer Dynamics*. Clarendon Press: Oxford, 1986.
59. de Gennes, P.-G., *Scaling Concepts in Polymer Physics*. Oxford University Press: Oxford, 1988.
60. Laurati, M.; Petekidis, G.; Koumakis, N.; Cardinaux, F.; Schofield, A. B.; Brader, J. M.; Fuchs, M.; Egelhaaf, S. U., *Structure, Dynamics, and Rheology of Colloid–Polymer Mixtures: From Liquids to Gels*. *J. Chem. Phys.* 2009, 130, 134907.
61. Hammouda, B., *Temperature Effect on the Nanostructure of SDS Micelles in Water*. *J. Res. Natl. Inst. Stand. Technol.* 2013, 118, 151–167.

4.9 Appendix

A4.1 Structural Characterisation of Mesophases Formed Across the CTAB–Polyacrylate Macrogel Interface by SAXS

Line scans were performed at the Australian Synchrotron, collecting SAXS patterns for 1 s at every 100 μm across the CTAB–PA macrogel interface employing an X-ray beam with a wavelength of 0.62 \AA (20 keV) and a sample to detector distance of 1533 mm providing a q -range between $0.019 < q < 1.042 \text{ \AA}^{-1}$.

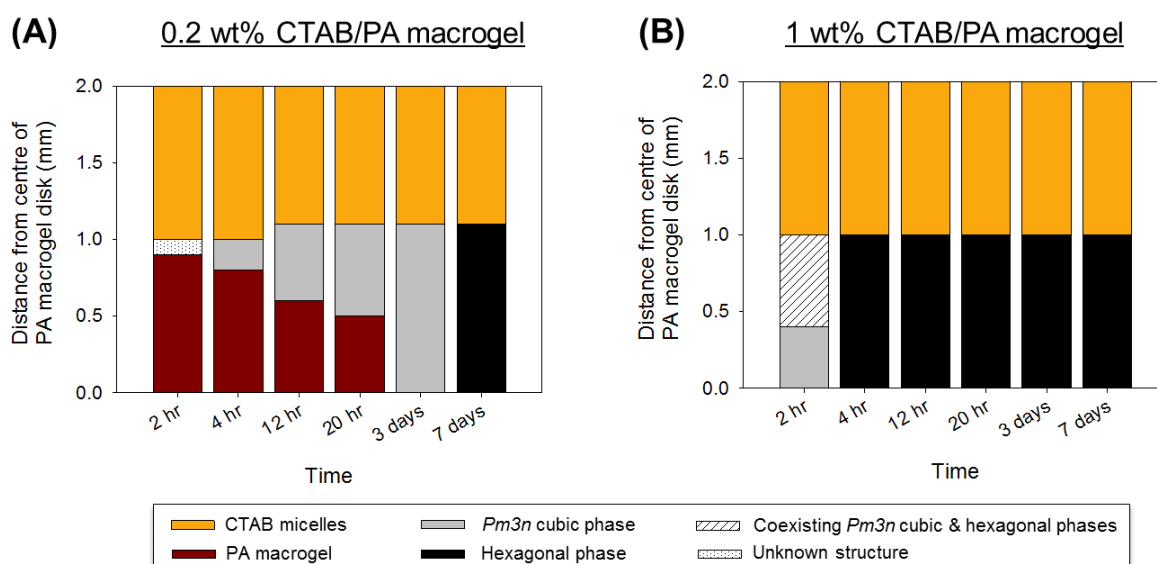


Figure A4.1 Effect of surfactant concentration on the kinetics of mesophase formation across the CTAB–PA macrogel interface. The bar charts highlight changes in the distance over which mesophases existed across the disk of PA gel after contact with the solution of CTAB. Selected SAXS profiles acquired across the CTAB–PA macrogel interface and plots of d -spacings vs. Miller indices are provided within the main text of this chapter (Figure 4.3 to Figure 4.6).

A4.2 Structural Characterisation of Bulk Aqueous Mixtures of SDS and PolyDADMAC by SAXS

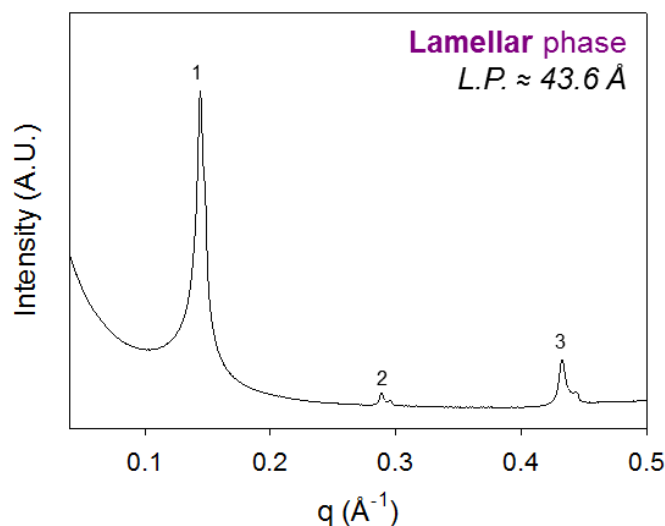


Figure A4.2 SAXS profile of an aqueous mixture comprised of 40 wt% SDS, 5 wt% polyDADMAC, and 55 wt% water showing the presence of a lamellar phase.

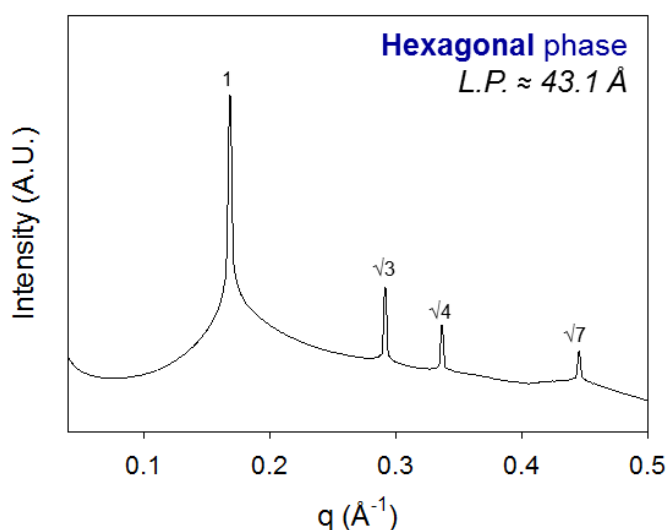


Figure A4.3 SAXS profile of an aqueous mixture comprised of 20 wt% SDS, 5 wt% polyDADMAC, and 75 wt% water showing the presence of a hexagonal phase with a lattice parameter of 43.1 Å.

Chapter 5: *Toward the Formation of Equilibrium
Structures in SDS and PolyDADMAC
Dispersions*

5. Toward the Formation of Equilibrium Structures in SDS and PolyDADMAC Dispersions

5.1 Introduction

Aqueous mixtures of oppositely charged surfactants and polymers have received great interest for personal care¹⁻⁴ and pharmaceutical⁵⁻⁸ applications, where the composition of the system is important in controlling the formation of ordered structures in solution. The phase behaviour of these systems has been demonstrated to consist of three distinct zones as the surfactant concentration is increased at fixed polymer concentrations. At low surfactant concentrations, a clear zone exists consisting of free surfactant molecules or micelles in solution (zone 1). As the concentration of surfactant is increased, surfactant molecules and/or micelles begin to bind with the polymer chains, a point that is termed the critical association concentration, which often occurs at least 2-fold lower than the critical micellar concentration of the surfactant solution in the absence of polymer.⁹ When charge equivalence is approached, the aggregates begin to lose their colloidal stability due to the absence of electrostatic repulsion between the opposite charges, leading to precipitation (zone 2). Usually an associative phase separation occurs, where one phase is surfactant and polymer rich, while the other aqueous phase consists of simple salts. When the concentration of surfactant is in excess, the surfactant molecules adsorb onto the surface of the complexes in solution, resulting in charge reversal and resolubilisation of the aggregates (zone 3).^{10, 11} Therefore, careful selection of the surfactant-to-polymer molar charge ratio is useful for tuning the size, morphology, and rheology of complexes formed in solution.¹²⁻¹⁴ However, it is unknown

whether the size of the internal structure (lattice parameter) of colloidal dispersions can also be influenced by the composition of the system.

The phase behaviour of dispersions of oppositely charged surfactant and polymer systems has been well characterised,^{10, 12, 13, 15-19} although an emphasis has been on the study of factors influencing the colloidal stability of nanoparticles from a formulations perspective. Kinetically stable dispersions are known to arise when the surfactant is present at high concentrations as the excess surfactant molecules are able to adsorb to the surface of the nanoparticles and increase the electrostatic barrier against aggregation.^{11, 20} Interestingly, the addition of nonionic surfactants can often be employed as a means to avoid phase separation.²¹⁻²³ Janiak *et al.* demonstrated the formation of bicontinuous cubic ($Ia3d$) or normal hexagonal (H_1) phases when a nonionic surfactant was introduced to the complex salt of poly(acrylic acid) and hexadecyltrimethylammonium hydroxide.^{24, 25} The order of addition and the speed of mixing used to prepare these dispersions can also significantly impact the size and stability of colloidal structures where they may often become kinetically trapped in a nonequilibrium state.^{21, 22, 26-29}

Both equilibrium and nonequilibrium nanostructures were found to exist locally across SDS–polyDADMAC interfaces as revealed in Chapter 3 and Chapter 4. The diffusivity of the surfactant and polymer molecules from their bulk regions and across the interface where mesophases formed due to associations between the oppositely charged species were the two main rate-limiting steps to achieving equilibrium. Studying the phase behaviour across these surfactant–polymer interfaces and in bulk aqueous mixtures at such reasonably high concentrations would inevitably result in a slow mixing process which is unfavourable for producing equilibrium structures. On the other hand, fewer surfactant and polymer molecules present in more dilute solutions would increase the speed of the self-assembly of

nanoparticles that more closely represent equilibrium nanostructures. For dilute dispersions, it is assumed that the composition within the individual complexes formed is comparable to the initial composition of the system and thus can be considered as a homogeneous mixture. It is therefore of interest to compare mesophases that are formed in dilute dispersions of SDS and polyDADMAC with those arising in concentrated bulk aqueous mixtures, as well as the liquid crystalline phases existing across SDS–polyDADMAC interfaces at equivalent global or local compositions. It is anticipated that the absolute concentration of components in aqueous mixtures of SDS and polyDADMAC at fixed surfactant-to-polymer molar charge ratios will influence the global morphology and size of nanostructures formed. Moreover, it is hypothesised that the state of equilibrium of structures formed upon mixing of SDS and polyDADMAC solutions in dispersions, concentrated mixtures, or across solution interfaces is determined by their local composition.

It is well reported that hexagonal phases often form in systems comprised of SDS and polyDADMAC,^{10, 30-35} however the type of phase, normal or inverse, has not yet been explicitly elucidated. Analogous lipid- or glycerate-based liquid crystalline systems often form inverse bicontinuous cubic phases or inverse hexagonal phases that when dispersed in excess solvent with stabilisers result in cubosomes or hexosomes, respectively, which have been proposed to have wide application in drug delivery.³⁶⁻³⁹ Incorporation of additives such as vitamin E acetate,⁴⁰ capric acid,⁴¹ or hexadecane⁴² into these formulations have demonstrated characteristic changes to the typical equilibrium phase behaviour exhibited by these inverse mesophases. Hexagonal phase structures formed in dispersions of SDS and polyDADMAC have been shown to dissociate upon addition of high concentrations of salt solution due to the ‘screening’ of the electrostatic attraction between the oppositely charged species, suggesting that the mesophase is of the normal type.^{11, 34} If hexosomes of the inverse

type were present, addition of salt would be expected to lead to swelling of the structure. Therefore, the phase behaviour observed in response to addition of ethanol or n-hexadecane to dispersions of SDS and polyDADMAC will enable classification of the type of hexagonal phase formed in SDS and polyDADMAC systems.

5.2 Hypotheses and Aims

Hypothesis 1

That the lattice parameter of liquid crystalline structures formed in aqueous mixtures of SDS and polyDADMAC is influenced by the polyDADMAC-to-SDS molar charge ratio.

Hypothesis 2

That the absolute concentration of components in aqueous mixtures of SDS and polyDADMAC at a fixed polyDADMAC-to-SDS molar charge ratio influences the global morphology and size of nanostructures formed.

Hypothesis 3

That the state of equilibrium of structures formed upon mixing of SDS and polyDADMAC solutions in dispersions, concentrated mixtures, or across solution interfaces is determined by their local composition.

Hypothesis 4

That hexagonal phase formed in systems comprised of SDS and polyDADMAC is of the normal (type I) phase.

In order to investigate these hypotheses, the following aims were achieved.

1. To structurally characterise a series of SDS and polyDADMAC dispersions at varying polyDADMAC-to-SDS molar charge ratios.

2. To compare the structures identified in SDS and polyDADMAC dispersions with those existing in bulk aqueous mixtures and across SDS–polyDADMAC interfaces at the same polyDADMAC–to–SDS molar charge ratio.
3. To identify the type of hexagonal phase formed in aqueous mixtures of SDS and polyDADMAC.

5.3 Materials

Sodium dodecyl sulphate (SDS, BioXtra, ≥ 99.0 %) and n-hexadecane (ReagentPlus[®], 99 %) were purchased from Sigma–Aldrich (Sydney, Australia). Poly(diallyldimethylammonium chloride) (polyDADMAC, Merquat[™] 100, molecular weight: 1.5×10^5 g/mol) was sourced from Nalco Company (Illinois, United States). The commercial solution of polyDADMAC obtained contained 53.3 % solid and 46.7 % water (standard deviation: ± 0.3 %) as determined by gravimetric analysis ($n = 10$). Merquat[™] 100 was dried prior to preparation of polyDADMAC stock solutions to form a waxy solid.

All materials were used without further purification. Milli-Q grade water purified through a Milli-pore system (Billerica, United States) was used throughout the studies.

5.4 Methods

5.4.1 Sample Preparation

Dispersions of SDS and polyDADMAC were prepared by dropwise addition of 5 wt% SDS solution to solutions of varying polyDADMAC concentration (0, 1, 2, 5, and 10 wt%) to obtain final mixtures with half the concentration of each component in the system. The samples were vortex mixed vigorously and centrifuged to ensure the absence of dust or

colloidally unstable particles in bulk dispersions. Dynamic light scattering (DLS) measurements and cryogenic-transmission electron microscopy (cryo-TEM) images were taken of the supernatant of each dispersed sample which were equilibrated for approximately 24 hr prior to analysis. Samples were identified based on their polyDADMAC-to-SDS molar charge ratio, expressed as $r = ([\text{polyDADMAC}] \times \text{charge per polymer molecule})/[\text{SDS}]$.

To study the influence of certain additives on the hexagonal phase that is often formed in systems comprised of SDS and polyDADMAC, ethanol (100 μL) and n-hexadecane (100 μL) were added into separate wells within a plastic 96-well plate ensuring saturation of a 100 μL aliquot of sample dispersion ($r = 1.8$) for subsequent analysis by small angle X-ray scattering.

5.4.2 Characterisation of Mesophases in SDS and PolyDADMAC Dispersions

5.4.2.1 *Dynamic Light Scattering*

Size measurements were performed with a Zetasizer Nano-ZS (Malvern Instruments, Worcestershire, United Kingdom). A laser power of 4 mW was used at a back scattering angle of 173° at room temperature. The bulk surfactant and polymer solutions, as well as the aqueous dispersion of SDS and polyDADMAC ($r = 0.4$) were separately loaded into low volume disposable sizing cuvettes (ZEN0112) and measured without further dilution. However, it was confirmed that further dilution of the sample did not change the particle size. As the dispersed coacervates were observed to be non-spherical under cryo-TEM, the apparent size rather than the absolute size measurements were obtained.

5.4.2.2 Small Angle X-ray Scattering

Structural characterisation of the SDS and polyDADMAC dispersions were conducted on the SAXS/WAXS beamline at the Australian Synchrotron.⁴³ Briefly, the sample dispersions (100 μL) were loaded into a 96-well plate, which was subsequently sealed with a silicone elastomer cover to prevent evaporation. A sampling robot equipped with gas-tight syringes drew up samples from each well into a quartz capillary (1.5 mm diameter) for analysis. The capillary was glued into a stainless steel holder that was mounted into a temperature-controlled block and connected by HPLC flanged fittings essentially without dead-space. The sample was exposed to the beam as it was drawn up and down the capillary to avoid beam damage. An X-ray beam with a wavelength of 1.512 Å (8.2 keV) was used, with a sample to detector distance of 1651 mm providing a q -range between $0.007 < q < 0.48 \text{ \AA}^{-1}$, where q is the magnitude of the scattering vector, defined as $q = 4\pi / \lambda \sin(\theta/2)$, λ being the wavelength and θ the scattering angle. The two-dimensional SAXS patterns were acquired for 1 s with 1 s delay between frames, using a Pilatus 1M detector (active area 169 x 179 mm² with a pixel size of 172 μm) and integrated into the one-dimensional scattering function $I(q)$ using the in-house developed software package ScatterBrain. Water was subtracted as background from all SAXS curves. The relative positions of the Bragg peaks allowed for assignment of mesophases present.⁴⁴

5.4.2.3 Cryogenic-Transmission Electron Microscopy

Dispersions of SDS and polyDADMAC were visually examined by cryogenic-transmission electron microscopy (cryo-TEM). Copper grids (200-mesh) coated with perforated carbon film (Lacey carbon film: ProSciTech, Queensland, Australia) were glow discharged in nitrogen to render them hydrophilic. Aliquots (4 μL) of the sample were pipetted

onto each grid prior to plunging into liquid ethane cooled by liquid nitrogen. Frozen grids were stored in liquid nitrogen until required. The samples were examined using a Gatan 626 cryoholder (California, United States) and Tecnai 12 Transmission Electron Microscope (Eindhoven, The Netherlands) at an operating voltage of 120 kV. Images were recorded using FEI Eagle 4k×4k CCD camera at magnifications ranging from 15 000× to 50 000×. Further details have been reported previously.⁴⁵

5.5 Results

5.5.1 Evolution of Nanostructures in Dispersed SDS and PolyDADMAC Systems

In the absence of polymer ($r = 0$), spherical micelles were present in a 2.5 wt% solution of SDS as represented by a broad peak in the SAXS pattern (Figure 5.1). Although micelles are too small to resolve on cryo-TEM, the micrographs preclude the presence of larger structures, and hence it is assumed that only micelles are logically present (Figure 5.2-A). This was expected given that the surfactant concentration was 10-fold greater than the reported critical micellar concentration determined by light scattering at 25 °C (~8 mM),⁴⁶ where the reported radius of SDS micelles in literature ranged between 1.6 to 2.1 nm.⁴⁷ In contrast, dynamic light scattering measurements showed no sign of particles formed in a solution of 0.5 wt% polyDADMAC in the absence of surfactant.

When these surfactant and polymer solutions were combined at equal volumes ($r = 0.4$), larger complexes with a broad size distribution resulted from the interaction of the oppositely charged species (Figure 5.3). The SAXS profile showed the initial appearance of a small peak at this composition (Figure 5.1). As the concentration of polymer was increased in

the sample dispersion ($r = 1.8$), the first order Bragg peak at $q \approx 0.1701 \text{ \AA}^{-1}$ became more resolved, grew in intensity, and was shifted slightly toward higher q values, which has not been reported previously. At $r = 3.6$ (Figure 5.1), the SAXS curve showed weak second and third order Bragg peaks indicative of a hexagonal phase with a lattice parameter of $\sim 41.8 \text{ \AA}$ (Appendix-Figure A5.1). In addition, the slope in the low q region fits a q^{-2} relationship, indicative of a combination of hexosomes and Gaussian coils formed upon interaction of SDS and polyDADMAC.⁴⁸ The scattering from a 5 wt% polyDADMAC solution in the absence of SDS did not show features indicative of coils or hexosomes (Appendix-Figure A5.4).

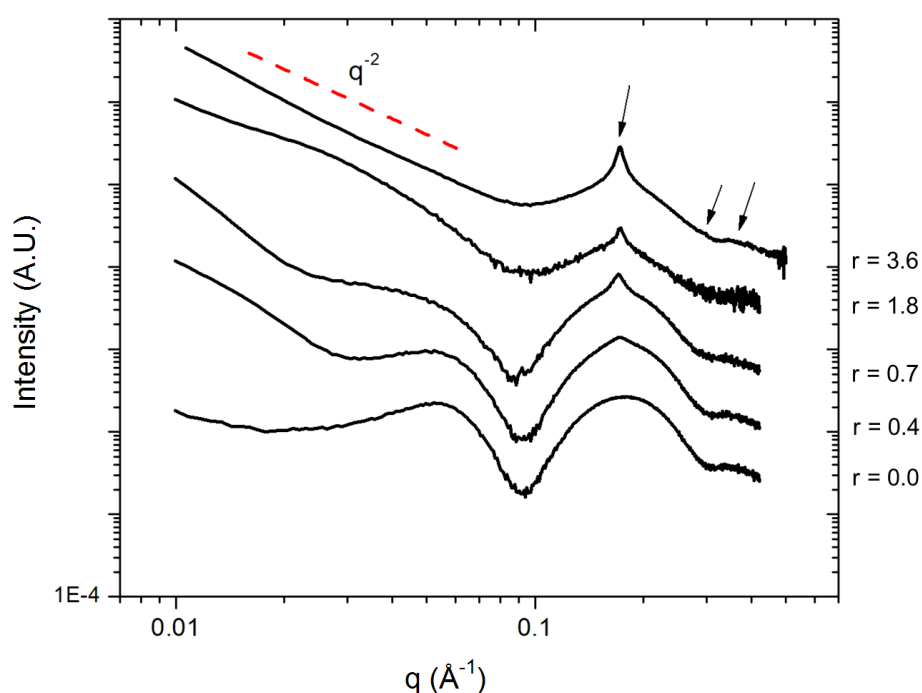


Figure 5.1 SAXS profiles of SDS/polyDADMAC dispersions with increasing polyDADMAC-to-SDS molar charge ratio, where $r = ([\text{polyDADMAC}] \times \text{charge per polymer molecule})/[\text{SDS}]$. SDS micelles were present at $r = 0.0$, and structures with a hexagonal lattice, indicated by the arrows, appeared as the concentration of polymer increased. The q^{-2} slope indicates the presence of one-dimensional complexes ($r = 3.6$).

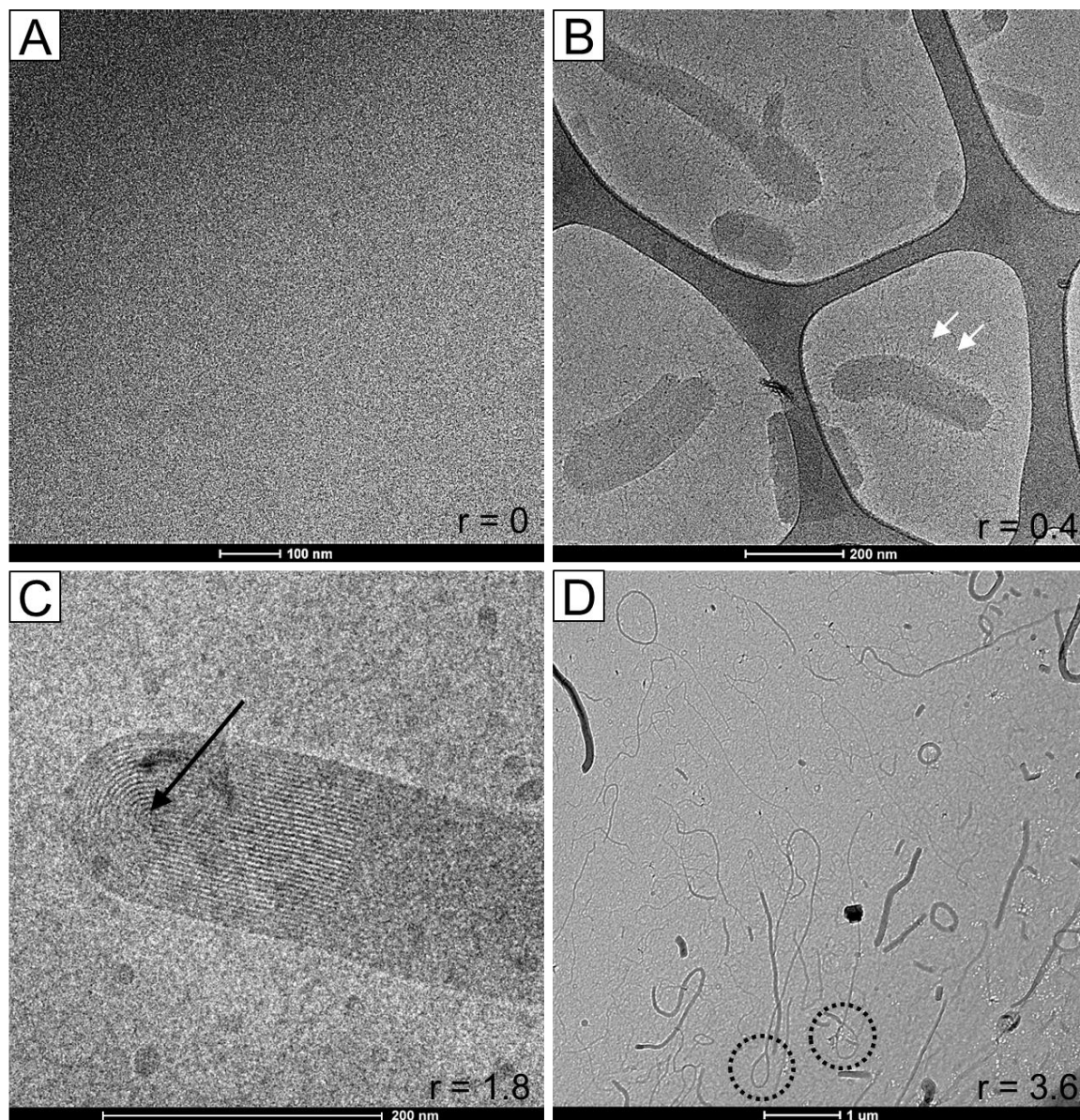


Figure 5.2 Cryo-TEM images of SDS/polyDADMAC dispersions with increasing polyDADMAC-to-SDS molar charge ratio at a fixed surfactant concentration. Micelles were present at 2.5 wt% SDS (A). Arrows indicate the presence of worm-like micelles adsorbed onto the elongated hexosomes (B) and the characteristic ‘stripe’ texture exhibited by the hexagonal phase (C). Stringy, looped, elongated and textured assemblies with a polydispersed size distribution were formed in excess polyDADMAC (D).

Cryo-TEM images reinforced the significance of the surfactant and polymer composition on the resulting structures in the dispersions. Elongated structures with a diameter of around 50 nm decorated with worm-like micelles were observed at $r = 0.4$ (Figure 5.1-B).⁴⁹ The presence of hexosomes at $r = 1.8$ was confirmed by the appearance of fingerprint-like fringes (Figure 5.1-C).¹⁰ Networks of elongated structures with a diversity of sizes and conformations, as well as hexosomes, existed in samples comprised of higher polymer concentration ($r = 3.6$, Figure 5.2-D and Appendix-Figure A5.2).

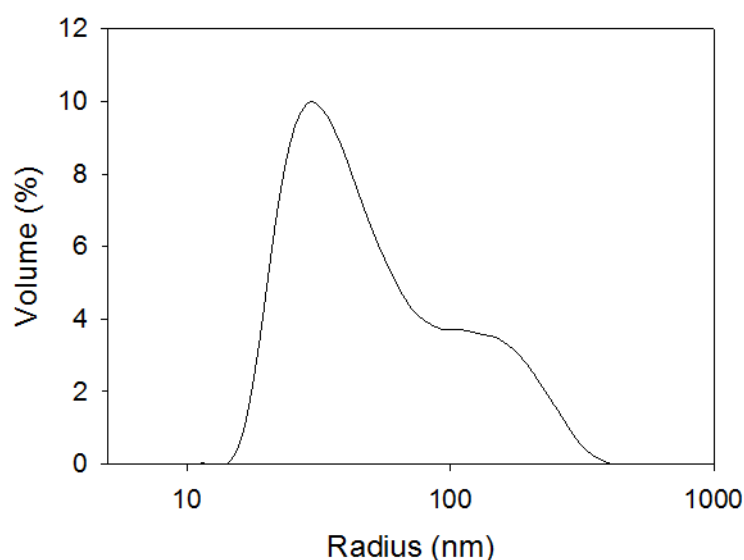


Figure 5.3 Formation of a polydispersed mixture of SDS/polyDADMAC complexes upon interaction between oppositely charged surfactant (2.5 wt% SDS) and polymer (0.5 wt% polyDADMAC) molecules prepared at $r = 0.4$. The correlation function for this system measured by dynamic light scattering is presented in the appendix (Figure A5.3).

5.5.2 Effect of Additives on Nanostructure Phase Behaviour

In this study, n-hexadecane and ethanol were incorporated into hexosomal dispersions of SDS and polyDADMAC ($r = 1.8$) to evaluate their influence on the phase

behaviour of nanostructures formed. The SAXS data indicated a slight shift in the first order Bragg peak of the hexagonal phase to a lower q value upon saturation with n-hexadecane (Figure 5.4-top). In comparison, saturation of the dispersion of SDS and polyDADMAC with ethanol ($r = 1.8$) led to the disappearance of the Bragg reflection of the hexagonal phase (Figure 5.4-bottom). An increase in intensity at low q was due to the presence of large particles and a correlation peak at $q \approx 0.2 \text{ \AA}^{-1}$ was also observed.

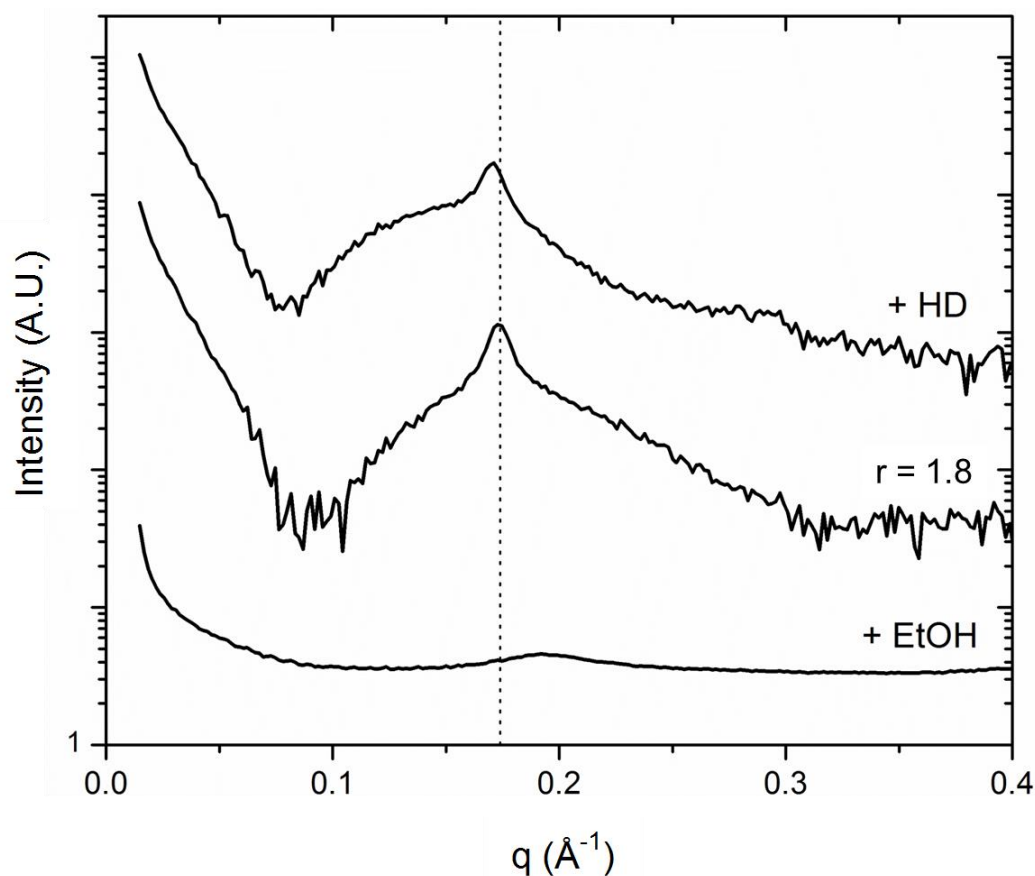


Figure 5.4 SAXS profiles demonstrating the effect of introducing n-hexadecane (+HD) or ethanol (+EtOH) on the equilibrium nanostructure formed in the SDS/polyDADMAC dispersion at $r = 1.8$. The dashed line acts as a guide to signify any shift in the q position of the first order Bragg peak of the hexagonal phase formed.

5.6 Discussion

5.6.1 Effect of the PolyDADMAC-to-SDS Molar Charge Ratio on the Lattice Parameter of Hexagonal Phases Formed in SDS/PolyDADMAC Mixtures

It is well known that the surfactant-to-polymer molar charge ratio significantly influences the size, zeta-potential, morphology, rheology, and colloidal stability of structures formed in dispersions of oppositely charged surfactants and polymers. Here, SAXS profiles and cryo-TEM images revealed an evolution of structures existing in dispersions of SDS and polyDADMAC with varying composition, which were in agreement with previous reports. Nizri *et al.* also demonstrated the progression of nanoparticles from spherical micelles, to lace-like aggregates, and to hexosomes with thread-like micelles attached to their surfaces with increasing polyDADMAC-to-SDS molar charge ratio.¹⁰

The hexagonal structures formed in these mixtures have been described as SDS rod-like micelles ‘bridged’ between or ‘decorated’ with chains of polyDADMAC.^{10, 50} A slight shift of the first Bragg peak of the hexagonal structure toward lower q values in the SAXS curves indicates that the lattice parameter of the mesophase increased with increasing SDS concentration. These findings can be supported by the results given by Pojják *et al.*, where the mean size of complexes formed in mixtures consisting of the cationic surfactant, cetyltrimethylammonium chloride, and the anionic polymer, poly(styrenesulphonate) decreased with increasing surfactant concentration.⁵¹ Higher concentrations of SDS and polyDADMAC led to an increase in the ionic strength of the system and an increase in the repulsive forces between the oppositely charged species. Therefore, the SDS rod-like micelles and polyDADMAC chains become loosely associated, which accounts for the increase in the

lattice parameter, and subsequent transition from relatively large hexosomes to smaller micellar aggregates. Kong *et al.* reported a significant decrease in the viscosity of SDS and polyDADMAC mixtures in this composition range due to the expansion of the polymer chains in solution.⁹ There have been some occurrences where the size of globular particles suddenly increases at higher surfactants concentrations due to aggregation of micelles.^{10, 50} However, monodispersed spherical nanoparticles are often formed when the molar concentration of the surfactant is in excess, such as those existing in dispersions of poly(ethylene oxide)-block-polymethacrylate anions and N-alkylpyridinium cations.¹⁴

In summary, the surfactant-to-polymer molar charge ratio not only plays an important role in controlling the size, morphology, and rheology of complexes formed in dispersions of oppositely charged surfactants and polymers, but also the lattice parameter of the mesophases formed. Thus, finer tuning of the structural attributes of such systems can be achieved.

5.6.2 The Importance of the Absolute Concentration in Determining the Global Morphology of Mesophases Formed in SDS/PolyDADMAC Mixtures

The absolute concentrations of oppositely charged surfactant and polymer in aqueous mixtures of such systems have important implications in the overall structures existing in the bulk. Trabelsi *et al.* demonstrated that the size of the *Pm3n* cubic phase structure of complexes formed in dispersions of dodecyltrimethylammonium bromide and carboxymethylcellulose was not influenced by the concentration regime studied.¹⁵ Although the global morphology of the mixtures differed, the internal structure present at low and high polymer concentrations remained unchanged. Contrary to their findings, the lattice parameter of

hexagonal phases formed in more concentrated SDS and polyDADMAC systems was influenced by the polyDADMAC-to-SDS molar charge ratio (Figure 5.5).

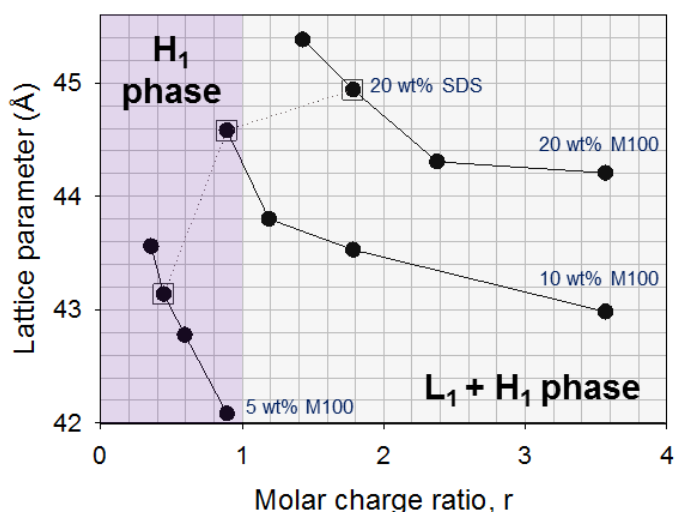


Figure 5.5 Effect of the molar charge ratio on the lattice parameter of hexagonal phase structures formed in concentrated mixtures of SDS and polyDADMAC, where $r = ([\text{polyDADMAC}] \times \text{charge per polymer molecule})/[\text{SDS}]$. Reproduced from Figure 3.3-A.

At fixed polyDADMAC concentrations, the lattice parameter of hexagonal phase structures increased with increasing SDS concentration ($r \ll 1$). The same explanation can be given to this phase behaviour, where an increase in the ionic strength of the system introduced greater repulsive forces between the charged species leading to mesophases with large internal dimensions (Figure 5.5). This trend was also observed for the dispersions of SDS and polyDADMAC, however the global morphology displayed by the mixtures differed greatly between the concentration regimes studied. In dilute conditions, it is not surprising that hexosomes coexisted with micelles in solution when SDS was in excess as the concentration of SDS was within the micellar phase region existing in the SDS/water binary phase diagram

at room temperature.⁵² On the other hand, at higher absolute concentrations where SDS was in excess only hexagonal phase was present. In addition to the effect ionic strength has on the lattice parameter of the mesophases formed, it appears that the hexagonal phase structure formed upon interactions between SDS and polyDADMAC becomes closer in resemblance to that of the hexagonal phase structures that are known to form at higher SDS concentrations in the absence of polymer.^{30, 52} Findings from Chapter 2 demonstrated an approximate linear decrease in the lattice parameter of the hexagonal phase from ~ 55 Å to ~ 45 Å with increasing surfactant concentration from 35 wt% to 58 wt% SDS (Figure 2.10-B), which further supports the theory that hexagonal phases formed in concentrated mixtures of SDS and polyDADMAC behave more like an SDS/water binary system as the composition deviates from charge neutrality.

Likewise at fixed SDS concentrations, the lattice parameter of hexagonal phases increased with increasing polyDADMAC concentration. The concentration range over which polymer was in excess comprised of coexisting micellar and hexagonal phases. Again, an increase in the ionic strength within the system most probably would have led to the reduction in the degree of order in the packing of SDS micelles and polyDADMAC chains within a hexagonal lattice, and subsequently the dissociation and release of SDS micelles into the bulk solution. A further increase in the polymer concentration (> 20 wt% polyDADMAC) would have caused a complete loss of electrostatic interactions between the oppositely charged species resulting in an aqueous mixture comprised most likely of free micelles and polymer coils (Figure 3.2-A). An alternative explanation could be that the increased inherent viscosity of the mixture upon addition of a low molar concentration of SDS into a concentrated solution of polyDADMAC¹² may have retarded the diffusivity of the charged species through the bulk

mixture, preventing associations between the oppositely charged molecules and the self-assembly of ordered structures in solution aside from SDS micelles.

A direct comparison can also be made between mixtures comprising of SDS and polyDADMAC at the same polyDADMAC-to-SDS molar charge ratio prepared in both the dilute and concentrated regimes. For example, coexisting micellar and hexagonal phases were formed at $r \approx 1.8$, where the lattice parameter of the hexagonal phase was found to decrease as the system became more dilute. Specifically, the internal dimensions of the hexagonal phases were measured as $\sim 45 \text{ \AA}$ (Figure 5.5), $\sim 43.5 \text{ \AA}$ (Figure 5.5), and $\sim 41.8 \text{ \AA}$ (Appendix-Figure A5.1) in systems comprised of 20 wt%, 10 wt%, and 2.5 wt% SDS, respectively. These findings indicate that more compact nanostructures are formed with dilute concentrations of SDS and polyDADMAC.

In summary, the absolute molar concentrations of SDS and polyDADMAC in aqueous mixtures of such systems significantly influence the internal dimensions of nanostructures formed, as well as the overall morphology of the bulk mixture.

5.6.3 Understanding the Relationship Between the Local Composition and the Existence of Equilibrium Structures in Surfactant/Polymer Mixtures

The existence of kinetically trapped electrostatically stable nonequilibrium structures has been acknowledged in mixtures of oppositely charged surfactant and polymer systems.^{28, 51, 53–55} Some efforts have been made to compare the phase behaviour within bulk solution and at the air–water interface. In particular, Campbell *et al.* performed surface tension measurements and employed neutron reflectometry to study the interfacial properties and morphologies of adsorbed layers, respectively, formed at the air–water interface and the bulk

solution of SDS and polyDADMAC mixtures.⁵⁴ Addition of polyDADMAC to a low concentration solution of SDS resulted in a decrease in the surface tension due to the self-assembly of different interfacial morphologies, namely thick layers of complexes and a compact layer.⁵⁴ For freshly mixed samples, the composition within the interfacial layers remained constant, however it was found to change in the bulk solution.⁵⁴ Aged samples that were left to ‘equilibrate’ for three days became transparent due to the sedimentation of the precipitate formed at compositions close to charge equivalence.⁵⁴ These particles were found to contain kinetically trapped structures due to concentration gradients created during the initial mixing process.⁵⁴ Release of surface active material upon inversion of these samples reversed the effects of equilibration, therefore demonstrates the nonequilibrium nature of the SDS and polyDADMAC system studied.⁵⁴

A week after initial contact between solutions of 20 wt% SDS and 20 wt% polyDADMAC, a gradient of mesophases were formed across the SDS–polyDADMAC interface, where the lattice parameter of hexagonal phases differed significantly depending on the local composition. Notably, two regions comprised of coexisting micellar and hexagonal phases existed in the middle of a region where only hexagonal phase was present (Figure 3.6). Interestingly, an apparent equilibrium hexagonal phase with a lattice parameter of as low as ~ 42 Å appeared across the SDS–polyDADMAC interface within 2 hr from initial contact between the two solutions (Figure 3.6 and Figure 3.9). These structural attributes closely resembled those of the hexosomes formed in the dispersed systems studied in this chapter, suggesting that apparent equilibrium hexagonal phases may form instantaneously upon mixing of SDS and polyDADMAC solutions regardless of the initial composition of the system. The diffusivity of the remaining molecules in solution that have yet to form interactions with the oppositely charged species after this stage will therefore influence the

structures existing globally within the system and the existence of nonequilibrium structures. This was supported by the average value of the lattice parameter of hexagonal phases formed locally across the SDS–polyDADMAC interface (~ 43 Å, Figure 3.7) being very similar to the lattice parameter of the hexagonal phase coexisting with SDS micelles in the equivalent bulk aqueous mixture (~ 43.5 Å, Appendix–Figure A3.2). The study of the phase behaviour across the SDS–polyDADMAC interface thus presents a new approach for predicting the nanostructures that will exist in bulk mixtures that may or may not reach true equilibrium.

In summary, hexagonal phases that are apparently at equilibrium can form spontaneously upon mixing of SDS and polyDADMAC solutions irrespective of the initial polymer–to–surfactant molar charge ratio in the system.

5.6.4 Formation of Normal Hexagonal (H_1) Phase in SDS and PolyDADMAC Systems

Hexagonal phases are known to form in systems of SDS and polyDADMAC,^{10, 30-35} however the type of phase formed, normal or inverse, has not been established yet. Small angle X-ray scattering is unable to directly differentiate a H_1 phase from a H_2 phase, however the type of hexagonal phase can be determined by studying the phase transition exhibited by the system upon incorporation of additives, such as alkanes or alcohols.

Upon addition of n-hexadecane, a shift in the first order Bragg peak of the hexagonal phase formed in the dispersion of SDS and polyDADMAC prepared at $r = 1.8$ to a lower q value resulted from the swelling of the internal dimensions within the ordered lattice. Similarly, Bernardes *et al.* demonstrated an increase in the lattice parameter of hexagonal phase formed in aqueous mixtures of the complex salt, CTAPA, due to incorporation of alkanes within the surfactant aggregates.⁵⁶ This phase behaviour is characteristic of the normal ‘type

1' hexagonal (H_1) phase as described by its critical packing parameter, a model for understanding the correlation between geometry of the molecules and the resulting structure.⁵⁷ For inverse phases, the addition of increasing concentrations of hexadecane is expected to shift the peak to higher q values, thereby reducing the lattice parameter.⁴²

The hexosomes existing in dispersions of SDS and polyDADMAC at $r = 1.8$ were destroyed upon addition of ethanol to the system. Ethanol has been found to interact preferably with the hydrophilic head groups of the structure, resulting in an increase in the critical packing parameter which favours a decrease in curvature.⁵⁸⁻⁶⁰ Bernardes *et al.* described this as a 'co-solvent effect' where the reduced miscibility of the alcohol in water leads to formation of disordered structures.⁶⁰ Baglioni *et al.* described a similar effect exhibited by alcohols on the structural integrity of micelles. It was reported that the degree to which the alcohol molecule could penetrate the micellar interface and disrupt the packing of the surfactant molecules to induce dissociation of micelles in solution was dependent upon its chain length.⁶¹ This could explain why the hexosomes may alternatively transition into an intermediate phase comprised of lamellar structures rather than breaking down into micellar aggregates after addition of ethanol.

The phase behaviour demonstrated by hexosomes formed in SDS and polyDADMAC dispersions upon introduction of additives indicate that these structures are H_1 phases.

5.6.5 Implications for Use as Bioactive Delivery Systems

Hexosomes have become an interesting vehicle for the solubilisation, encapsulation, and transportation of a range of active pharmaceutical compounds. Dispersions of inverse hexagonal (H_2) phase have been shown to enhance the permeation of drug through the skin for transdermal, dermal, and transmucosal delivery,⁶² and remain stable under sink

conditions.³⁸ However, in order to produce hexosomes comprised of an inverse hexagonal phase, an emulsification process is often involved, which requires a high input of energy and the addition of stabilisers, such as Pluronic® F127.⁶³ These are major limitations associated with the scale-up manufacturing of dispersed liquid crystalline formulations. In contrast, the mixing of dilute solutions of SDS and polyDADMAC results in the self-assembly of H₁ phase particles in water with no input of energy and the resulting dispersion is kinetically stable upon dilution. These properties make them potentially cost-effective and advantageous for the delivery of drugs, in particular for active ingredients that are sensitive to shear force or high energy input. Additionally, an appealing example of a delivery system would be incorporating charged cargo within or as a component of the self-assembled nanostructures, where the mesophase can be tailored to be responsive to certain stimuli, such as changes in temperature,⁶⁴ salt concentration,^{7, 34} or solution pH⁶⁵⁻⁶⁷ and trigger drug release.

5.7 Conclusions

This chapter has highlighted the significance of the absolute molar concentration and ionic strength in aqueous mixtures of SDS and polyDADMAC systems in the formation of nanostructures that are apparently at equilibrium or become kinetically trapped in nonequilibrium states. In addition, SDS and polyDADMAC mixtures prepared at fixed polyDADMAC-to-SDS molar charge ratios can yield similar mesophases, but exhibit different lattice parameters and global morphologies.

The hexosomes arising in the dispersions of SDS and polyDADMAC were established to be of the normal ‘type I’ phase. Moreover, employing additives, such as n-hexadecane and ethanol to study the loading of guest molecules provide a means of manipulating the liquid crystalline structures formed in oppositely charged surfactant and polymer systems.

5.8 References

1. Clauzel, M.; Johnson, E. S.; Nylander, T.; Panandiker, R. K.; Sivik, M. R.; Piculell, L., *Surface Deposition and Phase Behavior of Oppositely Charged Polyion–Surfactant Ion Complexes. Delivery of Silicone Oil Emulsions to Hydrophobic and Hydrophilic Surfaces*. ACS Appl. Mater. Interfaces. 2011, 3, 2451–2462.
2. Svensson, A. V.; Johnson, E. S.; Nylander, T.; Piculell, L., *Surface Deposition and Phase Behavior of Oppositely Charged Polyion–Surfactant Ion Complexes. 2. A Means to Deliver Silicone Oil to Hydrophilic Surfaces*. ACS Appl. Mater. Interfaces. 2010, 2, 143–156.
3. Wilgus, L. A.; Davis, K.; Labeaud, L.; Gandolfi, L.; Lochhead, R. Y., *A Study of the Distribution of Polymer/Surfactant Coacervate between Solution and Foam in Archetypal Shampoo Systems*. J. Cosmet. Sci. . 2011, 62, 179–189.
4. Desbrieres, J.; Bousquet, C.; Babak, V., *Surfactant–Chitosan Interactions and Application to Emulsion Stabilization*. Cellul. Chem. Technol. 2010, 44, 395–406.
5. Bronich, T. K.; Nehls, A.; Eisenberg, A.; Kabanov, V. A.; Kabanov, A. V., *Novel Drug Delivery Systems Based on the Complexes of Block Ionomers and Surfactants of Opposite Charge*. Colloids Surf., B. 1999, 16, 243–251.
6. Amar-Yuli, I.; Adamcik, J.; Blau, S.; Aserin, A.; Garti, N.; Mezzenga, R., *Controlled Embedment and Release of DNA from Lipidic Reverse Columnar Hexagonal Mesophases*. Soft Matter. 2011, 7, 8162–8168.
7. Morán, M. C.; Miguel, M. G.; Lindman, B., *Surfactant–DNA Gel Particles: Formation and Release Characteristics*. Biomacromolecules. 2007, 8, 3886–3892.
8. Takka, S.; Çali, A. G., *Bile Salt–Reinforced Alginate–Chitosan Beads*. Pharm. Dev. Technol. 2012, 17, 23–29.
9. Kong, L.; Cao, M.; Hai, M., *Investigation on the Interaction between Sodium Dodecyl Sulfate and Cationic Polymer by Dynamic Light Scattering, Rheological, and Conductivity Measurements*. J. Chem. Eng. Data. 2007, 52, 721–726.

10. Nizri, G.; Magdassi, S.; Schmidt, J.; Cohen, Y.; Talmon, Y., *Microstructural Characterisation of Micro- and Nanoparticles Formed by Polymer–Surfactant Interactions*. Langmuir. 2004, 20, 4380–4385.
11. Abraham, A.; Mezei, A.; Meszaros, R., *The Effect of Salt on the Association Between Linear Cationic Polyelectrolytes and Sodium Dodecyl Sulfate*. Soft Matter. 2009, 5, 3718–3726.
12. Mukherjee, S.; Dan, A.; Bhattacharya, S. C.; Panda, A. K.; Moulik, S. P., *Physicochemistry of Interaction between the Cationic Polymer Poly(diallyldimethylammonium chloride) and the Anionic Surfactants Sodium Dodecyl Sulfate, Sodium Dodecylbenzenesulfonate, and Sodium N-Dodecanoylsarcosinate in Water and Isopropyl Alcohol–Water Media*. Langmuir. 2011, 27, 5222–5233.
13. Nizri, G.; Makarsky, A.; Magdassi, S.; Talmon, Y., *Nanostructures Formed by Self-Assembly of Negatively Charged Polymer and Cationic Surfactants*. Langmuir. 2009, 25, 1980–1985.
14. Bronich, T. K.; Kabanov, A. V.; Kabanov, V. A.; Yu, K.; Eisenberg, A., *Soluble Complexes from Poly(ethylene oxide)–block–polymethacrylate Anions and N-Alkylpyridinium Cations*. Macromolecules. 1997, 30, 3519–3525.
15. Trabelsi, S.; Guillot, S.; Ritacco, H.; Boué, F.; Langevin, D., *Nanostructures of Colloidal Complexes Formed in Oppositely Charged Polyelectrolyte/Surfactant Dilute Aqueous Solutions*. Eur. Phys. J. E. 2007, 23, 305–311.
16. Kabanov, A. V.; Bronich, T. K.; Kabanov, V. A.; Yu, K.; Eisenberg, A., *Spontaneous Formation of Vesicles from Complexes of Block Ionomers and Surfactants*. J. Am. Chem. Soc. 1998, 120, 9941–9942.
17. Percebom, A. M.; Bernardes, J. S.; Loh, W., *Complex Salts Formed by Anionic Copolymers with Hexadecyltrimethylammonium: Phase Equilibrium and Structural Characterisation using SAXS*. AIP Conf. Proc. 2009, 1092, 173–175.
18. Percebom, A. M.; Piculell, L.; Loh, W., *Polyion–Surfactant Ion Complex Salts Formed by a Random Anionic Copolyacid at Different Molar Ratios of Cationic Surfactant: Phase Behavior with Water and n-Alcohols*. J. Phys. Chem. B. 2012, 116, 2376–2384.

19. Percebom, A. M.; Janiak, J.; Schillen, K.; Piculell, L.; Loh, W., *Micellization of Water-Soluble Complex Salts of an Ionic Surfactant with Hairy Polymeric Counterions*. *Soft Matter*. 2013, 9, 515–526.
20. Mezei, A. I.; Ábrahám, A. G.; Pojják, K.; Mészáros, R. B., *The Impact of Electrolyte on the Aggregation of the Complexes of Hyperbranched Poly(ethyleneimine) and Sodium Dodecyl Sulfate*. *Langmuir*. 2009, 25, 7304–7312.
21. Fegyver, E.; Meszaros, R., *Fine-Tuning the Nonequilibrium Behavior of Oppositely Charged Macromolecule/Surfactant Mixtures via the Addition of Nonionic Amphiphiles*. *Langmuir*. 2014.
22. Pojják, K.; Mészáros, R., *Novel Self-Assemblies of Oppositely Charged Polyelectrolytes and Surfactants in the Presence of Neutral Polymer*. *Langmuir*. 2009, 25, 13336–13339.
23. Percebom, A. M.; Barbosa, L. R. S.; Itri, R.; Loh, W., *How Does the Ethoxylated Grafting of Polyelectrolytes Affect the Self-Assembly of Polyanion–Cationic Surfactant Complex Salts?* *Langmuir*. 2014.
24. Janiak, J.; Tomšič, M.; Lundberg, D.; Olofsson, G.; Piculell, L.; Schillén, K., *Soluble Aggregates in Aqueous Solutions of Polyion–Surfactant Ion Complex Salts and a Nonionic Surfactant*. *J. Phys. Chem. B*. 2014.
25. Janiak, J.; Bayati, S.; Galantini, L.; Pavel, N. V.; Schillén, K., *Nanoparticles with a Bicontinuous Cubic Internal Structure Formed by Cationic and Non-Ionic Surfactants and an Anionic Polyelectrolyte*. *Langmuir*. 2012, 28, 16536–16546.
26. Mezei, A.; Mészáros, R.; Varga, I.; Gilányi, T., *Effect of Mixing on the Formation of Complexes of Hyperbranched Cationic Polyelectrolytes and Anionic Surfactants*. *Langmuir*. 2007, 23, 4237–4247.
27. Mezei, A. I.; Pojják, K.; Mészáros, R. B., *Nonequilibrium Features of the Association between Poly(vinylamine) and Sodium Dodecyl Sulfate. The Validity of the Colloid Dispersion Concept*. *J. Phys. Chem. B*. 2008, 112, 9693–9699.
28. Naderi, A.; Claesson, P. M.; Bergström, M.; Dédinaite, A., *Trapped Non-Equilibrium States in Aqueous Solutions of Oppositely Charged Polyelectrolytes and Surfactants*.

- Effects of Mixing Protocol and Salt Concentration.* Colloids and Surfaces A: Physicochem. Eng. Aspects. 2005, 253, 83–93.
29. Naderi, A.; Claesson, P. M., *Association between Poly(vinylamine) and Sodium Dodecyl Sulfate: Effects of Mixing Protocol, Blending Procedure, and Salt Concentration.* J. Dispersion Sci. Technol. 2005, 26, 329–340.
30. Yeh, F.; Sokolov, E. L.; Khokhlov, A. R.; Chu, B., *Nanoscale Supramolecular Structures in the Gels of Poly(diallyldimethylammonium chloride) Interacting with Sodium Dodecyl Sulfate.* J. Am. Chem. Soc. 1996, 118, 6615–6618.
31. Sokolov, E. L.; Yeh, F.; Khokhlov, A.; Chu, B., *Nanoscale Supramolecular Ordering in Gel–Surfactant Complexes: Sodium Alkyl Sulfates in Poly(diallyldimethylammonium chloride).* Langmuir. 1996, 12, 6229–6234.
32. Sokolov, E.; Yeh, F.; Khokhlov, A.; Grinberg, V. Y.; Chu, B., *Nanostructure Formation in Polyelectrolyte–Surfactant Complexes.* J. Phys. Chem. B. 1998, 102, 7091–7098.
33. Chu, B.; Yeh, F.; Sokolov, E. L.; Starodoubtsev, S. G.; Khokhlov, A. R., *Interaction of Slightly Cross-Linked Gels of Poly(diallyldimethylammonium chloride) with Surfactants.* Macromolecules. 1995, 28, 8447–8449.
34. Mironov, A. V.; Starodoubtsev, S. G.; Khokhlov, A. R.; Dembo, A. T.; Dembo, K. A., *Effect of Chemical Nature of 1,1-Salt on Structure of Polyelectrolyte Gel–Surfactant Complexes.* J. Phys. Chem. B. 2001, 105, 5612–5617.
35. Zhou, S.; Yeh, F.; Burger, C.; Chu, B., *Highly Ordered Supramolecular Structures From Self-Assembly of Ionic Surfactants in Oppositely Charged Polyelectrolyte Gels.* In Scattering from polymers, American Chemical Society: 1999; Vol. 739, pp 244–260.
36. Mulet, X.; Kennedy, D. F.; Conn, C. E.; Hawley, A.; Drummond, C. J., *High Throughput Preparation and Characterisation of Amphiphilic Nanostructured Nanoparticulate Drug Delivery Vehicles.* Int. J. Pharm. 2010, 395, 290–297.
37. Nguyen, T.-H.; Hanley, T.; Porter, C. H.; Boyd, B., *Nanostructured Reverse Hexagonal Liquid Crystals Sustain Plasma Concentrations for a Poorly Water-Soluble Drug after Oral Administration.* Drug Deliv. and Transl. Res. 2011, 1, 429–438.

38. Boyd, B. J.; Whittaker, D. V.; Khoo, S.-M.; Davey, G., *Hexosomes Formed from Glycerate Surfactants—Formulation as a Colloidal Carrier for Irinotecan*. *Int. J. Pharm.* 2006, 318, 154–162.
39. Fong, C.; Krodkiewska, I.; Wells, D.; Boyd, B. J.; Booth, J.; Bhargava, S.; McDowall, A.; Hartley, P. G., *Submicron Dispersions of Hexosomes Based on Novel Glycerate Surfactants*. *Aust. J. Chem.* 2005, 58, 683–687.
40. Dong, Y.-D.; Larson, I.; Hanley, T.; Boyd, B. J., *Bulk and Dispersed Aqueous Phase Behavior of Phytantriol: Effect of Vitamin E Acetate and F127 Polymer on Liquid Crystal Nanostructure*. *Langmuir*. 2006, 22, 9512–9518.
41. Tran, N.; Mulet, X.; Hawley, A. M.; Conn, C. E.; Zhai, J.; Waddington, L. J.; Drummond, C. J., *First Direct Observation of Stable Internally Ordered Janus Nanoparticles Created by Lipid Self-Assembly*. *Nano Lett.* 2015, 15, 4229–4233.
42. Phan, S.; Fong, W.-K.; Kirby, N.; Hanley, T.; Boyd, B. J., *Evaluating the Link Between Self-Assembled Mesophase Structure and Drug Release*. *Int. J. Pharm.* 2011, 421, 176–182.
43. Kirby, N. M.; Mudie, S. T.; Hawley, A. M.; Cookson, D. J.; Mertens, H. D. T.; Cowieson, N.; Samardzic-Boban, V., *A Low-Background-Intensity Focusing Small-Angle X-ray Scattering Undulator Beamline*. *J Appl. Crystallogr.* 2013, 46, 1670–1680.
44. Hyde, S., *Chapter 16– Identification of Lyotropic Liquid Crystalline Mesophases*. In *Handbook of Applied Surface and Colloid Chemistry*, Holmberg, K., Ed. John Wiley & Sons, Ltd. 2001 pp 299–332.
45. Phan, S.; Hawley, A.; Mulet, X.; Waddington, L.; Prestidge, C.; Boyd, B., *Structural Aspects of Digestion of Medium Chain Triglycerides Studied in Real Time using sSAXS and Cryo-TEM*. *Pharm. Res.* 2013, 30, 3088–3100.
46. Williams, R. J.; Phillips, J. N.; Mysels, K. J., *The Critical Micelle Concentration of Sodium Lauryl Sulphate at 25°C*. *Trans. Faraday Soc.* 1955, 51, 728–737.
47. Bruce, C. D.; Berkowitz, M. L.; Perera, L.; Forbes, M. D. E., *Molecular Dynamics Simulation of Sodium Dodecyl Sulfate Micelle in Water: Micellar Structural Characteristics and Counterion Distribution*. *J. Phys. Chem. B.* 2002, 106, 3788–3793.

48. Arrighi, V.; Higgins, J. S., *Structural Investigation of Polymers by Neutron Scattering*. *Plast, Rubber Compos.* 2004, 33, 313–330.
49. Bernheim-Groswasser, A.; Zana, R.; Talmon, Y., *Sphere-to-Cylinder Transition in Aqueous Micellar Solution of a Dimeric (Gemini) Surfactant*. *J. Phys. Chem. B.* 2000, 104, 4005–4009.
50. Hoffmann, I.; Heunemann, P.; Prévost, S.; Schweins, R.; Wagner, N. J.; Gradzielski, M., *Self-Aggregation of Mixtures of Oppositely Charged Polyelectrolytes and Surfactants Studied by Rheology, Dynamic Light Scattering and Small-Angle Neutron Scattering*. *Langmuir.* 2011, 27, 4386–4396.
51. Pojják, K.; Bertalanits, E.; Mészáros, R., *Effect of Salt on the Equilibrium and Nonequilibrium Features of Polyelectrolyte/Surfactant Association*. *Langmuir.* 2011, 27, 9139–9147.
52. Kékicheff, P.; Grabielle-Madémont, C.; Ollivon, M., *Phase Diagram of Sodium Dodecyl Sulfate–Water System*. *J. Colloid Interface Sci.* 1989, 131, 112–132.
53. Dedinaite, A.; Claesson, P. M.; Bergström, M., *Polyelectrolyte–Surfactant Layers: Adsorption of Preformed Aggregates versus Adsorption of Surfactant to Preadsorbed Polyelectrolyte*. *Langmuir.* 2000, 16, 5257–5266.
54. Campbell, R. A.; Yanez Arteta, M.; Angus-Smyth, A.; Nylander, T.; Varga, I., *Effects of Bulk Colloidal Stability on Adsorption Layers of Poly(diallyldimethylammonium chloride)/Sodium Dodecyl Sulfate at the Air–Water Interface Studied by Neutron Reflectometry*. *J. Phys. Chem. B.* 2011, 115, 15202–15213.
55. Braem, A. D.; Biggs, S.; Prieve, D. C.; Tilton, R. D., *Control of Persistent Nonequilibrium Adsorbed Polymer Layer Structure by Transient Exposure to Surfactants*. *Langmuir.* 2003, 19, 2736–2744.
56. Bernardes, J. S.; Norrman, J.; Piculell, L.; Loh, W., *Complex Polyion–Surfactant Ion Salts in Equilibrium with Water: Changing Aggregate Shape and Size by Adding Oil*. *J. Phys. Chem. B.* 2006, 110, 23433–23442.
57. Israelachvili, J. N.; Mitchell, D. J.; Ninham, B. W., *Theory of Self-Assembly of Hydrocarbon Amphiphiles into Micelles and Bilayers*. *J. Chem. Soc., Faraday Trans. 2.* 1976, 72, 1525–1568.

58. de Campo, L.; Yaghmur, A.; Garti, N.; Leser, M. E.; Folmer, B.; Glatter, O., *Five-Component Food-Grade Microemulsions: Structural Characterization by SANS*. J. Colloid Interface Sci. 2004, 274, 251–267.
59. Alam, M. M., *The Effect of Ethanol on the Phase Behaviour and Micro-Rheology of Liquid Crystals*. Liq. Cryst. 2012, 39, 1427–1434.
60. Bernardes, J. S.; Piculell, L.; Loh, W., *Self-Assembly of Polyion-Surfactant Ion Complex Salts in Mixtures with Water and n-Alcohols*. J. Phys. Chem. B. 2011, 115, 9050–9058.
61. Baglioni, P.; Kevan, L., *Structural Effects of Alcohol Addition to Sodium Dodecyl Sulfate Micelles Studied by Electron Spin-Echo Modulation of 5-Doxylstearic Acid Spin Probe*. J. Phys. Chem. 1987, 91, 1516–1518.
62. Lopes, L.; Ferreira, D.; de Paula, D.; Garcia, M. T.; Thomazini, J.; Fantini, M. A.; Bentley, M. V. B., *Reverse Hexagonal Phase Nanodispersion of Monoclein and Oleic Acid for Topical Delivery of Peptides: in Vitro and in Vivo Skin Penetration of Cyclosporin A*. Pharm Res. 2006, 23, 1332–1342.
63. Yaghmur, A.; de Campo, L.; Sagalowicz, L.; Leser, M. E.; Glatter, O., *Emulsified Microemulsions and Oil-Containing Liquid Crystalline Phases*. Langmuir. 2004, 21, 569–577.
64. Fong, W.-K.; Hanley, T.; Boyd, B. J., *Stimuli Responsive Liquid Crystals Provide 'On-Demand' Drug Delivery In Vitro and In Vivo*. J. Controlled Release. 2009, 135, 218–226.
65. Salentinig, S.; Tangso, K. J.; Hawley, A.; Boyd, B. J., *pH-Driven Colloidal Transformations Based on the Vasoactive Drug Nicergoline*. Langmuir. 2014, 30, 14776–14781.
66. Salentinig, S.; Phan, S.; Darwish, T. A.; Kirby, N.; Boyd, B. J.; Gilbert, E. P., *pH-responsive Micelles Based on Caprylic Acid*. Langmuir. 2014, 30, 7296–7303.
67. Negrini, R.; Fong, W.-K.; Boyd, B. J.; Mezzenga, R., *pH-responsive Lyotropic Liquid Crystals and Their Potential Therapeutic Role in Cancer Treatment*. Chem. Commun. 2015, 51, 6671–6674.

5.9 Appendix

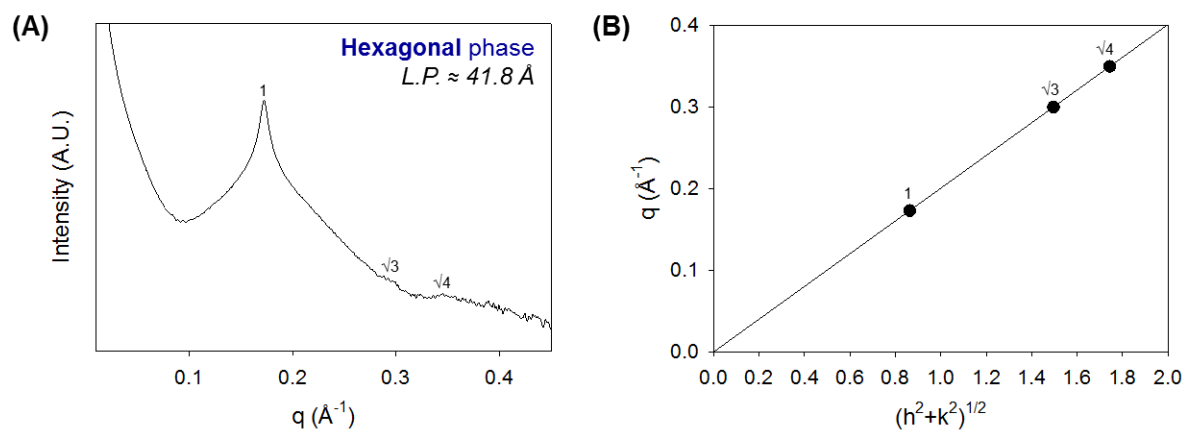


Figure A5.1 SAXS profile of a dilute aqueous mixture of SDS and polyDADMAC prepared at $r = 3.6$ (A) which was indexed as hexagonal phase (B).

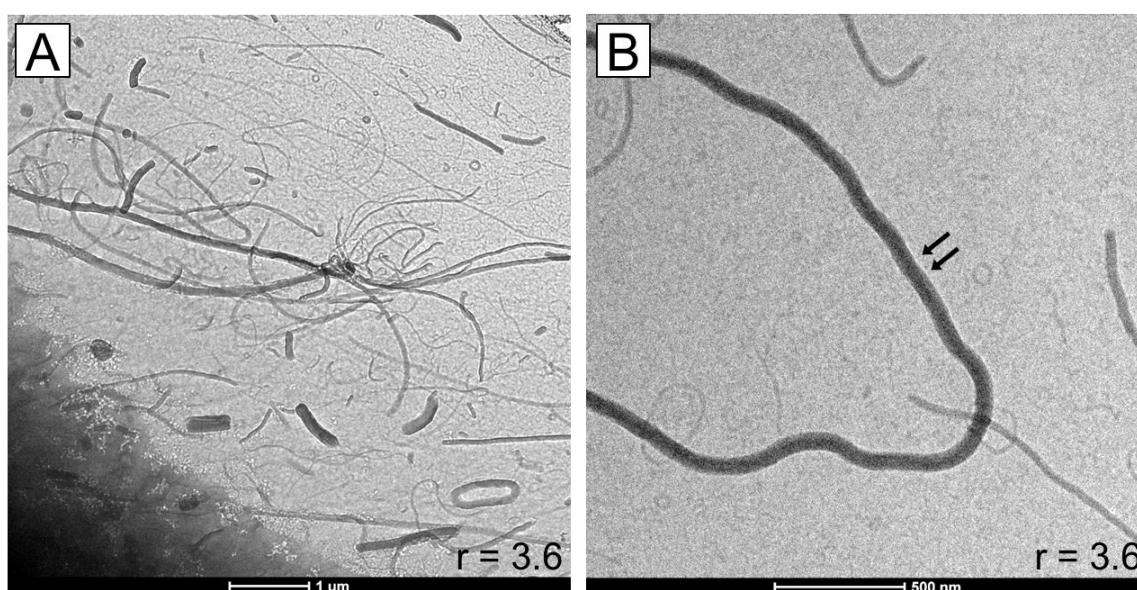


Figure A5.2 Cryo-TEM images of dispersed mixtures of SDS and polyDADMAC at $r = 3.6$ displaying stringy, looped, elongated, and textured assemblies with a polydispersed size distribution (A). Arrows indicate the characteristic 'stripe' texture exhibited by the hexagonal phase (B).

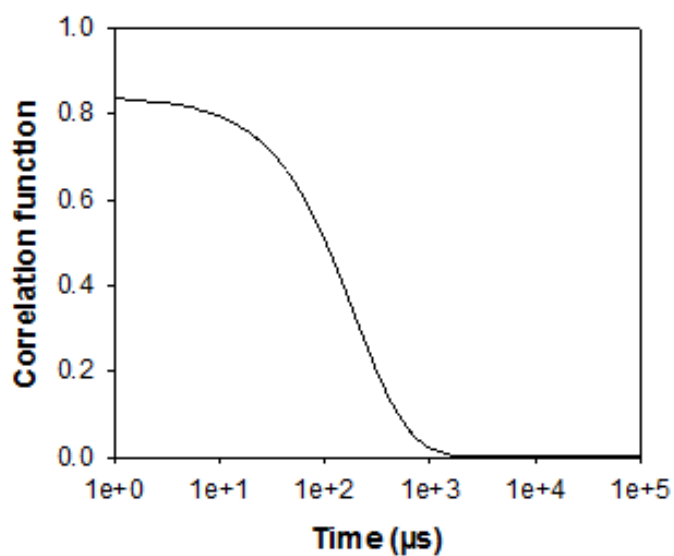


Figure A5.3 Correlation function of the particle size distribution measured by DLS for a dispersion comprised of 2.5 wt% SDS and polymer 0.5 wt% polyDADMAC at $r = 0.4$.

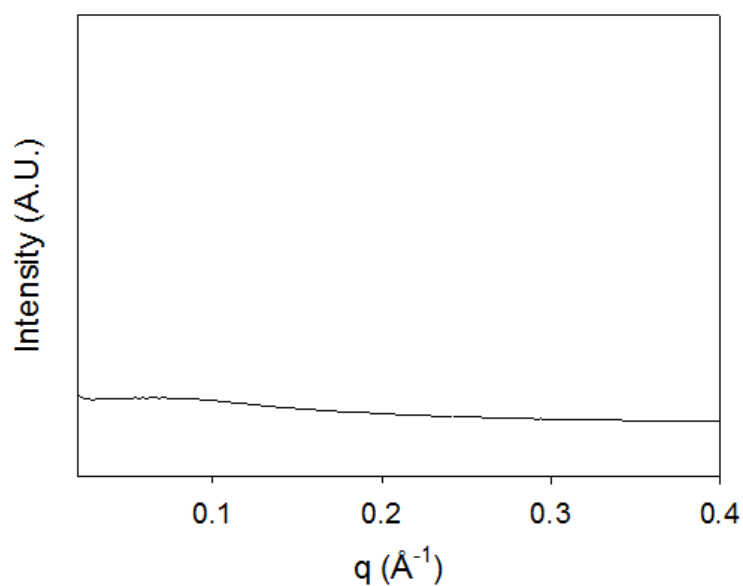


Figure A5.4 SAXS profile of a solution of 5 wt% polyDADMAC.

Chapter 6: *Novel Stimuli-Responsive Drug Delivery
Systems Created Using Nanostructures
Formed Across Surfactant-Polymer
Interfaces*

6. Novel Stimuli-Responsive Drug Delivery Systems Created Using Nanostructures Formed Across Surfactant-Polymer Interfaces

6.1 Introduction

Stimuli-responsive nanomaterials have become prevalent as a means of delivering drugs in a controlled manner. Layer-by-layer technology has been widely employed to engineer capsules using oppositely charged polyelectrolytes with functionalised surfaces that enable release of cargo at targeted sites upon introduction to certain stimuli.⁴ Although layer-by-layer assembled nanoparticles are considered to be ‘smart’ nanodevices, there has not been any known report of the formation of ordered structures in these materials and thus it is difficult to attain reproducible control over structure. On the other hand, the self-assembly of liquid crystalline structures in mixtures of oppositely charged surfactant and polymer solutions has been known since the late 1970s.^{5, 6} These complex nanostructures have potential applications in the cosmetic, food, consumer, and pharmaceutical industries.⁷⁻¹⁰ Hence, development of oppositely charged surfactant and polymer systems is anticipated to provide increased control over material structure and subsequently payload release in controlled delivery applications.

Liquid crystalline systems are excellent candidates as drug carriers for their ability to solubilise therapeutics with a diverse range of physicochemical properties. It is also well known that the nanostructure controls the rate of drug release from these matrices,^{11, 12} therefore it is advantageous to have dynamic control over the structural attributes of the mesophases formed. This may be achieved by introducing variables that can modulate the

electrostatic and/or hydrophobic interactions between the oppositely charged species, which in turn influences the molecular organisation within the resulting highly ordered structures. These experimental parameters which could act as triggers for a change in nanostructure and consequent drug release include temperature,^{8, 13-17} ionic strength,¹⁸⁻²⁰ and pH.^{21, 22}

There is evidence of structured materials formed from solutions of oppositely charged surfactants and polymers that deliver sustained or burst release of therapeutics or other organic compounds.^{18, 23, 24} Bronich *et al.* demonstrated the solubilisation of chemotherapeutic agents, such as paclitaxel and doxorubicin, in complexes formed with block ionomers and the sodium salt of oleic acid, which were protected from the reticulo-endothelial system, increasing its circulation time in the bloodstream.¹⁸ In addition, Lapitsky *et al.* showed encapsulation of an aromatic oil, cymene, into SDS-cat-HEC gel particles and its rapid release by diffusion through polydispersed pores.²³ In recent times, cationic lipids, surfactants, and/or polymers have become very attractive in the development of non-viral vectors that enhance transfection of DNA in gene therapy.²⁵ Moran *et al.* showed that the release of DNA entrapped in such complexes was controlled by the swelling or dissolution behaviour of the gel particles, which also may be triggered by addition of high salt concentrations.⁷

There have been limited reports of oppositely charged surfactant and polymer systems demonstrating triggered drug release. Therefore, this chapter investigates various industrially and biologically relevant oppositely charged surfactant and polymer systems to exploit the formation of kinetically trapped nanostructures at the surfactant-polymer interface for their application as stimuli-responsive drug delivery systems.

6.1.1 SDS/PolyDADMAC System

The anionic surfactant, sodium dodecyl sulphate (SDS), and the cationic polymer, poly(diallyldimethylammonium chloride) (polyDADMAC) (chemical structures shown in Figure 6.1), are common ingredients found in hair care products and are known to form hexagonal phases at certain surfactant-to-polymer molar charge ratios.^{15, 26–29}

The self-assembly of such mesophases upon mixing of oppositely charged surfactants and polymers in solution occurs as a result of association between the charged species. PolyDADMAC is a high charge density polymer, thus the electrostatic attractions between the anionic surfactant molecules or micelles and the positive charges on polyDADMAC chains would be the main forces that are important in determining the strength of the interactions between SDS and polyDADMAC.

The interactions dominating the nanostructures formed in surfactant/polymer complexes in turn influences their structural integrity, which is often determined by studying the effect addition of salt or application of heat has on the existing mesophases. The addition of high concentrations of salt has been shown to destroy highly ordered structures in such complexes due to the screening of the electrostatic interactions between the oppositely charged species.^{30, 31} Furthermore, phase transitions between different mesophases have also been induced by changes in temperature, which depend on the strength of the hydrophobic interactions and/or hydrogen bonding between the molecules in the system.^{11, 15, 32} Therefore, it is hypothesised that the addition of salt and changes in solution temperature may be used to modify the geometric packing within hexagonal phases formed across SDS–polyDADMAC interfaces and subsequently be employed as a means to trigger the release of a drug from nanostructured capsules in response to stimuli.

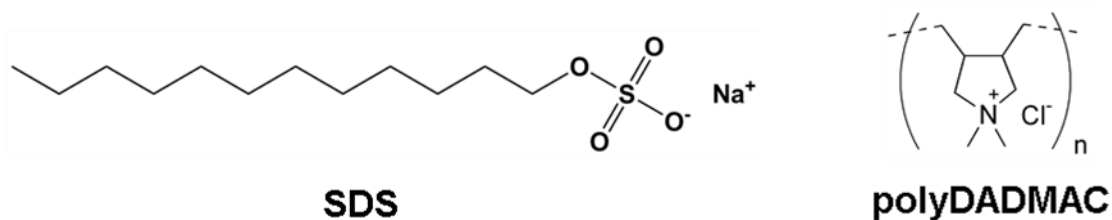


Figure 6.1 Chemical structures of sodium dodecyl sulphate (SDS) and poly(diallyldimethylammonium chloride) (polyDADMAC).

6.1.2 CTAB/PAAm-AA System

The formation of highly ordered structures that are responsive to pH is of particular interest as a variety of physiological and disease states involve changes in pH, and consequently can be used in biomedical applications to act as a trigger for the release of active components from surfactant/polymer complexes.^{33, 34} In order for a material to be responsive to changes in pH it must possess a functional group that is susceptible to ionisation. Poly(acrylic acid), poly(*N,N*-dimethylaminoethyl methacrylate), alginate, and hyaluronic acid are examples of synthetic and natural polyelectrolytes that fall under this category.³⁵ They are commonly utilised as hydrogels, where differences in their swelling behaviour at varying pH are exploited as a means of stimulating the delivery of therapeutics. Mahdavinia *et al.* reported how pH and salt influenced the swelling capacity of cross-linked hydrogels comprised of poly(acrylamide-acrylic acid) grafted with chitosan. Their findings presented pH-dependent reversible swelling between pH 3 ('on') and pH 10 ('off'), respectively, and that its swelling capacity was controlled by the degree of cross-linking.³⁶ While interesting, these materials do not form ordered nanostructures as is often found in oppositely charged surfactant and polymer systems.

Nizri *et al.* demonstrated that highly ordered nanostructures, namely hexagonal phases, can arise upon interaction between polyacrylate and alkyltrimethylammonium salts with a surfactant chain greater than eight carbons in length.³⁷ Cross-linking of polyacrylate produced macrogels which when in contact with a solution of cetyltrimethylammonium chloride (CTAB) resulted in its deswelling. This was explained by the diffusion of micelles into the stagnant macrogel and the subsequent formation of *Pm3n* cubic phase onto its surface, which transformed into hexagonal phase over time.³⁸ Hierarchical complex columnar phases have also been encountered when combining polyelectrolytic random copolymers with oppositely charged surfactants.³⁹

In this chapter, the formation of mesophases across the interface between solutions of the cationic surfactant, CTAB, and the random copolymer, poly(acrylamide–acrylic acid) (PAAm-AA) (chemical structures shown in Figure 6.2) is also investigated. The combination of these materials are hypothesised to be responsive to the solution pH, which in turn can modify the rate of release of a model hydrophilic drug from nanostructured capsules.

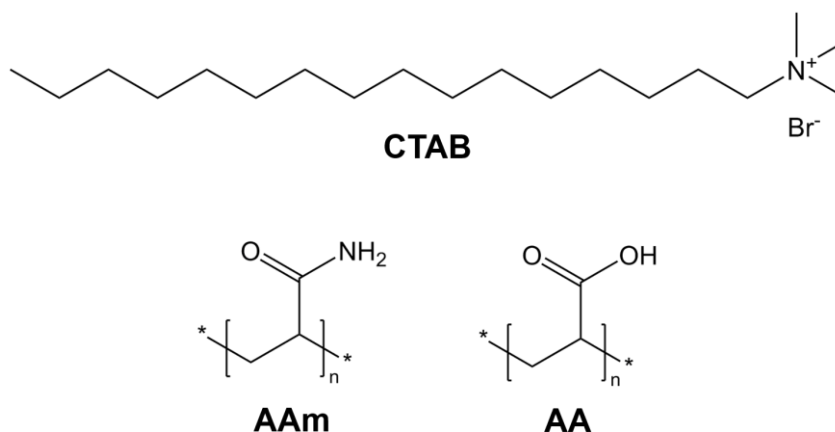


Figure 6.2 Chemical structures of the cationic surfactant, cetyltrimethylammonium bromide (CTAB), and the monomer units, acrylamide (AAm) and acrylic acid (AA), that comprise the random copolymer poly(acrylamide–acrylic acid) (PAAm-AA).

6.1.3 Bile Salt/Chitosan System

There has been much research into cationic lipids and DNA for use in gene therapy,^{20, 25, 40} however, studies on biocompatible anionic surfactant and cationic polymer systems have received little attention.

Bile acids, or bile salts, are biological anionic amphiphiles that exhibit great solubilisation capacity for lipids, such as lecithin and cholesterol,⁴¹ through formation of micelles at dilute concentrations. At higher concentrations, bile salts can form more highly ordered liquid crystalline phases, such as the hexagonal phase.⁴²

Chitosan is a cationic polysaccharide produced from the deacetylation of chitin, a natural element abundantly sourced from the shells of crustaceans. Its biocompatibility, biodegradability, low toxicity, and mucoadhesive properties enable chitosan to be used in skin products, cosmetic, and biomedical materials and it also has potential to function as a novel carrier of drugs for oral and intravenous administration.⁴³ Drug delivery via the buccal route is advantageous as it provides a rich blood supply, good accessibility for self-medication, patient compliance and safety, and most importantly bypasses the hepatic first-pass metabolism and degradation within the gastrointestinal tract. However, this route of drug administration also possesses a few limitations, including poor permeability of high molecular weight molecules,^{44, 45} thus requiring penetration enhancers that tend to cause mucosal damage, as well as needing protection from enzymes introduced within the saliva.

Systems comprising a combination of both bile salt and chitosan have recently become a growing field of interest. Lameiro *et al.* demonstrated encapsulation of protein into microparticles prepared with sodium deoxycholate and chitosan, where it remained protected from aqueous media until released by the onset of degradation of the microparticles after interaction with cell monolayers; offering a route to mucosal delivery of adenovirus vaccine.⁴⁶

Sodium taurodeoxycholate (STDC) is a bile salt commonly employed in the *in vitro* model developed for studying the digestion of lipid based formulations.^{47, 48} There is evidence that complexes are formed after association of molecules in aqueous mixtures of bile salts and chitosan.^{49, 50} Therefore, it is highly probable that ordered structures could arise across the interface between solutions of sodium taurodeoxycholate and chitosan (chemical structures shown in Figure 6.3). The structural integrity of mesophases formed across this bile salt-chitosan interface is also anticipated to be susceptible to changes in salt concentration and temperature. Therefore, it is hypothesised that the addition of salt and application of heat can be used to trigger the release of a model hydrophilic drug from these nanostructured capsules in response to the stimuli.

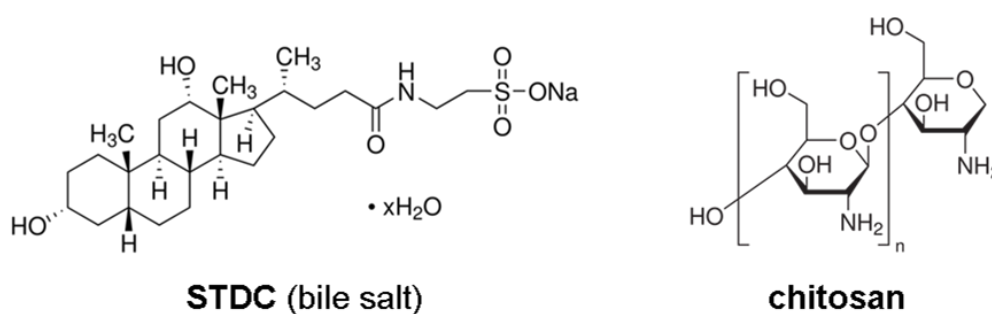


Figure 6.3 Chemical structures of sodium taurodeoxycholate (STDC) and chitosan.

6.1.4 Studying the Release Behaviour from Structured Capsules

The formation of gel capsules after dropwise addition of a solution of polyelectrolyte into a bulk solution of oppositely charged surfactant has been demonstrated by Babak and Lapitsky *et al.*^{23, 51-55} By employing a similar approach described in their studies, the diffusion behaviour of a model hydrophilic drug encapsulated within the nanostructured SDS/polyDADMAC, CTAB/PAAm-AA, and bile salt/chitosan capsules in response to changes in salt concentration, solution pH, and temperature can be determined.

6.2 Hypotheses and Aims

Hypotheses

That the diffusivity of a model hydrophilic drug from oppositely charged surfactant and polymer capsules can be modulated by changes in the structural integrity of the mesophases in response to certain stimuli. Specifically:

- i. Nanostructures formed across the SDS-polyDADMAC and bile salt-chitosan interfaces are expected to be responsive to changes in solution temperature and salt concentration.
- ii. Nanostructures formed across the CTAB-PAAm-AA interface are expected to be specifically responsive to changes in solution pH.

In order to investigate these hypotheses, the following aims were achieved:

1. To develop a method to study the responsiveness of nanostructures formed across the SDS-polyDADMAC, CTAB-PAAm-AA, and bile salt-chitosan interfaces before and after changes in salt concentration, solution pH, and temperature.
2. To develop a method to study the release behaviour of a model hydrophilic drug from nanostructured macro-sized capsules upon changes in solution conditions and use the method to study the rate of release from SDS/polyDADMAC, CTAB/PAAm-AA, and bile salt/chitosan nanostructured capsules upon changes in salt concentration, solution pH, and temperature.

6.3 Materials

Sodium dodecyl sulphate (SDS, BioXtra, $\geq 99.0\%$), sodium taurodeoxycholate hydrate (STDC, BioXtra, $\geq 97\%$), chitosan (low molecular weight, $\geq 75.0\%$ deacetylation), acetic acid (ReagentPlus[®], $\geq 99\%$), and Rhodamine B (RhB, dye content $\sim 90\%$) were purchased from Sigma-Aldrich (Sydney, Australia). Hexadecyltrimethylammonium bromide (CTAB, 98%) was obtained from Alfa Aesar (Lancashire, United Kingdom). Poly(diallyldimethylammonium chloride) (polyDADMAC, Merquat[™] 100, molecular weight: 1.5×10^5 g/mol) was obtained from Nalco Company (Illinois, United States). The commercial solution of polyDADMAC obtained contained 53.3% solid and 46.7% water (standard deviation: $\pm 0.3\%$) as determined by gravimetric analysis ($n = 10$). Merquat[™] 100 was dried prior to preparation of polyDADMAC stock solutions to form a waxy solid. Poly(acrylamide-acrylic acid, sodium salt) (PAAm-AA, 40% carboxy, molecular weight: $>10,000,000$ g/mol) was acquired from Polysciences Inc. (Warrington, United States). Sodium hydroxide pellets (Univar) were sourced from Ajax Chemicals (New South Wales, Australia). Hydrochloric acid (32% concentrated, Univol) was obtained from Asia Pacific Specialty Chemicals Limited (Australia). Sodium chloride analytical reagent was acquired from Chem-Supply (South Australia, Australia).

All materials were used without further purification. Milli-Q grade water purified through a Milli-pore system (Billerica, United States) was used throughout the studies.

6.3.1 Surfactant/Polymer System Composition

6.3.1.1 SDS/PolyDADMAC System

As the equilibrium phase behaviour across SDS-polyDADMAC interfaces was established in Chapter 3 and Chapter 4, it was of interest to further study the structural

attributes of the hexagonal phase formed in this model system in response to stimuli. The system prepared at 20 wt% SDS and 20 wt% polyDADMAC was selected for these studies for ease of handling.

6.3.1.2 CTAB/PAAm-AA System

Leonard *et al.* showed the existence of *Pm3n* cubic phase in mixtures of PAAm-AA and CTAB at charge stoichiometric amount, where the concentration of the polymer (40 % carboxylate content) was fixed at 1 wt%.¹⁹ In order to favour the formation of liquid crystalline structures in the system of interest, PAAm-AA was also prepared at 1 wt% in Milli-Q water. The concentration of CTAB required to ensure that stoichiometric charge equivalence was achieved was calculated to be 2.5 wt%. Hence, all studies were performed at this composition. Aqueous solutions prepared for investigation were adjusted to either pH 7 or 2 by dropwise addition of 0.1 M NaOH or 32 % concentrated HCl as required.

6.3.1.3 Bile Salt/Chitosan System

All stock solutions were prepared by weight. Chitosan is known to be readily soluble in acidic conditions where it predominantly exists in its protonated form. For this reason, stock solutions of bile salt and chitosan were both prepared in 10 % (v/v) acetic acid; where the solution pH was not adjusted. The liquid crystalline structure formed in systems comprised of fixed bile salt-to-chitosan composition was not influenced by pH (Appendix-Figure A6.1). To ensure that the molar concentration of bile salt was in excess of chitosan to favour the formation of mesophase, the concentration of bile salt was prepared at 30 wt% STDC, while solutions of chitosan were prepared at 4 wt%.

6.4 Methods

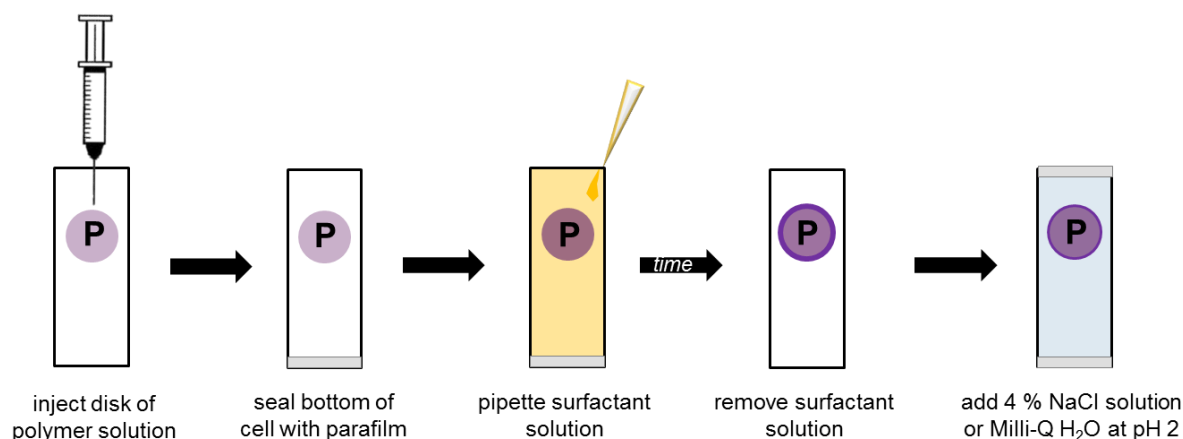
6.4.1 Characterisation of the Internal Structure of Liquid Crystalline Phases

6.4.1.1 Mesophases Across Surfactant-Polymer Interfaces

Sample Preparation

The phase behaviour of nanostructures formed across the oppositely charged surfactant-polymer interfaces was spatially characterised as described previously in Chapter 2. Briefly, polymer solution was drawn up from the bottom of an open-ended glass flat cell and sealed with parafilm. Surfactant solution was then carefully pipetted into the top-end of the flat cell and the top sealed again with parafilm. This method allowed a neat interface to be created between aqueous solutions of surfactant and polymer, which was marked as the ‘point of origin’ to monitor the development of nanostructures across the surfactant-polymer interfaces over time.

A second configuration was employed to study the influence of changes in salt concentration and solution pH on the mesophases formed across the various surfactant-polymer interfaces investigated. Here, a circular interface was produced by delivering a disk of polymer solution inside the flat cell via a 29G needle, which was subsequently flooded with surfactant solution to achieve complete contact between the two components. Liquid crystalline structures were allowed to form at the circular interface over a given time, after which the surrounding surfactant solution was removed from the cell and replaced with either 4 % NaCl solution or Milli-Q water adjusted to pH 2 (Schematic 6.1).



Schematic 6.1 Sample preparation in flat cells for studying the effect of salt concentration or solution pH on the stability of nanostructures formed across surfactant-polymer interfaces.

Crossed-Polarised Light Microscopy

Crossed-polarised light microscopy was employed to visualise the growth of anisotropic liquid crystalline phases formed across the surfactant-polymer interfaces as described in Section 2.4.3.1. To optically examine the effect of added salt or changes in solution pH on the stability of liquid crystalline phases formed across the surfactant-polymer interfaces, images were taken of the samples before and after addition of salt solution or Milli-Q water adjusted to pH 2, respectively. The concentration of sodium chloride solution was 4 %. This value was the theoretical concentration calculated to be excess of the amount required to drive the equilibrium reaction $SDS + polyDADMAC \rightleftharpoons polyDADMADS + NaCl$ to the left, which would favour the dissociation of the mesophases formed.

Hot Stage Crossed-Polarised Light Microscopy

Hot stage microscopy was employed to probe structural changes to the mesophases in response to heating. Samples loaded in flat cells were gradually heated at a rate of 5 °C/min from 25 °C to 60 °C using a Mettler Toledo FP82HT hot stage fitted with a FP90 Central

Processor temperature controller and viewed under Nikon ECLIPSE Ni-U upright microscope fitted with crossed-polarising filters and a DS-U3 digital camera control unit (Nikon, Japan).

Synchrotron Small Angle X-ray Scattering

For spatial resolution of structures formed across the surfactant-polymer interfaces, samples prepared in flat cells were mounted in line with the X-ray beam (energy ≈ 11 keV, wavelength ≈ 1.1271 Å) on a remotely operated XYZ translation stage at the Australian Synchrotron SAXS/WAXS beamline. An automated line scan was conducted which involved rastering across the interface from the bulk polymer to surfactant solution at 100 μm steps (beam size: 200 x 100 μm , horizontal x vertical), acquiring 2D SAXS patterns for 1 s at each position using a 1M Pilatus detector (active area 169 x 179 mm^2 with a pixel size of 172 μm) with a sample-to-detector distance of 1650 mm (SDS/polyDADMAC and bile salt/chitosan) or 1532 mm (CTAB/PAAm-AA). Scattering curves were obtained across the surfactant-polymer interfaces before and after solution conditions were changed.

6.4.1.2 Temperature Scan of Bulk Mixtures

As a complementary technique to hot stage microscopy, a benchtop SAXS instrument at the Bragg Institute at the Australian Nuclear Science and Technology Organisation was used to verify the structural integrity of nanostructures formed in aqueous mixtures of SDS and polyDADMAC (20 wt%: 20 wt%), CTAB and PAAm-AA (2.5 wt%: 1 wt%), and bile salt and chitosan (30 wt%: 4 wt%) in response to heating.

Sample mixtures were prepared by dropwise addition of surfactant solution (500 μL) into polymer solution (500 μL), vortex mixed, and then left to equilibrate at 37 °C for approximately a week prior to analysis. Samples were packed into quartz glass capillaries (Capillary Tube Supplies Ltd, Germany) with a path length of 2.0 mm, sealed with wax and

then inserted into a thermostatted metal heating block controlled by a Peltier system accurate to $\pm 0.1^\circ\text{C}$. The samples were introduced to the beam of a Bruker Nanostar SAXS instrument with pinhole collimation for point focus geometry. The instrument source was a copper rotating anode (0.3 m filament) operating at 45 kV and 110 mA, fitted with cross-coupled Göbel mirrors, resulting in $\text{CuK}\alpha$ radiation wavelength of 1.54 Å. The SAXS instrument was fitted with a Hi-star 2D detector (effective pixel size: 100 μm) which was located 650 mm from the sample to provide a q -range of 0.008–0.3910 \AA^{-1} . Scattering patterns were collected over 30 min under vacuum to minimise air scatter. Samples were heated stepwise from 25 $^\circ\text{C}$ to 60 $^\circ\text{C}$ at 5 $^\circ\text{C}$ increments.

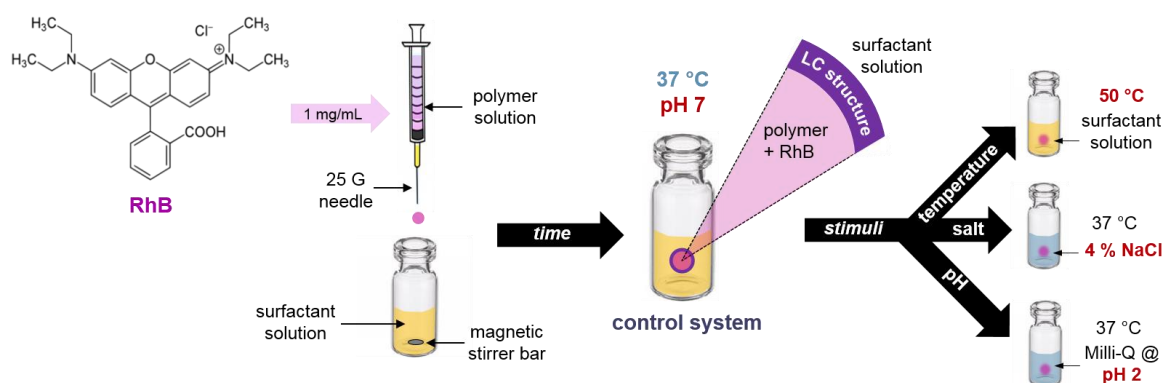
It should be noted that the scattering resolution obtained from the benchtop SAXS instrument was not as highly resolved as those obtained by synchrotron SAXS. If only one peak is observed then a definitive phase assignment is not possible. Therefore, if the second order Bragg reflection in the scattering profile obtained by the benchtop SAXS appeared at a comparable q value as shown in the scattering curve acquired with a synchrotron source then it was assumed that the nanostructures formed in the bulk aqueous mixture was comparable to those existing across the corresponding surfactant-polymer interface.

6.4.2 *In Vitro* Release Studies

6.4.2.1 Release of Model Drug from Nanostructured Capsules

Proof of concept release studies were conducted in triplicate with the purpose of determining the diffusivity of the model hydrophilic drug, Rhodamine B (RhB), across oppositely charged surfactant-polymer interfaces. Babak *et al.* demonstrated the formation of capsules after addition of a droplet of chitosan solution to a solution of SDS where the thickness of the gel bead, comprised of lamellar phase, grew over time.^{51, 53} Employing a

similar approach, nanostructured spherical capsules with reproducible surface areas were prepared by delivering a droplet of polymer solution loaded with 1 mg/mL Rhodamine B dye into a stirred solution of surfactant (1 mL in a 2 mL glass vial) via a 25G needle syringe. The liquid crystalline structure formed within the ‘outer shell’ was allowed to develop over time while maintained at physiological temperature (37 °C). Aliquots (200 μ L) of the release medium were sampled at pre-determined time points and replaced with 200 μ L of fresh dye-free solution. The release medium was comprised of the surfactant solution to initially form ordered structures across the surfactant–polymer interface and remained as the control system to avoid disruption of the capsule. For the systems tested with different stimuli, either (i) the temperature was increased from 37 °C to 50 °C, (ii) the surfactant solution was replaced with 4 % NaCl solution and kept at 37 °C, or (iii) the CTAB solution was replaced with Milli-Q water adjusted to pH 2 at a specific time after initial capsule formation (Schematic 6.2). The percentage of mass recovered was determined at the end of the study by comparing the initial mass of RhB loaded in the capsule with the mass of RhB measured in the release medium at the final time point.



Schematic 6.2 Approach for studying the effect of temperature, salt, and pH on the rate of release of model drug, Rhodamine B (RhB), from nanostructured capsules.

6.4.2.2 Rhodamine B Assay by Fluorescence Spectroscopy

Aliquots of the release medium (surfactant solution) were taken during the release study and diluted with the corresponding solvent, either 10% (v/v) acetic acid or Milli-Q water adjusted at a particular pH, and loaded into a 96-well plate. The fluorescence intensity of Rhodamine B in solution was measured at 37 °C using an EnSpire® Multimode Plate Reader (PerkinElmer, Singapore) with an excitation and emission wavelength of 554 nm and 627 nm, respectively. The concentration of dye released was quantified using a calibration curve of Rhodamine B in blank media (Appendix-Figure A6.7).

6.4.2.3 Data Analysis

In order to determine the apparent diffusion coefficient, D (cm^2/s), of drug across the single-sided matrix, the quantity expressing the moles of drug released per unit area, Q (mol/cm^2), was plotted against the square root of time, $t^{1/2}$ ($\text{s}^{1/2}$). The gradient of the linear curve from this plot was determined, which allowed for the calculation of D by applying the Higuchi equation⁵⁶:

$$Q = 2 \cdot C_0 \cdot \sqrt{\frac{D \cdot t}{\pi}} \quad [6.1]$$

where C_0 is the initial concentration of drug in the capsule (mol/cm^3). As previous studies have shown that liquid crystalline systems display diffusion-controlled release,^{11, 12} data were plotted as % RhB released vs. time^{1/2}. The Higuchi equation is based on Fickian diffusion, which allows for the direct comparison between the different release rates of the same drug from mesophases with different structures.⁵⁷

6.5 Results

6.5.1 Nanostructures Across the SDS–PolyDADMAC Interface

6.5.1.1 Effect of Temperature on Hexagonal Phases

It was established in Chapter 3 that coexisting hexagonal and micellar phases were formed across the SDS–polyDADMAC interface. These structures were found to persist at elevated temperatures with a lattice parameter of ~ 43 Å (Figure 6.4). The structural stability exhibited by these complexes may have been the result of very strong electrostatic interactions governing the associations between the charged species rather than weaker hydrophobic forces. In either case, a high degree of energy is required to disrupt the packing of the molecules within the hexagonal lattice in order for a phase change to occur.

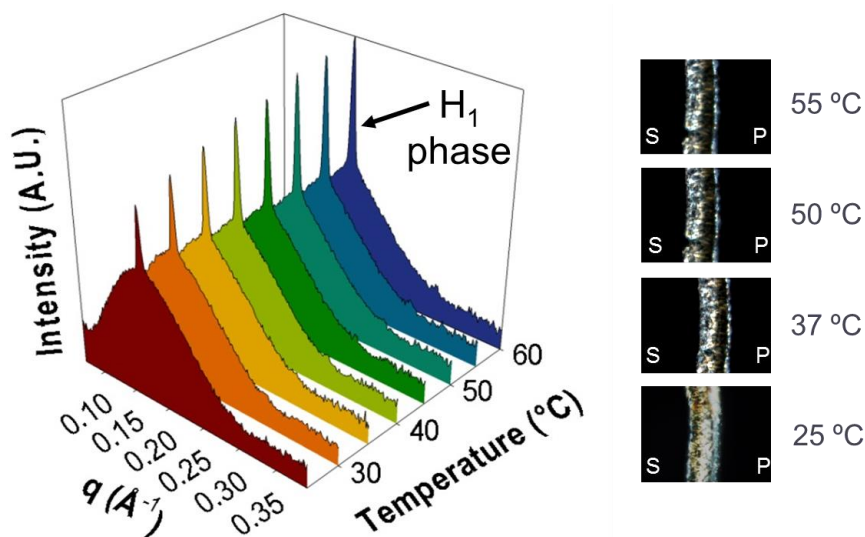


Figure 6.4 Temperature stable hexagonal phase formed in a system comprised of 20 wt% SDS and 20 wt% polyDADMAC. SAXS scattering profiles obtained of the mixture when heated from 25 °C to 60 °C at 5 °C increments (left). A birefringent band formed across the SDS–polyDADMAC interface persisted at high temperatures as observed under CPLM (right).

6.5.1.2 Effect of Salt Concentration on Hexagonal Phases

Scattering data acquired across the SDS–polyDADMAC interface after replacing the surfactant solution with a 4 % NaCl solution presented a decrease in the intensity of the first reflection peak indicative of a loss of hexagonal phase structure and a reduction in the distance over which the mesophase spanned across the SDS–polyDADMAC interface (Figure 6.5). This was emphasised in the image taken under crossed-polarisers where the previously intact band of anisotropic structure formed across the interface dissociated after addition of salt (Figure 6.5). These findings demonstrate that the electrostatic interactions between the oppositely charged surfactant and polymer molecules were the dominating forces that dictate the structural integrity of the mesophases formed in these complexes.

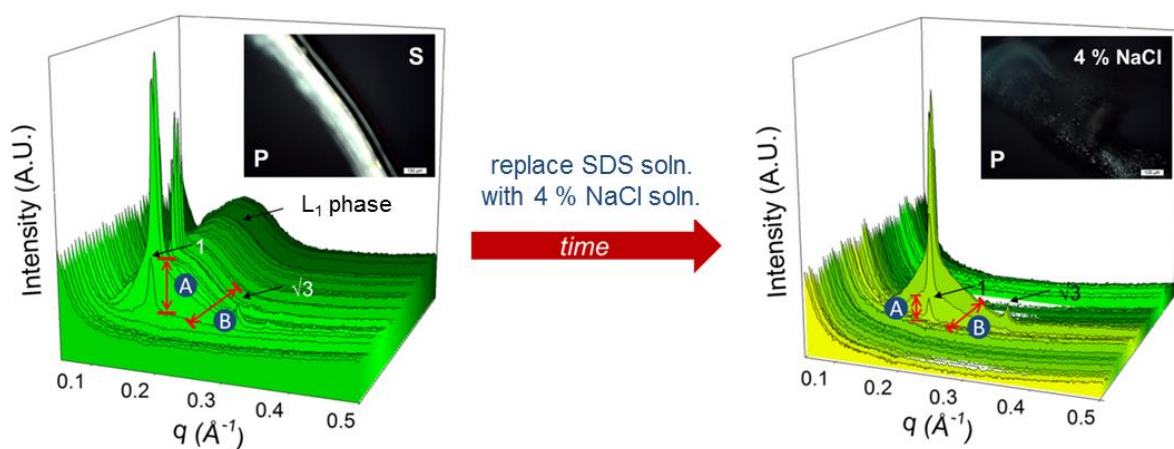


Figure 6.5 SAXS profiles across the SDS–polyDADMAC interface before (left) and after (right) addition of 4 % NaCl solution. Up–down arrows indicate a change in peak intensity, which correlates to the relative concentration of the hexagonal phase (A) and the relative changes in the distance over which the mesophase spanned across the interface (z-axis). Insets: CPLM images.

6.5.2 Nanostructures Across the CTAB-PAAm-AA Interface

6.5.2.1 Growth and Development of Coexisting $Pm\bar{3}n$ Cubic and Hexagonal Phases

Upon initial contact between the oppositely charged solutions of surfactant and polymer, the CTAB molecules already existed as micelles as indicated by the broad peak in the SAXS profile, whilst the PAAm-AA molecules displayed weak scattering (Figure 6.6-left). Highly ordered structures that spanned ~ 2 mm across the interface were identified as coexisting $Pm\bar{3}n$ cubic ($\sqrt{2}:\sqrt{4}:\sqrt{5}:\sqrt{6}\dots$) and hexagonal ($1:\sqrt{3}:\sqrt{4}\dots$) phases by indexing the Bragg reflections present in the SAXS scattering curves acquired across the surfactant-polymer interface (Appendix-Figure A6.4 and Figure A6.5). It should be reiterated that synchrotron SAXS offers a high flux of X-rays and signal-to-noise ratio that enables acquisition of highly resolved scattering profiles that is superior in comparison with those obtained from a benchtop SAXS instrument. This was emphasised in the appearance of the Bragg peak at $\sqrt{2}$ for $Pm\bar{3}n$ cubic phases when characterised by synchrotron SAXS (Appendix-Figure A6.4 and Figure A6.5). However, it was unresolved in the SAXS profiles obtained during the temperature scan with a benchtop SAXS instrument (Appendix-Table A6.1, Table A6.2, and Figure A6.6). These self-assembled mesophases grew predominantly towards the bulk CTAB micellar solution after 1 week (Figure 6.6).

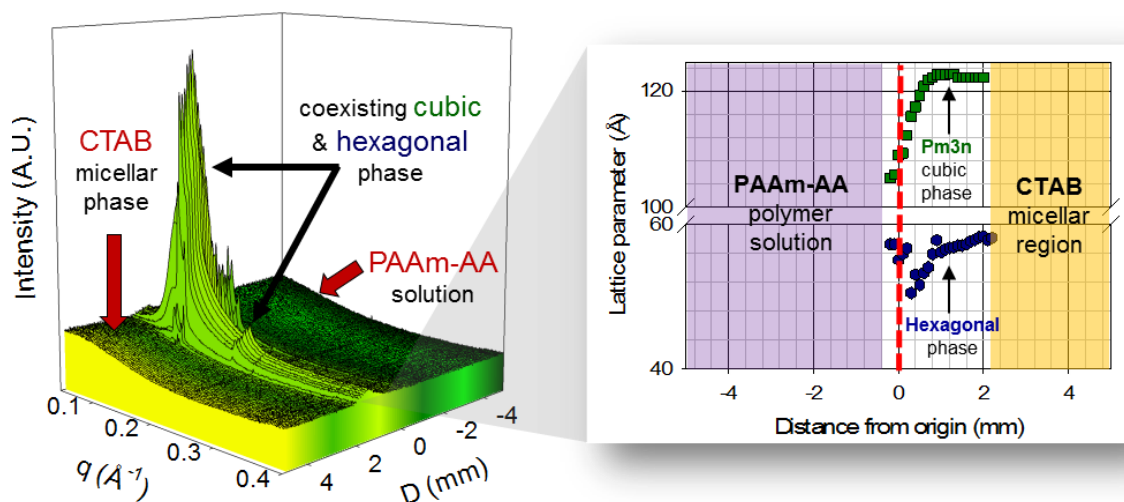


Figure 6.6 SAXS profiles as a function of distance from origin, D , across the interface created between solutions of 2.5 wt% CTAB and 1 wt% PAAm-AA. Coexisting cubic and hexagonal phases grew predominantly toward the bulk CTAB region after 1 week from initial contact (0 mm). The differences in the internal size of the $Pm3n$ cubic (squares) and hexagonal (circles) phases formed across the interface are mapped on the right panel. See the appendix for q vs. intensity profiles at three pertinent representative D values (Figure A6.4).

Further examination of the structures formed across the interface showed distinct spatial trends in their lattice dimensions (Figure 6.6–right). Notably, the lattice parameter of the $Pm3n$ cubic phase followed a somewhat sigmoidal trend, where the minimum was located near the bulk polymer region indicating the position of the least swollen structure of the cubic phase, whereas the maximum was situated towards the bulk micellar region. Interestingly, the point of inflection in the change in lattice parameter for the cubic phase corresponded to the position across the interface where a significant drop in the internal dimensions of the hexagonal phase was observed, however the point of minimal swelling of the two phases was not spatially coincident.

6.5.2.2 Effect of Temperature on CTAB-PAAm-AA Mesophases

Following the characterisation of structures formed across the CTAB-PAAm-AA interface, their structural stability in response to changes in temperature was assessed. The coexisting *Pm3n* cubic and hexagonal phases persisted throughout heating of the bulk aqueous mixture of CTAB and PAAm-AA from 25 °C to 60 °C (Figure 6.7-A), although the ratio between them changed (see Table A6.1 and Table A6.2 in the appendix for how the mesophases were indexed). As the temperature was increased, a number of the Bragg reflections indexed as *Pm3n* cubic phase gradually disappeared giving rise to a system primarily of hexagonal phase. In addition, the Bragg peaks shifted towards higher q values upon heating, which correlated to an approximate linear decrease in the lattice parameter with increasing temperature (Figure 6.7-B).

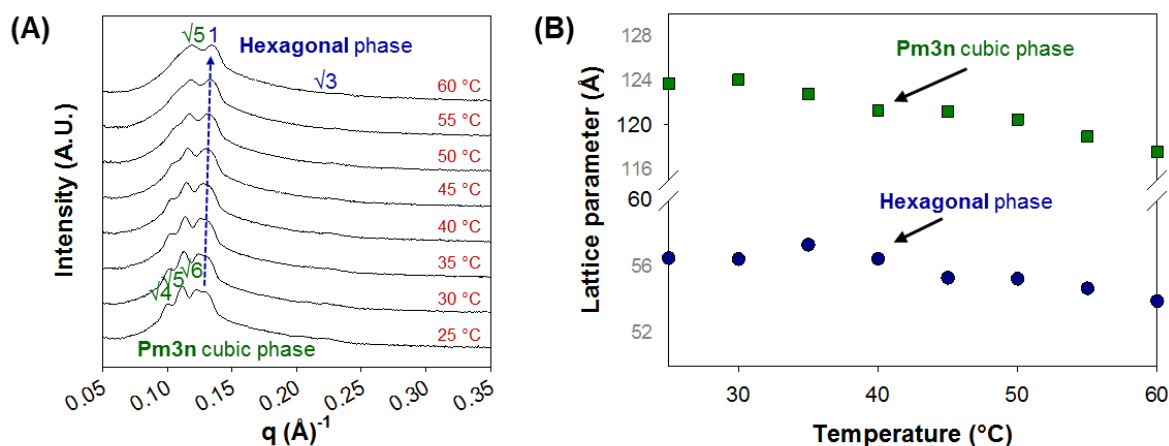


Figure 6.7 Influence of temperature on the equilibrium phase behaviour of coexisting cubic and hexagonal phases in a mixture comprised of 2.5 wt% CTAB and 1 wt% PAAm-AA. SAXS profiles obtained for the system when heated from 25 °C to 60 °C at 5 °C increments (A). Changes in the lattice parameter of coexisting *Pm3n* cubic (squares) and hexagonal (circles) phases in response to heating (B).

6.5.2.3 Effect of pH on CTAB–PAAm–AA Mesophases

In contrast to the weak dependence on temperature displayed by the liquid crystalline phases present across the CTAB–PAAm–AA interface, these nanostructures were strongly susceptible to a change in pH (Figure 6.8). At pH 7, the carboxylic acid group ($pK_a \sim 5.4$)³⁰ on the polymer backbone was deprotonated giving it a negative net charge. Ionisation of this functional group promoted its interaction with the cationic surfactant and the formation of coexisting cubic and hexagonal phases across the CTAB–PAAm–AA interface (Figure 6.8–left). At pH 2, the opposite effect occurred, where the acrylic acid portion of the polymer became protonated, thus losing its negative charge. This, along with a fraction of the acrylamide ($pK_a \sim 2.45$) monomer units attaining a positive charge introduced repulsive forces that were greater than the hydrophobic interactions involved in maintaining its structural integrity led to the dissociation of the highly ordered structures in acidic environments as indicated in the disappearance of Bragg peaks in the SAXS profile and a loss of birefringence under crossed-polarisers (Figure 6.8–right).

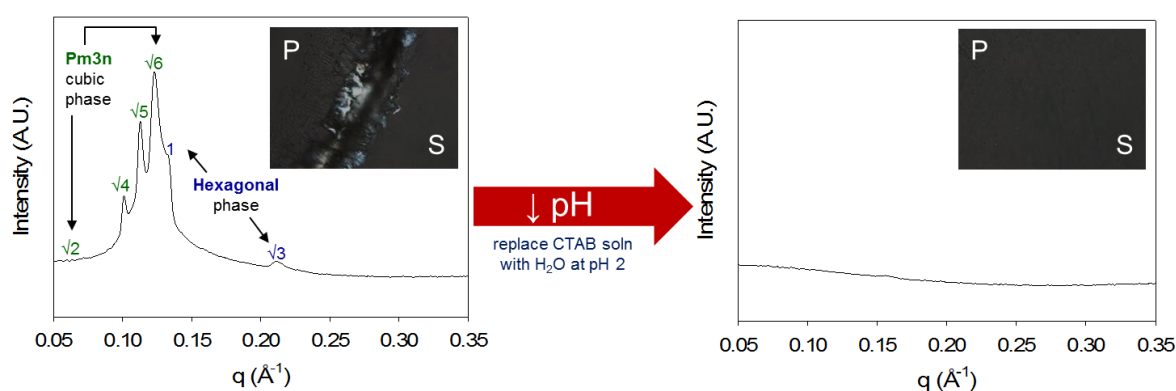


Figure 6.8 Effect of solution pH on the structural integrity of coexisting *Pm3n* cubic and hexagonal phases formed across the CTAB–PAAm–AA interface. SAXS profile shows the loss of structures after reducing the solution pH from 7 to 2. Insets: CPLM images.

6.5.3 Nanostructures Across Bile Salt-Chitosan Interfaces

6.5.3.1 Growth and Development of Bile Salt-Chitosan Mesophases

When approximately equal volumes of bile salt solution (sodium taurodeoxycholate, STDC) was contacted with a solution of chitosan, a band exhibiting birefringence was observed under a crossed-polarised light microscope at room temperature (Appendix-Figure A6.2). Lamellar phases with a lattice parameter of ~ 32 Å (Bragg reflections at spacing ratios 1 and 2-Figure 6.9) were spatially identified across the bile salt-chitosan interface, which grew predominantly toward the bulk chitosan solution after 1 week from initial contact. Micellar phase was present within the bulk 30 wt% STDC solution, which was indicated by the broad peak at low q values in the SAXS profiles (Figure 6.9).

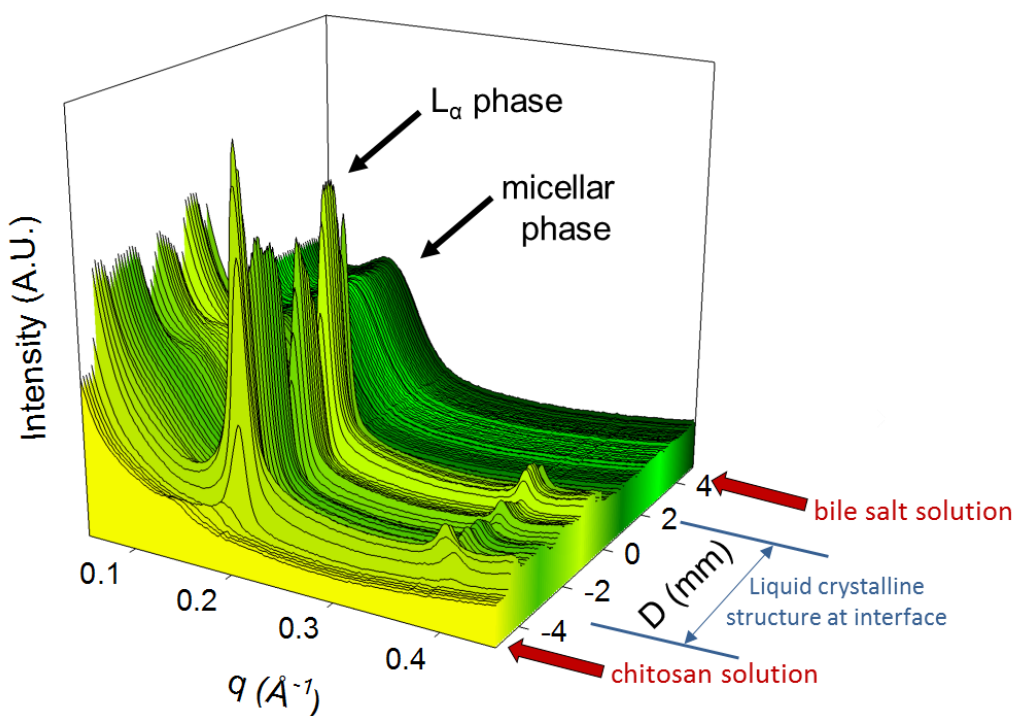


Figure 6.9 Scattering profiles as a function of distance from origin, D , across an interface between 4 wt% chitosan (bottom) and 30 wt% STDC solution (top) indicating the formation of lamellar (L_{α}) phases across the bile salt-chitosan interface.

6.5.3.2 Effect of Temperature on Bile Salt-Chitosan Lamellar Phase

Following the identification of lamellar phase formed in systems containing solutions of bile salt and chitosan, the structural integrity of the lamellar phase was examined in response to temperature. Temperature was employed to probe the nature of the hydrophobic interactions between the bile salt and chitosan. In the 30 wt% STDC: 4 wt% chitosan system, a lamellar phase existed at room temperature (Figure 6.9). During the temperature scan, scattering indicative of lamellar phase persisted up until ~ 45 °C, above which the ordered structure disappeared. Images taken of the sample under a crossed-polarised light microscope coupled with a hot stage were in agreement with the SAXS data (Figure 6.10-left), where the intensity of the birefringent band across the surfactant-polymer interface decreased with increasing temperature (Figure 6.10-right).

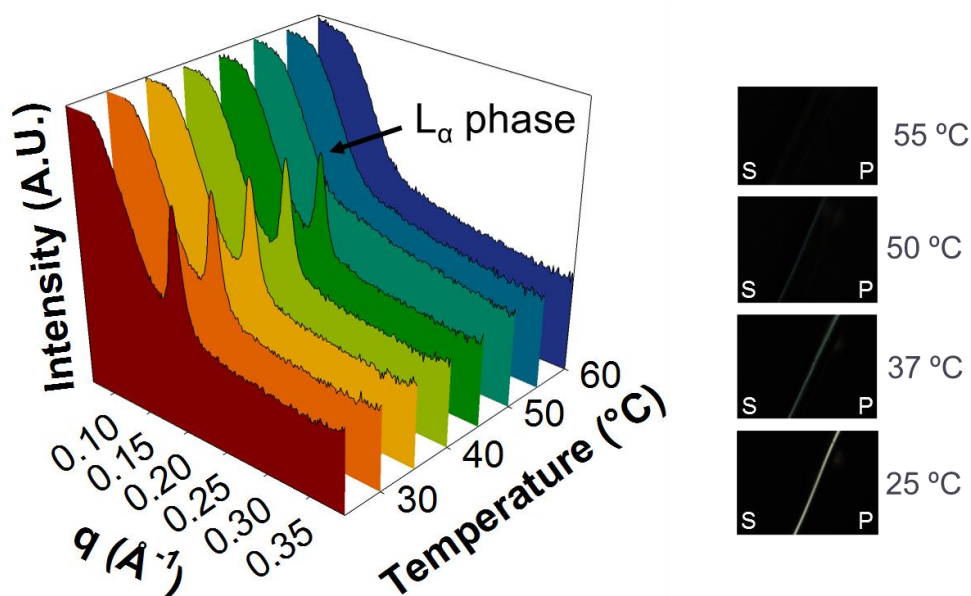


Figure 6.10 Temperature-sensitive lamellar phase formed in a system comprised of 30 wt% STDC and 4 wt% chitosan. SAXS profiles obtained of the mixture when heated from 25 °C to 60 °C at 5 °C increments (left). Loss of birefringence across the bile salt-chitosan interface above 50 °C was observed with CPLM (right).

6.5.3.3 Effect of Salt Concentration on Bile Salt-Chitosan Lamellar Phase

The electrostatic interactions between the oppositely charged species were probed by introducing a salt solution containing 4 % NaCl to the nanostructure formed across the interface. The amount of lamellar phase formed across the bile salt-chitosan interface was found to decrease upon exposure to salt solution, which was evident in a decrease in the scattering intensity of the first Bragg reflection peak and a blurred appearance of the band exhibiting birefringence across the surfactant-polymer interface under crossed-polarisers (Figure 6.11).

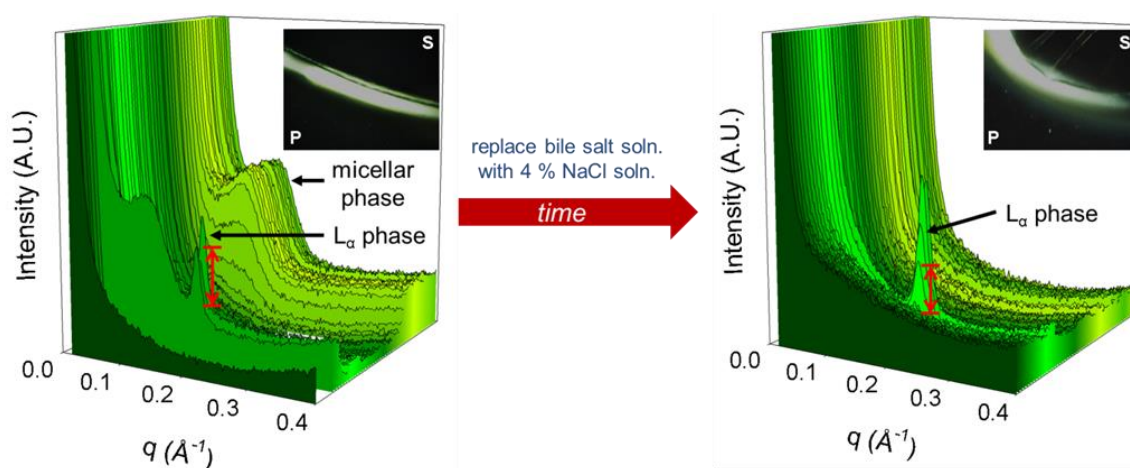


Figure 6.11 SAXS profiles across the bile salt-chitosan interface before (left) and after (after) addition of 4 % NaCl solution. Up-down arrows indicate changes in peak intensity, which correlates to the relative concentration of the lamellar phase existing as a function of the distance from origin (z -axis). Insets: CPLM images.

6.5.4 Diffusivity of Rhodamine B from Nanostructured Capsules

Having established that the coexisting micellar/hexagonal phases, coexisting cubic/hexagonal phases, and lamellar phases were destabilised with an increase in salt concentration, a decrease in solution pH, or heating to above 45 °C, respectively, it was of interest to determine whether the SDS/polyDADMAC, CTAB/PAAm-AA, and bile salt/chitosan systems may be useful as controlled release drug delivery systems. This concept was examined by determining the rate of diffusion of the model hydrophilic drug, Rhodamine B, from within macro-sized capsules comprised of an outer shell of highly ordered structures and how its diffusivity changes in response to the appropriate stimuli.

The rate of release of Rhodamine B from nanostructured capsules into the release medium displayed a slow diffusion-controlled process at physiological temperature as indicated by a linear increase of the percentage of Rhodamine B released with the square root of time. The diffusivity of the dye molecules was fastest from cubic/hexagonal phases, followed by lamellar phases, and slowest from hexagonal phases (Figure 6.12).

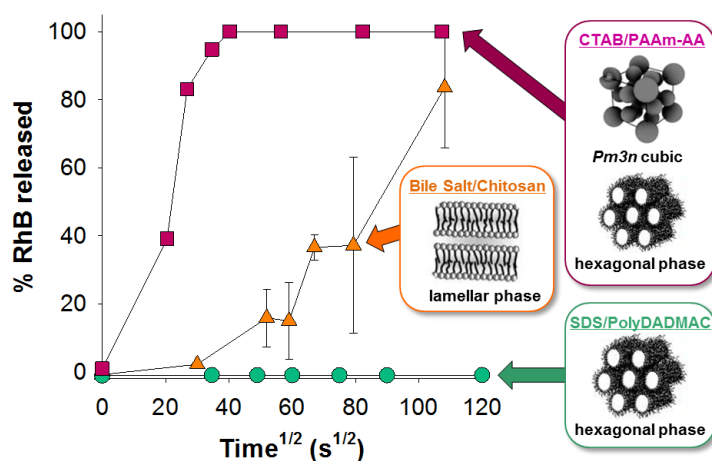


Figure 6.12 Inherent release behaviour of Rhodamine B (RhB) from the surfactant/polymer nanostructured capsules at physiological temperature without any applied stimulus ($n = 3 \pm$ S.D.). Images of mesophases reproduced from Kim *et al.*,¹ Marques *et al.*,² and Pileni *et al.*³

6.5.4.1 Triggered Release from Nanostructured Capsules

Thermally Stable Hexagonal Phase SDS/PolyDADMAC Capsules

At 2.25 hr after the SDS/polyDADMAC capsules were initially formed, the sample environment was either elevated to 50 °C or the SDS solution was replaced with a solution of 4 % NaCl. For the first scenario, no significant change in the rate of Rhodamine B release was observed, which was in agreement with structural data (Figure 6.4). It was expected that the rate of release may increase upon addition of salt. A slight increase in % RhB released was observed when this stimulus was introduced (Figure 6.13-A). This in part can be explained by a small amount of hexagonal phase still present across the SDS-polyDADMAC after the addition of salt as demonstrated in the SAXS data (Figure 6.5).

pH-Responsive Cubic/Hexagonal Phase CTAB/PAAm-AA Capsules

The coexisting *Pm3n* cubic and hexagonal phases formed across the CTAB-PAAm-AA interface were pH-sensitive. The percentage of dye molecules released from the structured capsules increased approximately linearly as a function of square root of time (Figure 6.13-B) with a calculated diffusion coefficient of $0.087 \pm 0.013 \times 10^{-6} \text{ cm}^2\text{s}^{-1}$ at physiological pH (Table 6.1). When the pH of the release medium was adjusted from pH 7 to pH 2 approximately 30 min after the capsules were initially formed, the gradient of the release curve significantly increased, reaching complete release within 5 min of the pH switch.

Temperature-Responsive Lamellar Phase Bile Salt/Chitosan Capsules

After approximately 2.25 hr from when the capsules were initially formed, the temperature of a set of triplicate samples was elevated to 50 °C whereupon a significant increase in the gradient of the release curve was observed (Figure 6.13-C). Similarly, when

the bile salt solution was replaced with a 4 % NaCl solution in a different set of triplicate samples maintained at 37 °C, a significant rise in the slope of the % RhB released vs. time^{1/2} profile was also exhibited by the system in response to a change in the concentration of salt in the release medium.

The calculated diffusion coefficient, *D*, of Rhodamine B from the lamellar phase bile salt-chitosan capsules at the various experimental conditions studied (Table 6.1) were in agreement with the release profiles (Figure 6.13-C). Initially at 37 °C, the rate of model drug release from the nanostructured capsules was $0.7 \times 10^{-6} \text{ cm}^2 \text{ s}^{-1}$. When the temperature was elevated to 50 °C after 2.25 hr, the release of dye greatly increased, which was reflected in a 40-fold increase in *D* when compared to the system at 37 °C. On the other hand, when the bile salt solution was replaced with a solution of 4 % NaCl at 37 °C, the rate of diffusion of model drug across the liquid crystalline matrix rose only by 10-fold, a lower increase in comparison with the effect of temperature.

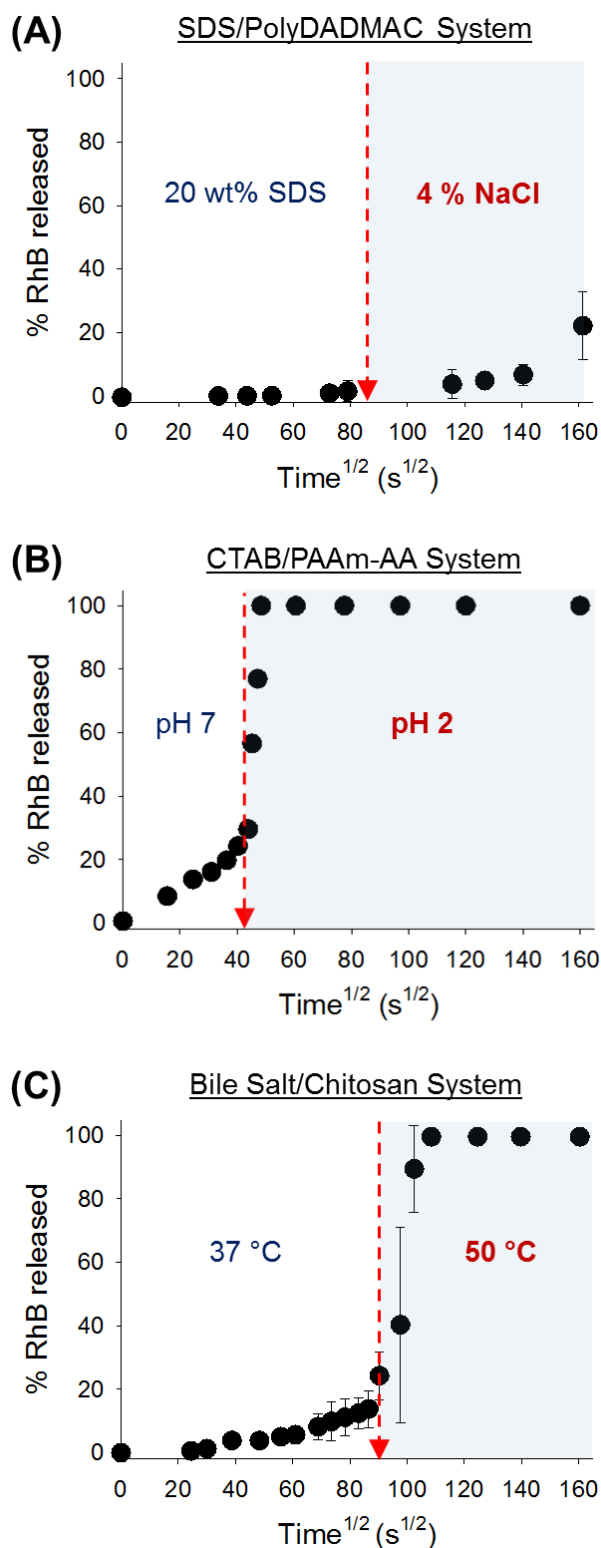


Figure 6.13 Release profiles for Rhodamine B (RhB) from nanostructured capsules under different stimuli ($n = 3 \pm \text{S.D.}$). The dashed arrow indicates when the external stimuli were introduced to the system to trigger a change in the rate of model drug release.

Table 6.1 Comparison of the rate of diffusion of Rhodamine B (RhB) from nanostructured capsules comprised of both industrially and biologically relevant materials at varying temperatures, from 37 °C (control) to 50 °C, and when the surfactant solution (release medium) was replaced with either 4 % NaCl solution or Milli-Q water adjusted to pH 2.

Solution condition		Diffusion coefficient of RhB ($\times 10^{-6} \text{ cm}^2 \text{ s}^{-1}$) $n = 3 \pm \text{S.D.}$		
		SDS/PolyDADMAC Micellar/hexagonal phases	CTAB/PAAm-AA Cubic/hexagonal phases	Bile Salt/Chitosan Lamellar phase
Control	37 °C	0.0002 \pm 0.0001	0.087 \pm 0.013	0.07 \pm 0.1
Stimuli	50 °C	0.0004 \pm 0.0001	-	3 \pm 2
	4 % NaCl	0.03 \pm 0.07	-	0.7
	pH 2	-	Burst release	-

Literature value for the diffusion coefficient of RhB at 25 °C measured by a static imaging method in an aqueous solution was determined to be $4.27 \pm 0.040 \times 10^{-6} \text{ cm}^2 \text{ s}^{-1}$ ($n = 13$).⁵⁸

6.6 Discussion

6.6.1 Nanostructure-Controlled Diffusion of Molecules from Surfactant/Polymer Complexes

As expected, the diffusivity of the model hydrophilic drug, Rhodamine B (RhB), from capsules of various oppositely charged surfactant and polymer systems differed significantly depending on the nanostructures formed across the surfactant-polymer interface. Specifically, the diffusion coefficient of RhB was determined to be the slowest from

SDS/polyDADMAC micellar/hexagonal phases, followed by bile salt/chitosan lamellar phases, and fastest from CTAB/PAAm-AA cubic/hexagonal phases.

Philippova and Söderman *et al.* reported the diffusion coefficient of surfactant micelles in aqueous mixtures of SDS and polyDADMAC in the magnitude of 10^{-6} and 10^{-7} cm^2s^{-1} , respectively.^{59, 60} These values were much higher in comparison with the rate of diffusion of RhB from SDS/polyDADMAC capsules studied here, which was approximately in the magnitude of 10^{-10} cm^2s^{-1} . A relatively small molecule, such as SDS, is likely to have greater mobility in solution, so it was not surprising that the existence of a highly compact hexagonal phase structure across the SDS-polyDADMAC interface retarded the diffusion of RhB molecules into the surrounding release media.

In contrast, the diffusion coefficient of CTAB molecules in solutions of polyacrylate has been reported to be comparable with that determined for RhB from CTAB/PAAm-AA capsules (10^{-7} cm^2s^{-1}).³⁷ This could be explained by the lattice parameter of the cubic phase being more than double in size compared to the hexagonal phase alone, suggesting that the cubic phase is the dominant structure that exists across the CTAB-PAAm-AA interface in the duration of the study, and is therefore the key determinant of the release behaviour observed (Figure 6.6).

Surprisingly, the frontal diffusion of SDS molecules toward a solution of chitosan was shown to be slightly slower than the diffusion of RhB from bile salt/chitosan capsules.⁵³ Although the chemical structures of SDS and bile salt (sodium taurodeoxycholate) differ significantly, both systems demonstrated the formation of lamellar phase upon contact of surfactant and chitosan solutions.⁵³ A difference between the lattice parameters of the lamellar phases formed in the respective systems (~ 34 Å and ~ 32 Å) may account for the difference in the rate of the diffusion of the various molecules across the nanostructured

materials. However, this was not the case. Therefore, the packing geometry and physicochemical properties exhibited by lamellar phases formed upon interactions between bile salt and chitosan must differ greatly with those formed in the SDS and chitosan system, leading to a leakier matrix which RhB molecules can diffuse through.

Overall, these findings have demonstrated that the interactions that govern the formation of nanostructures in oppositely charged surfactant and polymer systems play a notable bearing on their degree of order and physicochemical properties, such as their intrinsic viscosity, which could in turn influence the diffusion of molecules through the liquid crystalline phases. Moreover, the differences in the lattice parameter of the ordered structures partly support the distinct release behaviour demonstrated from the various nanostructured capsules.

6.6.2 Potential Applications of Thermally Stable and Salt-Sensitive SDS/PolyDADMAC Micellar/Hexagonal Phases

The coexisting micellar and hexagonal phases formed across the SDS-polyDADMAC interface remained stable when introduced to high temperatures up to 60 °C, however their structural integrity was compromised upon addition of 4 % NaCl solution.

The percent of model hydrophilic drug released from these nanostructured capsules increased linearly as a function of square root of time even after the solution temperature was increased from 25 °C to 50 °C. As anionic surfactants and cationic polymers are commonly found in shampoos and conditioners, these findings have implications in designing such hair products with improved functionalities. For example, active ingredients, such as proteins, amino acids, and/or silicone oils that help repair and strengthen damaged hair,^{61, 62} may be solubilised within the self-assembled ordered structures existing in the formulation. Upon

surface deposition of a thin layer of the material,^{63, 64} these molecules can be delivered in a controlled manner during hair washing with warm water. Use of cationic polymers with a more ‘branched’ structure, such as Polyquaternium 44, as conditioning agents in shampoos in combination with sodium lauryl ether sulphate has shown better wet compatibility, a creamier lather, and the feel of hair in comparison to the efficacy demonstrated with the use of polyDADMAC.¹⁰ Hössel *et al.* postulated that the uncharged regions of the polymer form loops that orientate away from the hair, which reduces the friction between the hairs.¹⁰

On the other hand, immersing the nanostructured capsules into a solution containing 4 % NaCl did not induce as significant an effect on the rate of drug release as may have been expected. This perhaps may have depended on the time allowed for the mesophases to form across the SDS-polyDADMAC interface before the stimulus was introduced; where a thicker ‘membrane barrier’ would be produced when left for a longer duration, which in turn would require higher salt concentrations and/or extended time for diffusion of molecules to occur and disturb the electrostatic interactions between the charged species. The sensitivity of the material toward exposure to concentrated salt solutions may be exploited in the formulation of moisturising conditioners to protect the hair from becoming dry and damaged in seawater or hard water.⁶⁵ It is envisaged that the product can be applied onto the hair prior to entering the ocean or hair washing, after which the release of conditioning agents, such as humectants, fatty alcohols, fatty esters, vegetable oils, mineral oils, and other additives,⁶⁶ can be triggered upon contact with salty water to form an occlusive film on the surface of the hair to attract and retain moisture.

6.6.3 Novel Cubic/Hexagonal Phase Cetyltrimethylammonium Bromide-Poly(acrylamide-acrylic acid) Capsules for pH Stimulated Release

pH is often a desirable means of imparting responsiveness to liquid crystalline structures by changing the extent of ionisation state of a particular component of a drug carrier system. Directly linking the *in situ* formation (and loss) of structure in these systems with changes in pH, and consequently demonstrating release of an encapsulated molecule is new for systems comprised of CTAB and PAAm-AA. This behaviour can be used to take advantage of changes in cellular pH,⁶⁷ for example in tumours,^{68, 69} or even the range of pH across the gastrointestinal tract.⁷⁰

Of particular interest is the exploitation of hyaluronic acid, which is a naturally occurring polysaccharide involved in, but not limited to, the maintenance of connective tissues in living organisms.⁷¹ Its biodegradability, biocompatibility, and low toxicity is advantageous in the field of targeted drug delivery, where the carboxyl group functions as a ligand to hyaluronan CD-44 receptors that are overexpressed in solid tumour cells.⁷² When conjugated with the anticancer drug, paclitaxel, nanoparticles coated with chitosan to protect it from degradation by hyaluronidase, were found to accumulate in tumours cells via cell-mediated endocytosis, providing a platform for oral delivery of hydrophobic drugs.⁷³ Furthermore, when hyaluronic acid was conjugated with poly(L-histidine), the ionisation of the imidazole ring of poly(L-histidine) in response to changes in solution pH was shown to dictate the swelling behaviour of the copolymer micelles and subsequent release of the encapsulated chemotherapeutic drug, doxorubicin.⁷⁴ In addition, hyaluronic acid has been blended with poloxamers to increase the stability and mechanical properties of gels formed

in situ in response to physiological temperature.⁷⁵ Mayol *et al.* demonstrated that the ionisation of hyaluronic acid enhanced the mucoadhesion of the poloxamer, which in turn increased the residence time and bioavailability of the drug, acyclovir. Here, temperature was used to control the viscosity of the formulation through changes in the degree of molecular entanglements and secondary chemical bonds within the poloxamer, offering a potential system for sustained-release ocular drug delivery.⁷⁵

CTAB and PAAm-AA are not biocompatible and are considered unsuitable for the delivery of actives in the body. Nevertheless, this system serves as a confirmatory system for such behaviour providing confidence that analogous biocompatible oppositely charged surfactant and polymer systems will show similar pH responsive behaviour. The use of these materials is not excluded in external applications either, such as fragrance release, or in sensing and diagnostic applications where the materials could provide a highly controllable amplification function.

6.6.4 Novel Temperature-Sensitive Lamellar Phase Bile Salt/Chitosan Oral Dosage Forms

The lamellar phase formed across the bile salt-chitosan interface was found to be sensitive to temperature. The most significant result that arose from the temperature scan was the complete loss of lamellar structure above ~ 45 °C (Figure 6.10). This suggests that the hydrophobic interactions were relatively weak, where only a small input of energy was required to increase the mobility of the associating molecules and cause a disruption to the packing within the liquid crystalline nanostructure. The temperature at which the lamellar phase was lost was significant in the context of this system to act as a novel stimuli-responsive drug delivery system. Drugs can be encapsulated within the capsule or the lamellar phase

itself and the mesophase would remain stable at physiological temperature. Introducing heat via a heat pack, for example, to the site of administration would disrupt packing within the liquid crystalline matrix, leading to the disintegration of the ordered structure and trigger the release of the therapeutic.

Outcomes from the temperature scans correlated well with the *in vitro* release studies. Release of Rhodamine B from the lamellar phase increased significantly at 50 °C due to the loss of structure. Interestingly, the time-scale of drug release from lamellar phase (Figure 6.13-C) was consistent with the time oral dosage forms transit within the upper region of gastrointestinal tract (3–4 hr);⁷⁶ where absorption of drug is at its highest owing to the large surface area provided by the small intestine.⁷⁷

6.6.4.1 *In Situ Self-Assembly of Mesophase in Simulated Gastrointestinal Fluids*

Chitosan has been well studied for use in oral and buccal delivery due to its mucoadhesiveness, biocompatibility, biodegradability, and low toxicity.⁴³ Thongngam *et al.* demonstrated (i) the temperature dependence of the hydrophobic interactions within insoluble complexes formed in systems comprised of chitosan and sodium taurocholate,⁴⁹ and (ii) the exothermic binding of SDS with chitosan, the interactions of which were determined to be electrostatic of origin.⁷⁸ Both systems were proposed for an approach to lowering cholesterol levels in the blood.

When a solution of chitosan was introduced into a solution of 5 mM sodium taurodeoxycholate, the concentration of bile salt which was comparable to the amount present in the gastrointestinal tract during the ‘fasted’ state,⁴⁷ no ordered structures were identified by SAXS (Figure A6.3-A). Interestingly, with a 4-fold increase in bile salt

concentration, a lamellar phase possessing a similar lattice parameter to that of the mesophase formed in the previously studied 30 wt% STDC: 4 wt% chitosan system was evident (Figure A6.3-B). This suggests that at high bile salt concentrations, which simulates the amount present in the gastrointestinal tract upon the digestion of even small traces of lipids (referred to as the ‘fed’ state),⁴⁷ there was a sufficient amount of micelles in the local microenvironment to associate with the oppositely charged chitosan to form lamellar phase. When administered orally, it is envisaged that the bile salt and chitosan system could offer a novel route to the *in situ* self-assembly of liquid crystalline nanostructures in the gut and subsequent sustained release of therapeutics or in response to changes in temperature.

6.6.5 Novel Colistin/Heparin Lamellar Phase Complexes for Antimicrobial Coating of Biomedical Devices

Although not stimuli-responsive, a further biocompatible system comprising a cationic antimicrobial peptide and a negatively charged biopolymer were also studied during this thesis that is worth briefly mentioning here. In this case, the ‘drug’ actively participates in the self-assembly behaviour.

Infections arising in hospitalised patients, particularly those who have undergone surgery and are reliant on receiving treatment through biomedical devices, continue to be a rising concern.⁷⁹ Colistin is a re-emerging antibiotic used against multidrug-resistant Gram negative bacteria.⁸⁰ The structure of colistin consists of a lipopeptide whose headgroup contains five positive charges, and a C₈-C₉ branched fatty acid tail. Its amphiphilic structure allows it to form micellar aggregates in solution.⁸¹ Thus, preliminary studies were performed to determine whether structured complexes are formed between colistin and negatively charged biopolymers, such as the highly sulphated anticoagulant, heparin.

CPLM and synchrotron SAXS were employed to visualise and identify the formation of a birefringent lamellar phase with a lattice parameter of ~ 40 Å across the colistin-heparin interface. In addition, *in vitro* release studies showed slow release of colistin from the lamellar phase gel complexes into the bulk media and disk diffusion bioassays revealed antimicrobial activity against *Pseudomonas aeruginosa*.

These findings demonstrate the novelty of the therapeutic itself participating in the formation of highly ordered mesophases, rather than being loaded into a matrix that provided 'passive release' such as previously shown with the SDS/polyDADMAC, CTAB/PAAm-AA, and bile salt/chitosan systems. The viscosity of the lamellar gel phase would be important during the application process, where it is envisaged that a more freely flowing formulation would allow the delivery system to, for instance, be easily painted on surfaces with a brush-like tool. This can be achieved by determining the optimal colistin-to-heparin molar charge ratio at dilute concentrations that will produce similar outcomes reported.

6.7 Conclusions

Gaining an understanding of how structural attributes of mesophases formed across oppositely charged surfactant-polymer interfaces can be influenced by changes in the environmental conditions has provided an interesting route to designing tailored release nanomaterials. In this chapter, various industrially and biologically relevant surfactant and polymer systems were assessed for their potential applications as drug delivery systems.

The micellar and hexagonal phases formed in complexes of sodium dodecyl sulphate and poly(diallyldimethylammonium chloride) can offer sustained release of actives and remain stable at high temperatures, or triggered release of materials in environments where the salt concentration is high. This feature along with the knowledge attained regarding the equilibrium phase behaviour of this system can be exploited in the development of new and/or improved formulations, such as hair care products.

pH triggered release of a model hydrophilic dye from *Pm3n* cubic/hexagonal phase capsules formed across the interface between solutions of cetyltrimethylammonium bromide and poly(acrylamide-acrylic acid) serves as a platform for devising systems that are responsive to changes in solution pH, particularly in the application of biomaterials.

When administered orally, it is envisaged that the bile salt/chitosan system could offer a novel route to the *in situ* self-assembly of lamellar phase in the gut, and subsequent sustained release of therapeutics or in response to changes in temperature or salt concentrations.

In summary, these studies have revealed many possibilities for employing oppositely charged surfactant and polymer systems as stimuli-responsive drug delivery systems.

6.8 References

1. Kim, D.; Jon, S.; Lee, H.-K.; Baek, K.; Oh, N.-K.; Zin, W.-C.; Kim, K., *Anion-Directed Self-Organization of Thermotropic Liquid Crystalline Materials Containing a Guanidinium Moiety*. Chem. Commun. 2005, 5509–5511.
2. Marques, E.; Silva, B. B., *Surfactants, Phase Behavior*. In Encyclopedia of Colloid and Interface Science, Tadros, T., Ed. Springer Berlin Heidelberg: 2013; pp 1290–1333.
3. Pileni, M.-P., *The Role of Soft Colloidal Templates in Controlling the Size and Shape of Inorganic Nanocrystals*. Nat. Mater. 2003, 2, 145–150.
4. Johnston, A. P. R.; Cortez, C.; Angelatos, A. S.; Caruso, F., *Layer-by-Layer Engineered Capsules and Their Applications*. Curr. Opin. Colloid Interface Sci. 2006, 11, 203–209.
5. Goddard, E.; Hannan, R., *Polymer/Surfactant Interactions*. J. Am. Oil Chem. Soc. 1977, 54, 561–566.
6. Goddard, E. D.; Hannan, R. B., *Cationic Polymer/Anionic Surfactant Interactions*. J. Colloid Interface Sci. 1976, 55, 73–79.
7. Morán, M. C.; Miguel, M. G.; Lindman, B., *Surfactant-DNA Gel Particles: Formation and Release Characteristics*. Biomacromolecules. 2007, 8, 3886–3892.
8. Hsu, W.-L.; Li, Y.-C.; Chen, H.-L.; Liou, W.; Jeng, U. S.; Lin, H.-K.; Liu, W.-L.; Hsu, C.-S., *Thermally-Induced Order-Order Transition of DNA-Cationic Surfactant Complexes*. Langmuir. 2006, 22, 7521–7527.
9. Rosa, M.; del Carmen Morán, M.; da Graça Miguel, M.; Lindman, B., *The Association of DNA and Stable Catanionic Amino Acid-Based Vesicles*. Colloids Surf., A. 2007, 301, 361–375.
10. Hössel; Dieing; Nörenberg; Pfau; Sander, *Conditioning Polymers in Today's Shampoo Formulations—Efficacy, Mechanism and Test Methods*. Int. J. Cosmet. Sci. 2000, 22, 1–10.
11. Fong, W.-K.; Hanley, T.; Boyd, B. J., *Stimuli Responsive Liquid Crystals Provide 'On-Demand' Drug Delivery In Vitro and In Vivo*. J. Controlled Release. 2009, 135, 218–226.

12. Phan, S.; Fong, W.-K.; Kirby, N.; Hanley, T.; Boyd, B. J., *Evaluating the Link Between Self-Assembled Mesophase Structure and Drug Release*. *Int. J. Pharm.* 2011, 421, 176–182.
13. Loyen, K.; Iliopoulos, I.; Audebert, R.; Olsson, U., *Reversible Thermal Gelation in Polymer/Surfactant Systems. Control of the Gelation Temperature*. *Langmuir*. 1995, 11, 1053–1056.
14. Thongngam, M.; McClements, D. J., *Influence of pH, Ionic Strength, and Temperature on Self-Association and Interactions of Sodium Dodecyl Sulfate in the Absence and Presence of Chitosan*. *Langmuir*. 2004, 21, 79–86.
15. Sokolov, E.; Yeh, F.; Khokhlov, A.; Grinberg, V. Y.; Chu, B., *Nanostructure Formation in Polyelectrolyte-Surfactant Complexes*. *J. Phys. Chem. B*. 1998, 102, 7091–7098.
16. Merta, J.; Torkkeli, M.; Ikonen, T.; Serimaa, R.; Stenius, P., *Structure of Cationic Starch (CS)/Anionic Surfactant Complexes Studied by Small-Angle X-ray Scattering (SAXS)*. *Macromolecules*. 2001, 34, 2937–2946.
17. Janiak, J.; Bayati, S.; Galantini, L.; Pavel, N. V.; Schillén, K., *Nanoparticles with a Bicontinuous Cubic Internal Structure Formed by Cationic and Non-Ionic Surfactants and an Anionic Polyelectrolyte*. *Langmuir*. 2012, 28, 16536–16546.
18. Bronich, T. K.; Nehls, A.; Eisenberg, A.; Kabanov, V. A.; Kabanov, A. V., *Novel Drug Delivery Systems Based on the Complexes of Block Ionomers and Surfactants of Opposite Charge*. *Colloids Surf., B*. 1999, 16, 243–251.
19. Leonard, M. J.; Strey, H. H., *Phase Diagrams of Stoichiometric Polyelectrolyte-Surfactant Complexes*. *Macromolecules*. 2003, 36, 9549–9558.
20. Bilalov, A.; Olsson, U.; Lindman, B., *DNA-Lipid Self-Assembly: Phase Behaviour and Phase Structures of a DNA-Surfactant Complex Mixed with Lecithin and Water*. *Soft Matter*. 2011, 7, 730–742.
21. Alatorre-Meda, M.; Taboada, P.; Sabin, J.; Krajewska, B.; Varela, L. M.; Rodriguez, J. R., *DNA-Chitosan Complexation: A Dynamic Light Scattering Study*. *Colloids Surf., A*. 2009, 339, 145–152.
22. Chiappisi, L.; Prévost, S.; Grillo, I.; Gradzielski, M., *Chitosan/Alkylethoxy Carboxylates: A Surprising Variety of Structures*. *Langmuir*. 2014, 30, 1778–1787.

23. Lapitsky, Y.; Kaler, E. W., *Surfactant and Polyelectrolyte Gel Particles for Encapsulation and Release of Aromatic Oils*. *Soft Matter*. 2006, 2, 779–784.
24. Wang, W.; Sande, S. A., *Kinetics of Re-Equilibrium of Oppositely Charged Hydrogel-Surfactant System and Its Application in Controlled Release*. *Langmuir*. 2013, 29, 6697–6705.
25. Amar-Yuli, I.; Adamcik, J.; Blau, S.; Aserin, A.; Garti, N.; Mezzenga, R., *Controlled Embedment and Release of DNA from Lipidic Reverse Columnar Hexagonal Mesophases*. *Soft Matter*. 2011, 7, 8162–8168.
26. Nizri, G.; Magdassi, S.; Schmidt, J.; Cohen, Y.; Talmon, Y., *Microstructural Characterisation of Micro- and Nanoparticles Formed by Polymer-Surfactant Interactions*. *Langmuir*. 2004, 20, 4380–4385.
27. Mironov, A. V.; Starodoubtsev, S. G.; Khokhlov, A. R.; Dembo, A. T.; Dembo, K. A., *Effect of Chemical Nature of 1,1-Salt on Structure of Polyelectrolyte Gel-Surfactant Complexes*. *J. Phys. Chem. B*. 2001, 105, 5612–5617.
28. Sokolov, E. L.; Yeh, F.; Khokhlov, A.; Chu, B., *Nanoscale Supramolecular Ordering in Gel-Surfactant Complexes: Sodium Alkyl Sulfates in Poly(diallyldimethylammonium chloride)*. *Langmuir*. 1996, 12, 6229–6234.
29. Chu, B.; Yeh, F.; Sokolov, E. L.; Starodoubtsev, S. G.; Khokhlov, A. R., *Interaction of Slightly Cross-Linked Gels of Poly(diallyldimethylammonium chloride) with Surfactants*. *Macromolecules*. 1995, 28, 8447–8449.
30. Annaka, M., *Salt Effect on Microscopic Structure and Stability of Colloidal Complex Obtained from Neutral/Polyelectrolyte Block Copolymer and Oppositely Charged Surfactant*. *Colloids Surf., B*. 2012, 99, 127–135.
31. Hellebust, S.; Blokhus, A. M.; Nilsson, S., *Associative and Segregative Phase Behaviour of a Mixed Aqueous Cationic Surfactant and Anionic Hydrophilic Polymer System*. *Colloid Surface Physicochem. Eng. Aspect*. 2004, 243, 133–138.
32. Lee, W. B.; Mezzenga, R.; Fredrickson, G. H., *Anomalous Phase Sequences in Lyotropic Liquid Crystals*. *Phys. Rev. Lett*. 2007, 99, 187801.
33. Negrini, R.; Mezzenga, R., *pH-Responsive Lyotropic Liquid Crystals for Controlled Drug Delivery*. *Langmuir*. 2011, 27, 5296–5303.

34. Rahanyan-Kägi, N.; Aleandri, S.; Speziale, C.; Mezzenga, R.; Landau, E. M., *Stimuli-Responsive Lipidic Cubic Phase: Triggered Release and Sequestration of Guest Molecules*. Chem Eur J. 2015, 21, 1873-1877.
35. Dai, S.; Ravi, P.; Tam, K. C., *pH-Responsive Polymers: Synthesis, Properties and Applications*. Soft Matter. 2008, 4, 435-449.
36. Mahdavinia, G. R.; Pourjavadi, A.; Hosseinzadeh, H.; Zohuriaan, M. J., *Modified Chitosan 4. Superabsorbent Hydrogels from Poly(acrylic acid-co-acrylamide) Grafted Chitosan with Salt- and pH-Responsiveness Properties*. European Polymer Journal. 2004, 40, 1399-1407.
37. Nizri, G.; Makarsky, A.; Magdassi, S.; Talmon, Y., *Nanostructures Formed by Self-Assembly of Negatively Charged Polymer and Cationic Surfactants*. Langmuir. 2009, 25, 1980-1985.
38. Nilsson, P.; Hansson, P., *Regular and Irregular Deswelling of Polyacrylate and Hyaluronate Gels Induced by Oppositely Charged Surfactants*. J. Colloid Interface Sci. 2008, 325, 316-323.
39. Li, C.; Schluüter, A. D.; Zhang, A.; Mezzenga, R., *A New Level of Hierarchical Structure Control by Use of Supramolecular Self-Assembled Dendronized Block Copolymers*. Adv Mater. 2008, 20, 4530-4534.
40. Miguel, M. G.; Pais, A. A. C. C.; Dias, R. S.; Leal, C.; Rosa, M.; Lindman, B., *DNA-Cationic Amphiphile Interactions*. Colloids Surf., A. 2003, 228, 43-55.
41. Admirand, W. H.; Small, D. M., *The Physicochemical Basis of Cholesterol Gallstone Formation in Man*. J. Clin. Investig. 1968, 47, 1043-1052.
42. Marques, E. F.; Edlund, H.; La Mesa, C.; Khan, A., *Liquid Crystals and Phase Equilibria Binary Bile Salt-Water Systems*. Langmuir. 2000, 16, 5178-5186.
43. Hirano, S.; Seino, H.; Akiyama, Y.; Nonaka, I., *Chitosan: A Biocompatible Material for Oral and Intravenous Administrations*. In Prog. Biomed. Polym., Gebelein, C.; Dunn, R., Eds. Springer US: 1990; pp 283-290.
44. Hoogstraate, J. A. J.; Wertz, P. W., *Drug Delivery via the Buccal Mucosa*. Pharm. Sci. Technol. Today. 1998, 1, 309-316.

45. Harris, D.; Robinson, J. R., *Drug Delivery via the Mucous Membranes of the Oral Cavity*. J. Pharm. Sci. 1992, 81, 1-10.
46. Lameiro, M. H.; Malpique, R.; Silva, A. C.; Alves, P. M.; Melo, E., *Encapsulation of Adenoviral Vectors into Chitosan-Bile Salt Microparticles for Mucosal Vaccination*. J. Biotechnol. 2006, 126, 152-162.
47. Kaukonen, A.; Boyd, B.; Porter, C. H.; Charman, W., *Drug Solubilisation Behavior During In vitro Digestion of Simple Triglyceride Lipid Solution Formulations*. Pharmaceut. Res. 2004, 21, 245-253.
48. Porter, C. J. H.; Charman, W. N., *In vitro Assessment of Oral Lipid Based Formulations*. Adv. Drug Delivery Rev. 2001, 50, Supplement 1, S127-S147.
49. Thongngam, M.; McClements, D. J., *Isothermal Titration Calorimetry Study of the Interactions between Chitosan and a Bile Salt (Sodium Taurocholate)*. Food Hydrocolloids. 2005, 19, 813-819.
50. Lameiro, M. H.; Lopes, A.; Martins, L. O.; Alves, P. M.; Melo, E., *Incorporation of a Model Protein into Chitosan-Bile Salt Microparticles*. Int. J. Pharm. 2006, 312, 119-130.
51. Babak, V. G.; Merkovich, E. A.; Desbrières, J.; Rinaudo, M., *Formation of An Ordered Nanostructure in Surfactant-Polyelectrolyte Complexes Formed by Interfacial Diffusion*. Polym. Bull. 2000, 45, 77-81.
52. Vikhoreva, G. A.; Babak, V. G.; Galich, E. F.; Gal'braikh, L. S., *Complex Formation in the Sodium Dodecyl Sulfate-Chitosan System*. Polym. Sci., Ser. A. 1997, 39, 617-622.
53. Babak, V. G.; Merkovich, E. A.; Galbraikh, L. S.; Shtykova, E. V.; Rinaudo, M., *Kinetics of Diffusionally Induced Gelation and Ordered Nanostructure Formation in Surfactant-Polyelectrolyte Complexes Formed at Water/Water Emulsion Type Interfaces*. Mendeleev Commun. 2000, 10, 94-95.
54. Lapitsky, Y.; Kaler, E. W., *Formation of Surfactant and Polyelectrolyte Gel Particles in Aqueous Solutions*. Colloids Surf, A. 2004, 250, 179-187.
55. Lapitsky, Y.; Kaler, E. W., *Formation and Structural Control of Surfactant and Polyelectrolyte Gels*. Colloids Surf., A. 2006, 282-283, 118-128.

56. Higuchi, W. I., *Diffusional Models Useful in Biopharmaceutics. Drug Release Rate Processes*. J. Pharm. Sci. 1967, 56, 315–324.
57. Zabara, A.; Negrini, R.; Baumann, P.; Onaca-Fischer, O.; Mezzenga, R., *Reconstitution of OmpF Membrane Protein on Bended Lipid Bilayers: Perforated Hexagonal Mesophases*. Chem. Commun. . 2014, 50, 2642–2645.
58. Haglund, B. O.; Sundelöf, L.-O.; Upadrashta, S. M.; Wurster, D. E., *Effect of SDS Micelles on Rhodamine-B Diffusion in Hydrogels*. J. Chem. Educ. 1996, 73, 889.
59. Philippova, O. E.; Starodoubtzev, S. G., *Interaction of Slightly Cross-linked Gels of Poly(diallyldimethylammonium bromide) with Sodium Dodecyl Sulfate. Diffusion of Surfactant Ions in Gel*. J. Polym. Sci., Part B: Polym. Phys. 1993, 31, 1471–1476.
60. Söderman, O.; Stilbs, P.; Price, W. S., *NMR Studies of Surfactants*. Concepts Magn. Reson., Part A. 2004, 23A, 121–135.
61. Swift, J. A., *The Mechanics of Fracture of Human Hair*. Int. J. Cosmet. Sci. 1999, 21, 227–239.
62. Madnani, N.; Khan, K., *Hair Cosmetics*. Indian J. Dermatol. Venereol. Leprol. 2013, 79, 654–667.
63. Svensson, A. V.; Johnson, E. S.; Nylander, T.; Piculell, L., *Surface Deposition and Phase Behavior of Oppositely Charged Polyion-Surfactant Ion Complexes. 2. A Means to Deliver Silicone Oil to Hydrophilic Surfaces*. ACS Appl. Mater. Interfaces. 2010, 2, 143–156.
64. Clauzel, M.; Johnson, E. S.; Nylander, T.; Panandiker, R. K.; Sivik, M. R.; Piculell, L., *Surface Deposition and Phase Behavior of Oppositely Charged Polyion-Surfactant Ion Complexes. Delivery of Silicone Oil Emulsions to Hydrophobic and Hydrophilic Surfaces*. ACS Appl Mater Interfaces. 2011, 3, 2451–2462.
65. Srinivasan, G.; Srinivas, C. R.; Mathew, A. C.; Duraiswami, D., *Effects of Hard Water on Hair*. Int. J. Trichology. 2013, 5, 137–139.
66. Draelos, Z. D., *Essentials of Hair Care often Neglected: Hair Cleansing*. Int. J. Trichology. 2010, 2, 24–29.

67. Yu, H.; Zou, Y.; Wang, Y.; Huang, X.; Huang, G.; Sumer, B. D.; Boothman, D. A.; Gao, J., *Overcoming Endosomal Barrier by Amphotericin B-Loaded Dual pH-Responsive PDMA-*b*-PDPA Micelleplexes for siRNA Delivery*. ACS Nano. 2011, 5, 9246-9255.
68. Negrini, R.; Fong, W.-K.; Boyd, B. J.; Mezzenga, R., *pH-Responsive Lyotropic Liquid Crystals and Their Potential Therapeutic Role in Cancer Treatment*. Chem. Commun. 2015.
69. Kim, B.-S.; Lee, H.-i.; Min, Y.; Poon, Z.; Hammond, P. T., *Hydrogen-Bonded Multilayer of pH-Responsive Polymeric Micelles with Tannic Acid for Surface Drug Delivery*. Chem. Commun. 2009, 4194-4196.
70. Salentinig, S.; Phan, S.; Darwish, T. A.; Kirby, N.; Boyd, B. J.; Gilbert, E. P., *pH-Responsive Micelles Based on Caprylic Acid*. Langmuir. 2014, 30, 7296-7303.
71. Liao, Y.-H.; Jones, S. A.; Forbes, B.; Martin, G. P.; Brown, M. B., *Hyaluronan: Pharmaceutical Characterisation and Drug Delivery*. Drug Delivery. 2005, 12, 327-342.
72. Mero, A.; Campisi, M., *Hyaluronic Acid Bioconjugates for the Delivery of Bioactive Molecules*. Polymers. 2014, 6, 346.
73. Li, J.; Huang, P.; Chang, L.; Long, X.; Dong, A.; Liu, J.; Chu, L.; Hu, F.; Liu, J.; Deng, L., *Tumor Targeting and pH-Responsive Polyelectrolyte Complex Nanoparticles Based on Hyaluronic Acid-Paclitaxel Conjugates and Chitosan for Oral Delivery of Paclitaxel*. Macromol. Res. 2013, 21, 1331-1337.
74. Qiu, L.; Li, Z.; Qiao, M.; Long, M.; Wang, M.; Zhang, X.; Tian, C.; Chen, D., *Self-Assembled pH-Responsive Hyaluronic Acid-*g*-Poly(*l*-histidine) Copolymer Micelles for Targeted Intracellular Delivery of Doxorubicin*. Acta Biomater. 2014, 10, 2024-2035.
75. Mayol, L.; Quaglia, F.; Borzacchiello, A.; Ambrosio, L.; Rotonda, M. I. L., *A Novel Poloxamers/Hyaluronic Acid In situ Forming Hydrogel for Drug Delivery: Rheological, Mucoadhesive and In vitro Release Properties*. Eur. J. Pharm. Biopharm. 2008, 70, 199-206.

76. Yu, L. X.; Crison, J. R.; Amidon, G. L., *Compartmental Transit and Dispersion Model Analysis of Small Intestinal Transit Flow in Humans*. Int. J. Pharm. 1996, 140, 111–118.
77. Ritschel, W. A., *Targeting in the Gastrointestinal Tract. New Approaches*. Methods Find. Exp. Clin. Pharmacol. 1991, 13, 313–336.
78. Thongngam, M.; McClements, D. J., *Characterisation of Interactions between Chitosan and an Anionic Surfactant*. J. Agr. Food Chem. 2004, 52, 987–991.
79. Kleinpell, R. M.; Munro, C. L.; Giuliano, K. K., Targeting Health Care-Associated Infections: Evidence-Based Strategies. In *Patient Safety and Quality: An Evidence-Based Handbook for Nurses*, Hughes, R. G., Ed. Rockville (MD): Agency for Healthcare Research and Quality (US), 2008.
80. Li, J.; Nation, R. L.; Turnidge, J. D.; Milne, R. W.; Coulthard, K.; Rayner, C. R.; Paterson, D. L., *Colistin. The Re-Emerging Antibiotic for Multidrug-Resistant Gram-Negative Bacterial Infections*. Lancet Infect. Dis. 2006, 6, 589–601.
81. Wallace, S. J.; Li, J.; Nation, R. L.; Prankerd, R. J.; Velkov, T.; Boyd, B. J., *Self-Assembly Behaviour of Colistin and Its Prodrug Colistin Methanesulfonate. Implications for Solution Stability and Solubilisation*. J. Phys. Chem. B. 2010, 114, 4836–4840.
82. Phan, S.; Hawley, A.; Mulet, X.; Waddington, L.; Prestidge, C.; Boyd, B., *Structural Aspects of Digestion of Medium Chain Triglycerides Studied in Real Time using sSAXS and Cryo-TEM*. Pharm. Res. 2013, 30, 3088–3100.

6.9 Appendix

A6.1 Effect of pH on the Bile Salt/Chitosan System

Solutions of 4 wt% chitosan (low molecular weight) and 30 wt% sodium taurodeoxycholate hydrate were prepared in 10 % acetic acid. Each solution (500 μL) was combined into a 1.5 mL glass vial and vigorously mixed until the mixture appeared homogeneous. To each sample, 1 M NaOH was added dropwise until the desired pH was reached (tested with pH strips), then topped with Milli-Q water to a total mass of 1.5 g. The samples were allowed to equilibrate for a week, after which a white precipitate had formed in a turbid solution. SAXS data demonstrated that the formation of lamellar phase (lattice parameter $\sim 32 \text{ \AA}$) was not influenced by solution pH (Figure A6.1); apart from the slightly viscous opaque mixture at pH 10 where no scattering was observed. This justified the preparation of the capsules studied in the *in vitro* release studies in 10 % acetic acid ($\sim \text{pH } 2$).

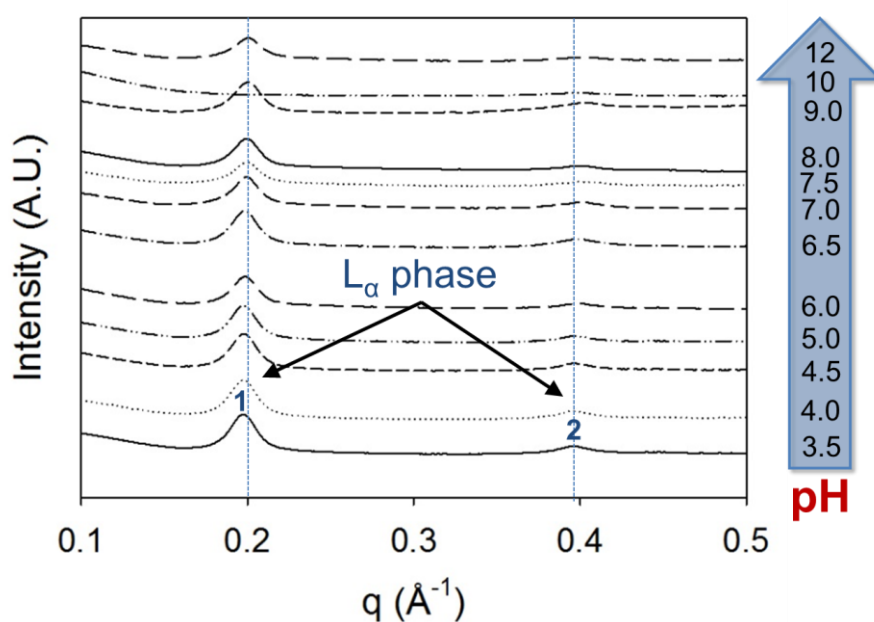


Figure A6.1 Effect of pH on the lamellar (L_{α}) phase formed in mixtures comprised of 30 wt% STDC and 4 wt% chitosan.

A6.2 Visualising the Growth of Nanostructures Across the Bile Salt-Chitosan Interface by CPLM

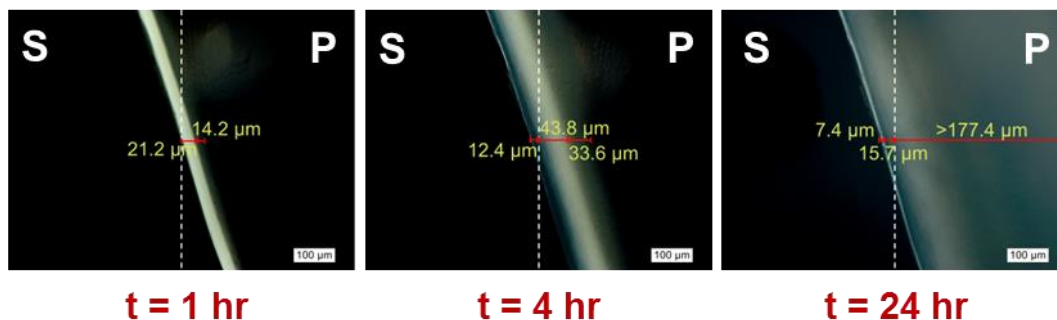


Figure A6.2 The growth and development of bands exhibiting birefringence across the interface created between solutions of 30 wt% sodium taurodeoxycholate (S) and 4 wt% chitosan (P) under crossed-polarisers, which was directed predominantly towards the bulk polymer region. The dashed line marks the point of origin.

A6.3 Phase Behaviour of Chitosan in Biorelevant Bile Solutions

To investigate the feasibility of the bile salt and chitosan system for forming liquid crystalline structures in a more biological environment, solutions of chitosan were introduced to solutions of bile salt with varying concentrations that mimicked the amount of micelles released in the gut during either the ‘fasted’ or ‘fed’ state.^{47, 82} Fed micelles were comprised of 20 mM STDC and 5 mM DOPC in digestion buffer at pH 6.6. Fasted micelles were prepared by a 1 in 4 dilution of the fed micelle solution. A disk of 4 wt% chitosan was delivered into a flat cell and flushed with either of the micellar solutions. A line scan with 100 μm spatial resolution was conducted across the bile solution-chitosan solution interfaces at the Australian Synchrotron SAXS/WAXS beamline to identify the formation of any mesophases.

Upon the introduction of two different bile salt-lecithin mixed micellar solutions to a disk of 4 wt% chitosan solution, the concentration of micelles in the ‘fasted’ state (low bile salt) was determined to be insufficient to produce any highly ordered structures (Figure A6.3-A). In contrast, lamellar phase with a lattice parameter of ~ 34 Å was formed when surrounded by a higher concentration of micelles in the ‘fed’ state (Figure A6.3-B).

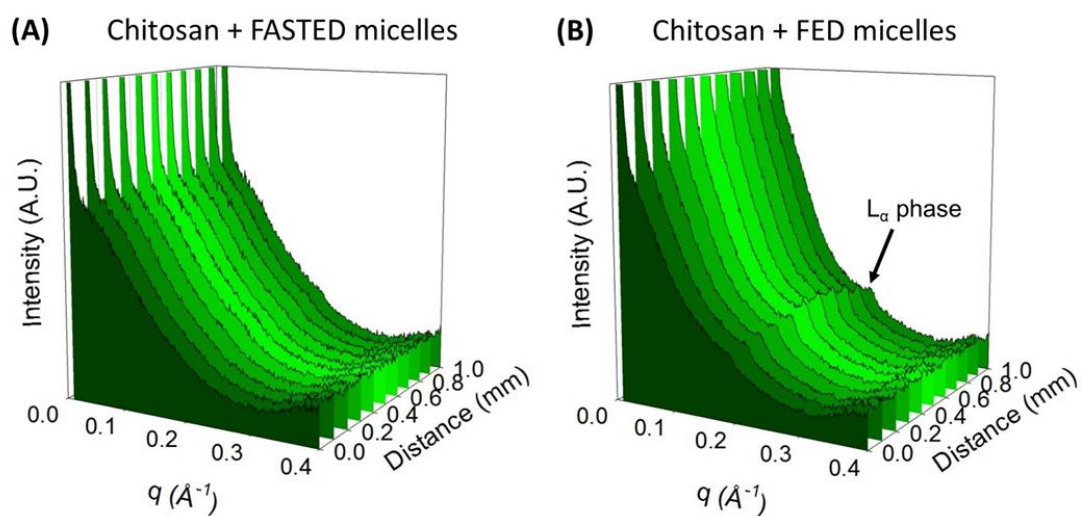


Figure A6.3 SAXS profiles across interfaces created between solutions of chitosan and simulated gastrointestinal fluid with micellar concentrations comparable to those present during the ‘fasted’ (A) or ‘fed’ (B) state of digestion.

A6.4 Characterisation of Mesophases Formed Across the CTAB- PAAm-AA Interface by Synchrotron SAXS

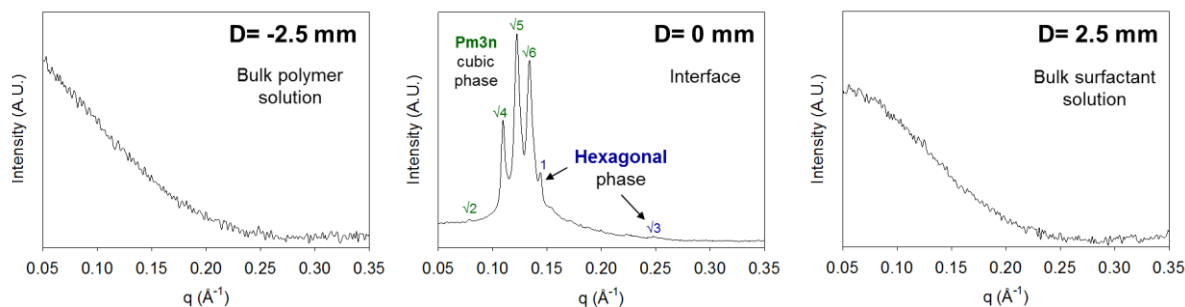


Figure A6.4 SAXS profiles of pertinent D (distance from origin) values across the CTAB-PAAm-AA interface in Figure 6.6.

Note. The high flux of X-rays and signal-to-noise ratio provided by a synchrotron SAXS source allowed the Bragg peak at $\sqrt{2}$ for *Pm3n* cubic phases formed across the surfactant-polymer interface to be resolved.

A6.5 Identification of Coexisting *Pm3n* Cubic and Hexagonal Phases Across the CTAB-PAAm-AA Interface

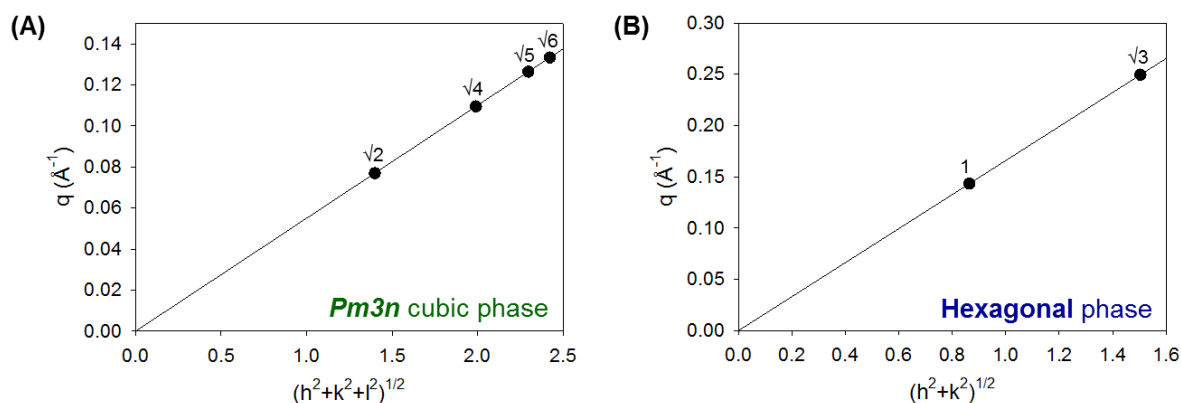


Figure A6.5 Graphs of d -spacing vs. Miller indices generated from the corresponding Bragg reflections observed in the SAXS profile (Figure A6.4) at $D = 0$ mm across the CTAB-PAAm-AA interface indicating the coexistence of *Pm3n* cubic (A) and hexagonal (B) phases.

A6.6 Temperature-Dependent Equilibrium Phase Behaviour of the CTAB and PAAm-AA System

Table A6.1 Effect of temperature on the spacing ratio of Bragg peaks indexed for *Pm3n* cubic phase in mixtures of CTAB and PAAm-AA.

Bragg peak	Temperature															
	25 °C		30 °C		35 °C		40 °C		45 °C		50 °C		55 °C		60 °C	
	q (Å ⁻¹)	d (Å)														
√2	*	*	*	*	*	*	*	*	*	*	*	*	*	*	*	*
√4	0.1003	63	0.101	62	0.102	61	0.104	61	*	*	*	*	*	*	*	*
√5	0.117	54	0.113	56	0.114	55	0.115	55	0.116	54	0.117	54	0.118	53	0.12	53
√6	0.1223	51	0.125	50	0.126	50	0.127	49	*	*	*	*	*	*	*	*

Note. The Bragg peak at √2 for *Pm3n* cubic phases were not evident in the SAXS profile obtained during the temperature scan of this sample mixture as the benchtop SAXS instrument was not able to produce highly resolved scattering curves as with synchrotron SAXS (Figure A6.4). This is true for Bragg reflections marked with asterisks. However, above 45 °C the disappearance of the previously existing Bragg peaks characteristic of *Pm3n* cubic phase was a result of a change in its proportion in the mixed mesophases rather than a limitation of the technique.

Table A6.2 Effect of temperature on the spacing ratio of Bragg peaks indexed for hexagonal phase in mixtures of CTAB and PAAm-AA.

Bragg peak	Temperature															
	25 °C		30 °C		35 °C		40 °C		45 °C		50 °C		55 °C		60 °C	
	q (Å ⁻¹)	d (Å)														
1	0.1284	49	0.129	49	0.126	50	0.127	49	0.131	48	0.132	48	0.132	47	0.134	47
√3	0.2224	28	0.222	28	0.221	28	0.225	28	0.228	28	0.227	28	0.23	27	0.233	27

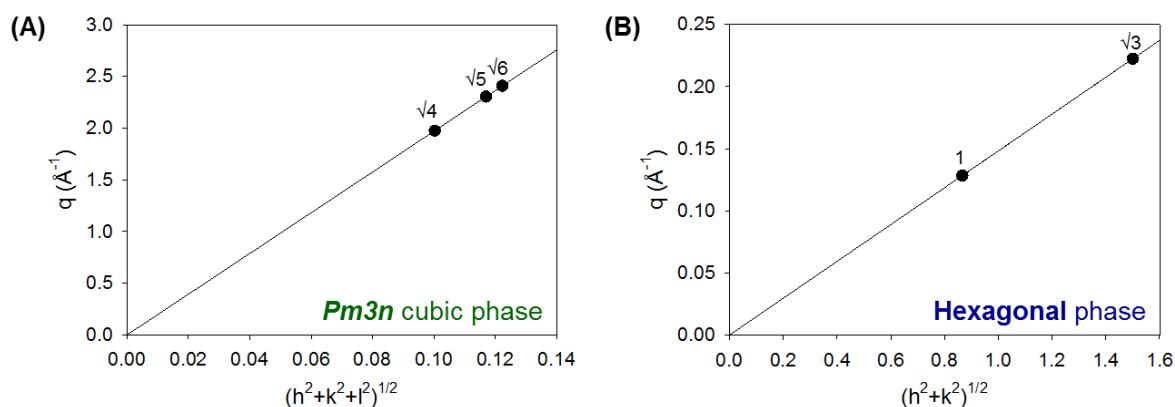


Figure A6.6 Graphs of d-spacing vs. Miller indices generated from the corresponding Bragg reflections observed in the SAXS profile of the bulk aqueous mixture of CTAB and PAAm-AA at 25°C with coexisting *Pm3n* cubic (A) and hexagonal (B) phases (Figure 6.7).

Note. The Bragg peak at $\sqrt{2}$ for *Pm3n* cubic phases was not evident in the SAXS profiles obtained during the temperature scan of this sample mixture as the benchtop SAXS instrument was not able to produce highly resolved scattering curves as with synchrotron SAXS (Figure A6.4).

A6.7 Calibration Curve for Rhodamine B by Fluorescence Spectroscopy

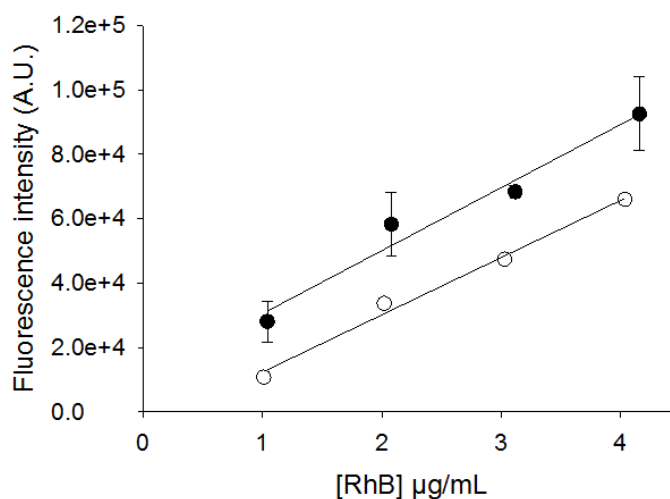


Figure A6.7 Calibration curve for Rhodamine B prepared in either 10% acetic acid ($\sim\text{pH}$ 2–filled circles) or Milli-Q water ($\sim\text{pH}$ 7–open circles).

Chapter 7: *Summary and Outlook*

7. Summary and Outlook

7.1 Summary of Findings

Oppositely charged surfactant and polymer systems have become a growing field of research over the past four decades for their use in a wide range of applications particularly in the personal care¹⁻³ and pharmaceutical⁴⁻⁷ industries. With a large selection of synthetic and biocompatible materials available that have diverse molecular structures, the formation of liquid crystalline phases in such systems can be controlled to produce complexes with different internal structure, particle size, surface morphology, viscosity, and phase behaviour at varying compositions and solution conditions. Mixing of these charged species in bulk solutions is often not an instantaneous process. There have been reports of kinetically trapped nonequilibrium structures existing in bulk aqueous mixtures of oppositely charged surfactants and polymers.⁸⁻¹¹ However, there is little understanding of how local changes in structure and composition influences the overall equilibrium behaviour of the system. This thesis presents approaches to study the formation of nanostructures and the distribution of components across surfactant–polymer interfaces over time, as well as the release behaviour of a model hydrophilic drug from nanostructured capsules to assess their potential as novel stimuli-responsive drug delivery systems.

7.1.1 Novel Approaches to Study the Dynamics of Structure Formation Across Solution Interfaces

In Chapter 2, novel approaches were developed to study the kinetics of structure formation across oppositely charged surfactant–polymer interfaces.

The growth of anisotropic materials exhibiting birefringence across surfactant–polymer interfaces were visualised with crossed–polarised light microscopy.

Line scans performed with synchrotron small angle X-ray scattering (SAXS) enabled acquisition of scattering curves across these interfaces with 100 μm spatial resolution. The SAXS curves obtained allowed the identification of liquid crystalline structures and determination of their lattice parameters. Specifically, the lattice parameter determined for hexagonal phases existing in solutions of SDS with or without polyDADMAC was used to approximately quantify the concentrations of surfactant and water locally across SDS–polyDADMAC interfaces. In addition, the shape of the broad peak indicative of micelles in the low q range of the SAXS curves provided discrimination between the formation of spherical and rod–like SDS micelles, as well as an indication of the concentration range of SDS present in different micellar regions as demonstrated in Section 2.5.3.2.

More generally, the approach developed here using synchrotron SAXS to study surfactant–polymer interfaces may also be employed to examine the evolution of structures upon contact between other types of materials in real–time. Ideally, the viscosity of one component should be greater than the other to ensure the formation of a neat interface, thus contact experiments may also be feasible with dispersions, emulsions, polymer gels, and lipids where ordered structures are expected to form. Additionally, using the ‘disk’ approach described in Section 4.4.2.1 and Section 6.4.2.1, the phase behaviour exhibited across such interfaces may also be studied as other components are sequentially added and/or removed (Schematic 6.1). The order of addition of surfactant and polymer solutions has shown to significantly influence the physicochemical properties of complexes formed.¹⁰ It is also known that hair products, such as shampoos, contain multiple ingredients.¹² Thus, it is envisaged that the ‘step–by–step’ addition of pure or mixed components to creating such

interfaces described may provide a new means of gaining further insight into the formation of nanostructures upon mixing of all ingredients within a formulation. Lastly, achieving smaller beam sizes with synchrotron SAXS would allow investigation of the dynamics of structure formation with better resolution for earlier stages in interface formation and/or where the region of interest is very thin, such as microparticles produced by microfluidic devices.¹³

Raman microspectroscopy has been widely employed for mapping the distribution of chemicals across various types of materials.¹⁴ Line scans performed with Raman microscopy enabled acquisition of Raman spectra across surfactant–polymer interfaces also with 100 μm spatial resolution. It is believed that this is the first time that Raman microscopy has been used in this way. In some cases, the concentrations of surfactant, polymer, and water present locally across SDS–polyDADMAC interfaces could be quantified by determining the area under the curve of peaks representative of the key components in the system. However, this technique was not able to resolve the concentration of SDS where hexagonal phases existed as demonstrated in Section 2.5.3.1. In addition, since water is a weak Raman scatterer, a property which often makes this technique favourable over infrared microscopy, Raman microscopy was not reliable for the measurement of water content of materials analysed. To overcome these limitations, the relative concentrations of each specified component were mapped across the surfactant–polymer interface, given as the polyDADMAC-to-SDS molar charge ratio, rather than their absolute concentrations as presented in Section 3.5.4. Thus, the distribution behaviour of surfactant, polymer, and water molecules across SDS–polyDADMAC interfaces was studied by determining the changes in composition with the formation of mesophases over time.

7.1.2 New Insights into the Formation of Equilibrium and Nonequilibrium Structures in Oppositely Charged Surfactant and Polymer Systems

The phase behaviour of the model system comprising of the anionic surfactant, SDS, and the cationic polymer, polyDADMAC, was studied in concentrated regimes as bulk mixtures, dilute regimes as dispersions, and across solution interfaces.

The method of preparation of mixtures of surfactant and polymer solutions is important in determining the physicochemical properties of such systems.¹⁵ In Chapter 3, it was found that the ternary phase diagram generated for samples prepared by dropwise addition and vortex mixing of SDS and polyDADMAC solutions, which was defined as the conventional mixing protocol, was similar for samples prepared with the complex salt, polyDADMADS. Therefore, taking different routes to achieving the same final composition can result in comparable nanostructures. These findings suggest that the complex salt can be formed *in situ*, meaning that the additional time, cost, and labour associated with synthesising the complex salt for addition into formulations can be avoided.

A gradient of structures were formed across the SDS–polyDADMAC interface, which was a consequence of a concentration gradient created after contact between solutions of 20 wt% SDS and 20 wt% polyDADMAC as described in Section 3.5.3. The distance over which the region comprised of equilibrium hexagonal phases existed across the SDS–polyDADMAC interface increased over time. While the area over which coexisting micellar and hexagonal nonequilibrium structures existing on either side of this structured region decreased over time. These findings emphasise that true equilibrium may not be reached within the time scale of only a week. It was understood that the inherent viscosity of the starting bulk surfactant

and/or polymer solution and the mesophases formed significantly influenced the diffusion of molecules across the surfactant–polymer interface, which overall determined the state of equilibrium achieved.

The development of nanostructures toward the bulk SDS region across this SDS–polyDADMAC interface was a peculiar phenomenon. In Chapter 4, constraining the mobility of a component influenced the rate and direction of structure formation across the surfactant–polymer interface. Upon contact of an SDS hexagonal phase region with a dilute solution of polyDADMAC, SDS micelles were able to diffuse efficiently across the SDS–polyDADMAC interface to form highly ordered structures in the bulk polymer region. In this case, the diffusion of polyDADMAC molecules into the highly concentrated surfactant region was hindered by the rheological barrier exhibited by the SDS hexagonal phase. Furthermore, the SDS molecules that were initially organised into a hexagonal lattice behaved as a ‘donor’ phase of micelles, where their transport across the interface was the key rate limiting factor toward the formation of mesophases. The phase behaviour demonstrated across this particular SDS–polyDADMAC interface revealed a means of producing similar structures with the use of less water, which will consequently reduce the costs associated in the manufacturing of hair products, for example. The cross-linking of charged polymers offers an additional approach for controlling the diffusion of oppositely charged surfactants and the formation of ordered structures within gels. Oppositely charged therapeutics may also be loaded by this process, where its release can be controlled by the swelling behaviour of the gel or the response of the nanostructure to certain stimuli.

In Chapter 5, the global morphology and lattice parameter of nanostructures formed in aqueous mixtures of SDS and polyDADMAC were considerably influenced by the absolute molar concentrations and molar charge ratio of surfactant and polymer in the system.

Generally, hexagonal phases with larger internal dimensions were formed in more concentrated mixtures due to an increase in the ionic strength within the system, which in turn resulted in an increase in repulsive forces existing between the oppositely charged species. In contrast, more compact structures were formed in more dilute regimes since there were greater chances for the charged species to interact with each other in solution. Moreover, the diffusion of the molecules in dilute dispersions was not significantly retarded as a result of an increased viscosity which was often encountered at higher compositions and the formation of liquid crystalline structures. Most importantly, the relationship existing between the local composition and viscosity of complexes formed in aqueous mixtures of SDS and polyDADMAC was found to play a crucial role in determining whether the nanostructures exist at equilibrium or become kinetically trapped at a nonequilibrium state.

7.1.3 Tailored Release Nanomaterials

Chapter 6 showcased a range of oppositely charged surfactant and polymer systems for their potential application as stimuli-responsive drug delivery systems. The release behaviour of a model hydrophilic drug from macro-sized capsules was controlled by the mesophases formed across the surfactant-polymer interfaces, as well as the response of the structure to changes in solution conditions.

Coexisting hexagonal and micellar phases formed across the SDS-polyDADMAC interface were temperature-stable, but sensitive to high salt concentrations, which render them useful in hair care products. While, the structural integrity of coexisting $Pm3n$ cubic and hexagonal phases formed across the CTAB-PAAm-AA interface were lost in acidic environments, providing a platform for the design of pH-responsive systems comprised of biomaterials. Lastly, the temperature- and salt-sensitive lamellar phase formed upon contact between chitosan and bile salts offers a novel *in situ* forming drug delivery system.

7.2 Future Directions

The work in this thesis has demonstrated new methods to study the correlation between changes in the local structure and composition across surfactant–polymer solution interfaces as the system approaches equilibrium. It was highlighted that the inherent viscosity of bulk solutions and of mesophases formed upon mixing may have been one of the key parameters to significantly influence the diffusion of charged species in solution and that possibly lead to kinetically trapped nonequilibrium structures. Hence, it would be of interest to further study the relationship between structure, composition, and viscosity across surfactant–polymers interfaces. Techniques commonly employed for probing the microrheology of complex fluids include optical tweezers,^{16, 17} particle tracking^{18, 19} and magnetic nanowire^{20, 21} microrheology, as well as diffusive wave spectroscopy.²²⁻²⁴ A major advantage these methodologies have over rheometers typically used to measure the viscosity of bulk solutions is that only microlitre volumes of the sample are required. Additionally, confocal microscopy may enable full real-space visualisation of the trajectory of tracer particles and measurements of the viscoelastic moduli of anisotropic materials.¹⁸

Not only can therapeutics be encapsulated within gel particles formed from the interactions between oppositely charged surfactants and polymers in solution, but they themselves may be able to participate in the formation of structured complexes. Charged peptides are attracting interest as anticancer, antiviral, and antimicrobial agents.²⁵ It is envisioned that when these molecules are delivered in combination with anionic biomaterials that can be found ubiquitously within the body, such as heparin sulphate²⁶ or hyaluronic acid²⁷, their release can be triggered in response to elevated levels of heparinase²⁸ or hyaluronidase^{29, 30} present in certain disease states. Thus, these systems offer vast opportunities for designing novel targeted and controlled drug delivery devices.

7.3 References

1. Clauzel, M.; Johnson, E. S.; Nylander, T.; Panandiker, R. K.; Sivik, M. R.; Piculell, L., *Surface Deposition and Phase Behavior of Oppositely Charged Polyion–Surfactant Ion Complexes. Delivery of Silicone Oil Emulsions to Hydrophobic and Hydrophilic Surfaces*. ACS Appl Mater Interfaces. 2011, 3, 2451–2462.
2. Wilgus, L. A.; Davis, K.; Labeaud, L.; Gandolfi, L.; Lochhead, R. Y., *A Study of the Distribution of Polymer/Surfactant Coacervate between Solution and Foam in Archetypal Shampoo Systems*. J. Cosmet. Sci. . 2011, 62, 179–189.
3. Desbrieres, J.; Bousquet, C.; Babak, V., *Surfactant–Chitosan Interactions and Application to Emulsion Stabilization*. Cellul. Chem. Technol. 2010, 44, 395–406.
4. Bronich, T. K.; Nehls, A.; Eisenberg, A.; Kabanov, V. A.; Kabanov, A. V., *Novel Drug Delivery Systems Based on the Complexes of Block Ionomers and Surfactants of Opposite Charge*. Colloids Surf., B. 1999, 16, 243–251.
5. Amar-Yuli, I.; Adamcik, J.; Blau, S.; Aserin, A.; Garti, N.; Mezzenga, R., *Controlled Embedment and Release of DNA from Lipidic Reverse Columnar Hexagonal Mesophases*. Soft Matter. 2011, 7, 8162–8168.
6. Morán, M. C.; Miguel, M. G.; Lindman, B., *Surfactant–DNA Gel Particles: Formation and Release Characteristics*. Biomacromolecules. 2007, 8, 3886–3892.
7. Takka, S.; Çali, A. G., *Bile Salt-Reinforced Alginate–Chitosan Beads*. Pharm. Dev. Technol. 2012, 17, 23–29.
8. Fegyver, E.; Mészáros, R., *Fine-Tuning the Nonequilibrium Behavior of Oppositely Charged Macromolecule/Surfactant Mixtures via the Addition of Nonionic Amphiphiles*. Langmuir. 2014, 30, 15114–15126.
9. Mezei, A.; Mészáros, R.; Varga, I.; Gilányi, T., *Effect of Mixing on the Formation of Complexes of Hyperbranched Cationic Polyelectrolytes and Anionic Surfactants*. Langmuir. 2007, 23, 4237–4247.
10. Naderi, A.; Claesson, P. M.; Bergström, M.; Dédinaite, A., *Trapped Non-Equilibrium States in Aqueous Solutions of Oppositely Charged Polyelectrolytes and Surfactants*.

- Effects of Mixing Protocol and Salt Concentration.* Colloids and Surfaces A: Physicochem. Eng. Aspects. 2005, 253, 83–93.
11. Naderi, A.; Claesson, P. M., *Association between Poly(vinylamine) and Sodium Dodecyl Sulfate: Effects of Mixing Protocol, Blending Procedure, and Salt Concentration.* J. Dispersion Sci. Technol. 2005, 26, 329–340.
 12. Draelos, Z. D., *Essentials of Hair Care often Neglected: Hair Cleansing.* Int. J. Trichology. 2010, 2, 24–29.
 13. Vladisavljević, G. T.; Shahmohamadi, H.; Das, D. B.; Ekanem, E. E.; Tauanov, Z.; Sharma, L., *Glass Capillary Microfluidics for Production of Monodispersed Poly(dl-lactic acid) and Polycaprolactone Microparticles: Experiments and Numerical Simulations.* J. Colloid Interface Sci. 2014, 418, 163–170.
 14. Mansour, H. M.; Hickey, A. J., *Raman Characterization and Chemical Imaging of Biocolloidal Self-Assemblies, Drug Delivery Systems, and Pulmonary Inhalation Aerosols: A Review.* AAPS PharmSciTech. 2007, 8, 140–155.
 15. Qi, L.; Fresnais, J.; Berret, J.-F.; Castaing, J.-C.; Grillo, I.; Chapel, J.-P., *Influence of the Formulation Process in Electrostatic Assembly of Nanoparticles and Macromolecules in Aqueous Solution: The Mixing Pathway.* J. Phys. Chem. C. 2010, 114, 12870–12877.
 16. Bennett, J. S.; Gibson, L. J.; Kelly, R. M.; Brousse, E.; Baudisch, B.; Preece, D.; Nieminen, T. A.; Nicholson, T.; Heckenberg, N. R.; Rubinsztein-Dunlop, H., *Spatially-Resolved Rotational Microrheology with an Optically-Trapped Sphere.* Scientific Reports. 2013, 3, 1759.
 17. Tassieri, M.; Giudice, F. D.; Robertson, E. J.; Jain, N.; Fries, B.; Wilson, R.; Glidle, A.; Greco, F.; Netti, P. A.; Maffettone, P. L.; Bicanic, T.; Cooper, J. M., *Microrheology with Optical Tweezers: Measuring the Relative Viscosity of Solutions ‘At A glance’.* Scientific Reports. 2015, 5, 8831.
 18. Mason, T. G.; Ganesan, K.; van Zanten, J. H.; Wirtz, D.; Kuo, S. C., *Particle Tracking Microrheology of Complex Fluids.* Phys. Rev. Lett. 1997, 79, 3282–3285.
 19. Ortega, F.; Ritacco, H.; Rubio, R. G., *Interfacial Microrheology: Particle Tracking and Related Techniques.* Curr. Opin. Colloid Interface Sci. 2010, 15, 237–245.

-
20. Lee, M. H.; Lapointe, C. P.; Reich, D. H.; Stebe, K. J.; Leheny, R. L., *Interfacial Hydrodynamic Drag on Nanowires Embedded in Thin Oil Films and Protein Layers*. Langmuir. 2009, 25, 7976–7982.
 21. Lee, M. H.; Reich, D. H.; Stebe, K. J.; Leheny, R. L., *Combined Passive and Active Microrheology Study of Protein-Layer Formation at an Air–Water Interface*. Langmuir. 2010, 26, 2650–2658.
 22. Alexander, M.; Dalgleish, D. G., *Diffusing Wave Spectroscopy of Aggregating and Gelling Systems*. Curr. Opin. Colloid Interface Sci. 2007, 12, 179–186.
 23. Breedveld, V.; Pine, D. J., *Microrheology as a Tool for High-Throughput Screening*. J. Mater. Sci. 2003, 38, 4461–4470.
 24. Dasgupta, B. R.; Weitz, D. A., *Microrheology of Cross-linked Polyacrylamide Networks*. Phys. Rev. E. 2005, 71, 021504.
 25. Mulder, K. C. L.; Lima, L. A.; Miranda, V. J.; Dias, S. C.; Franco, O. L., *Current Scenario of Peptide-Based Drugs: The Key Roles of Cationic Antitumor and Antiviral Peptides*. Front. Microbiol. 2013, 4, 321.
 26. Simon Davis, D. A.; Parish, C. R., *Heparan Sulfate: A Ubiquitous Glycosaminoglycan with Multiple Roles in Immunity*. Front. Immunol. 2013, 4, 470.
 27. Brown, M. B.; Jones, S. A., *Hyaluronic Acid: A Unique Topical Vehicle for the Localized Delivery of Drugs to the Skin*. J. Eur. Acad. Dermatol. Venereol. 2005, 19, 308–318.
 28. Shafat, I.; Barak, A. B.; Postovsky, S.; Elhasid, R.; Ilan, N.; Vlodaysky, I.; Arush, M. W. B., *Heparanase Levels Are Elevated in the Plasma of Pediatric Cancer Patients and Correlate with Response to Anticancer Treatment*. Neoplasia (N. Y., NY, U. S.). 2007, 9, 909–916.
 29. Lokeshwar, V. B.; Lokeshwar, B. L.; Pham, H. T.; Block, N. L., *Association of Elevated Levels of Hyaluronidase, a Matrix-degrading Enzyme, with Prostate Cancer Progression*. Cancer Res. 1996, 56, 651–657.
 30. Bertrand, P.; Girard, N.; Duval, C.; d'Anjou, J.; Chauzy, C.; Ménard, J.-F.; Delpech, B., *Increased Hyaluronidase Levels in Breast Tumor Metastases*. Int. J. Cancer. 1997, 73, 327–331.
-